Developing new routes towards precision and function in materials synthesis and properties

Dafni Moatsou

submitted for the degree of Doctor of Philosophy

Department of Chemistry

THE UNIVERSITY OF WARWICK

2015

Table of Contents

List of Figures, Schemes, and Tables

Figures

Schemes

Tables

Acknowledgements

This PhD has not been easy, but I have had a lot of support in the past three (and a bit) years and, now, I feel like time flew.

I want to thank all of the people whom I have collaborated with around the world: Prof. Michael Jewett, Dr. Arnaz Ranji, and Dr. Jian Li from NU; Dr. Kei Saito and Dr. Gagan Kaur from Monash University; Prof. Andreas Kilbinger and Dr. Amit Nagarkar from the University of Fribourg; Dr. Annhelen Lu from the University of Warwick. I would also like to acknowledge EPSRC for funding.

I cannot thank enough Rachel (Professor O'Reilly to you) for bringing me here in the first place, helping me through some rough patches, and always being the diligent guide she is. I sometimes cannot believe how many exciting things have happened because of her.

If this thesis makes sense to anyone, that is a result of the kind help from Mat, Lewis, Becky, Zan, Rob, Guillaume, Alice, Anaïs, Helen, Anne, and James that were volunteered to proof-read. I also want to thank everyone in the Do'Reilly (O'Dovelly?) groups, including Annie, for making life as a lab rat more social, and for always leaving snacks at the tea point. I couldn't leave out of this the O'Reilly try-athletes, and their successors, who introduced me to a lifestyle that allows me to go for a run to relax. Special thanks to the people that didn't give up on me even on my grumpiest days; well, I don't need to explain why, it's my thesis, so "thanks".

I know my family still has no idea what my PhD thesis is about, but they have influenced a great deal its outcome. Thank you for supporting me though all of these years in education, which are now coming to an end. Probably… Αλέξανδρε, I hope you like science because this is going to be one hell of a bedtime story!

Declaration of Authorship

This thesis is submitted to the University of Warwick in support of my application for the degree of Doctor of Philosophy. It has been composed by myself and has not been submitted in any previous application for any degree. The work presented (including data generated and data analysis) was carried out by the author except in the case of Chapter 4, which was carried out in collaboration with Arnaz Ranji and Jian Li from Professor Michael Jewett's group at Northwestern University, USA, Chapter 5, which was carried out in collaboration with Annhelen Lu, from Professor Rachel O'Reilly's group at the University of Warwick, UK, and in the case of Chapter 6, that was carried out with the help of Dominic Gray from Professor Rachel O'Reilly's group at the University of Warwick, UK. Any materials synthesized or data analyses carried out by persons other than the author are clearly labelled in the text of that chapter.

List of Publications

1. "Tuning the Catalytic Activity of L-Proline Functionalized Hydrophobic Nanogel Particles in Water", A. Lu,‡ D. Moatsou,‡ D. A. Longbottom, R. K. O'Reilly, *Chem. Sci.*, 2013, **4**, 965-96 (**Chapter 5**)
2. "Studying the activity of the McMillan catalyst embedded within hydrophobic crosslinked polymeric nanostructures", B. Moore, D. Moatsou, A. Lu, R. K. O'Reilly, *Polym. Chem.*, 2014, **5**, 3487-3494
3. "Precision Polymers: A Kinetic Approach for Functional Poly(norbornenes)", D. Moatsou, C. F. Hansell, R. K. O'Reilly, *Chem. Sci.*, 2014, **5**, 2246-2250 (**Chapter 2**)
4. "The effect of polymer nanostructure on diffusion of small molecules using Tryptophan as a FRET probe", B. L. Moore, A. Lu, D. Moatsou, R. K. O'Reilly, *Eur. Polym. J.*, 2015, **62**, 380-3853
5. "Recyclable L-Proline Functional Nanoreactors with Temperature-Tuned Activity Based on Core-Shell-Corona Nanogels", A. Lu,‡ D. Moatsou,‡ I. Hands-Portman, D. A. Longbottom, R. K. O'Reilly, *ACS Macro Lett.*, 2014, **3**, 1235–1239 (**Chapter 5**)
6. "Biofunctionalizable flexible bucky paper by combination of multi-walled carbon nanotubes and polynorbornene-pyrene. Application to the bioelectrocatalytic reduction of oxygen", S. Cosnier, R. Haddad, D. Moatsou, R. K. O'Reilly, *Carbon*, *accepted*
7. "Self-assembly of temperature-responsive protein-polymer bioconjugates", D. Moatsou,‡ J. Li,‡ A. Ranji, A. Pitto-Barry, I. Ntai, M. C. Jewett, R. K. O'Reilly, *Bioconjugate Chemistry*, *accepted* (**Chapter 4**)

‡ *denotes equal contribution by authors*

Summary of Thesis

This thesis explores three methods for the synthesis of materials with precise sequence and functions.

Chapter 1 gives a brief introduction to the main concepts that underpin the methods used throughout the thesis.

Chapter 2 examines the use of norbornenes for the synthesis of precision polymers *via* ring-opening metathesis polymerization by taking advantage of the different reactivity of different isomers of the monomers.

Chapter 3 suggests the use of dioxepins for single monomer insertion in the ring-opening metathesis polymerization of norbornenes.

Chapter 4 describes the synthesis of a temperature-responsive protein-polymer bioconjugate and the study of its properties.

Chapter 5 evaluates the synthetic parameters of L-proline-containing nanogels as a function of their ability to catalyze organic reactions.

Chapter 6 discusses the attempt to modulate the cross-linking of nanogels by a photo-reactive cross-linker based on thymine.

Abbreviations

^3J	proton coupling constant (commonly written as $^3J_{HH}$)
ADMET	acyclic diene metathesis
AIBN	2,2′-azobis(2-methylpropionitrile)
ALTMET	alternating diene metathesis
ATRP	atom transfer radical polymerization
BuMA	*n*-butyl methacrylate
CLD	cross-linking density
CRP	controlled radical polymerization
CTA	chain transfer agent
CuAAC	copper-catalyzed azide-alkyne cycloaddition
d	doublet
DCM	dichloromethane
D_h	hydrodynamic diameter
DLS	dynamic light scattering
$Đ_M$	molecular weight distribution (M_w/M_n)
DMAP	4-(dimethylamino) pyridine
DMF	*N*,*N*-dimethylformamide
DMSO	dimethylsulfoxide
DNA	deoxyribonucleic acid
DoF	degree of functionalization
DOSY	diffusion-ordered spectroscopy
DP	degree of polymerization
DRI	differential refractive index

DxpPhe	2-phenyl-4,7-dihydro-2*H*-1,3-dioxepin
ee	enantiomeric excess
EGDMA	ethylene glycol dimethacrylate
EMA	ethyl methacrylate
*endo*NbHex	*N*-hexyl-*endo*-norbornene-5,6-dicarboximide
eq.	equivalents
ESI	electrospray ionization
EVE	ethyl vinyl ether
*exo*NbCoum	7-coumarinyl-*exo*-5-norbornene-2-carboxylate
*exo*NbHex	*N*-hexyl-*exo*-norbornene-5,6-dicarboximide
*exo*NbPFP	pentafluorophenyl *exo*-5-norbornene-2-carboxylate
*exo*NbPyr	(1-pyrenyl)methyl-*exo*-5-norbornene-2-carboxylate
*exo*NbTMS	trimethylsilyl *exo*-5-norbornene-2-carboxylate
FDA	food and drug administration
G1	Grubbs Catalyst, 1st Generation (bis(tricyclohexylphosphine)benzylidine ruthenium(IV) dichloride)
GO	graphene oxide
HPLC	High performance liquid chromatography
HRMS	high resolution mass spectrometry
k_i	initiation rate constant
k_p	propagation rate constant
LC	liquid chromatography
LMA	lauryl methacrylate

m	multiplet
MALDI	matrix-assisted laser desorption ionization
MMA	methyl methacrylate
M_n	number-average molecular weight distribution
MS	mass spectrometry
M_w	weight-average molecular weight distribution
MW	molecular weight
MWCO	molecular weight cut-off
NIPAM	*N*-isopropylacrylamide
NMBA	*N*-*N*'-methylenebis(acrylamide)
NMP	nitroxide-mediated polymerization
NMR	nuclear magnetic resonance
PAGE	poly(acrylamide) gel electrophoresis
PEG	poly(ethylene glycol)
PEGMA	poly[oligo(ethylene glycol) methyl ether methacrylate]
PEO	poly(ethylene oxide)
ProMA	*O*-methacryloyl-*trans*-4-hydroxy-L-proline hydrochloride
RAFT	reversible addition-fragmentation chain-transfer
RDRP	reversible-deactivation radical polymerization
R_f	retardation factor
RNA	ribonucleic acid
ROIMP	ring-opening-insertion-metathesis polymerization
ROMP	ring-opening metathesis polymerization
SDS	sodium dodecyl sulfate

SEC	size exclusion chromatography
t	triplet
TEA	triethylamine
TEM	transmission electron microscopy
T_g	glass transition temperature
THF	tetrahydrofuran
TLC	thin layer chromatography
TMS-PSA	3-(trimethylsilyl)propanesulfonic acid
ToF	time of flight
UV	ultraviolet
UV-vis	ultraviolet-visible
VBT	1-(vinylbenzyl)thymine
wt%	weight percent
δ	chemical shift
λ	wavelength

Chapter 1 - Introduction

1.1. Sequence in Nature

Nature has always outperformed synthetic chemists when it comes to controlling the sequence of macromolecules. With an arsenal consisting of just over two dozen building blocks, a remarkable repertoire of functional natural polymers such as DNA and proteins is now known to be the basis of life. Decades before Watson and Crick solved the double-helical structure of DNA in 1953,[1] Albrecht Kossel had isolated the five nucleobases that are to a great extent responsible for the remarkable properties of DNA and RNA.[2] The fact that intricate functions are dictated by such a small number of building blocks highlights the importance of the sequence in which these building blocks are connected. The importance is emphasized when genetic disorders are considered, whereby the sequence of the genome is compromised potentially having damaging effects on the host organism. The implications of sequence-ordered macromolecules are equally prominent in proteins where the primary structure, that is the sequence of the amino acid residues, is to a large extent responsible for the three-dimensional tertiary structure, and thus the function of the protein. Small variations in the sequence of the protein result in significantly different properties, ensuing tremendous variation in naturally occurring proteins. As each protein is synthesized in order for a specific function to be accomplished, multiple biological processes ensure that the sequence of a synthesized protein is correct. However, often proteins with dissimilar sequences have similar functions as a result of homologous three-dimensional microstructures in the way the sequences fold. While there is still a lot of ground to cover in our understanding of how sequences correlate to specific functions, a large amount of work is dedicated to mimicking these functions by combining materials with known attributes (top-down approach), and more recently by harnessing the sequence in

synthetic macromolecules in order to evaluate their properties (bottom-up approach) (Figure 1.1).[3]

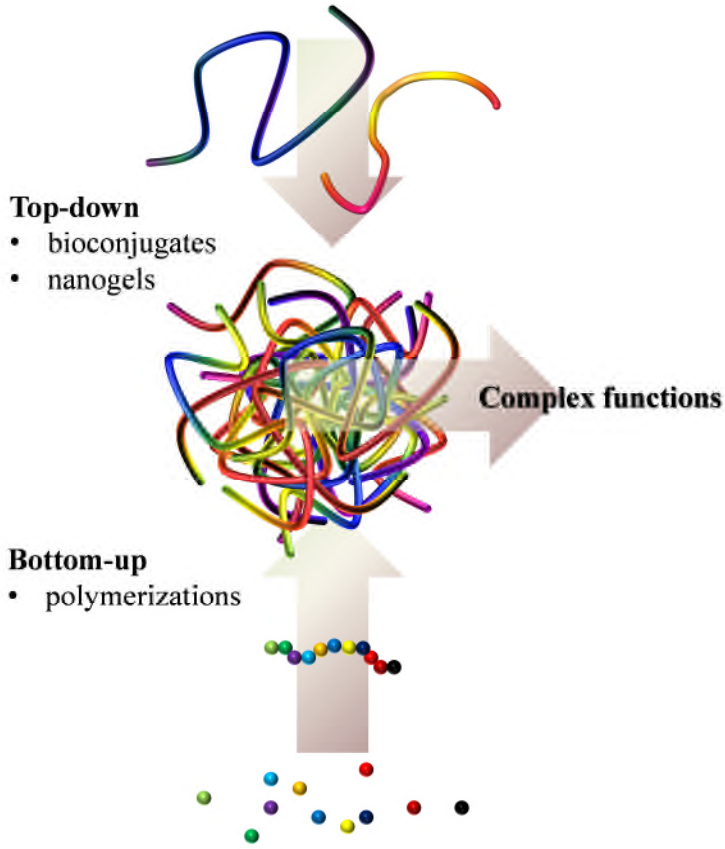

Figure 1.1. Top-down and bottom-up strategies followed to obtain nanostructures mimicking protein and enzyme functions.

1.2. Protein conjugates

Proteins that are conjugated with synthetic non-peptide molecules have drawn the attention of the scientific community as they offer the potential of enhancing the properties of the biomolecule. This has become more tangible with the development of methods that allow incorporation of non-natural amino acids into proteins.[4, 5] Non-natural amino acids can bear functionalities that are not commonly found in natural systems, and that can directly alter the protein properties, such as fluorescence,[6-8] magnetism,[9] glycosylation,[10] and activity triggering.[11, 12] Perhaps even more attractive

are non-natural amino acids that allow further orthogonal reactions, post-synthetically; for example amino acids bearing groups capable of undergoing "Click" reactions. "Click" chemistry represents a range of reactions that, as described by Sharpless *et al.*, and later specified for macromolecules, should be equimolar, easy to purify, rapid, high yielding, but perhaps more importantly they should be chemoselective.[13, 14] The ability to perform a reaction between two groups in the presence of other commonly reactive moieties renders "Click" reactions an invaluable tool in protein conjugation. Non-natural amino acids that have been previously incorporated into proteins and that bear functionalities that can undergo such reactions bear alkyne,[15-17] azide,[18-20] maleimide,[21] halide,[22] aminothiol,[23] allyl,[24] tetrazole,[25] keto,[26] and norbornene[18, 27] moieties. While these functionalities significantly broaden the range of molecules that can be conjugated onto the host protein, there is an increasing interest in the conjugation of proteins with synthetic polymers. This concept will be extensively discussed in Chapter 4. Other substrates for protein conjugation leading to potentially interesting applications include surfaces,[28] quantum dots,[29] chemotherapeutic agents,[30] and nanoparticles.[31] The prevailing motivation for all these conjugates is to combine the protein properties with those of the conjugated substrate, potentially enhancing them, therefore making such systems more attractive for applications such as in industrial,[32] biomedical,[33, 34] and biotechnological fields.[35, 36]

1.3. Enzyme mimics

An example of sequence-control leading to function is enzymes which are proteins often referred to as "Nature's catalysts" because of their ability to accommodate complex reactions.[37] Synthetic approaches towards the synthesis of proteins such as enzymes are constantly developed in an attempt to render attainable those proteins of high

importance to healthcare and industrial applications.[38] Nonetheless, a large body of work has been dedicated to the alteration of the properties of such biomolecules in an attempt to enhance and expand their functions. As an alternative approach, polymeric nanoreactors have emerged as reproducible and scalable mimics of enzymes.[39]

1.3.1. Polymeric nanoreactors

While enzymes are highly efficient catalysts, a substantial effort has been made to replicate their potential using synthetic materials, in an attempt to understand their catalytic mechanisms and enhance the modern catalytic methods used in industry. Polymer chemistry is one of the fields that have significantly contributed, as synthetic macromolecules offer the potential to replicate the properties of enzymes that promote those catalytic functions; one of those properties being the presence of a hydrophobic compartment while the enzyme is dispersed in water.

An important aspect of enzyme catalytic activity is the sequence of the amino acid residues that form active catalytic sites. These sites are often only accessible by substrates with specific size, shape, hydrophilicity and hydrogen bonding ability.[40] As such, a recent development in polymeric enzyme mimics is the use of molecularly imprinted polymers. These are highly cross-linked polymers synthesized in the presence of a template molecule that, upon removal, produces a cavity containing specific functional groups at well-defined positions and orientations.[41] With regards to systems dispersed in water, polymer chemistry also offers the potential to mimic the nanoenvironment of the enzyme catalytic sites based on nanostructures such as micelles, vesicles, and cross-linked polymers.[42, 43]

1.3.1.1. Self-assembled polymers

Ever since the introduction of controlled polymerizations, the range of copolymer architectures that can be synthesized has significantly widened with perhaps the most commonly studied being block copolymers. These are often pursued given the ability of two blocks to segregate when exposed to selective media. As such, by combining a hydrophobic and a hydrophilic block, an amphiphilic copolymer is formed which, when in water, self-assembles into high order structures (Figure 1.2), with the hydrophobic block being shielded from the water phase by the hydrophilic block.[44] This effectively forms a hydrophobic pocket, resembling that often found surrounding the catalytic active site of enzymes, thus encouraging their use as bio-mimetic materials.[45] As such, a polymeric nanoreactor can be produced when a catalytic moiety that is inefficient in aqueous environments, is either tethered onto the polymer, or encapsulated within the hydrophobic compartment of the aggregate.[46]

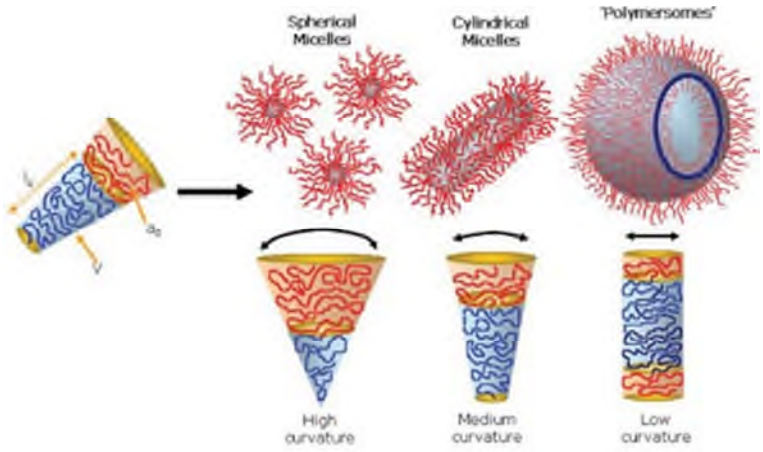

Figure 1.2. Schematic representation of various self-assembled structures formed by block copolymers in a block-selective solvent.[44]

There are a few examples that have demonstrated the formation of catalytic nanoreactors by incorporating the catalytic functionality onto a copolymer which then was self-assembled in water. The formation of the hydrophobic environment with a high

concentration of the catalyst results in accelerated catalysis, as opposed to the results obtained from either the free catalyst in water or polymer micelles in the absence of the catalytic moiety.[47, 48]

Although a large number of enzyme-mimicking nanostructures rely on well-defined copolymers, random copolymers have also proven popular catalytic systems as they are easy to obtain lowering their commercial cost.[49] Based on the formation of "local micelles", the copolymers exhibit superior catalytic activity in water (Figure 1.3).[50-53]

1.3.1.2. Nano-sized particles

The catalytic nanoreactors described so far rely on the self-assembly of copolymers in water, however hydrophobic pockets in aqueous media can also be obtained by dispersions/solutions of dendritic polymers,[54] or *via* heterogeneous polymerizations that result in the formation of particles dispersed in the medium. These particles can be readily loaded with the catalytic moiety and used as catalytic nanoreactors in water (Figure 1.3A).[55-58] Other examples involve the use of such particles as templates for the synthesis of polymeric hollow capsules that bear the catalytic moiety (Figure 1.3B),[59] while in some cases the polymer was synthesized around the dispersed catalyst in order to modulate its properties (Figure 1.3C).[60, 61] One other example is the synthesis of a core-shell particle in water, whereby the shell was cross-linked and the hydrophobic core was exploited as a nanoreactor for the polymerization of a hydrophobic monomer.[62]

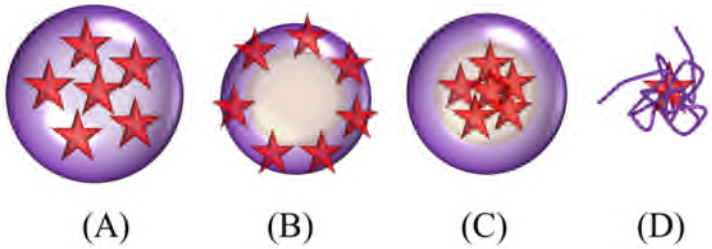

Figure 1.3. Schematic representation of the catalytic dispersed particles (A), catalytic hollow capsules (B-C), and the free catalyst-loaded polymer (D).

Such dispersed particles do not only serve as excellent nanoreactors, but they have also been studied in a variety of applications,[63] such as rheological modifiers,[64] wastewater treatments,[65] drug delivery,[66, 67] photonic crystals,[68] and sensors.[69, 70] Perhaps the main reason why dispersed particles find so many applications in such diverse fields is the ease of obtaining large quantities of particles *via* simple reactions (with the exception of dendritic particles). Generally, these can be distinguished into four categories: emulsion, suspension, and precipitation polymerization, and microfluidics, while other synthetic procedures based on these processes have also been reported, such as miniemulsion and inverse emulsion polymerization.[71-75] In all cases the final polymer is insoluble in the reaction medium; however the solubility of the reaction components is different. One prominent difference is the use of a water-soluble initiator in emulsion and precipitation polymerization, as opposed to an insoluble initiator in the case of suspension polymerization. Additionally, while the monomer is insoluble in the reaction medium in emulsion and suspension polymerization, it is soluble in the case of dispersion polymerization.

1.3.1.2.1. Emulsion polymerization

Emulsion polymerization has become popular since 1947 when Harkins proposed the currently accepted mechanism of the reaction.[76, 77] As the name suggests, emulsion

polymerization requires the presence of an emulsifier (*i.e.* surfactant) that allows dispersion of the hydrophobic components of the reaction in the aqueous medium. Common emulsifiers are either charged such as sodium dodecyl sulfate, or nonionic such as Triton X. With the concentration of the surfactant being higher than its critical micelle concentration (CMC), small surfactant micelles form (Figure 1.4). These encapsulate small amounts of the hydrophobic monomer, however the majority of the monomer is dispersed in large droplets whose size depends on the stirring rate, while a small fraction of the monomer is dissolved in the aqueous phase (depending on its water solubility). The initiator is also dissolved in water. Upon initiation of the polymerization the water soluble initiating radicals migrate into the micelles where the polymerization propagates in a manner similar to bulk polymerization. The reaction proceeds with diffusion of the water-dissolved monomer into the micelles, while the monomer droplets reduce in size as monomer dissolves into the water. It should be noted that the rate of the polymerization is different at three distinct intervals of the reaction (Figure 1.4).

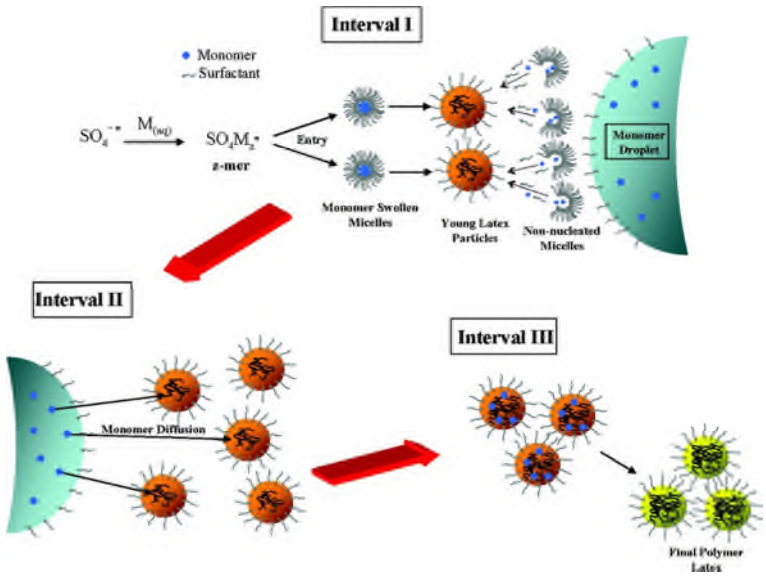

Figure 1.4. Schematic representation of the three intervals of emulsion polymerization.[42]

Initially, the reaction rate increases until the amount of micelles is constant, then, the rate is constant and dependent on the diffusion of monomer into the polymer-containing micelles. In the third stage, the rate constantly drops as the monomer droplets have been consumed and all monomer is contained in the micelles.[78] The size distribution of the resulting particles is usually narrow and can range from the nanometer to the micron scale.[79] Often the polymers synthesized by heterogeneous polymerizations are cross-linked in order to retain their shape at different conditions. As such, the resulting particles are essentially nano-sized polymer gels (*i.e.* nanogels) dispersed in the medium.

1.3.1.2.2. Responsive particles

Dispersed particles, and more specifically cross-linked particles such as nanogels, have characteristic soft particle-particle interactions with the ability to form highly packed suspensions, as a result of their elastic composition.[80, 81] The balance between osmotic pressure and polymer elasticity determines the size of the particles, which can be fine-tuned *via* the amount of crosslinker and the polymer-solvent interactions. This can be further adjusted using systems that selectively respond to external stimuli thus allowing the particles to selectively swell and de-swell, while degradation and dissolution can also be achieved.[82] A range of responsive systems have been reported in the literature, with the most common examples being responsive to changes in temperature,[83] pH,[84] irradiation wavelength,[85] and current.[86] Upon exposure to such changes, the physicochemical properties of the polymer chains are altered, resulting in change of their solvation, and thus swelling or de-swelling of the particles. Such changes, for example are the coil-to-globule transition of temperature-responsive polymers, resulting in the expulsion of water from the particle and its effective shrinkage,[87] and the

electrostatic repulsion forces that cause pH-responsive polymer particles to reversibly swell upon increase of the concentration of ions.[88]

1.4. Sequence-controlled polymerizations

Since the seminal work on synthetic polymers by Staudinger and Carothers,[89-91] the range of macromolecules that can be obtained is diverse not only in terms of composition, but also in their architecture. Intricate structures such as block, alternating/periodic, gradient, cyclic, star, graft, (hyper)branched, and dendrimer (co)polymers can be achieved, as greater precision in the way monomers are polymerized is achieved. With the development of controlled and "living" polymerizations, macromolecules with predictable compositions and properties are synthesized, while a wealth of strategies allow materials with more precise sequence distributions to be obtained.

Although generally perceived as poorly-controlled reactions in terms of the resulting polymer characteristics, step-growth polymerizations can be exploited for the synthesis of sequence-defined polymers. Based on the orthogonal reaction between monomers, solid-supported synthesis of such polymers has been proven highly efficient and has been extensively used for the synthesis of peptides.[92] Although complete control over monomer sequence is achieved, this method is limited by incomplete coupling reactions with the use of protecting groups often being necessary, and non-native folding of the products, therefore allowing the synthesis of only small polymers (up to 50 repeat units).[93] Nonetheless, a wealth of reactions and monomers has been reported in the literature regarding the iterative addition-activation process that results in sequence-defined polymers. [94-100]

Another elegant approach involves the use of Nature's toolbox for the synthesis of sequence-controlled materials. Mimicking the natural paths, such as complementary nucleobases, on-demand sequences of DNA strands can be obtained, thus leading to higher order materials, such as DNA origami (Figure 1.5).[101-104]

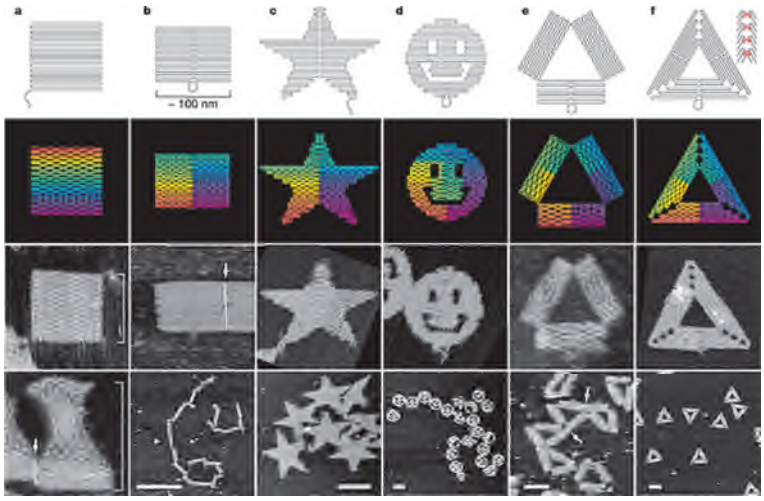

Figure 1.5. DNA origami.[105]

As Nature creates sequences based on templates, another promising approach for the synthesis of well-defined sequences involves the use of specific interactions between building blocks and a template. As such, conventional monomers can be introduced in a synthetic pathway that dictates their polymerization with high precision.[106-111]

Although far from the examples shown with DNA origami, intricate polymer structures can also be obtained by "living" and reversible-deactivation radical polymerizations (RDRP). Additionally, recent reports have explored the ability to kinetically control these polymerizations in order to achieve higher order copolymer structures and achieve sequence control.[112] These will be further discussed in Chapter 2.

1.4.1. Reversible deactivation radical polymerizations

Reversible deactivation radical polymerizations (RDRP)[113] are a family of polymerizations that combine the advantages of traditional free radical polymerization and living polymerizations. As such, a range of vinyl monomers can be polymerized under conditions less demanding than classical anionic polymerization. Most common such processes are nitroxide-mediated polymerization (NMP), reversible addition-fragmentation chain transfer (RAFT) polymerization, and transition metal-catalyzed radical polymerizations – including atom transfer radical polymerization (ATRP) and Cu^0-mediated polymerizations. These techniques emerged within the past thirty years and have been extensively used for the synthesis of polymers with well-defined molecular weights, dispersities (typically $Đ_M < 1.5$), and architectures.[114, 115]

1.4.1.1. Nitroxide-mediated polymerization (NMP)

NMP is historically the first of RDRPs to be developed and it relies on the equilibrium between an active species that involves active radical chain ends and a dormant species whereby the polymer end is capped by combination with nitroxide radicals (Scheme 1.1).[116-120]

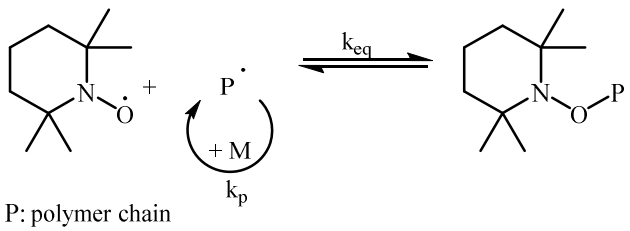

Scheme 1.1. Schematic representation of the equilibrium in NMP.

The alkoxyamine initiators introduced in the reaction are commonly 2,2,6,6-tetramethyl-1-piperidinyloxy (TEMPO) and 2,2,5-trimethyl-4-phenyl-3-azahexane-*N*-oxyl (TIPNO) (Scheme 1.2).

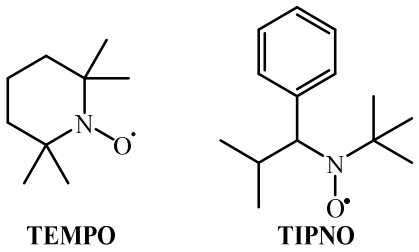

Scheme 1.2. Chemical structures of commonly used nitroxides in NMP.

Although efficient and compatible with a range of monomer functionalities, NMP suffers from low polymerization rates that require high temperatures (commonly above 100 ^{o}C), while polymerization of methacrylates is challenging.[121]

1.4.1.2. Transition metal-catalyzed polymerizations

Matyjaszewski *et al.* and Sawamoto *et al.* separately described the polymerization of styrene and methyl methacrylate, respectively, in the presence of transition metal complexes.[122, 123] Widely known as atom transfer radical polymerization (ATRP), this method relies on the equilibrium provided by the metal catalyst between the propagating polymer and its dormant species. Since the dormant form of the polymer is dominant, side reactions are suppressed, providing the desired control over the polymer characteristics. Upon transfer of the (pseudo)halogen from the polymer to the transition metal complex, the propagating radical is formed while the transition metal adopts a higher oxidation state (Scheme 1.3).[124]

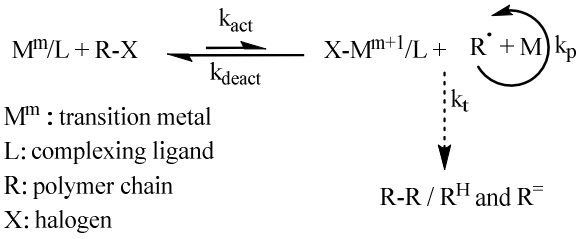

Scheme 1.3. Reaction mechanism of ATRP.

ATRP is a versatile polymerization method with the ability to polymerize a wide range of monomers under mild conditions and in a variety of solvents (as well as in bulk), thus making it attractive in many applications. An interesting development has also been the use of zerovalent metals as the catalytic species in polar solvents (DMSO and water).[125] While the mechanism (and the nomenclature) is still under debate,[114] it has proven to be a powerful tool in the synthesis of well-defined polymers.

1.4.1.3. Reversible addition-fragmentation chain transfer (RAFT) polymerization

RAFT polymerization emerged in 1998 as a type of RDRP that allows the synthesis of complex architectures using a thiocarbonylthio-based chain transfer agent (CTA) with very low dispersities.[126] Although some aspects had been under debate,[127, 128] the mechanism of the polymerization is similar to free radical polymerization with two added equilibria steps; chain transfer and equilibration.[129] These are depicted in Scheme 1.4.

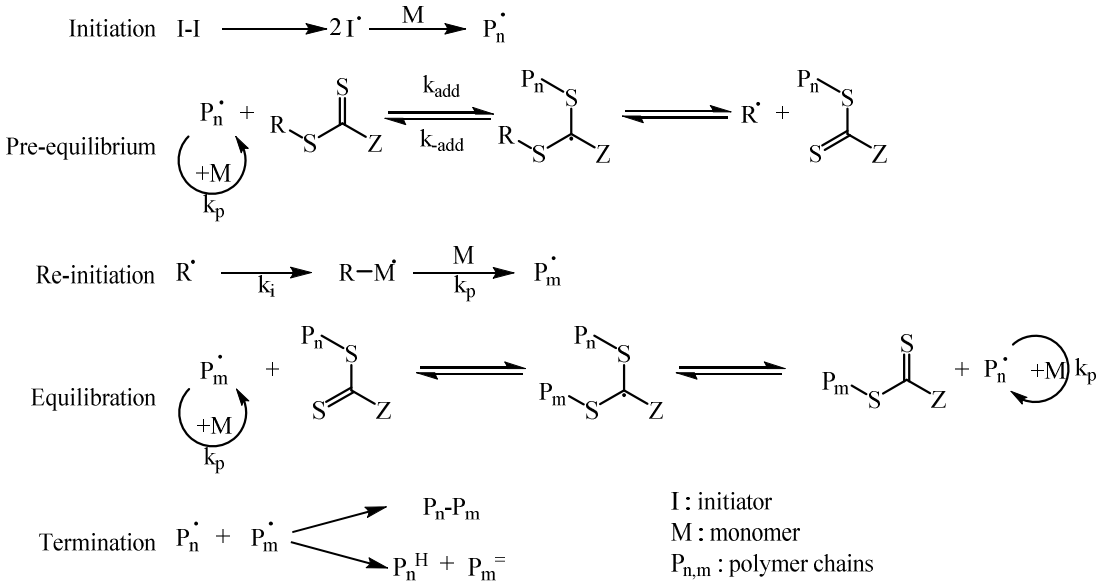

Scheme 1.4. Proposed mechanism for RAFT polymerization.

The key aspect of the RAFT mechanism the rapid equilibrium between dormant and propagating species that provides equal probability for all the chains to grow. Thus, control of the polymer molecular weight is achieved *via* the monomer and CTA stoichiometry. Termination reactions are minimal as a result of the low radical concentration. It is generally accepted that different CTAs can polymerize different monomers, with the determining parameter being the selection of the R and the Z groups.[129, 130] The R group governs the pre-equilibrium and thus should be stable for fragmentation to be favored, while also being able to re-initiate. On the other hand, the Z group determines the stability of the thiocarbonylthio bond and therefore the retention of a radical in the main equilibrium. Additionally, both the R and the Z group can be accordingly modified in order to provide the final polymer with functional end groups. Nonetheless, polymers synthesized by RAFT can readily undergo post-polymerization end-group modification, as a result of the good end-group fidelity.[131]

1.4.2. "Living" polymerizations

Polymers that have lost their capacity to further grow were characterized as "dead", therefore when styrene under anionic polymerization conditions was observed to be able to further react upon addition of monomer, the term "living" polymer was coined.[132] Since then, living polymerizations are identified as those that "retain their ability to propagate for a long time and grow to a desired maximum size while their degree of termination or chain transfer is still negligible".[132] Most common such polymerizations are anionic,[133] cationic,[134] group-transfer,[135] ring-opening,[136] and ring-opening metathesis polymerizations.[137]

1.4.2.1. Ring-opening metathesis polymerization (ROMP)

Amongst the mechanisms that govern living polymerizations, the knowledge of the mechanism of olefin metathesis is perhaps the youngest.[138-141] Based on the generic olefin metathesis mechanism, ROMP was explained by the mechanism proposed by Chauvin (Scheme 1.5).[142]

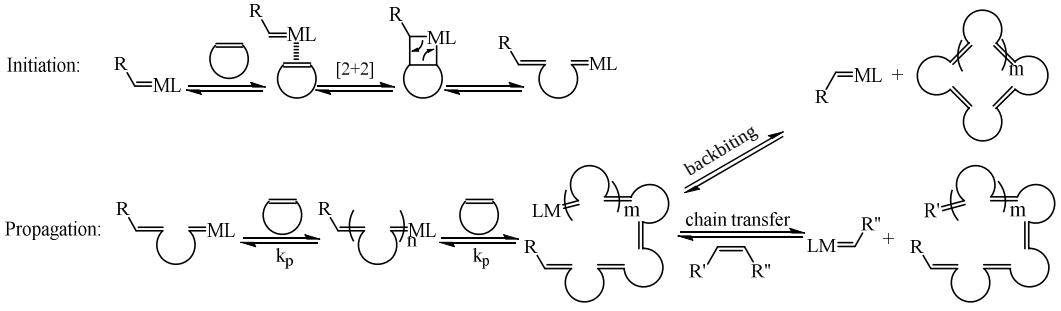

Scheme 1.5. Mechanism of ROMP.

The metal carbene initiator (Figure 1.6) initially coordinates with a cyclic olefin to form a metallacyclobutane intermediate *via* a [2+2] cycloaddition, followed by its cycloreversion to form a new olefin and a new metal carbene. This new complex has the

same reactivity as the metal carbene and thus in the presence of excess olefin propagates the reaction in a similar manner. Termination can occur *via* the addition of a quenching agent that removes and deactivates the metal from the end of the polymer chain *via* cross metathesis. Some concerns over the living nature of ROMP stem from two key characteristics: metathesis reactions are reversible, and backbiting is possible *via* olefin metathesis. Nevertheless, owing to the fact that the driving force in ROMP is relief of the ring strain of the monomer, a variety of cyclic monomers can by polymerized, with the exception of six-membered rings that are not likely to undergo ring-opening.[143] Most commonly used monomers are norbornenes, cyclooctenes, cyclopentenes, and their derivatives; however a constantly increasing range of reactive monomers is reported. While both concerns over the living nature of ROMP are considered, the efficiency of the polymerization is ultimately determined by the catalyst and the monomer.

1.4.2.1.1. ROMP catalysts

Initial catalysts used in ROMP involved transition metal chlorides, however the reactions were heterogeneous and the polymerizations were uncontrolled. [144] Initial examples of catalysts able to efficiently mediate ROMP were based on titanium and tantalum. Schrock *et al.* introduced the first tungsten catalysts that were able to catalyze ROMP in a controlled manner.[145, 146] The main difference with previously used catalysts was the metal-carbene complex, a motif that was later repeated for the synthesis of efficient molybdenum and ruthenium-based catalysts (Figure 1.6).[147, 148]

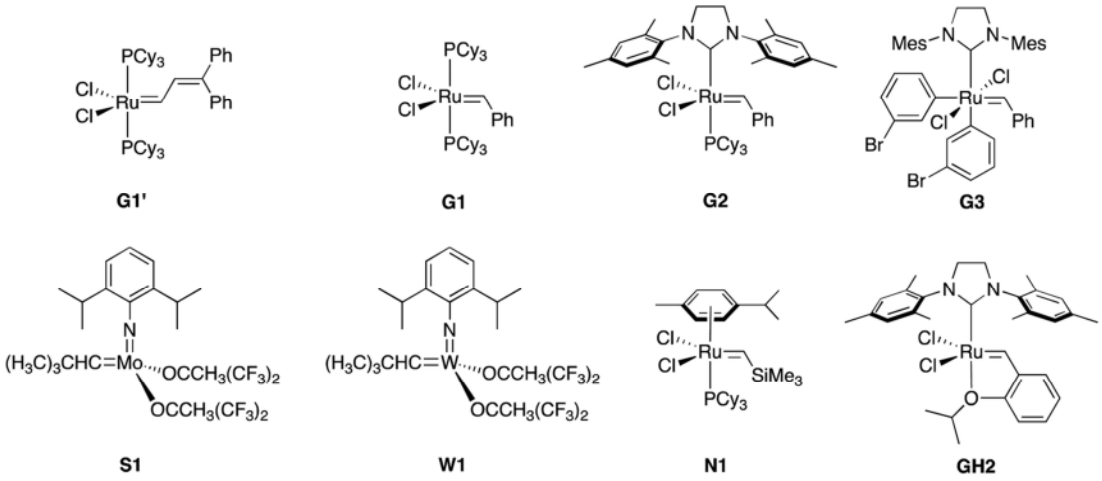

Figure 1.6. Common ROMP catalysts.[149]

The importance of the introduction of ruthenium-based catalysts (mainly by Grubbs *et al.*) is highlighted from its greater tolerance towards functional groups.[137] This was initially observed for catalyst **G1'** (Figure 1.6) only to be surpassed by catalyst **G1**, nowadays known as Grubbs 1st generation catalyst.[150-154] Later developed catalysts were also proven powerful, however suffered from uncontrolled polymerizations or demanding syntheses.[155]

Based on these catalysts, several reports have emerged whereby a functional group is introduced onto the metal alkylidene in order to obtain α-end-functional polymers, as a direct result of the living nature of the polymerization. As such, fluorescent moieties,[156] pre-synthesized polymers,[157] and ATRP initiating groups[158] are amongst the functionalities obtained on the polymer chain-end in this manner.

1.4.2.1.2. Quenching agents

As previously mentioned, ROMP is considered a living polymerization, and as such it requires quenching in order for termination to take place (Scheme 1.5). This is often exploited for the ω-chain-end functionalization of the polymer. Early reports where highly reactive catalysts such as Mo- and W-based catalysts are used demonstrate the

successful chain end functionalization with commercially available aldehydes.[159-161] However, with the rise of Ru-based catalysts, such reagents can no longer be employed, as their quenching efficiency is limited. On the other hand, polymerizations catalyzed by ruthenium can be quenched with the use of vinyl ethers.[162] This strategy has been followed to introduce biotin,[163] ATRP-initiating groups,[164] hydrogen-bonding functionalities,[165] hydroxyl groups,[166] and aldehydes.[167] Commercially available acrylates are also effective ROMP quenchers, however metatheses of acrylates are only partially efficient leading to mixture of products.[168] Most of the aforementioned end-group functionalization methods rely on the fast metathesis with the quenching agent; however this is often not the case, thus large excess of the quencher is required for efficient termination.

1.5. Conclusions

Based on our understanding of how some complex processes are efficiently carried out by natural macromolecules, such as enzymes, the wealth of literature dedicated to replicate them can be assigned to two categories: top-down and bottom-up. In the first case, materials provided by Nature are used and altered in order to enhance their potential while in other cases the components responsible for the desired functionality are placed in a system that will allow their improved performance. As such, the use of protein conjugates was seen often to provide the biomacromolecule with new attributes, while polymeric nanoreactors have demonstrated excellent potential as catalytic enzyme mimics. In the second case, the macromolecules are synthesized from small building blocks, attempting to replicate the precision in the sequence of model natural polymers, such as enzymes. This is the result of the newly introduced controlled polymerizations that are constantly being developed so as to achieve higher sequence precision.

1.6. References

1. J. D. Watson and F. H. C. Crick, *Nature*, 1953, **171**, 737-738.
2. M. E. Jones, *Yale J. Biol. Med.*, 1953, **26**, 80-97.
3. Z. Dong, Q. Luo and J. Liu, *Chem. Soc. Rev.*, 2012, **41**, 7890-7908.
4. C. J. Noren, S. J. Anthony-Cahill, M. C. Griffith and P. G. Schultz, *Science*, 1989, **244**, 182-188.
5. A. Dumas, L. Lercher, C. D. Spicer and B. G. Davis, *Chem. Sci.*, 2015, **6**, 50-69.
6. D. Summerer, S. Chen, N. Wu, A. Deiters, J. W. Chin and P. G. Schultz, *Proc. Natl. Acad. Sci. U. S. A.*, 2006, **103**, 9785-9789.
7. A. T. Krueger and B. Imperiali, *ChemBioChem*, 2013, **14**, 788-799.
8. M. Amaro, J. Brezovský, S. Kováčová, J. Sýkora, D. Bednář, V. Němec, V. Lišková, N. P. Kurumbang, K. Beerens, R. Chaloupková, K. Paruch, M. Hof and J. Damborský, *J. Am. Chem. Soc.*, 2015, **137**, 4988-4992.
9. M. J. Schmidt, J. Borbas, M. Drescher and D. Summerer, *J. Am. Chem. Soc.*, 2014, **136**, 1238-1241.
10. N. E. Fahmi, L. Dedkova, B. Wang, S. Golovine and S. M. Hecht, *J. Am. Chem. Soc.*, 2007, **129**, 3586-3597.
11. D. Mendel, J. A. Ellman and P. G. Schultz, *J. Am. Chem. Soc.*, 1991, **113**, 2758-2760.
12. A. Gautier, D. P. Nguyen, H. Lusic, W. An, A. Deiters and J. W. Chin, *J. Am. Chem. Soc.*, 2010, **132**, 4086-4088.
13. H. C. Kolb, M. G. Finn and K. B. Sharpless, *Angew. Chem. Int. Ed.*, 2001, **40**, 2004-2021.
14. C. Barner-Kowollik, F. E. Du Prez, P. Espeel, C. J. Hawker, T. Junkers, H. Schlaad and W. Van Camp, *Angew. Chem. Int. Ed.*, 2011, **50**, 60-62.
15. A. Deiters, T. A. Cropp, M. Mukherji, J. W. Chin, J. C. Anderson and P. G. Schultz, *J. Am. Chem. Soc.*, 2003, **125**, 11782-11783.
16. D. P. Nguyen, H. Lusic, H. Neumann, P. B. Kapadnis, A. Deiters and J. W. Chin, *J. Am. Chem. Soc.*, 2009, **131**, 8720-8721.
17. M. Pott, M. J. Schmidt and D. Summerer, *ACS Chem. Biol.*, 2014, **9**, 2815-2822.
18. J. W. Chin, S. W. Santoro, A. B. Martin, D. S. King, L. Wang and P. G. Schultz, *J. Am. Chem. Soc.*, 2002, **124**, 9026-9027.

19. N. J. Agard, J. A. Prescher and C. R. Bertozzi, *J. Am. Chem. Soc.*, 2004, **126**, 15046-15047.
20. H. Neumann, K. Wang, L. Davis, M. Garcia-Alai and J. W. Chin, *Nature*, 2010, **464**, 441-444.
21. S. Marburg, A. C. Neckers and P. R. Griffin, *Bioconjugate Chem.*, 1996, **7**, 612-616.
22. J. W. Chin, T. A. Cropp, J. C. Anderson, M. Mukherji, Z. Zhang and P. G. Schultz, *Science*, 2003, **301**, 964-967.
23. D. P. Nguyen, T. Elliott, M. Holt, T. W. Muir and J. W. Chin, *J. Am. Chem. Soc.*, 2011, **133**, 11418-11421.
24. Z. Zhang, L. Wang, A. Brock and P. G. Schultz, *Angew. Chem. Int. Ed.*, 2002, **41**, 2840-2842.
25. J. Wang, W. Zhang, W. Song, Y. Wang, Z. Yu, J. Li, M. Wu, L. Wang, J. Zang and Q. Lin, *J. Am. Chem. Soc.*, 2010, **132**, 14812-14818.
26. L. Wang, Z. Zhang, A. Brock and P. G. Schultz, *Proc. Natl. Acad. Sci. U. S. A.*, 2003, **100**, 56-61.
27. K. Lang, L. Davis, J. Torres-Kolbus, C. Chou, A. Deiters and J. W. Chin, *Nature Chem.*, 2012, **4**, 298-304.
28. I. Willner and E. Katz, *Angew. Chem. Int. Ed.*, 2000, **39**, 1180-1218.
29. J. C. Claussen, A. Malanoski, J. C. Breger, E. Oh, S. A. Walper, K. Susumu, R. Goswami, J. R. Deschamps and I. L. Medintz, *J. Phys. Chem. C*, 2015, **119**, 2208-2221.
30. J. M. Lambert, *Curr. Opin. Pharmacol.*, 2005, **5**, 543-549.
31. E. Katz and I. Willner, *Angew. Chem. Int. Ed.*, 2004, **43**, 6042-6108.
32. J.-M. Choi, S.-S. Han and H.-S. Kim, *Biotechnol. Adv.*, 2015, doi:10.1016/j.biotechadv.2015.1002.1014.
33. B. R. Knudsen, M. L. Jepsen and Y.-P. Ho, *Expert Rev. Mol. Diagn.*, 2013, **13**, 367-375.
34. E. V. Suprun, V. V. Shumyantseva and A. I. Archakov, *Electrochim. Acta*, 2014, **140**, 72-82.
35. I. Willner, B. Willner and E. Katz, *Rev. Mol. Biotechnol.*, 2002, **82**, 325-355.
36. I. Willner, B. Basnar and B. Willner, *FEBS J.*, 2007, **274**, 302-309.
37. A. R. H. Narayan and D. H. Sherman, *Science*, 2013, **339**, 283-284.

38. C. Chiarabelli, P. Stano and P. L. Luisi, *Curr. Opin. Biotechnol.*, 2009, **20**, 492-497.
39. R. J. R. W. Peters, I. Louzao and J. C. M. van Hest, *Chem. Sci.*, 2012, **3**, 335-342.
40. R. Breslow, S. Bandyopadhyay, M. Levine and W. Zhou, *ChemBioChem*, 2006, **7**, 1491-1496.
41. G. Wulff, *Chem. Rev.*, 2002, **102**, 1-28.
42. M. J. Monteiro, *Macromolecules*, 2010, **43**, 1159-1168.
43. A. Lu and R. K. O'Reilly, *Curr. Opin. Biotechnol.*, 2013, **24**, 639-645.
44. A. Blanazs, S. P. Armes and A. J. Ryan, *Macromol. Rapid Commun.*, 2009, **30**, 267-277.
45. Y. Zhao, F. Sakai, L. Su, Y. Liu, K. Wei, G. Chen and M. Jiang, *Adv. Mater.*, 2013, **25**, 5215-5256.
46. A. Khaskel, P. Barman and U. Jana, *R. Soc. Chem. Adv.*, 2015, **5**, 13366-13373.
47. L. Liu, M. Rozenman and R. Breslow, *J. Am. Chem. Soc.*, 2002, **124**, 12660-12661.
48. Y. Yin, L. Wang, H. Jin, C. Lv, S. Yu, X. Huang, Q. Luo, J. Xu and J. Liu, *Soft Matter*, 2011, **7**, 2521-2529.
49. Y. Yin, Z. Dong, Q. Luo and J. Liu, *Prog. Polym. Sci.*, 2012, **37**, 1476-1509.
50. R. Svensson, V. Pamedytyt, J. Juodaityt, R. Makuška and R. Morgenstern, *Toxicology*, 2001, **168**, 251-258.
51. W. B. Motherwell, C. E. Atkinson, A. E. Aliev, S. Y. F. Wong and B. H. Warrington, *Angew. Chem. Int. Ed.*, 2004, **43**, 1225-1228.
52. R. Skouta, S. Wei and R. Breslow, *J. Am. Chem. Soc.*, 2009, **131**, 15604-15605.
53. E. Huerta, P. J. M. Stals, E. W. Meijer and A. R. A. Palmans, *Angew. Chem. Int. Ed.*, 2013, **52**, 2906-2910.
54. A.-M. Caminade, A. Ouali, M. Keller and J.-P. Majoral, *Chem. Soc. Rev.*, 2012, **41**, 4113-4125.
55. B.-B. Jang, K.-P. Lee, D.-H. Min and J. Suh, *J. Am. Chem. Soc.*, 1998, **120**, 12008-12016.
56. L. J. Twyman, A. S. H. King and I. K. Martin, *Chem. Soc. Rev.*, 2002, **31**, 69-82.
57. T. Endo, T. Yoshimura and K. Esumi, *J. Colloid Interface Sci.*, 2005, **286**, 602-609.

58. N. Welsch, M. Ballauff and Y. Lu, in *Chemical Design of Responsive Microgels*, eds. A. Pich and W. Richtering, Springer Berlin Heidelberg, 2011, vol. 234, pp. 129-163.
59. Y. Lan, L. Yang, M. Zhang, W. Zhang and S. Wang, *ACS Appl. Mater. Interfaces*, 2010, **2**, 127-133.
60. Y. Lu, Y. Mei, M. Drechsler and M. Ballauff, *Angew. Chem. Int. Ed.*, 2006, **45**, 813-816.
61. S. Wu, J. Dzubiella, J. Kaiser, M. Drechsler, X. Guo, M. Ballauff and Y. Lu, *Angew. Chem. Int. Ed.*, 2012, **51**, 2229-2233.
62. M. Zhang and W. Zhang, *J. Polym. Sci. Part A: Polym. Chem.*, 2010, **48**, 5446-5455.
63. J. Thorne, G. Vine and M. Snowden, *Colloid Polym. Sci.*, 2011, **289**, 625-646.
64. V. Schmitt and V. Ravaine, *Curr. Opin. Colloid Interface Sci.*, 2013, **18**, 532-541.
65. G. E. Morris, B. Vincent and M. J. Snowden, *J. Colloid Interface Sci.*, 1997, **190**, 198-205.
66. S. V. Vinogradov, T. K. Bronich and A. V. Kabanov, *Adv. Drug Delivery Rev.*, 2002, **54**, 135-147.
67. V. C. Lopez, J. Hadgraft and M. J. Snowden, *Int. J. Pharm.*, 2005, **292**, 137-147.
68. S. Xu, J. Zhang, C. Paquet, Y. Lin and E. Kumacheva, *Adv. Funct. Mater.*, 2003, **13**, 468-472.
69. K. Iwai, Y. Matsumura, S. Uchiyama and A. P. de Silva, *J. Mater. Chem.*, 2005, **15**, 2796-2800.
70. G. Zenkl, T. Mayr and I. Klimant, *Macromol. Biosci.*, 2008, **8**, 146-152.
71. J. M. Asua, *Prog. Polym. Sci.*, 2002, **27**, 1283-1346.
72. P. B. Zetterlund, Y. Kagawa and M. Okubo, *Chem. Rev.*, 2008, **108**, 3747-3794.
73. N. Sanson and J. Rieger, *Polym. Chem.*, 2010, **1**, 965-977.
74. A. Pich and W. Richtering, in *Chemical Design of Responsive Microgels*, eds. A. Pich and W. Richtering, Springer Berlin Heidelberg, 2011, vol. 234, pp. 1-37.
75. S. Seiffert, *Macromol. Rapid Commun.*, 2011, **32**, 1600-1609.
76. W. D. Harkins, *J. Am. Chem. Soc.*, 1947, **69**, 1428-1444.
77. W. V. Smith and R. H. Ewart, *J. Chem. Phys.*, 1948, **16**, 592-599.

78. G. Odian, in *Principles of Polymerization*, John Wiley & Sons, Inc., 2004, pp. 350-371.
79. W. Funke, O. Okay and B. Joos-Müller, in *Microencapsulation Microgels Iniferters*, eds. S. DiMari, W. Funke, M. A. Haralson, D. Hunkeler, B. Joos-Müller, A. Matsumoto, O. Okay, T. Otsu, A. C. Powers, A. Prokop, T. G. Wang and R. R. Whitesell, Springer Berlin Heidelberg, 1998, vol. 136, pp. 139-234.
80. A. Le Grand and G. Petekidis, *Rheol. Acta*, 2008, **47**, 579-590.
81. N. Koumakis, A. Pamvouxoglou, A. S. Poulos and G. Petekidis, *Soft Matter*, 2012, **8**, 4271-4284.
82. S. Seiffert and J. Sprakel, *Chem. Soc. Rev.*, 2012, **41**, 909-930.
83. R. Pelton, *Adv. Colloid Interface Sci.*, 2000, **85**, 1-33.
84. H. Nur, V. T. Pinkrah, J. C. Mitchell, L. S. Benée and M. J. Snowden, *Adv. Colloid Interface Sci.*, 2010, **158**, 15-20.
85. S. Kadlubowski, *Radiat. Phys. Chem.*, 2014, **102**, 29-39.
86. P. F. Kiser, G. Wilson and D. Needham, *Nature*, 1998, **394**, 459-462.
87. D. Gan and L. A. Lyon, *J. Am. Chem. Soc.*, 2001, **123**, 8203-8209.
88. T. Sawai, S. Yamazaki, Y. Ikariyama and M. Aizawa, *Macromolecules*, 1991, **24**, 2117-2118.
89. H. Staudinger, *Ber. Dtsch. Chem. Ges.*, 1920, **53**, 1073-1085.
90. W. H. Carothers, *J. Am. Chem. Soc.*, 1929, **51**, 2548-2559.
91. W. H. Carothers, *Chem. Rev.*, 1931, **8**, 353-426.
92. R. B. Merrifield, *J. Am. Chem. Soc.*, 1963, **85**, 2149-2154.
93. J. E. Oh and K. H. Lee, *Bioorg. Med. Chem.*, 1999, **7**, 2985-2990.
94. L. Hartmann, E. Krause, M. Antonietti and H. G. Börner, *Biomacromolecules*, 2006, **7**, 1239-1244.
95. L. Hartmann, *Macromol. Chem. Phys.*, 2011, **212**, 8-13.
96. S. Mosca, F. Wojcik and L. Hartmann, *Macromol. Rapid Commun.*, 2011, **32**, 197-202.
97. F. Wojcik, S. Mosca and L. Hartmann, *J. Org. Chem.*, 2012, **77**, 4226-4234.
98. P. Espeel, L. L. G. Carrette, K. Bury, S. Capenberghs, J. C. Martins, F. E. Du Prez and A. Madder, *Angew. Chem. Int. Ed.*, 2013, **52**, 13261-13264.
99. S. C. Solleder and M. A. R. Meier, *Angew. Chem. Int. Ed.*, 2014, **53**, 711-714.

100. T. T. Trinh, L. Oswald, D. Chan-Seng and J.-F. Lutz, *Macromol. Rapid Commun.*, 2014, **35**, 141-145.
101. J. J. Storhoff and C. A. Mirkin, *Chem. Rev.*, 1999, **99**, 1849-1862.
102. Z. J. Gartner, M. W. Kanan and D. R. Liu, *J. Am. Chem. Soc.*, 2002, **124**, 10304-10306.
103. C. T. Calderone and D. R. Liu, *Angew. Chem. Int. Ed.*, 2005, **44**, 7383-7386.
104. G. De Bo, S. Kuschel, D. A. Leigh, B. Lewandowski, M. Papmeyer and J. W. Ward, *J. Am. Chem. Soc.*, 2014, **136**, 5811-5814.
105. P. W. K. Rothemund, *Nature*, 2006, **440**, 297-302.
106. S. Ida, T. Terashima, M. Ouchi and M. Sawamoto, *J. Am. Chem. Soc.*, 2009, **131**, 10808-10809.
107. P. K. Lo and H. F. Sleiman, *J. Am. Chem. Soc.*, 2009, **131**, 4182-4183.
108. Y. Hibi, S. Tokuoka, T. Terashima, M. Ouchi and M. Sawamoto, *Polym. Chem.*, 2011, **2**, 341-347.
109. R. McHale, J. P. Patterson, P. B. Zetterlund and R. K. O'Reilly, *Nature Chem.*, 2012, **4**, 491-497.
110. Y. Kang, A. Lu, A. Ellington, M. C. Jewett and R. K. O'Reilly, *ACS Macro Lett.*, 2013, **2**, 581-586.
111. N. ten Brummelhuis, *Polym. Chem.*, 2015, **6**, 654-667.
112. J.-F. Lutz, *ACS Macro Lett.*, 2014, **3**, 1020-1023.
113. A. D. Jenkins, R. G. Jones and G. Moad, *Pure Appl. Chem.*, 2010, **82**, 483-491.
114. D. Konkolewicz, Y. Wang, P. Krys, M. Zhong, A. A. Isse, A. Gennaro and K. Matyjaszewski, *Polym. Chem.*, 2014, **5**, 4396-4417.
115. W. Wang, J. Zhao, N. Zhou, J. Zhu, W. Zhang, X. Pan, Z. Zhang and X. Zhu, *Polym. Chem.*, 2014, **5**, 3533-3546.
116. M. K. Georges, R. P. N. Veregin, P. M. Kazmaier and G. K. Hamer, *Macromolecules*, 1993, **26**, 2987-2988.
117. C. J. Hawker, *J. Am. Chem. Soc.*, 1994, **116**, 11185-11186.
118. D. Benoit, V. Chaplinski, R. Braslau and C. J. Hawker, *J. Am. Chem. Soc.*, 1999, **121**, 3904-3920.
119. D. Benoit, S. Grimaldi, S. Robin, J.-P. Finet, P. Tordo and Y. Gnanou, *J. Am. Chem. Soc.*, 2000, **122**, 5929-5939.
120. C. J. Hawker, A. W. Bosman and E. Harth, *Chem. Rev.*, 2001, **101**, 3661-3688.

121. R. B. Grubbs, *Polym. Rev.*, 2011, **51**, 104-137.
122. M. Kato, M. Kamigaito, M. Sawamoto and T. Higashimura, *Macromolecules*, 1995, **28**, 1721-1723.
123. J.-S. Wang and K. Matyjaszewski, *J. Am. Chem. Soc.*, 1995, **117**, 5614-5615.
124. W. A. Braunecker and K. Matyjaszewski, *Prog. Polym. Sci.*, 2007, **32**, 93-146.
125. V. Percec, A. V. Popov, E. Ramirez-Castillo, M. Monteiro, B. Barboiu, O. Weichold, A. D. Asandei and C. M. Mitchell, *J. Am. Chem. Soc.*, 2002, **124**, 4940-4941.
126. J. Chiefari, Y. K. Chong, F. Ercole, J. Krstina, J. Jeffery, T. P. T. Le, R. T. A. Mayadunne, G. F. Meijs, C. L. Moad, G. Moad, E. Rizzardo and S. H. Thang, *Macromolecules*, 1998, **31**, 5559-5562.
127. B. Klumperman, E. T. A. van den Dungen, J. P. A. Heuts and M. J. Monteiro, *Macromol. Rapid Commun.*, 2010, **31**, 1846-1862.
128. G. Moad, *Macromol. Chem. Phys.*, 2014, **215**, 9-26.
129. J. Chiefari, R. T. A. Mayadunne, C. L. Moad, G. Moad, E. Rizzardo, A. Postma and S. H. Thang, *Macromolecules*, 2003, **36**, 2273-2283.
130. Y. K. Chong, J. Krstina, T. P. T. Le, G. Moad, A. Postma, E. Rizzardo and S. H. Thang, *Macromolecules*, 2003, **36**, 2256-2272.
131. H. Willcock and R. K. O'Reilly, *Polym. Chem.*, 2010, **1**, 149-157.
132. M. Szwarc, *J. Polym. Sci. Part A: Polym. Chem.*, 1998, **36**, IX-XV.
133. M. Szwarc, M. Levy and R. Milkovich, *J. Am. Chem. Soc.*, 1956, **78**, 2656-2657.
134. S. Aoshima and S. Kanaoka, *Chem. Rev.*, 2009, **109**, 5245-5287.
135. O. W. Webster, W. R. Hertler, D. Y. Sogah, W. B. Farnham and T. V. RajanBabu, *J. Am. Chem. Soc.*, 1983, **105**, 5706-5708.
136. S. Penczek, M. Cypryk, A. Duda, P. Kubisa and S. Słomkowski, *Prog. Polym. Sci.*, 2007, **32**, 247-282.
137. C. W. Bielawski and R. H. Grubbs, *Prog. Polym. Sci.*, 2007, **32**, 1-29.
138. K. Ziegler, E. Holzkamp, H. Breil and H. Martin, *Angew. Chem.*, 1955, **67**, 426-426.
139. Y. Chauvin, *Angew. Chem. Int. Ed.*, 2006, **45**, 3740-3747.
140. R. H. Grubbs, *Angew. Chem. Int. Ed.*, 2006, **45**, 3760-3765.
141. R. R. Schrock, *Angew. Chem. Int. Ed.*, 2006, **45**, 3748-3759.

142. J.-L. Hérisson and Y. Chauvin, *Die Makromolekulare Chemie*, 1971, **141**, 161-176.
143. S. W. Benson, F. R. Cruickshank, D. M. Golden, G. R. Haugen, H. E. O'Neal, A. S. Rodgers, R. Shaw and R. Walsh, *Chem. Rev.*, 1969, **69**, 279-324.
144. C. Pariya, K. N. Jayaprakash and A. Sarkar, *Coord. Chem. Rev.*, 1998, **168**, 1-48.
145. R. R. Schrock, J. Feldman, L. F. Cannizzo and R. H. Grubbs, *Macromolecules*, 1987, **20**, 1169-1172.
146. M. B. O'Donoghue, R. R. Schrock, A. M. LaPointe and W. M. Davis, *Organometallics*, 1996, **15**, 1334-1336.
147. T. M. Trnka and R. H. Grubbs, *Acc. Chem. Res.*, 2001, **34**, 18-29.
148. R. R. Schrock and A. H. Hoveyda, *Angew. Chem. Int. Ed.*, 2003, **42**, 4592-4633.
149. H. Martinez, N. Ren, M. E. Matta and M. A. Hillmyer, *Polym. Chem.*, 2014, **5**, 3507-3532.
150. S. T. Nguyen, L. K. Johnson, R. H. Grubbs and J. W. Ziller, *J. Am. Chem. Soc.*, 1992, **114**, 3974-3975.
151. S. T. Nguyen, R. H. Grubbs and J. W. Ziller, *J. Am. Chem. Soc.*, 1993, **115**, 9858-9859.
152. Z. Wu, A. D. Benedicto and R. H. Grubbs, *Macromolecules*, 1993, **26**, 4975-4977.
153. P. Schwab, M. B. France, J. W. Ziller and R. H. Grubbs, *Angew. Chem. Int. Ed.*, 1995, **34**, 2039-2041.
154. P. Schwab, R. H. Grubbs and J. W. Ziller, *J. Am. Chem. Soc.*, 1996, **118**, 100-110.
155. S. Sutthasupa, M. Shiotsuki and F. Sanda, *Polym. J.*, 2010, **42**, 905-915.
156. D. Burtscher, R. Saf and C. Slugovc, *J. Polym. Sci. Part A: Polym. Chem.*, 2006, **44**, 6136-6145.
157. T. C. Castle, L. R. Hutchings and E. Khosravi, *Macromolecules*, 2004, **37**, 2035-2040.
158. C. W. Bielawski, J. Louie and R. H. Grubbs, *J. Am. Chem. Soc.*, 2000, **122**, 12872-12873.
159. D. Albagli, G. C. Bazan, R. R. Schrock and M. S. Wrighton, *J. Am. Chem. Soc.*, 1993, **115**, 7328-7334.

160. D. Albagli, G. C. Bazan, R. R. Schrock and M. S. Wrighton, *J. Phys. Chem.*, 1993, **97**, 10211-10216.

161. K. Nomura, S. Takahashi and Y. Imanishi, *Macromolecules*, 2001, **34**, 4712-4723.

162. E. J. Gordon, J. E. Gestwicki, L. E. Strong and L. L. Kiessling, *Chem. Biol.*, 2000, **7**, 9-16.

163. B. Chen, K. Metera and H. F. Sleiman, *Macromolecules*, 2005, **38**, 1084-1090.

164. J. B. Matson and R. H. Grubbs, *Macromolecules*, 2008, **41**, 5626-5631.

165. S. Kurzhals and W. H. Binder, *J. Polym. Sci. Part A: Polym. Chem.*, 2010, **48**, 5522-5532.

166. L. Ding, J. An and Z. Zhu, *Polym. Chem.*, 2014, **5**, 733-742.

167. A. A. Nagarkar and A. F. M. Kilbinger, *Chem. Sci.*, 2014, **5**, 4687-4692.

168. C. Lexer, R. Saf and C. Slugovc, *J. Polym. Sci. Part A: Polym. Chem.*, 2009, **47**, 299-305.

Chapter 2 - Controlling the sequence in the polymerization of norbornenes

2.1. Abstract

The potential control over monomer sequence in the ring-opening metathesis polymerization (ROMP) of functional norbornenes is explored based on the difference in reactivity of *endo* and *exo* isomers. This kinetic approach takes advantage of the slow polymerization of *endo* norbornenes as it allows the rapid consumption of *exo* norbornenes upon addition into the reaction. As a result, the addition of the *exo* norbornene onto the growing poly(norbornene) chain is achieved within a narrow region of the overall polymer chain, whilst maintaining a homogeneous backbone. By using readily accessible monomers, this method allows the introduction of a variety of functional groups onto a polymer in a precise manner.

2.2. Introduction

Ever since the realization that the most complex functions in Nature are achieved by macromolecules that gain their properties from the sequence of their building blocks, such as DNA and proteins, efforts to achieve the synthesis of sequence-controlled polymers have been made by chemists to replicate such properties.[1-5] Mainly using biologically relevant building blocks (such as nucleotides),[6] a large body of work is dedicated to the synthesis of biomolecule-mimicking polymers and the respective materials properties (such as DNA origami).[7] These elegant approaches to sequence control, such as DNA templating,[8-15] suffer from scale and cost issues. This is a considerable drawback when contemplating the use of such methods for the exploration of materials with properties derived from their sequence. Another straightforward and high yielding fashion to obtain sequence-controlled polymers is the use of pre-formed templates that dictate the order of the building blocks.[16-21]

Stemming from the introduction of reversible-reactivation radical polymerization techniques, these efforts have escalated in the past few decades with the synthesis of complex copolymers such as block, graft, alternating and gradient polymers.[22] Achieving truly sequence-controlled polymers is however still intangible as polymerizations only allow the statistical control of the synthesized macromolecule, thus resulting in compositional drift even within the same polymerization mixture.

It has been recently shown that in order to accurately control the monomer sequence of a macromolecule synthesized *via* RAFT polymerization, careful consideration of the kinetic parameters (*i.e.*, initiation rate, chain transfer rate, propagation rate, *etc.*) is necessary,[23] as deviation from complete and single monomer insertion results in the previously mentioned compositional drift. One proposed method to overcome this limitation is the extensive purification of small oligomers, as shown by Junkers *et al.* who performed single (on average) monomer insertions onto a RAFT chain transfer agent followed by "recycling size exclusion chromatography (SEC)", thus allowing the isolation of a monodisperse oligomer. Nevertheless, this approach is scrupulous and low yielding.[24] Truly monodisperse sequence-controlled polymers have been produced *via* step-growth techniques with extensive purification steps, such as solid-phase peptide synthesis.[25] Such monodisperse precision polymers are the result of the addition of one – and only one – repeat unit on the growing chain end and usually involve an iterative addition-activation process.[26-41]

One-pot methods for the synthesis of sequence-ordered polymers whereby the sequence is defined by cascade orthogonal reactions have been reported, although the most prominent limitation of this method is the demanding synthesis of the starting materials.[42-44] Hillmyer *et al.* reported the synthesis of a truly sequence-ordered polymer by ROMP whereby the synthesis of a multifunctional cyclooctene and its

subsequent polymerization afforded a polymer with the functionalities at regular intervals.[45,46]

Sawamoto *et al.* have also reported the tandem catalysis of the radical polymerization of methacrylates and the transesterification of the monomers. In the presence of a metal alkoxide and an alcohol, the ruthenium-catalyzed radical polymerization of primary methacrylates proceeded concurrently with the transesterification of the repeat units, depending on the reaction temperature, the alkoxide species, and the relative concentrations of the reagents. The resulting copolymers exhibited a somewhat regulated sequence attributed to the synchronization of the two processes, thus forming gradient block copolymers.[47]

Recently, the concept of multi-block copolymers has been extensively studied whereby the production of high molecular weight macromolecules with complex composition relies on the sequential oligomerization of different monomers. This has been achieved by controlled polymerizations such as ring-opening polymerization (ROP),[48] reversible addition-fragmentation chain transfer (RAFT) polymerization[49-52] and transition metal-catalyzed radical polymerizations (such as atom transfer radical polymerization, ATRP).[53-61]

Another interesting approach towards controlling the sequence of conventional polymers involves polymerization *via* temporal reactions. This approach allows the "on/off" switching of a dynamic system, such as polymerizations, and thus permitting greater control and precision.[62-65] Typically directed by a stimulus (such as irradiation), the propagating species of the polymerization reaction is reversibly rendered inactive only to be re-activated by a second stimulus. Such a system in ROMP was introduced by Sijbesma *et al.* whereby a latent ruthenium catalyst was mechanically activated and subsequently initiated the polymerization, however the

de-activation process was reported to be slow rendering the system inefficient for sequence-controlled polymerizations.[66]

An approach of interest involves processes whereby the sequence of the polymer is kinetically regulated and therefore minimal interference is required. These approaches commonly involve chain growth polymerizations and careful selection of the monomers and/or initiators that dictate the preferential cross-polymerization of the building blocks. Although limited by the specificity of the reagents, a few such examples have emerged in living anionic polymerizations,[67-69] while an early demonstration of such a method involved oligomerization of styrenic monomers and vinyl ethers *via* living cationic polymerization.[70] In a similar fashion, Russell *et al.* observed the different reactivities of styrene and maleic anhydride under nitroxide-mediated polymerization (NMP) conditions, thus allowing the synthesis of block copolymers in a one-pot reaction.[71] The favorable cross-propagation between the two monomers, which constitute an electron donor-acceptor pair, has been extensively exploited by Lutz *et al.* for the synthesis of "precision polymers"[4] – that is macromolecules whose structure is more sharply defined than typical (co)polymers (Figure 2.1). By taking advantage of the high reactivity of *N*-substituted maleimides towards styrenic monomers during their radical polymerization,[72] a series of functionalities have been incorporated into a polystyrene backbone in a sequential manner.[73] This strategy has been employed for the synthesis of polymers with a variety of pendent functionalities[74-81] as well as to achieve more complex structures (*i.e.* graft, branch, dendritic polymers).[82, 78, 83-85]

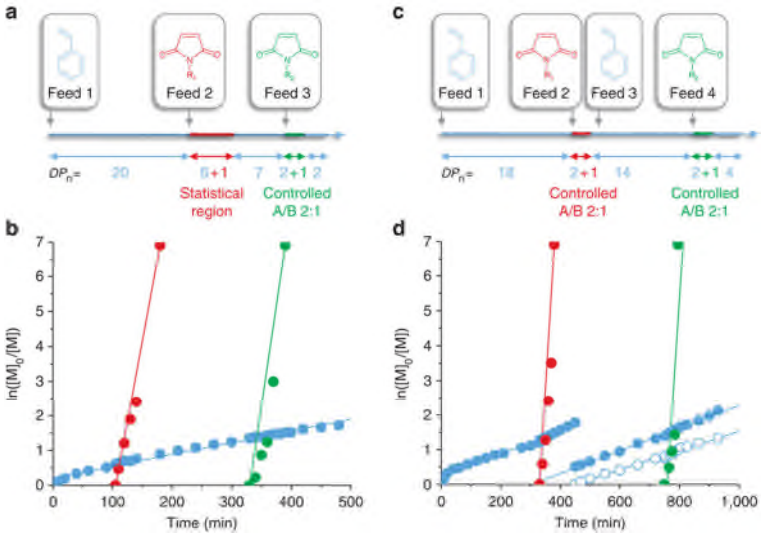

Figure 2.1. Microstrucures of the polymers and semilogarithmic plots from the copolymerization of maleimide-type monomers and styrene depending on the styrene conversion.[86]

Indeed, more recently Lutz *et al.* have shown the possibility of further controlling the sequence of the polymer by automated synthetic protocols.[87] These kinetic approaches are bridging the gap between selective and precise introduction of reactive functionalities and scalable and readily accessible polymeric materials. However, one fundamental drawback of the use of the styrenic/maleimide pair is the statistical,[88, 89] rather than precise monomeric, incorporation of the functional (maleimide) monomer at low conversion regimes of the auxiliary (styrenic) monomer. A solution has been shown to be time-controlled consecutive feeds of the two monomers, however it adds a further layer of complexity to the synthetic approach (Figure 2.1).[86]

Ring-opening metathesis polymerization (ROMP) is a living polymerization method,[90, 91] the simplicity and versatility of which has allowed its use in industrial processes.[92-94] Undeniably, the ability to synthesize nearly monodisperse polymers and complex architectures relies on the range of powerful catalysts available. These have allowed the synthesis of almost perfectly alternating copolymers based on the

thermodynamically driven selective bond formation between the explored monomers, such as in the case of dienes and diacrylates.[95-103, 12, 104-107] These examples demonstrate the tremendous potential of ROMP in its use towards the synthesis of sequence-defined polymers; however they often suffer from broad molecular weight distributions. It should also be noted that these unique monomer pairs have not been studied in systems where one functional monomer is added in precise locations on the polymer backbone of the auxiliary, in a fashion similar to the styrene-*N*-substituted maleimide monomer pair.

It has been shown that while *exo* norbornenes rapidly undergo ROMP in the presence of ruthenium-based catalysts, *endo* norbornenes exhibit far slower polymerization kinetics attributed primarily to steric interactions between the growing polymer chain and the incoming monomer.[108, 109] The two prevailing models (Figure 2.2) suggest that the substituents of *endo* monomers sterically interact either with the metallacyclobutane upon metathesis, or with the growing polymer chain upon coordination with the ruthenium atom, thus resulting in the decreased reactivity of *endo* norbornenes in ROMP. This has hitherto been perceived as a drawback to using an *endo*/*exo* monomer mixture as the overall polymerization rate decreases relative to a pure *exo* monomer feed.[110] Nonetheless, based on the kinetic regulation approach for the synthesis of sequence-controlled polymers, *endo* norbornenes are expected to slowly form the polymer backbone and addition of *exo* norbornene batches should therefore result in their rapid insertion onto the growing polymer chain.

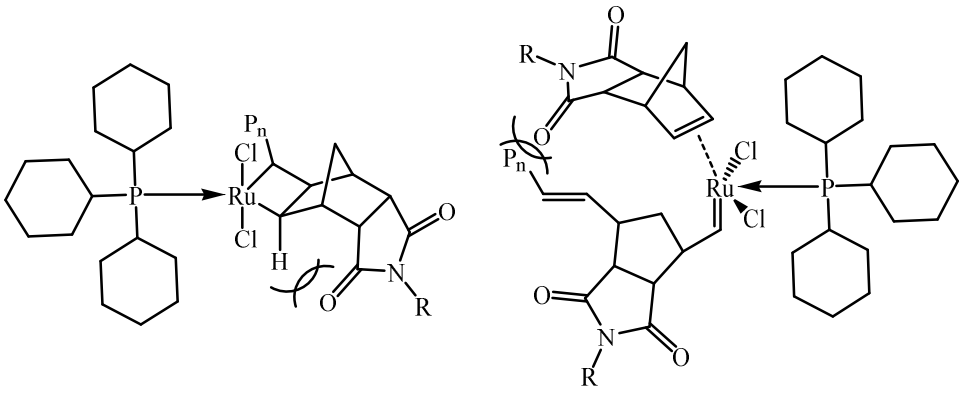

Figure 2.2. Schematic representation of (A) the steric interaction between the metallacyclobutane and the *endo* norbornene substituent and (B) the growing polymer chain and the *endo* norbornene substituent (adapted from the literature[108]).

Perhaps obvious, the prerequisites in this approach are that *endo* norbornenes undergo living polymerization, addition of the *exo* monomer does not alter the overall *endo* reaction rate, and that the difference in the relative reactivity is significant to allow a short sequence of incorporated *exo* monomers at a specific position along the chain. In terms of exploring the material properties of precision polymers, a significant advantage of this system is the homogeneous copolymer backbone, due to the fact that the generic *endo* and *exo* monomers are stereoisomers.

2.3. Results and discussion

Apart from their distinctive isomerism that results to different polymerization rates, norbornenes are of interest because of the range of functional derivatives that can be obtained *via* simple synthetic procedures. Pure isomers of hydroxy, carboxylic acid, and anhydride-functional norbornenes are some of the commercially available precursors to monomers that would allow studying their potential in the synthesis of precision polymers by ROMP.

2.3.1. Relative ratios

In an initial study to evaluate the relative rates of the reaction of *endo* and *exo* norbornenes, *N*-hexyl-*endo*-norbornene-5,6-dicarboximide (*endo*NbHex) and its *exo* isomer *N*-hexyl-*exo*-norbornene-5,6-dicarboximide (*exo*NbHex) were synthesized (Figure 2.3) and allowed to polymerize separately using Grubbs 1st generation ruthenium catalyst (**G1**) (Scheme 2.1) to yield **P2.1** and **P2.2**.

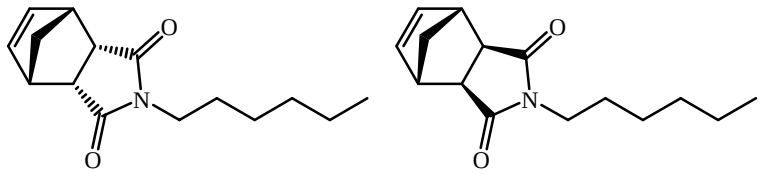

*endo*NbHex *exo*NbHex

Figure 2.3. Chemical structures of the norbornenes used for the evaluation of the relative ROMP rates.

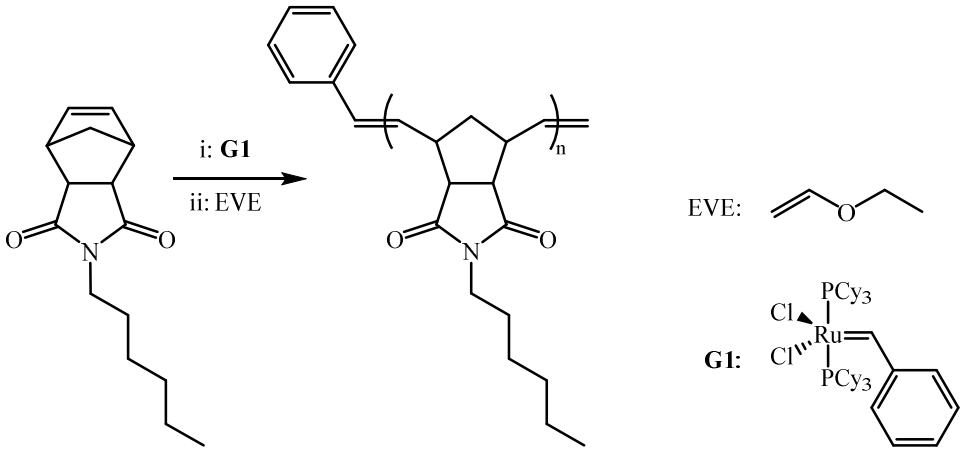

Scheme 2.1. Schematic representation of the polymerization of NbHex using **G1** as the catalyst and EVE as the quenching agent.

The monomer conversions in each polymerization were followed by ^{1}H NMR spectroscopy over time (Figure 2.4) by relative integration of the monomer and the polymer alkene proton signals at δ = 6.1 ppm, and δ = 5.5-6.0 ppm, respectively (Figure 2.5).

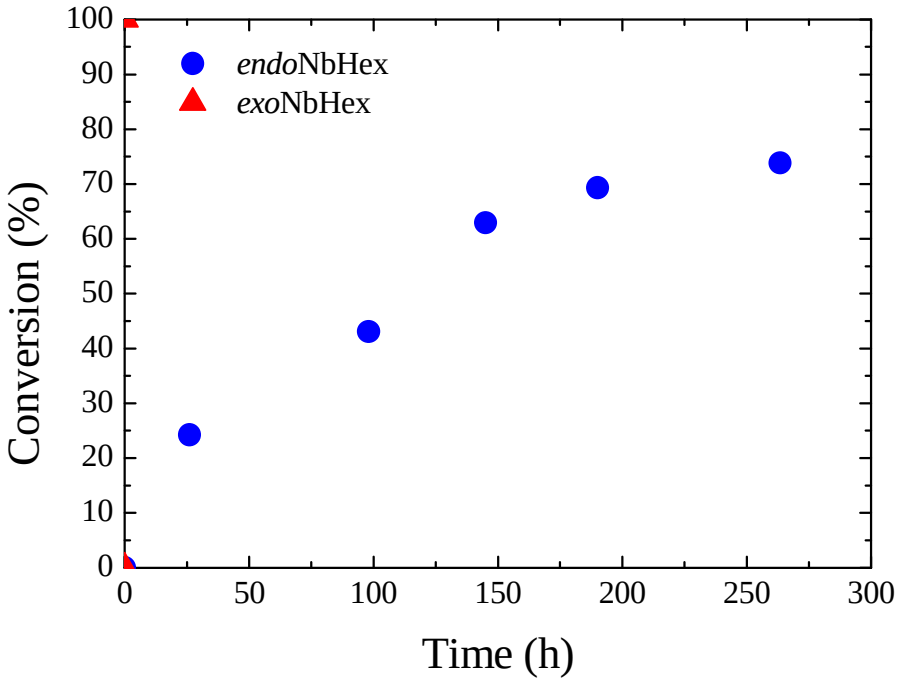

Figure 2.4. Monomer conversions for the ROMP of *endo*NbHex and *exo*NbHex, calculated by ^{1}H NMR spectroscopy.

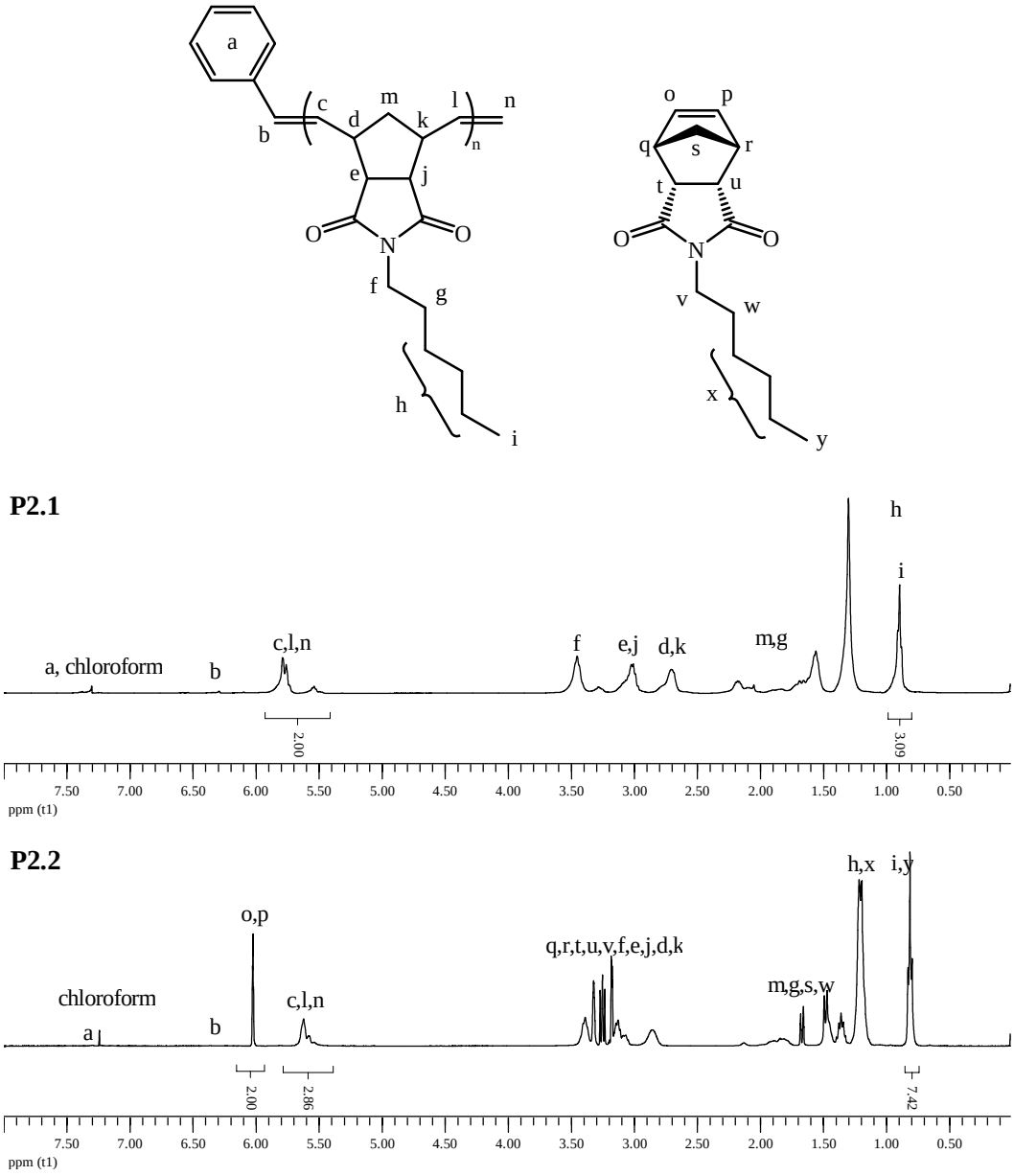

Figure 2.5. Assigned ^{1}H NMR spectra from the homopolymerizations of *exo*NbHex (top) and *endo*NbHex ($CDCl_3$, 400 MHz).

It is apparent that the reactivity of the two monomers is significantly different as the *exo*NbHex monomer was completely consumed when the first spectrum was collected (*ca*. 12 minutes after the addition of the catalyst), while the *endo*NbHex polymerization only reached 69% conversion after 190 hours (~8 days). It should be noted that the polymerization was continued for another 3 days but the conversion of the *endo* monomer did not significantly change. The polymers isolated from the

polymerization of *exo*NbHex (**P2.1**) and the polymerization of *endo*NbHex after 190 hours (**P2.2**) were also characterized by size exclusion chromatography (SEC) (Figure 2.6).

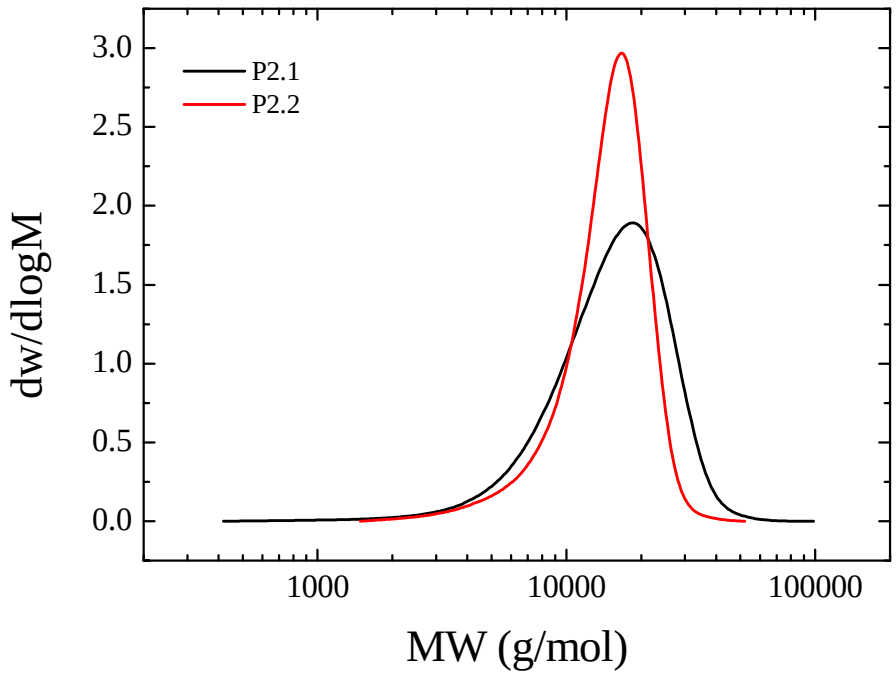

Figure 2.6. Molecular weight distributions obtained by SEC in THF for polymer **P2.1** and **P2.2**.

In both cases narrow molecular weight distributions were obtained, although in the case of **P2.2** (from the *endo* monomer) the distribution was significantly narrower, despite the much longer polymerization time. Nevertheless, the obtained dispersities were in both cases low, suggesting good control of the reaction (Table 2.1).

Table 2.1. Molecular weights and dispersities for the polymers synthesized by the ROMP of *exo*NbHex (**P2.1**) and *endo*NbHex (**P2.2**) (determined by SEC in THF against poly(styrene) standards).

	M_n (kDa)	M_w (kDa)	$Đ_M$
P2.1	12.2	16.8	1.38
P2.2	12.8	15.3	1.20

As expected, these results indicate that the polymerization rates for the two isomers are significantly different and therefore norbornenes are excellent candidates for the synthesis of precision polymers, as discussed previously. While their respective rates are different, it is important to study the rates of *endo* and *exo* norbornenes in a copolymerization. As shown in previous studies, the overall reaction rate of a mixture of isomers is dependent on the relative concentration of the monomers.[110] However the respective rates within the mixture have not been studied. While *endo*NbHex and *exo*NbHex are isomers of the same chemical formula, it was deemed very difficult to assess their relative rates, as the ^{1}H NMR signals from their respective polymers overlap. Therefore, the use of norbornene esters as the *exo* derivative was employed instead. As such, the ROMP of *endo*NbHex (50 equivalents) was initiated using **G1** and at different times an aliquot was removed and added to a solution of 7-coumarinyl-*exo*-5-norbornene-2-carboxylate (*exo*NbCoum) (10 equivalents) and the reaction was monitored by ^{1}H NMR spectroscopy. This would allow the evaluation of the relative rates of the two monomers at different conversions of *endo*NbHex (25%, 50%, and 75%), while using the same amount of *exo*NbCoum (Figure 2.7 and Scheme 2.2). The determination of the apparent polymerization rate for each monomer was determined based on the conversions measured by ^{1}H NMR spectroscopy (Figure 2.8).

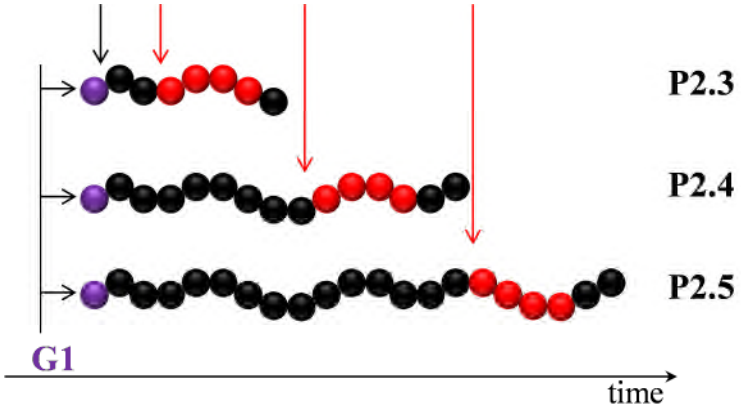

Figure 2.7. Schematic representation of the strategy followed for the synthesis of **P2.3**, **P2.4**, and **P2.5**. Arrows denote monomer addition.

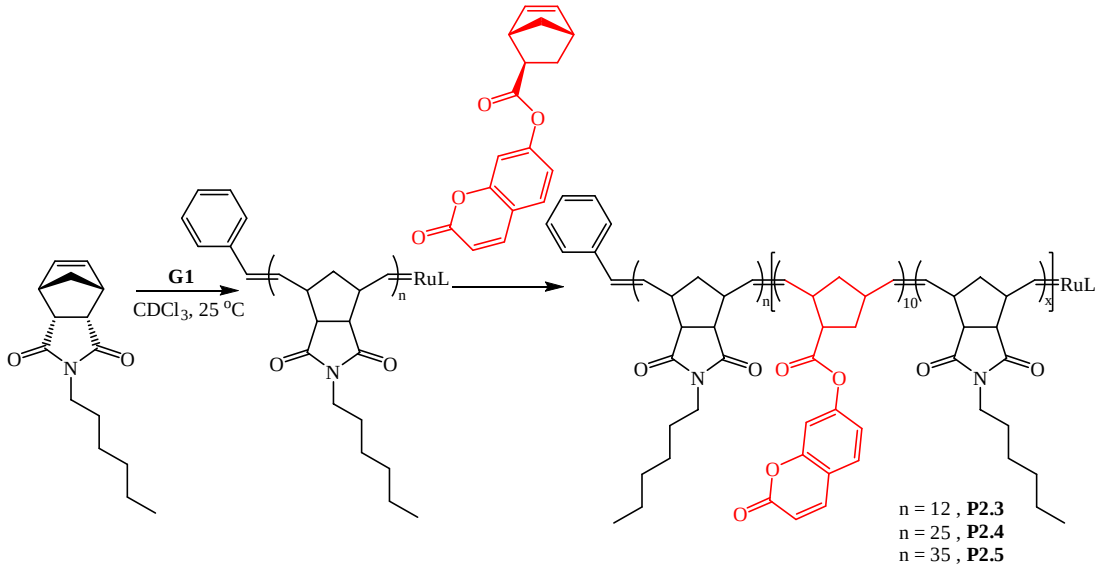

Scheme 2.2. Schematic representation of the strategy followed for the copolymerization of *endo*NbHex and *exo*NbCoum, resulting in three copolymers with different compositions.

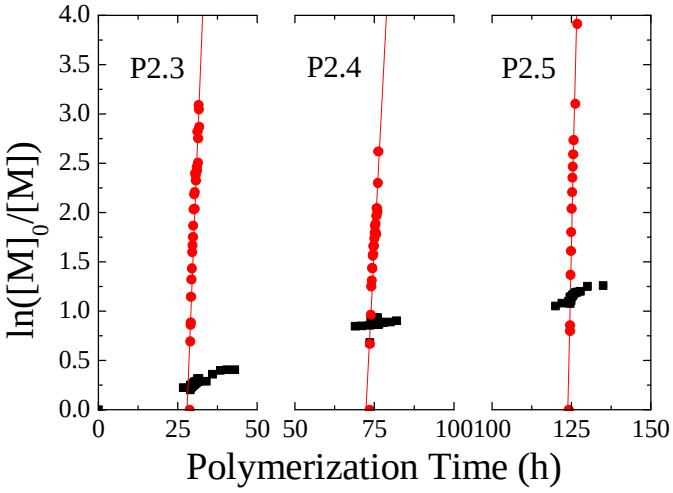

Figure 2.8. Semilogarithmic plots of monomer conversion versus time for the copolymerization of *endo*NbHex (squares) and *exo*NbCoum (circles) in $CDCl_3$ at room temperature at three *endo* monomer conversions: 25% (**P2.3**), 50% (**P2.4**) and 70% (**P2.5**).

It is apparent that *exo*NbCoum is consumed significantly faster than *endo*NbHex, regardless of the conversion of *endo*NbHex. From the slopes of the regression lines of the $\ln([M]_0/[M])$ versus time plots, the apparent polymerization rates (k_{app}) of both monomers at the different *endo* monomer conversions were determined. The overall polymerization rate of the *endo* monomer was found to be 2.68×10^{-6} s^{-1}, and the obtained values for the *exo* monomer were found to be 2.26×10^{-4} s^{-1} at low *endo* monomer conversion (25 %), 1.72×10^{-4} s^{-1} at 50% *endo* monomer conversion and 3.88×10^{-4} s^{-1} at higher conversion (70%), thus *ca*. 100 times faster than the *endo* monomer in all regimes. This demonstrates that the rate of polymerization for *exo*NbCoum is independent of the conversion of *endo*NbHex at which it was copolymerized. This is inconsistent with the observation of Lutz *et al.* whereby the consumption of a maleimide-type monomer when introduced in a radical polymerization of styrene is more rapid at "starvation" conditions when styrene has

reached high conversions.[86] This is perceived as an advantage as it allows precise insertion of the *exo* monomer throughout the polymerization process.

2.3.2. Multifunctional precision polymers

In order to further exploit the difference in reactivity of *endo* and *exo* norbornenes and the ability to obtain copolymers with relatively precise sequences, four different *exo* norbornenes were synthesized bearing functional handles. These were the previously used *exo*NbCoum that is fluorescent owing to the coumarin group, pentafluorophenyl *exo*-5-norbornene-2-carboxylate (*exo*NbPFP) that is an activated ester that can react with primary amines,[111] (1-pyrenyl)methyl *exo*-5-norbornene-2-carboxylate (*exo*NbPyr) that is fluorescent owing to the pyrene moiety, and trimethylsilyl *exo*-5-norbornene-2-carboxylate (*exo*NbTMS) which is a useful NMR spectroscopy handle as the trimethylsilyl protons have a chemical shift of 0 ppm. As such, these were added at different time points to the ROMP of *endo*NbHex (Scheme 2.3) in order to obtain the multifunctional copolymer. Initially, *endo*NbHex was allowed to polymerize for 24.5 hours, using **G1** as the catalyst, before the addition of two equivalents of *exo*NbPFP. The reaction was allowed to proceed for a further 5 hours before the addition of two equivalents of *exo*NbTMS that were further allowed to polymerize for 5.5 hours. Then, the third functional norbornene, *exo*NbPyr was added to the polymerization (two equivalents) and allowed to react for 4.5 hours followed by the addition of *exo*NbCoum (two equivalents).

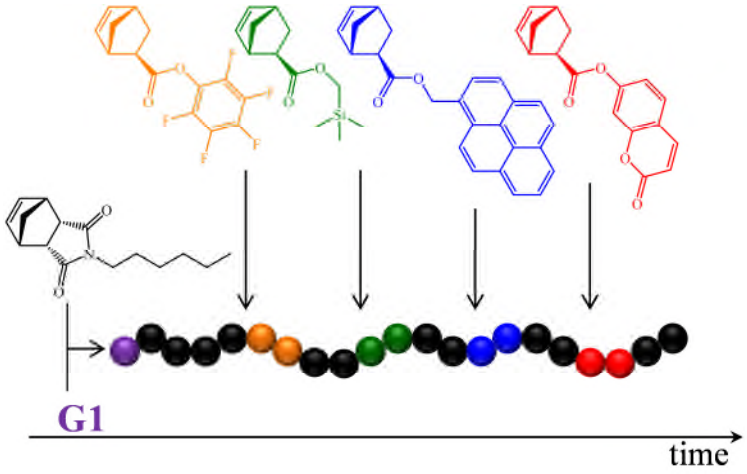

Scheme 2.3. Schematic representation of the strategy followed for the synthesis of the multifunctional **P2.6**.

The successful sequential addition of each *exo* norbornene was confirmed by NMR spectroscopy. In order to confirm the incorporation of *exo*NbPFP in the copolymer **P2.6**, ^{19}F NMR spectroscopy was employed (Figure 2.9).

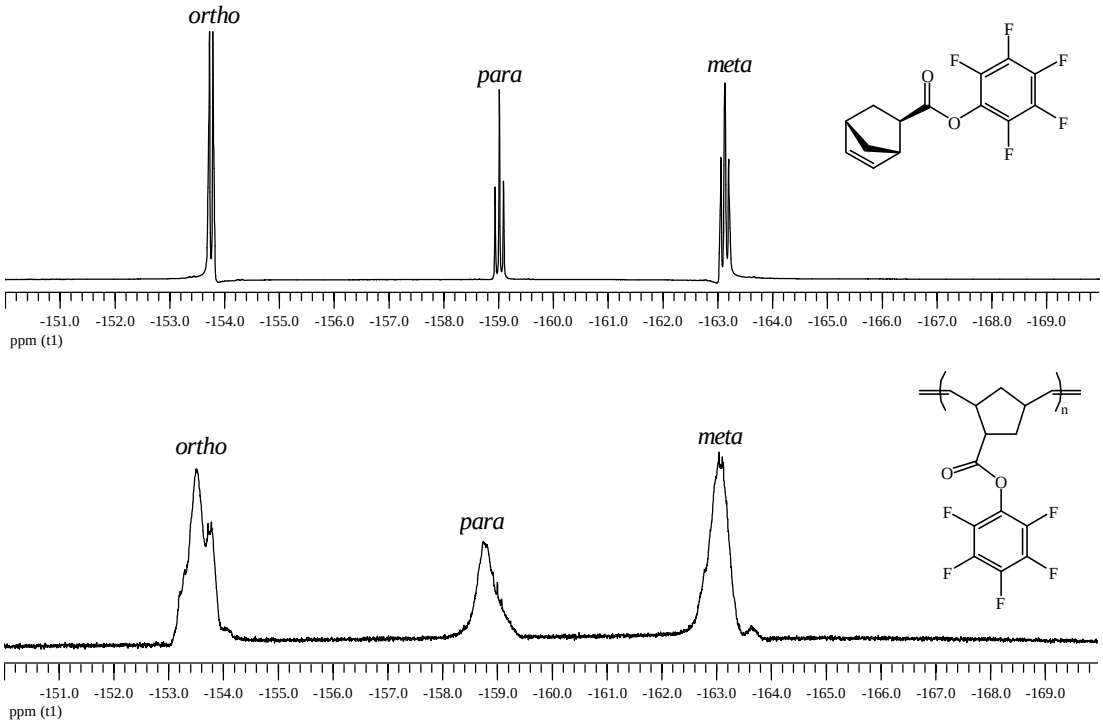

Figure 2.9. ^{19}F NMR spectra of *exo*NbPFP (top) and **P2.6** (bottom) showing the characteristic fluorine signals of pentafluorophenyl ($CDCl_3$, 282 MHz).

Signals corresponding to the fluorine atoms of the *exo*NbPFP group were observed for polymer **P2.6**, suggesting the successful incorporation of the monomer. While the absence of a reference peak does not allow integration, and thus quantification, the broadening of the peaks (compared to those obtained from the monomer) is consistent with polymerization of the monomer. Furthermore, ^{1}H NMR spectra of the reaction mixture before and after the addition of *exo*NbPFP into the polymerization were compared in order to confirm the consumption of the monomer (Figure 2.10).

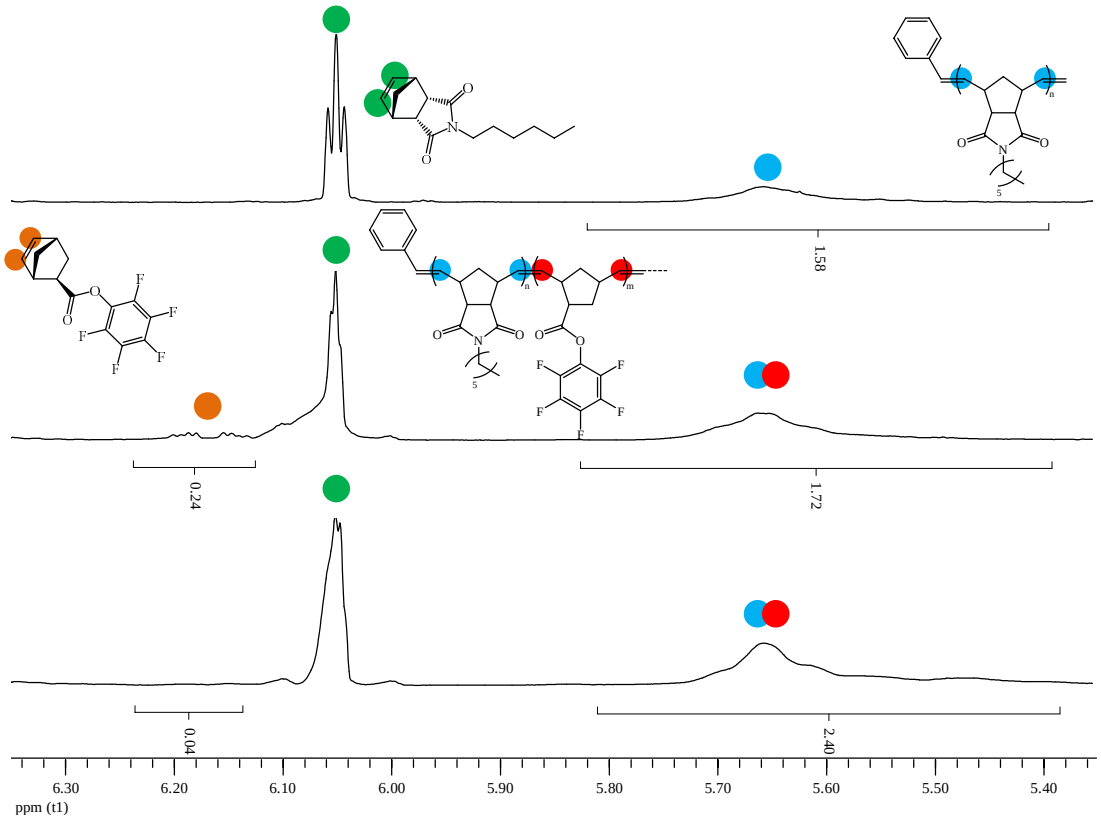

Figure 2.10. ^{1}H NMR spectra of the polymerization of *endo*NbHex before (top), 12 minutes after (middle) and 2 hours after (bottom) the addition of *exo*NbPFP in the reaction mixture ($CDCl_3$, 400 MHz).

Prior to the addition of *exo*NbPFP, the only signals observed in the alkene region (δ = 5.35-6.35 ppm) correspond to *endo*NbHex and the living poly(NbHex) backbone. Upon addition of *exo*NbPFP the increase of the relative integral of the

polymer backbone proton signals (δ = 5.4-5.8 ppm) suggest the rapid ROMP of the added *exo*NbPFP, while the signals at *ca.* δ = 6.18 ppm correspond to the *exo*NbPFP monomer alkene. These signals disappear after 2 hours, while the integration of the polymer backbone signals (δ = 5.4-5.8 ppm) has further increased. This further confirms the successful sequential addition of *exo*NbPFP with the living poly(NbHex).

Similarly, the polymerization was monitored by ^{1}H NMR spectroscopy upon addition of the second functional monomer, *exo*NbTMS (Figure 2.11).

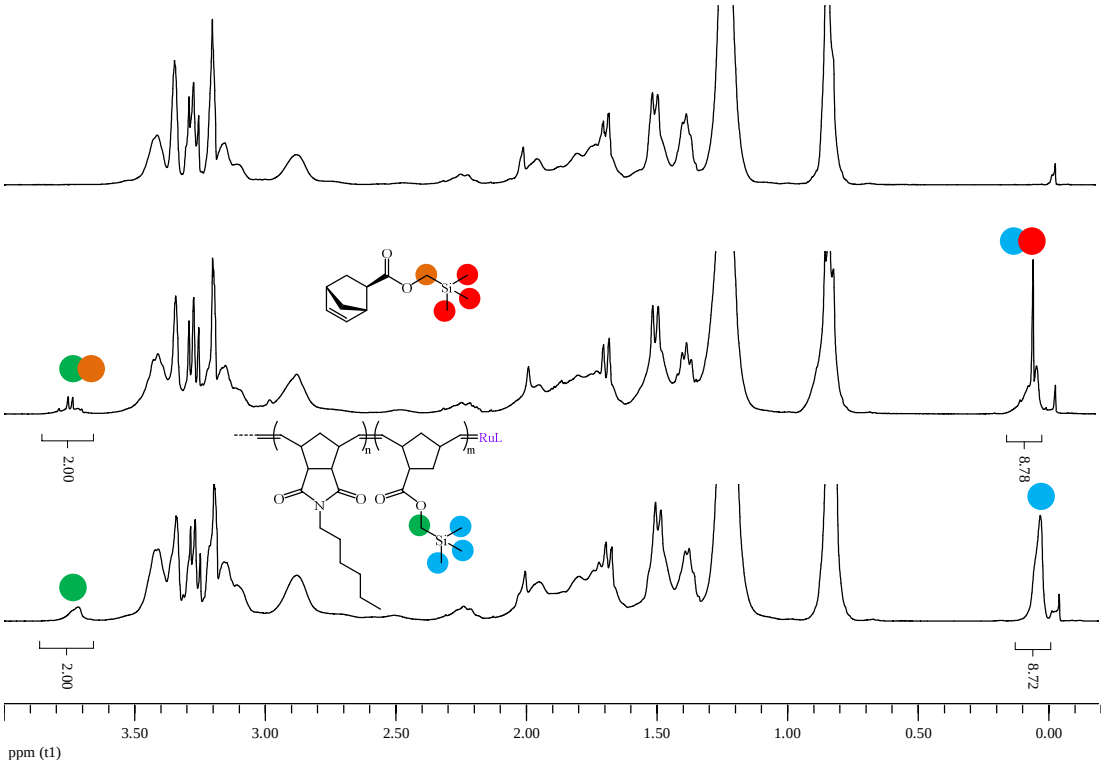

Figure 2.11. ^{1}H NMR spectra of the polymerization mixture before (top), 15 minutes after (middle) and two hours after (bottom) the addition of *exo*NbTMS ($CDCl_3$, 400 MHz).

Before the addition of *exo*NbTMS, in the δ = 0-0.2 ppm region of the ^{1}H NMR spectrum of the polymerization mixture, the only signal observed corresponds to the protons of the tetramethylsilane standard present in the NMR solvent. Upon addition

of *exo*NbTMS a sharp peak at *ca.* δ = 0.05 ppm appeared, attributed to the methyl protons of the TMS group of the monomer. A broad overlapping peak can also be observed which is attributed to polymerized *exo*NbTMS. Two hours after the addition, the sharp peak corresponding to the monomer has disappeared and the broader peak has dominated, thus signifying the consumption of the monomer. Similarly, when examining the δ = 3.5-4.0 ppm region of the spectra, a sharp doublet at *ca.* δ = 3.7 ppm appears upon addition of *exo*NbTMS, corresponding to the CH_2 protons. As a result of polymerization, the peak appears significantly broader two hours after the addition.

In a similar fashion, the addition of *exo*NbPyr into the polymerization was monitored by ^{1}H NMR spectroscopy (Figure 2.12).

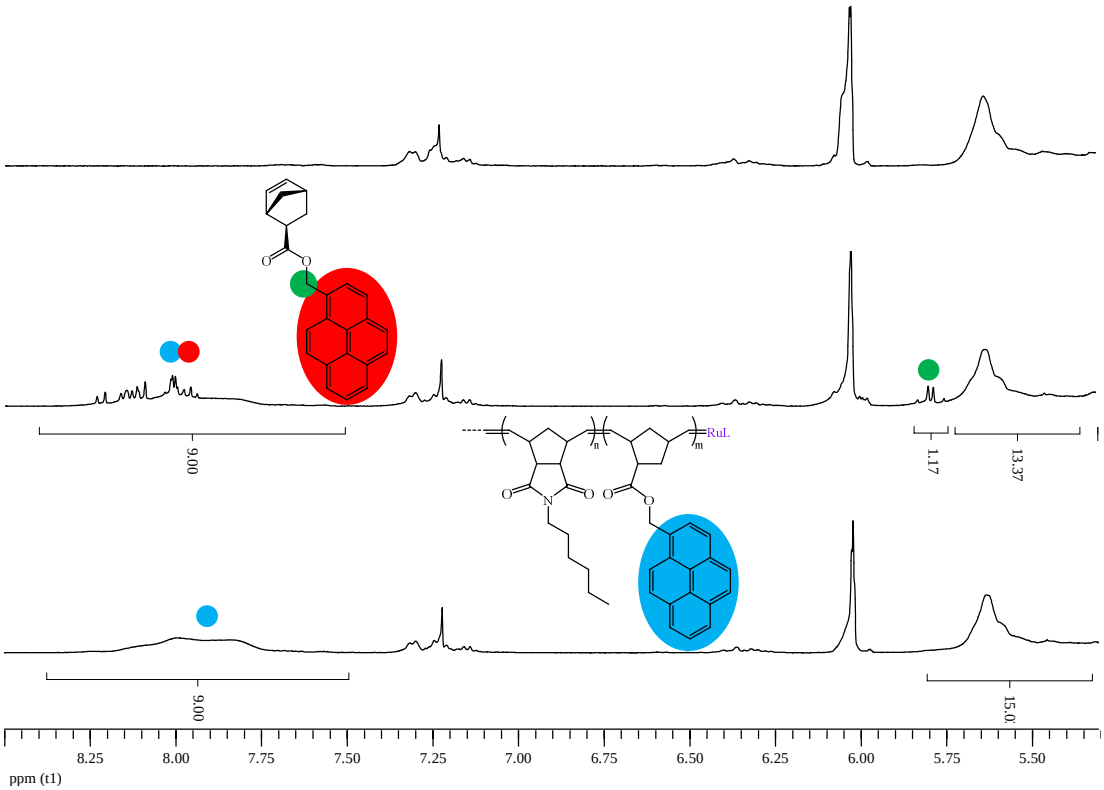

Figure 2.12. ^{1}H NMR spectra of the polymerization mixture before (top), 15 minutes after (middle) and three hours after (bottom) the addition of *exo*NbPyr ($CDCl_3$, 400 MHz).

Prior to the addition of *exo*NbPyr to the reaction mixture, there is an absence of peaks in the downfield region of the ^{1}H NMR spectrum, while upon addition of *exo*NbPyr multiple peaks attributed to protons of the pyrene group appear at *ca.* δ = 7.5-8.3 ppm. In addition, two peaks corresponding to the CH_2 protons appear at *ca.* δ = 5.7 ppm. Three hours after the monomer addition, all sharp peaks have dissappeared and broader ones, consistent with polymer proton peaks, have appeared thus signifying the consumption of the monomer.

Similarly, the addition of *exo*NbCoum into the polymerization mixture was followed by ^{1}H NMR spectroscopy (Figure 2.13).

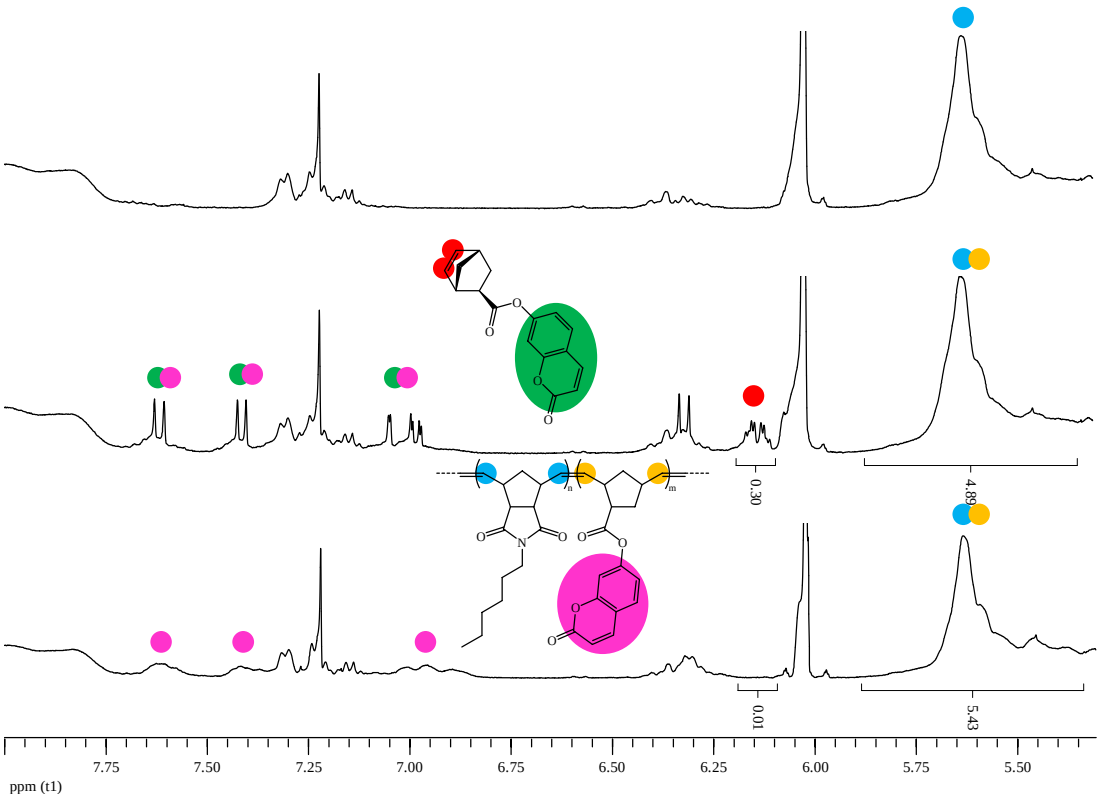

Figure 2.13. ^{1}H NMR spectra of the polymerization mixture before (top), 12 minutes after (middle) and three hours after (bottom) the addition of *exo*NbCoum ($CDCl_3$, 400 MHz).

Analysis of the ^{1}H NMR spectrum of the polymerization mixture before and after the addition of *exo*NbCoum in the reaction shows the appearance of the monomer alkene protons signals at *ca.* δ = 6.15 ppm. Additionally, some of the characteristic coumarin signals appear (*ca.* δ = 7-7.6 ppm) which upon completion of the polymerization after three hours were found to have broadened, thus corresponding to the respective polymer proton signals. This was accompanied by the complete disappearance of the aforementioned monomer alkene peaks.

After isolation of the polymer by precipitation in cold hexane to remove unreacted *endo*NbHex, the product was characterized by diffusion ordered NMR spectroscopy (DOSY) (Figure 2.14).

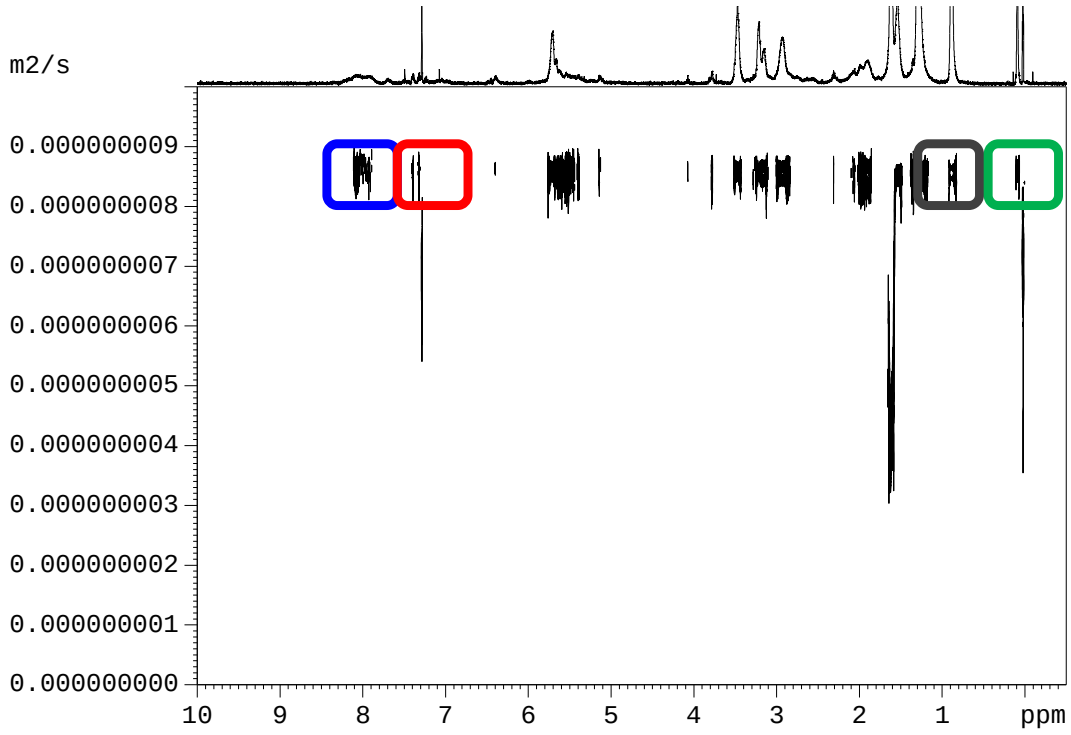

Figure 2.14. DOSY spectrum of the isolated copolymer **P2.6** with the signals corresponding to the functional groups highlighted (blue: NbPyr; red: NbCoum; grey: NbHex; green: NbTMS) ($CDCl_3$, 500 MHz).

The obtained spectrum revealed that all characteristic protons from the functional monomers exhibited the same diffusion coefficient (8.5×10^{-9} m/s^2), thus confirming that they are all present on the same polymer. The additional signals at lower diffusion coefficients correspond to the chloroform solvent (δ = 7.26 ppm), water (δ = 1.5 ppm) and tetramethylsilane, present in the deuterated solvent (δ = 0 ppm).

The rate of incorporation (k_{app}) of each functional monomer into the growing polymer chain was determined by analysis of the ^{1}H NMR spectra and from the respective slopes of the regression lines of the plots of ln([M]$_0$/[M]) versus time (Figure 2.15).

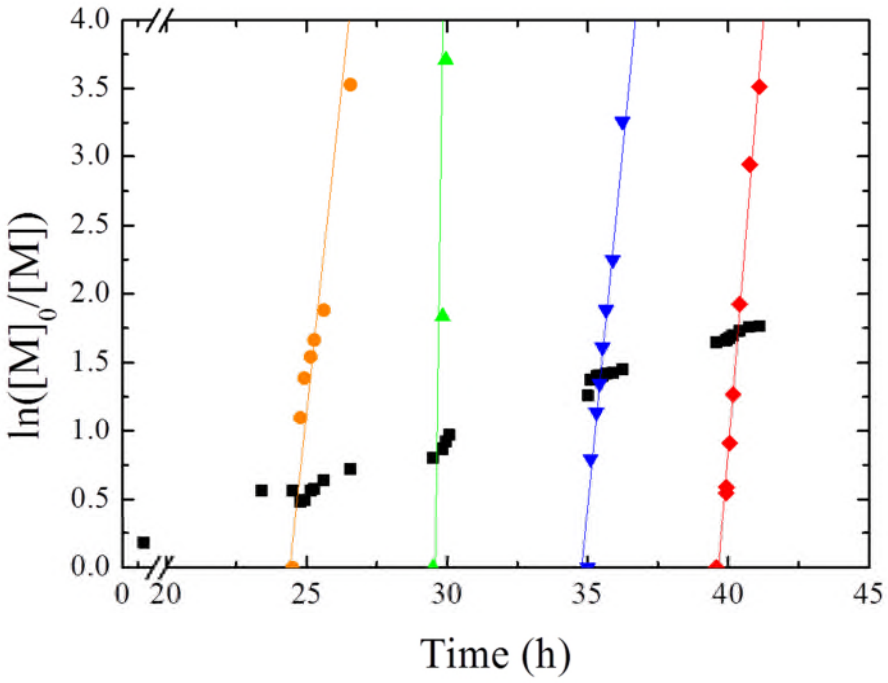

Figure 2.15. Semilogarithmic plots of monomer conversions versus time for the ROMP of *endo*NbHex (■) and the sequential addition of *exo*NbPFP (●), *exo*NbTMS (▲), *exo*NbPyr (▼), and *exo*NbCoum (♦) for the synthesis of the multifunctional copolymer **P2.6**.

Once again, the overall polymerization rate of the *endo* norbornene was low while each *exo* norbornene was copolymerized significantly faster, as evidenced by the difference in the gradient of the slopes. The k_{app} of *endo*NbHex was found to be 1.43×10^{-5} s^{-1}, while the k_{app} of the *exo* norbornenes were found to be 4.16×10^{-4} s^{-1} for *exo*NbPFP, 2.12×10^{-3} s^{-1} for *exo*NbTMS, 6.56×10^{-4} s^{-1} for *exo*NbPyr and 6.94×10^{-4} s^{-1} for *exo*NbCoum. It should be noted that compared to the previous calculations of the polymerization rates of *endo*NbHex and *exo*NbCoum, in this case both monomers were found to polymerize faster which was attributed to the higher catalyst concentration with respect to the monomer concentration. It should also be noted that *exo*NbTMS exhibited a significantly higher polymerization rate compared to the other *exo* monomers which was ascribed to the less bulky pendent group and suggests that relative reaction rates could be further adjusted based on the steric bulk of the *endo* and *exo* monomers. Nevertheless, the polymerization of the *exo* monomers was over 30 times faster than that of the auxiliary monomer indicating the successful synthesis of a multifunctional precision polymer (**P2.6**) through sequential monomer addition.

The final copolymer **P2.6** was characterized by SEC in order to examine the molecular weight distribution. Additional to the standard differential refractive index detector, a UV detector measuring the absorbance at 309 nm and at 344 nm was used (Figure 2.16). This would allow the detection of both the coumarin group on the *exo*NbCoum repeat units which absorbs at λ = 309 nm, as well as the pyrene group on the *exo*NbPyr repeat units that strongly absorbs at λ = 344 nm.

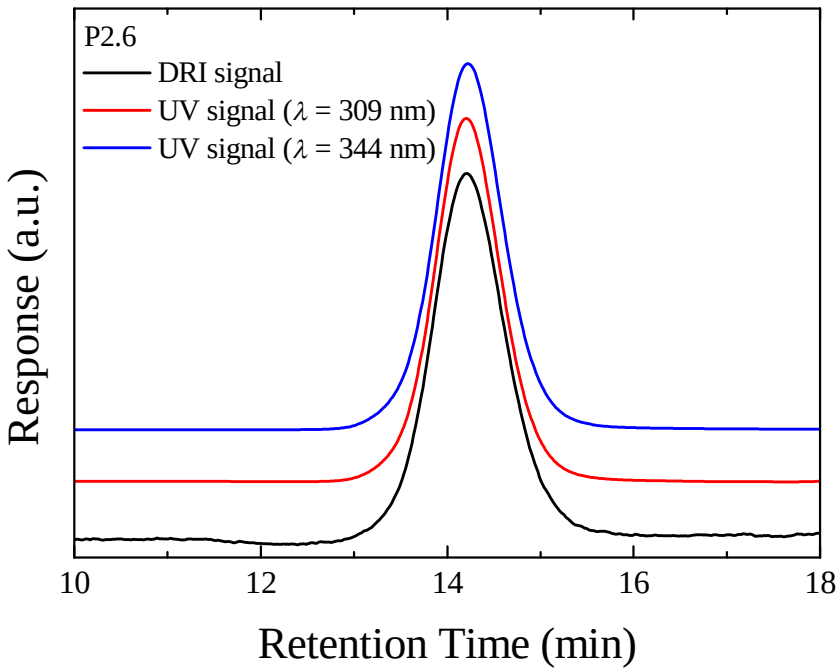

Figure 2.16. Size exclusion chromatograms of the multifunctional copolymer **P2.6** in THF using DRI detection as well as UV detection at λ = 309 nm and λ = 344 nm.

The final polymer exhibited a Gaussian distribution, indicating control of the polymerization, and the molecular weight was found to be M_n = 7,800 g/mol while the dispersity was $Đ_M$ = 1.16 (determined by SEC in THF against poly(styrene) standards). Additionally, the signals from all three detectors exhibit identical narrow distributions, suggesting the presence of both coumarin and pyrene moieties in all polymer chains of **P2.6**.

Additionally, in an attempt to further comprehend the efficiency of the sequential addition, the overall degree of polymerization (DP), as calculated from the monomer conversions as determined by ^{1}H NMR spectroscopy, was plotted against polymerization time (Figure 2.17).

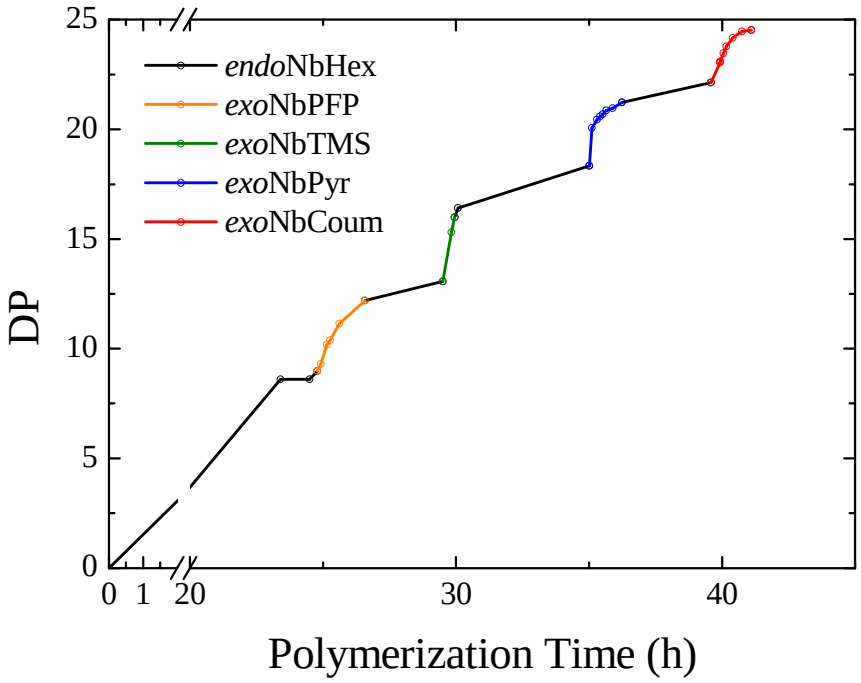

Figure 2.17. Overall DP as a function of polymerization time.

It is apparent that the addition of the *exo* norbornenes results in a rapid increase of the polymer DP, while between additions the DP still increases suggesting incorporation of *endo*NbHex units to the polymer. Additionally, while the addition of *exo*NbPFP results in an increase of the apparent overall DP by 3.5 units, subsequent additions of *exo* norbornenes result in a less prominent increase of the DP with the addition of *exo*NbCoum resulting in an increase by only 2.2 units. This increase of 2-4 repeat units suggests that all *exo* monomer (2 equivalents per addition) is consumed with less than two equivalents of *endo* norbornene adding to the growing polymer chain in the meantime. This highlights the precision of the reaction, as it indicates the successful synthesis of a multiblock copolymer with a well-defined structure. It should, however, be noted that although the observed rate of each *exo* monomer polymerization was found to be independent of the relative concentration of *endo* monomer, the precision of the *exo* monomer insertion is enhanced towards

the end of the reaction, as observed by the better correlation of the added monomer equivalents and the increase of the overall DP.

2.3.3. Single monomer insertions using *exo* norbornenes

A key issue that needs to be addressed when envisioning sequence control is the ability to insert the selected functionality on all growing polymer chains, while controlling the average equivalents added on each chain. To investigate how successful this is in the case of ROMP, the addition of a single *exo* norbornene onto a growing poly(norbornene) chain was attempted. As such, *endo*NbHex was again used as the auxiliary monomer and *exo*NbCoum was added, one equivalent at a time, at four different time points (Figure 2.18).

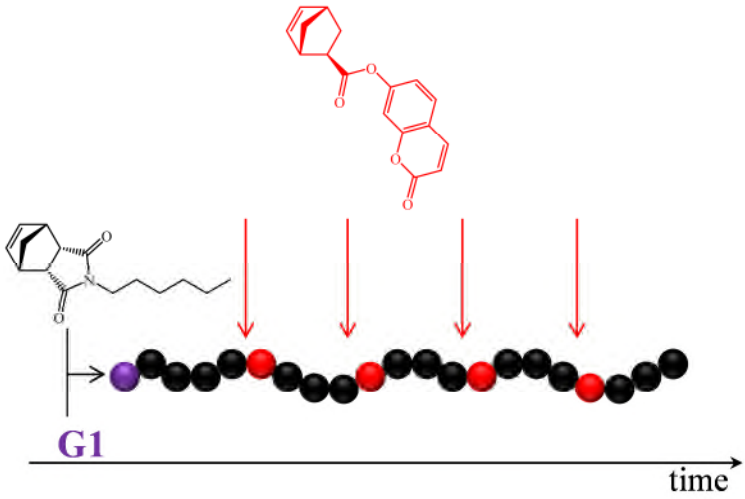

Figure 2.18. Schematic representation of the strategy followed for the single insertions of *exo*NbCoum in the ROMP of *endo*NbCoum.

The use of a coumarin-functional norbornene as the functional monomer provides a useful UV handle for characterization of the resultant copolymers. A sample was removed from the polymerization mixture before and after each addition of *exo*NbCoum and was characterized by SEC analysis (Figure 2.19).

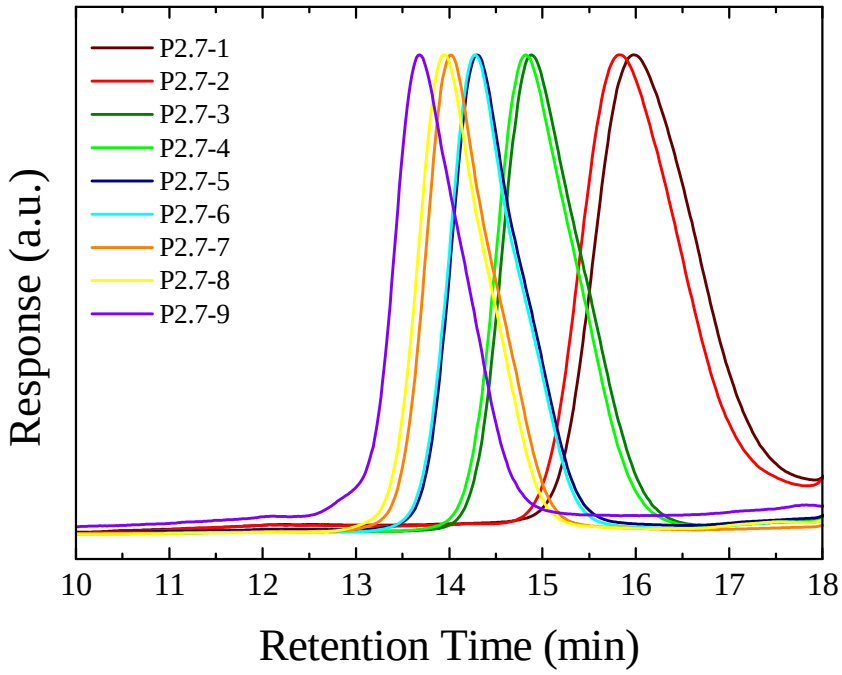

Figure 2.19. Size exclusion chromatograms from the polymerization of *endo*NbHex before (**P2.7-1**, **P2.7-3**, **P2.7-5**, and **P2.7-7**) and after (**P2.7-2**, **P2.7-4**, **P2.7-6**, and **P2.7-8**) addition of a single equivalent of *exo*NbCoum, as well as the final copolymer **P2.7-9**, in THF.

In all cases a Gaussian distribution is obtained indicating control of the polymerization. Additionally, the shifting of the retention time of the polymer peak suggests the increase of the molecular weight of the copolymer with time. The increase of the molecular weight, as determined by SEC, was found to increase after each addition of the *exo*NbCoum batch, however not significantly (Table 2.2).

Table 2.2. Molecular weights and dispersities for the polymerization of *endo*NbHex with single equivalents of *exo*NbCoum being added at t = 22, 71, 144, and 214 hours (determined by SEC in THF against poly(styrene) standards).

	t (h)	M_n (g/mol)	M_w (g/mol)	$Đ_M$
P2.7-1	22	2.2	2.7	1.23
P2.7-2	24	2.6	3.1	1.19
P2.7-3	71	6.2	7.2	1.16
P2.7-4	73	6.6	7.7	1.17
P2.7-5	144	11.0	12.4	1.13
P2.7-6	147	11.3	12.7	1.12
P2.7-7	214	14.3	16.2	1.13
P2.7-8	216	15.4	17.4	1.13
P2.7-9	355	19.9	22.3	1.12

The overall molecular weight was found to increase and the dispersity to decrease over a period of 355 hours in a manner consistent with controlled polymerizations. The final copolymer was also characterized by SEC coupled to an online photodiode array (PDA) detector to generate 2D SEC/UV-vis spectra.

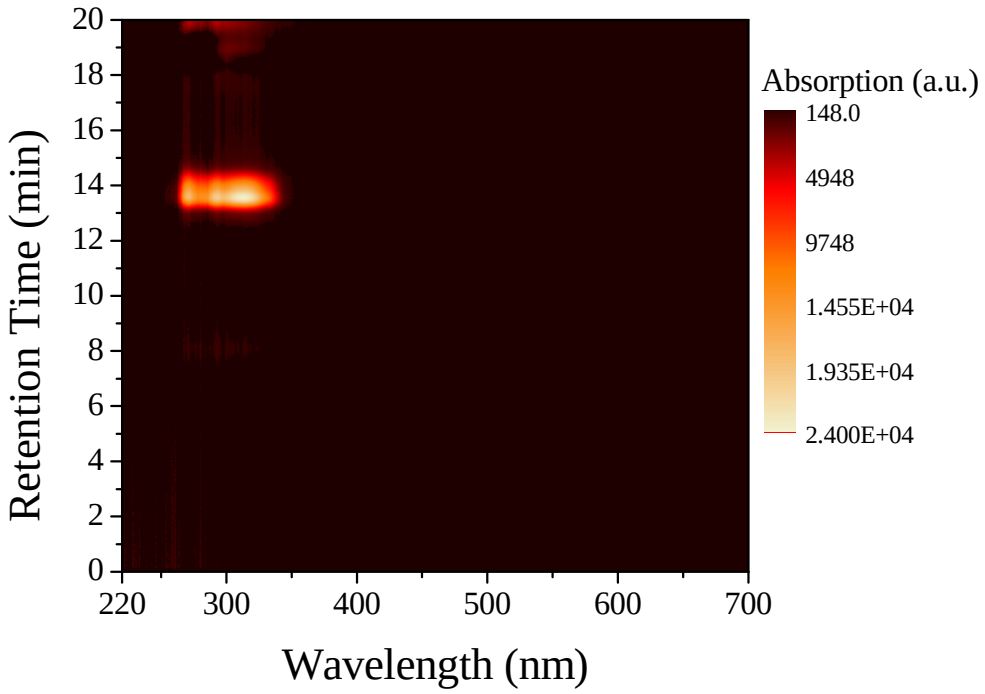

Figure 2.20. 2D SEC/UV-vis spectrum for the final polymer **P2.7-9** in THF.

The spectrum generated from the PDA detector reveals a single polymeric species with a retention time of *ca*. 13 minutes, absorbing at *ca.* 263-343 nm, attributed to the coumarin moiety. This suggests the *exo*NbCoum successfully copolymerized with the growing poly(NbHex), without forming oligomers, thus resulting in a uniform distribution of polymer chains all containing the coumarin moiety.

The overall rate of the polymerization was also investigated by ^{1}H NMR spectroscopy (Figure 2.21).

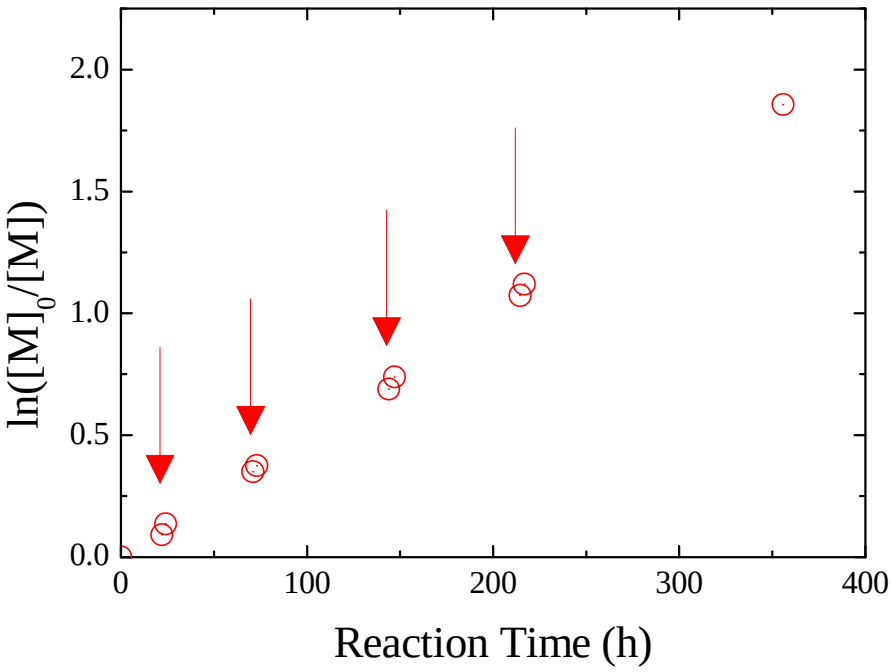

Figure 2.21. Semilogarithmic plot of monomer conversion versus time for the ROMP of *endo*NbHex and the sequential addition of four single equivalents of *exo*NbCoum. The arrows indicate the time points of the *exo*Coum addition.

A linear increase of $\ln([M]_0/[M])$ was observed while the apparent rate was calculated from the slope of the regression line and was found to be $1.44 \times 10^{-6}\ s^{-1}$, comparable to the rate of the homopolymerization of *endo*NbHex. The results obtained from SEC and ^1H NMR spectroscopic analysis suggest that the polymerization kinetics and living chain end are unperturbed by each single addition of the *exo* norbornene.

That being established, quantification of the average amount of coumarin moieties incorporated per polymer chain was attempted. To achieve this, the absorption spectra of each sample were measured in CH_2Cl_2 (Figure 2.22).

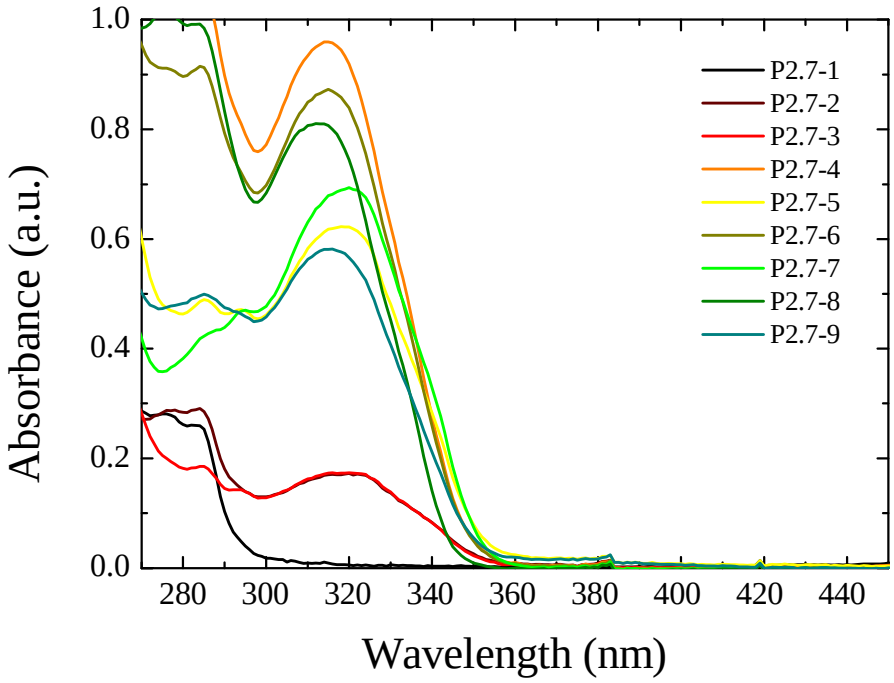

Figure 2.22. Absorption spectra of the isolated copolymers from the ROMP of *endo*NbHex before (**P2.7-1**, **P2.7-3**, **P2.7-5**, and **P2.7-7**) and after (**P2.7-2**, **P2.7-4**, **P2.7-6**, and **P2.7-8**) addition of a single equivalent of *exo*NbCoum, as well as the final copolymer **P2.7-9**, in CH_2Cl_2.

The measured absorption maxima (at $\lambda \sim 320$ nm) were then used to determine the concentration of the coumarin moiety in the solution, based on the Beer-Lambert law (equation 2.1).

$$A = \varepsilon l c \qquad \textbf{2.1}$$

With A being the absorption, l the path length of the UV-vis cell, and ε the extinction coefficient of the coumarin (found to be 8.4×10^3 M^{-1}), the concentration of the absorbing species, *c*. Additionally, based on the polymer concentration in each sample (*C*) and the molecular weight of the respective polymer (determined by SEC), the calculation of coumarin moieties per polymer chain (N_c) was determined based on equation 2.2.

$$N_c = \frac{A}{\varepsilon l C} \qquad \textbf{2.2}$$

The calculated average number of coumarin moieties per polymer chain (N_c) with respect to polymerization time was compared to the anticipated amount from the ratio of *exo*NbCoum to the catalyst present in the reaction mixture (Figure 2.23).

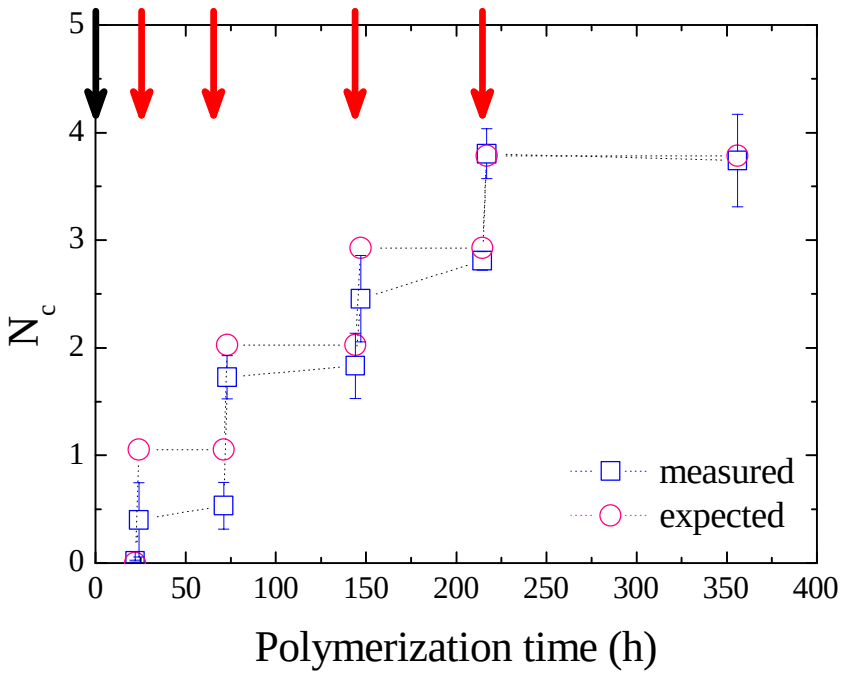

Figure 2.23. Amount of coumarin moieties per polymer chain (N_c) as calculated for each polymer obtained from the single equivalent addition of *exo*NbCoum into the ROMP of *endo*NbHex. Arrows denote monomer addition times.

Ideally, after each monomer addition the ratio increases by one, thus suggesting the incorporation of a single coumarin moiety per polymer chain on average. While at the initial stages of the polymerization the average coumarin content per polymer chain is low, suggesting incomplete incorporation of the *exo* monomer, upon the last addition, the measured average reaches the expected number of coumarin moieties per polymer chain. While this confirms that the average amount of *exo* monomers

inserted per growing polymer chain is controlled, it also shows that the precision with which that monomer is inserted is limited.

To further evaluate the success of the single insertion, the polymers before and after the first addition of *exo*NbCoum, **P2.7-1** and **P2.7-2**, were analyzed by MALDI-ToF (Figure 2.24).

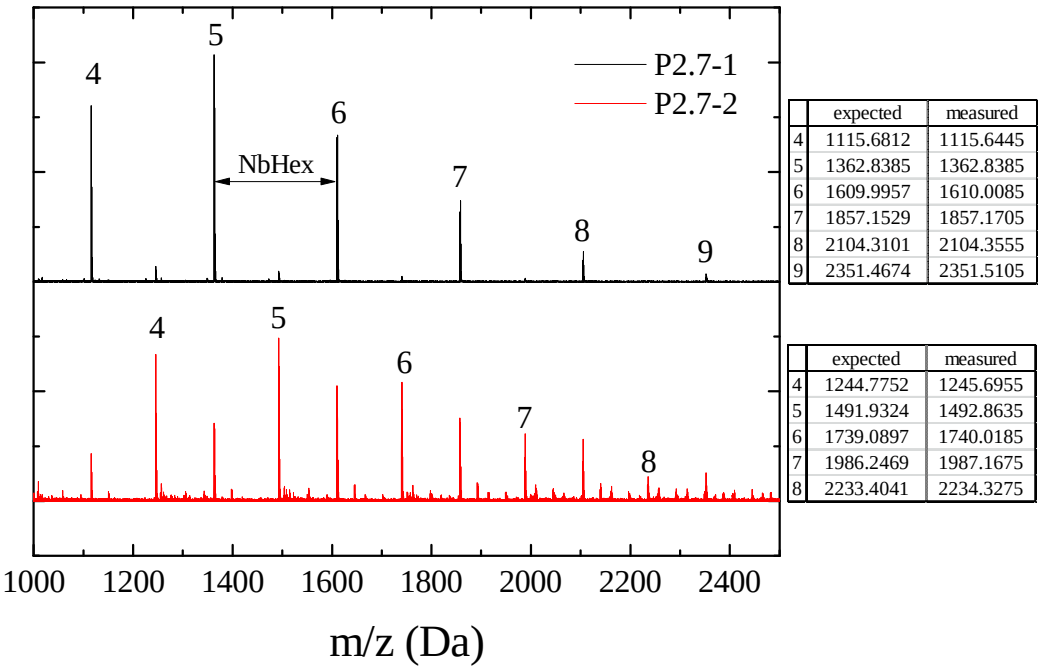

	expected	measured
4	1115.6812	1115.6445
5	1362.8385	1362.8385
6	1609.9957	1610.0085
7	1857.1529	1857.1705
8	2104.3101	2104.3555
9	2351.4674	2351.5105

	expected	measured
4	1244.7752	1245.6955
5	1491.9324	1492.8635
6	1739.0897	1740.0185
7	1986.2469	1987.1675
8	2233.4041	2234.3275

Figure 2.24. MALDI-ToF mass spectra of **P2.7-1** and **P2.7-2** after the addition of a single equivalent of *exo*NbCoum. Tables indicate the expected and measured masses in Da for the respective peaks.

For the polymer prior to the addition of *exo*NbCoum, **P2.7-1**, the obtained spectrum revealed a main population (sodium charged) with the mass difference between peaks corresponding to one NbHex unit. A minor population was also observed, however it could not be identified. Upon addition of *exo*NbCoum, the spectrum obtained for **P2.7-2** revealed peaks of the same mass as the homopolymer (**P2.7-1**), suggesting the incomplete functionalization. Unfortunately, the dominant population

was found to correspond to a single norbornene carboxylic acid being added to the polymer chain, suggesting that the ester linker to the coumarin moiety had been hydrolyzed, therefore rendering analysis by MALDI-ToF impractical. However, the error between the expected and measured values is large, therefore correct assigning of the peaks was not possible. Nevertheless, the appearance of smaller populations further indicates the presence of more than one equivalents of norbornene carboxylic acid on the polymer chain, thus confirming that single additions are not precise.

2.4. Conclusions

In this Chapter it has been shown that ROMP can be used to easily and relatively accurately control the position of functional moieties on the polymer chain, by taking advantage of the vastly different polymerization rates of *endo* and *exo* norbornene monomers. It was shown that when adding *exo* monomer in small, defined batches to the auxiliary *endo* polymerization, the presence of both monomers had little effect on their respective reactivity as the *endo* norbornene was consumed 30-100 times slower than the *exo* norbornene during their copolymerization. This method was employed to synthesize a multifunctional copolymer whereby four different functionalities were inserted at relatively precise positions on the polymer backbone. The accuracy of monomer addition was investigated by sequentially inserting an *exo* norbornene bearing a UV-active functionality into a growing *endo* polymer chain at the desired *endo* norbornene polymerization conversion. Although single monomer insertions proved to be problematic, the overall efficiency of the approach suggests that by simply taking advantage of the difference in the reactivity of norbornene isomers, reasonably precise sequences can be achieved *via* ROMP.

2.5. Materials and methods

Cis-5-norbornene-*endo*-2,3-dicarboxylic anhydride (97%) was purchased from VWR International. Hexylamine (99%), *cis*-5-norbornene-*exo*-2,3-dicarboxylic anhydride (95%), *exo*-5-norbornene-2-carboxylic acid (97%), umbelliferone (99%), *N,N'*-dicyclohexylcarbodiimide (99%), 4-(dimethylamino)pyridine (99%), pentafluorophenol (>99%), 1-pyrenemethanol (98%), trimethylsilyl methanol (98%), Grubbs catalyst 1st generation (97%), potassium 2-isocyanoacetate (85%), and ethyl vinyl ether (99%) were purchased from Sigma-Aldrich and were used without further purification. Solvents were purchased from Fisher Scientific and used as received.

Nuclear magnetic resonance (^{1}H, ^{13}C and ^{19}F NMR) spectra were recorded in $CDCl_3$ solution on a Bruker AC-250, a Bruker DPX-300, a Bruker AV-400 or a Bruker DPX- 400, and a Bruker AV II-700 spectrometer. Chemical shifts are reported as δ in parts per million (ppm) and referenced to the chemical shift of the residual solvent resonances ($CDCl_3$ ^{1}H: δ=7.26 ppm; ^{13}C: δ=77.16 ppm). SEC measurements were performed on an Agilent 390-MDS equipped with differential refractive index and UV detectors. The separation was achieved by a guard column (Varian PLGel 5 μm) and two mixed-D columns (Varian PLGel 5 μm) using THF (2% Et_3N mixture) or chloroform (2% Et_3N mixture) as the eluent at a flow rate of 1 mL/min. Data analysis was performed using Cirrus v3.3 with calibration curves produced using Varian Polymer Laboratories Easi-Vials linear poly(styrene) standards with molecular weights ranging from 162 to 2.4×10^5 g/mol. High resolution mass spectra (HRMS) were collected using a Bruker MaXis UHR-ESI-TOF. UV/vis spectroscopy was carried out on a Perkin Elmer Lambda 35 UV/vis spectrometer. Quartz cuvettes transparent above 230 nm were used for all experiments, and recorded absorbance

values corrected for background and solvent absorbance. MALDI ToF mass spectra were acquired on a Bruker Daltonics Ultraflex and an Autoflex MALDI-ToF mass spectrometer in positive ion ToF detection performed using an accelerating voltage of 25 kV. Solutions in THF of dithranol as matrix (30 mg/mL), sodium or potassium trifluoroacetate as ionization agent (2 mg/mL) and analyte (1 mg/mL) were mixed prior to being spotted on the MALDI plate and air-dried. The samples were measured in reflector ion mode and calibrated by comparison to SpheriCal (Polymer Factory) single molecular weight standards (1,200-8,000 Da).

2.5.1. Synthesis

2.5.1.1. Synthesis of *N*-hexyl-*endo*-norbornene-5,6-dicarboximide (*endo*NbHex)

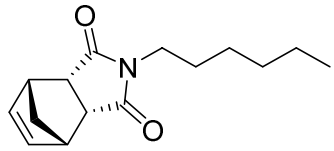

In a round bottom flask equipped with a magnetic stirrer bar, *cis*-5-norbornene-*endo*-2,3-dicarboxylic anhydride (10 g, 60.92 mmol, 1 eq.) was dissolved in toluene (200 mL) before addition of hexylamine (8.21 mL, 62.13 mmol, 1.02 eq.). The reaction mixture was stirred under reflux overnight. The solvent was then removed under reduced pressure and the crude product was dissolved in CH_2Cl_2 and passed through a short silica plug to remove unreacted hexylamine. The pure product was collected as off-yellow viscous oil (11 g, 73% isolated yield). ^{1}H NMR ($CDCl_3$, 400 MHz) δ (ppm): 6.09 (2H, app t, ^3J = 2.0 Hz, CH=CH), 3.39 (2H, m, =CH-C**H**), 3.31 (2H, t, ^3J = 7.5 Hz, N-CH_2), 3.24 (2H, dd, ^3J = 1.3, 1.5 Hz, -CH-C**H**), 1.55-1.74 (2H, m, CH_2 bridge), 1.42 (2H, tt, ^3J = 8.3, 6.5 Hz, N-CH_2-C**H**$_2$), 1.26 (6H, m,

$(CH_2)_3$), 0.87 (3H, t, ^3J = 6.8 Hz, CH_3); ^{13}C NMR ($CDCl_3$, 100 MHz) δ (ppm): 177.7, 134.4, 52.2, 45.7, 44.9, 38.4, 31.3, 27.7, 26.5, 22.5, 14.0; HRMS *m/z*: expected: 270.1470, found: 270.1468 $[M+Na]^+$.

2.5.1.2. Synthesis of *N*-hexyl-*exo*-norbornene-5,6-dicarboximide (*exo*NbHex)

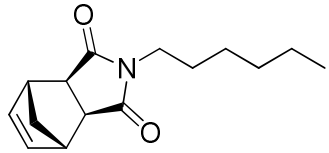

*Exo*NbHex was synthesized using the same procedure followed for the synthesis of *endo*NbHex using *cis*-5-norbornene-*exo*-2,3-dicarboxylic anhydride as a starting material. ^{1}H NMR ($CDCl_3$, 400 MHz) δ (ppm): 6.28 (2H, m, CH=CH), 3.45 (2H, m, =CH-C**H**), 3.26 (2H, m, N-CH_2), 2.65 (2H, d, ^3J = 1.1 Hz, =CH-CH-C**H**), 1.52 (2H, m, N-CH_2-C**H**$_2$-), 1.24-1.47 (2H, m, CH_2 bridge), 1.24-1.37 (6H, m, $(CH_2)_3$), 0.86 (3H, t, ^3J = 6.6 Hz, CH_3); ^{13}C NMR ($CDCl_3$, 75 MHz) δ (ppm): 177.5, 137.2, 17.2, 44.5, 42.1, 38.1, 30.7, 27.1, 26.0, 21.8, 13.4; HRMS *m/z*: expected: 270.1470, found: 270.1467 $[M+Na]^+$.

2.5.1.3. Synthesis of 7-coumarinyl-*exo*-5-norbornene-2-carboxylate (*exo*NbCoum)

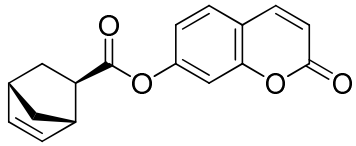

The synthesis of *exo*NbCoum was altered from the reported procedure.[112] In an ice cold round bottom flask *exo*-5-norbornene-2-carboxylic acid (0.785 g, 5.68 mmol, 1 eq.), umbelliferone (1.5 g, 9.25 mmol, 1.63 eq.), and *N,N'*-dicyclohexylcarbodiimide (1.4 g, 6.816 mmol, 1.2 eq.) were dissolved in

CH_2Cl_2 (20 mL) before the addition of 4-(dimethylamino)pyridine (45 mg, 0.37 mmol, 0.065 eq.). The reaction was allowed to warm to room temperature and was stirred overnight. Subsequently, the formed precipitate was removed by filtration and the pure product was collected as a white powder after recrystallization from hexane/methanol (1.2 g, 75% isolated yield). ^{1}H NMR ($CDCl_3$, 400 MHz) δ (ppm): 7.70 (1H, d, ^3J = 9.6 Hz, C**H**-CH-C=O), 7.48 (1H, d, ^3J = 8.4 Hz, C**H**-CH-CO), 7.12 (1H, d, ^3J = 2.2 Hz, C**H**-CO), 7.06 (1H, dd, ^3J = 2.2, 8.4 Hz, CH-C**H**-CO), 6.41 (1H, d, ^3J = 9.5 Hz, CH-C**H**-C=O), 6.19-6.22 (2H, m, CH=CH), 3.24 (1H, m, =CH-C**H**-CH), 3.02 (1H, s, =CH-C**H**-CH_2), 2.50 (1H, m, CH_2-C**H**-C=O), 1.55-2.05 (2H, m, CH_2), 1.48-1.53 (2H, m, CH_2 bridge); ^{13}C NMR ($CDCl_3$, 75 MHz) δ (ppm): 173.6, 159.8, 154.1, 152.9, 142.3, 137.8, 134.9, 127.9, 117.8, 115.9, 115.4, 109.8, 46.2, 45.8, 42.8, 41.2, 30.0; HRMS *m/z*: expected: 305.0790, found: 305.0783 $[M+Na]^+$.

2.5.1.4. Synthesis of pentafluorophenyl *exo*-5-norbornene-2-carboxylate (*exo*NbPFP)

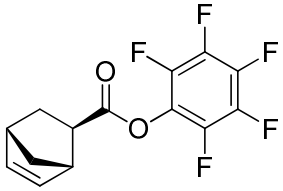

The synthesis of *exo*NbPFP was altered from the reported procedure.[113] In an ice-cold round bottom flask *exo*-5-norbornene-2-carboxylic acid (0.5 g, 3.619 mmol, 1.02 eq.), pentafluorophenol (0.653 g, 3.548 mmol, 1 eq.), and *N,N'*-dicyclohexylcarbodiimide (0.878 g, 4.258 mmol, 1.2 eq.) were dissolved in CH_2Cl_2 (10 mL) before the addition of 4-(dimethylamino)pyridine (28 mg, 0.23 mmol, 0.065 eq.). The reaction was allowed to warm to room temperature and

was stirred overnight. Subsequently, the formed precipitate was removed by filtration and the product was isolated by flash chromatography (silica, CH_2Cl_2) (0.32 g, 30% isolated yield). TLC (CH_2Cl_2): R_f = 0.67; ^{1}H NMR ($CDCl_3$, 300 MHz) δ (ppm): 6.19-6.23 (2H, m, CH=CH), 3.28 (1H, m, =CH-C**H**-CH), 3.03 (1H, m, =CH-C**H**-CH_2), 2.57-2.61 (1H, m, CH-C=O), 1.55-2.13 (2H, m, CH_2), 1.49-1.55 (2H, m, CH_2 bridge); ^{13}C NMR ($CDCl_3$, 75 MHz) δ (ppm): 171.7, 141.9, 138.3, 137.8, 137.3, 134.9, 125.5, 46.2, 45.8, 42.8, 41.2, 30.0; ^{19}F NMR ($CDCl_3$, 282 MHz) δ (ppm): -153.8 (2F, d, ^3J = 17.6 Hz, *ortho*), -159.0 (1F, t, ^3J = 21.8 Hz, *para*), -163.2 (2F, dd, ^3J = 17.9, 21.8 Hz, *meta*); elemental analysis (calcd., found) $C_{14}H_9F_5O_2$: C (54.11%, 54.02%), H (2.98%, 2.93%), F (31.23%, 30.80%).

2.5.1.5. Synthesis of (1-pyrenyl)methyl *exo*-5-norbornene-2-carboxylate (*exo*NbPyr)

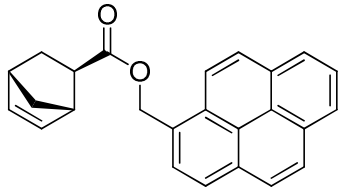

The synthesis of *exo*NbPyr was altered from the reported procedure.[114] In an ice-cold round bottom flask *exo*-5-norbornene-2-carboxylic acid (0.372 g, 2.7 mmol, 1 eq.), 1-pyrenemethanol (1 g, 4.3 mmol, 1.6 eq.) and *N,N'*-dicyclohexylcarbodiimide (0.665 g, 3.2 mmol, 1.2 eq.) were dissolved in CH_2Cl_2 (10 mL) before the addition of 4-(dimethylamino)pyridine (21 mg, 0.18 mmol, 0.065 eq.). The reaction was allowed to warm to room temperature and was stirred overnight. Then, the formed precipitate was removed by filtration and the product was isolated by flash chromatography (silica, CH_2Cl_2) (0.7 g, 74% isolated yield). TLC (CH_2Cl_2): R_f = 0.85; ^{1}H NMR ($CDCl_3$, 400 MHz) δ (ppm): 7.96-8.22 (9H, m, Ar), 6.02-6.07 (2H, m, CH=CH), 5.80

(2H, dd, ^{3}J = 12.4, 18.4 Hz, O-CH_2), 3.06 (1H, m, CH-C**H**-CH_2), 2.88 (1H, m, CH-C**H**-CH), 2.29 (1H, m, CH-CH-C**H**), 1.54-1.97 (2H, m, =CH-CH-C**H$_2$**), 1.33-1.35 (2H, m, CH_2 bridge); ^{13}C NMR ($CDCl_3$, 100 MHz) δ (ppm): 176.2, 138.1, 135.8, 131.7, 131.2, 130.7, 129.5, 129.2, 128.1, 127.8, 127.7, 127.4, 126.1, 125.5, 125.4, 124.9, 124.6, 123.0, 64.8, 53.5, 46.8, 46.5, 43.3, 41.7, 30.5; HRMS *m/z*: expected: 375.1361, found: 375.1356 $[M+Na]^+$.

2.5.1.6. Synthesis of (trimethylsilanyl)methyl *exo*-5-norbornene-2-carboxylate (*exo*NbTMS)

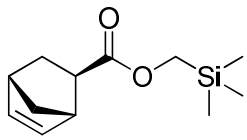

The synthesis of *exo*NbTMS was altered from the reported procedure.[115] In an ice-cold round bottom flask *exo*-5-norbornene-2-carboxylic acid (0.5 g, 3.62 mmol, 1.02 eq.), trimethylsilyl methanol (448 µL, 3.55 mmol, 1 eq.) and *N,N'*-dicyclohexylcarbodiimide (0.878 g, 4.26 mmol, 1.2 eq.) were dissolved in CH_2Cl_2 (10 mL) before the addition of 4-(dimethylamino)pyridine (28 mg, 0.23 mmol, 0.065 eq.). The reaction was allowed to warm to room temperature and was stirred overnight. After filtration to remove the precipitates, the product was isolated by flash chromatography (silica, CH_2Cl_2) (0.4 g, 50% isolated yield). TLC (CH_2Cl_2): R_f = 0.83; ^{1}H NMR ($CDCl_3$, 300 MHz) δ (ppm): 6.07 (2H, m, CH=CH), 3.75 (2H, m, Si-CH_2), 2.97 (1H, m, CH-C**H**-CH_2), 2.87 (1H, m, CH-C**H**-CH), 2.19 (1H, m, CH-C**H**-CH_2), 1.46-1.89 (2H, m, CH-C**H**$_2$-CH), 1.32 (2H, m, CH_2 bridge), 0.04 (9H, s, Si-$(CH_3)_3$); ^{13}C NMR ($CDCl_3$, 75 MHz) δ (ppm) 164.5, 137.3, 135.1, 57.1, 46.0, 45.8, 42.5, 41.0, 29.8, -3.6; HRMS *m/z*: expected: 247.1130, found: 247.1121 $[M+Na]^+$.

2.5.1.7. Homopolymerizations

For comparison of the polymerization rates of *endo*NbHex and *exo*NbHex the two monomers were separately homopolymerized employing similar conditions. For a typical polymerization *exo*NbHex (0.1 g, 0.40 mmol, 50 eq.) was added in an NMR glass tube equipped with a Young's tap together with **G1** (6.6 mg, 0.008 mmol, 1 eq.) dissolved in $CDCl_3$ (1 mL). The monomer conversion was followed by ^{1}H NMR spectroscopy. It should be noted that for the *exo*NbHex homopolymerization, the absence of monomer peaks in the first spectrum suggest the polymerization had reached full conversion within the 12 minutes required to acquire the spectrum.

2.5.1.8. Copolymerization of *endo*NbHex and *exo*NbCoum (**P2.3-2.5**)

To assess the effect of the presence of an *exo* norbornene on the polymerization rate of an *endo* norbornene and *vice versa*, *endo*NbHex (1 g, 4.04 mmol, 50 eq.) and **G1** (66.4 mg, 0.08 mmol, 1 eq.) were dissolved in $CDCl_3$ (5 mL). The solution was degassed by three freeze-pump-thaw cycles before allowing the reaction to proceed under a nitrogen blanket. After *ca.* 29 h, an aliquot (1 mL) was removed from the polymerization mixture and added to *exo*NbCoum (22.8 mg, 0.08 mmol, 5 eq.). The sample was then added to an NMR glass tube equipped with a Young's tap and flushed with nitrogen before monitoring the reaction by ^{1}H NMR spectroscopy. This process was repeated after *ca.* 73 h and *ca.* 124 h, in order to monitor the reactivity of the monomers at different *endo* norbornene conversions.

2.5.1.9. Synthesis of multi-functional poly(norbornene) (**P2.6**)

*Endo*NbHex (0.06 g, 0.243 mmol, 20 eq.) and **G1** (10 mg, 0.012 mmol, 1 eq.) were dissolved in $CDCl_3$ (0.6 mL) in an NMR glass tube equipped with a Young's tap. The solution was degassed by three freeze-pump-thaw cycles before allowing the reaction to proceed under a nitrogen blanket while being monitored by ^{1}H NMR spectroscopy. After 24.5 h, *exo*NbPFP (7.4 mg, 0.024 mmol, 2 eq.) was added and the polymerization was monitored for a further 5 h. Then, *exo*NbTMS (5.5 mg, 0.024 mmol, 2 eq.) was added and the reaction was followed for 5 h before the addition of *exo*NbPyr (8.5 mg, 0.024 mmol, 2 eq.) and further monitoring for 5 h. Lastly, *exo*NbCoum (6.8 mg, 0.024 mmol, 2 eq.) was added and the reaction was followed by ^{1}H NMR spectroscopy until all *exo* norbornene signals had disappeared. The final polymer was isolated by precipitation in cold hexane and characterized by ^{1}H NMR, ^{19}F NMR and DOSY.

2.5.1.10. Single *exo*NbCoum insertions into the ROMP of *endo*NbHex

For the attempted single norbornene additions, in an ampoule equipped with a magnetic stirrer bar *endo*NbHex (1 g, 4.04 mmol, 100 eq.) and **G1** (33.2 mg, 0.04 mmol, 1 eq.) were dissolved in $CHCl_3$ (10 mL). The solution was degassed by three freeze-pump-thaw cycles before filling the ampoule with nitrogen. The polymerization was allowed to proceed at room temperature. Before each addition of *exo* monomer, 1 mL of the polymerization mixture was removed, quenched with ethyl vinyl ether (EVE) and precipitated in cold hexane before drying and analyzing. *Exo*NbCoum (57 mg, 0.2 mmol, 5 eq.) was dissolved in chloroform (2.5 mL) and degassed by three freeze-pump-thaw cycles and stored at 4 ºC under nitrogen. For each addition to the polymerization, the amount of *exo*NbCoum solution required in

order to add one equivalent (with respect to the catalyst) of monomer to the polymerization mixture was calculated by taking into account the previously removed aliquots. After each addition, the reaction was allowed to proceed for 2 hours before removing a sample for analysis. Each sample was first characterized by ^{1}H NMR spectroscopy in order to determine the monomer conversions before quenching by the addition of EVE (100 μL). In all cases, further removal of catalyst residues was achieved by the addition of potassium cyanoacetate[116] (10 eq.) before precipitation in cold hexane.

2.6. References

1. R. Jones, *Nat. Nanotechnol.*, 2008, **3**, 699-700.
2. N. Badi and J.-F. Lutz, *Chem. Soc. Rev.*, 2009, **38**, 3383-3390.
3. J.-F. Lutz, *Polym. Chem.*, 2010, **1**, 55-62.
4. H. G. Börner, *Macromol. Rapid Commun.*, 2011, **32**, 115-126.
5. H. Colquhoun and J.-F. Lutz, *Nature Chem.*, 2014, **6**, 455-456.
6. J. J. Storhoff and C. A. Mirkin, *Chem. Rev.*, 1999, **99**, 1849-1862.
7. H. G. Börner and H. Schlaad, *Soft Matter*, 2007, **3**, 394-408.
8. Z. J. Gartner, M. W. Kanan and D. R. Liu, *J. Am. Chem. Soc.*, 2002, **124**, 10304-10306.
9. Z. J. Gartner, B. N. Tse, R. Grubina, J. B. Doyon, T. M. Snyder and D. R. Liu, *Science*, 2004, **305**, 1601-1605.
10. C. T. Calderone and D. R. Liu, *Angew. Chem. Int. Ed.*, 2005, **44**, 7383-7386.
11. M. L. McKee, P. J. Milnes, J. Bath, E. Stulz, A. J. Turberfield and R. K. O'Reilly, *Angew. Chem. Int. Ed.*, 2010, **49**, 7948-7951.
12. K. Vehlow, M. Lichtenheldt, D. Wang, S. Blechert and M. R. Buchmeiser, *Macromol. Symp.*, 2010, **296**, 44-48.
13. P. J. Milnes, M. L. McKee, J. Bath, L. Song, E. Stulz, A. J. Turberfield and R. K. O'Reilly, *Chem. Commun.*, 2012, **48**, 5614-5616.
14. Y.-Z. Ke, R.-J. Ji, T.-C. Wei, S.-L. Lee, S.-L. Huang, M.-J. Huang, C.-h. Chen and T.-Y. Luh, *Macromolecules*, 2013, **46**, 6712-6722.

15. G. De Bo, S. Kuschel, D. A. Leigh, B. Lewandowski, M. Papmeyer and J. W. Ward, *J. Am. Chem. Soc.*, 2014, **136**, 5811-5814.
16. S. Ida, T. Terashima, M. Ouchi and M. Sawamoto, *J. Am. Chem. Soc.*, 2009, **131**, 10808-10809.
17. P. K. Lo and H. F. Sleiman, *J. Am. Chem. Soc.*, 2009, **131**, 4182-4183.
18. Y. Hibi, S. Tokuoka, T. Terashima, M. Ouchi and M. Sawamoto, *Polym. Chem.*, 2011, **2**, 341-347.
19. R. McHale, J. P. Patterson, P. B. Zetterlund and R. K. O'Reilly, *Nature Chem.*, 2012, **4**, 491-497.
20. Y. Kang, A. Lu, A. Ellington, M. C. Jewett and R. K. O'Reilly, *ACS Macro Lett.*, 2013, **2**, 581-586.
21. N. ten Brummelhuis, *Polym. Chem.*, 2015, **6**, 654-667.
22. E. Saldívar-Guerra and E. Vivaldo-Lima, in *Handbook of Polymer Synthesis, Characterization, and Processing*, John Wiley & Sons, Inc., 2013, pp. 1-14.
23. S. Houshyar, D. J. Keddie, G. Moad, R. J. Mulder, S. Saubern and J. Tsanaktsidis, *Polym. Chem.*, 2012, **3**, 1879-1889.
24. J. Vandenbergh, G. Reekmans, P. Adriaensens and T. Junkers, *Chem. Commun.*, 2013, **49**, 10358-10360.
25. R. B. Merrifield, *J. Am. Chem. Soc.*, 1963, **85**, 2149-2154.
26. L. Hartmann, E. Krause, M. Antonietti and H. G. Börner, *Biomacromolecules*, 2006, **7**, 1239-1244.
27. M.-A. Berthet, Z. Zarafshani, S. Pfeifer and J.-F. Lutz, *Macromolecules*, 2009, **43**, 44-50.
28. L. Hartmann and H. G. Börner, *Adv. Mater.*, 2009, **21**, 3425-3431.
29. S. Pfeifer, Z. Zarafshani, N. Badi and J.-F. Lutz, *J. Am. Chem. Soc.*, 2009, **131**, 9195-9197.
30. L. Hartmann, *Macromol. Chem. Phys.*, 2011, **212**, 8-13.
31. S. Mosca, F. Wojcik and L. Hartmann, *Macromol. Rapid Commun.*, 2011, **32**, 197-202.
32. R. M. Stayshich, R. M. Weiss, J. Li and T. Y. Meyer, *Macromol. Rapid Commun.*, 2011, **32**, 220-225.
33. X. Tong, B.-h. Guo and Y. Huang, *Chem. Commun.*, 2011, **47**, 1455-1457.

34. E. H. H. Wong, M. H. Stenzel, T. Junkers and C. Barner-Kowollik, *J. Polym. Sci. Part A: Polym. Chem.*, 2011, **49**, 2118-2126.
35. D. Ponader, F. Wojcik, F. Beceren-Braun, J. Dernedde and L. Hartmann, *Biomacromolecules*, 2012, **13**, 1845-1852.
36. F. Wojcik, S. Mosca and L. Hartmann, *J. Org. Chem.*, 2012, **77**, 4226-4234.
37. P. Espeel, L. L. G. Carrette, K. Bury, S. Capenberghs, J. C. Martins, F. E. Du Prez and A. Madder, *Angew. Chem. Int. Ed.*, 2013, **52**, 13261-13264.
38. A. Lv, X.-X. Deng, L. Li, Z.-L. Li, Y.-Z. Wang, F.-S. Du and Z.-C. Li, *Polym. Chem.*, 2013, **4**, 3659-3662.
39. B. N. Norris, S. Zhang, C. M. Campbell, J. T. Auletta, P. Calvo-Marzal, G. R. Hutchison and T. Y. Meyer, *Macromolecules*, 2013, **46**, 1384-1392.
40. S. C. Solleder and M. A. R. Meier, *Angew. Chem. Int. Ed.*, 2014, **53**, 711-714.
41. T. T. Trinh, L. Oswald, D. Chan-Seng and J.-F. Lutz, *Macromol. Rapid Commun.*, 2014, **35**, 141-145.
42. K. Satoh, S. Ozawa, M. Mizutani, K. Nagai and M. Kamigaito, *Nat. Commun.*, 2010, **1**, 6.
43. J.-J. Yan, D. Wang, D.-C. Wu and Y.-Z. You, *Chem. Commun.*, 2013, **49**, 6057-6059.
44. L. Yu, L.-H. Wang, Z.-T. Hu, Y.-Z. You, D.-C. Wu and C.-Y. Hong, *Polym. Chem.*, 2015, **6**, 1527-1532.
45. J. Zhang, M. E. Matta and M. A. Hillmyer, *ACS Macro Lett.*, 2012, **1**, 1383-1387.
46. J. Zhang, M. E. Matta, H. Martinez and M. A. Hillmyer, *Macromolecules*, 2013, **46**, 2535-2543.
47. K. Nakatani, Y. Ogura, Y. Koda, T. Terashima and M. Sawamoto, *J. Am. Chem. Soc.*, 2012, **134**, 4373-4383.
48. C. Fetsch and R. Luxenhofer, *Macromol. Rapid Commun.*, 2012, **33**, 1708-1713.
49. G. Gody, T. Maschmeyer, P. B. Zetterlund and S. Perrier, *Nat. Commun.*, 2013, **4**, 2505.
50. C. Fu, J. Xu, L. Tao and C. Boyer, *ACS Macro Lett.*, 2014, **3**, 633-638.

51. G. Gody, T. Maschmeyer, P. B. Zetterlund and S. Perrier, *Macromolecules*, 2014, **47**, 3451-3460.
52. G. Gody, T. Maschmeyer, P. B. Zetterlund and S. Perrier, *Macromolecules*, 2014, **47**, 639-649.
53. C. Boyer, A. H. Soeriyadi, P. B. Zetterlund and M. R. Whittaker, *Macromolecules*, 2011, **44**, 8028-8033.
54. A. H. Soeriyadi, C. Boyer, F. Nyström, P. B. Zetterlund and M. R. Whittaker, *J. Am. Chem. Soc.*, 2011, **133**, 11128-11131.
55. C. Boyer, A. Derveaux, P. B. Zetterlund and M. R. Whittaker, *Polym. Chem.*, 2012, **3**, 117-123.
56. A. Anastasaki, C. Waldron, P. Wilson, C. Boyer, P. B. Zetterlund, M. R. Whittaker and D. Haddleton, *ACS Macro Lett.*, 2013, **2**, 896-900.
57. Q. Zhang, J. Collins, A. Anastasaki, R. Wallis, D. A. Mitchell, C. R. Becer and D. M. Haddleton, *Angew. Chem. Int. Ed.*, 2013, **52**, 4435-4439.
58. Q. Zhang, P. Wilson, Z. Li, R. McHale, J. Godfrey, A. Anastasaki, C. Waldron and D. M. Haddleton, *J. Am. Chem. Soc.*, 2013, **135**, 7355-7363.
59. A. Anastasaki, V. Nikolaou, G. S. Pappas, Q. Zhang, C. Wan, P. Wilson, T. P. Davis, M. R. Whittaker and D. M. Haddleton, *Chem. Sci.*, 2014, **5**, 3536-3542.
60. F. Alsubaie, A. Anastasaki, P. Wilson and D. M. Haddleton, *Polym. Chem.*, 2015, **6**, 406-417.
61. A. Anastasaki, V. Nikolaou, N. W. McCaul, A. Simula, J. Godfrey, C. Waldron, P. Wilson, K. Kempe and D. M. Haddleton, *Macromolecules*, 2015, **48**, 1404-1411.
62. F. A. Leibfarth, K. M. Mattson, B. P. Fors, H. A. Collins and C. J. Hawker, *Angew. Chem. Int. Ed.*, 2013, **52**, 199-210.
63. B. M. Neilson and C. W. Bielawski, *Chem. Commun.*, 2013, **49**, 5453-5455.
64. O. Coulembier, S. Moins, R. Todd and P. Dubois, *Macromolecules*, 2014, **47**, 486-491.
65. S. Shanmugam, J. Xu and C. Boyer, *Macromolecules*, 2014, **47**, 4930-4942.
66. R. T. M. Jakobs and R. P. Sijbesma, *Organometallics*, 2012, **31**, 2476-2481.
67. A. Natalello, J. N. Hall, E. A. L. Eccles, S. M. Kimani and L. R. Hutchings, *Macromol. Rapid Commun.*, 2011, **32**, 233-237.

68. P. P. Brooks, A. Natalello, J. N. Hall, E. A. L. Eccles, S. M. Kimani, K. Bley and L. R. Hutchings, *Macromol. Symp.*, 2013, **323**, 42-50.
69. L. R. Hutchings, P. P. Brooks, D. Parker, J. A. Mosely and S. Sevinc, *Macromolecules*, 2015, **48**, 610-628.
70. M. Minoda, M. Sawamoto and T. Higashimura, *Macromolecules*, 1990, **23**, 4889-4895.
71. D. Benoit, C. J. Hawker, E. E. Huang, Z. Lin and T. P. Russell, *Macromolecules*, 2000, **33**, 1505-1507.
72. S. Pfeifer and J.-F. Lutz, *J. Am. Chem. Soc.*, 2007, **129**, 9542-9543.
73. J.-F. Lutz, *Acc. Chem. Res.*, 2013, **46**, 2696-2705.
74. S. Pfeifer and J.-F. Lutz, *Chem. Eur. J.*, 2008, **14**, 10949-10957.
75. J.-F. Lutz, B. V. K. J. Schmidt and S. Pfeifer, *Macromol. Rapid Commun.*, 2011, **32**, 127-135.
76. R. Kakuchi, M. Zamfir, J.-F. Lutz and P. Theato, *Macromol. Rapid Commun.*, 2012, **33**, 54-60.
77. S. Srichan, D. Chan-Seng and J.-F. Lutz, *ACS Macro Lett.*, 2012, **1**, 589-592.
78. S. Srichan, L. Oswald, M. Zamfir and J.-F. Lutz, *Chem. Commun.*, 2012, **48**, 1517-1519.
79. N. Baradel, S. Fort, S. Halila, N. Badi and J.-F. Lutz, *Angew. Chem. Int. Ed.*, 2013, **52**, 2335–2339.
80. S. Srichan, H. Mutlu, N. Badi and J.-F. Lutz, *Angew. Chem. Int. Ed.*, 2014, **53**, 9231-9235.
81. S. Srichan, H. Mutlu and J.-F. Lutz, *Eur. Polym. J.*, 2015, **62**, 338-346.
82. B. V. K. J. Schmidt, N. Fechler, J. Falkenhagen and J.-F. Lutz, *Nature Chem.*, 2011, **3**, 234-238.
83. N. Baradel, O. Gok, M. Zamfir, A. Sanyal and J.-F. Lutz, *Chem. Commun.*, 2013, **49**, 7280-7282.
84. A. O. Moughton, T. Sagawa, W. M. Gramlich, M. Seo, T. P. Lodge and M. A. Hillmyer, *Polym. Chem.*, 2013, **4**, 166-173.
85. O. Shishkan, M. Zamfir, M. A. Gauthier, H. G. Borner and J.-F. Lutz, *Chem. Commun.*, 2014, **50**, 1570-1572.
86. M. Zamfir and J.-F. Lutz, *Nat. Commun.*, 2012, **3**, 1138.

87. D. Chan-Seng, M. Zamfir and J.-F. Lutz, *Angew. Chem.*, 2012, **124**, 12420-12423.
88. G.-Q. Chen, Z.-Q. Wu, J.-R. Wu, Z.-C. Li and F.-M. Li, *Macromolecules*, 1999, **33**, 232-234.
89. K. Ishizu, C. Takashimizu, T. Shibuya and S. Uchida, *Polym. Int.*, 2003, **52**, 1010-1015.
90. C. Slugovc, *Macromol. Rapid Commun.*, 2004, **25**, 1283-1297.
91. A. Leitgeb, J. Wappel and C. Slugovc, *Polymer*, 2010, **51**, 2927-2946.
92. J. C. Mol, *J. Mol. Catal. A: Chem.*, 2004, **213**, 39-45.
93. M. Yamazaki, *J. Mol. Catal. A: Chem.*, 2004, **213**, 81-87.
94. M. S. Trimmer, in *Handbook of Metathesis*, Wiley-VCH Verlag GmbH, 2008, pp. 407-418.
95. T.-L. Choi, I. M. Rutenberg and R. H. Grubbs, *Angew. Chem. Int. Ed.*, 2002, **41**, 3839-3841.
96. V. Amir-Ebrahimi and J. J. Rooney, *J. Mol. Catal. A: Chem.*, 2004, **208**, 115-121.
97. M. Bornand and P. Chen, *Angew. Chem. Int. Ed.*, 2005, **44**, 7909-7911.
98. M. Bornand, S. Torker and P. Chen, *Organometallics*, 2007, **26**, 3585-3596.
99. K. Vehlow, D. Wang, M. R. Buchmeiser and S. Blechert, *Angew. Chem. Int. Ed.*, 2008, **47**, 2615-2618.
100. M. Lichtenheldt, D. Wang, K. Vehlow, I. Reinhardt, C. Kühnel, U. Decker, S. Blechert and M. R. Buchmeiser, *Chem. Eur. J.*, 2009, **15**, 9451-9457.
101. A. Song, K. A. Parker and N. S. Sampson, *J. Am. Chem. Soc.*, 2009, **131**, 3444-3445.
102. A. Song, K. A. Parker and N. S. Sampson, *Org. Lett.*, 2010, **12**, 3729-3731.
103. S. Torker, A. Müller and P. Chen, *Angew. Chem. Int. Ed.*, 2010, **49**, 3762-3766.
104. M. R. Buchmeiser, I. Ahmad, V. Gurram and P. S. Kumar, *Macromolecules*, 2011, **44**, 4098-4106.
105. M. Abbas, J. Wappel and C. Slugovc, *Macromol. Symp.*, 2012, **311**, 122-125.
106. J. Romulus, L. Tan, M. Weck and N. S. Sampson, *ACS Macro Lett.*, 2013, **2**, 749-752.

107. L. Tan, K. A. Parker and N. S. Sampson, *Macromolecules*, 2014, **47**, 6572-6579.

108. J. D. Rule and J. S. Moore, *Macromolecules*, 2002, **35**, 7878-7882.

109. V. Lapinte, J.-C. Brosse and L. Fontaine, *Macromol. Chem. Phys.*, 2004, **205**, 824-833.

110. J. M. Pollino, L. P. Stubbs and M. Weck, *Macromolecules*, 2003, **36**, 2230-2234.

111. L. He, K. Szameit, H. Zhao, U. Hahn and P. Theato, *Biomacromolecules*, 2014, **15**, 3197-3205.

112. U.S. Patent 7,541,073, 2009.

113. D. D. Manning, X. Hu, P. Beck and L. L. Kiessling, *J. Am. Chem. Soc.*, 1997, **119**, 3161-3162.

114. D.-J. Liaw, K.-L. Wang, K.-R. Lee and J.-Y. Lai, *J. Polym. Sci. Part A: Polym. Chem.*, 2007, **45**, 3022-3031.

115. U.S. Patent 7,504,194, 2009.

116. B. R. Galan, K. P. Kalbarczyk, S. Szczepankiewicz, J. B. Keister and S. T. Diver, *Org. Lett.*, 2007, **9**, 1203-1206.

Chapter 3 - Single monomer additions in ring-opening metathesis polymerization

3.1. Abstract

In this chapter the possibility to introduce monomer sequence control of a growing poly(norbornene) *via* ring-opening metathesis polymerization is further examined. As discussed in Chapter 2, single monomer insertion is the ultimate goal towards that purpose. In order to efficiently determine the location of the incoming monomer onto the macromolecule backbone, the use of dioxepins was suggested to play the role of the single monomer, as upon polymerization their acid-labile acetal is found on the polymer backbone. This allows scission of the polymer at the point of the dioxepin insertion and thus provides an indirect way to determine the monomer location.

This work was carried out in collaboration with Dr. Amit Nagarkar from the Kilbinger group at the University of Fribourg, Switzerland.

3.2. Introduction

Naturally occurring macromolecules outperform synthetic ones from many points of view, one of them being the precision of the order in which the building blocks are linked. As discussed in the introduction of Chapter 2, the most prominent difference between naturally occurring and synthetic polymers is the ability to incorporate the building blocks in a specific sequence. However, attributes of macromolecules do not only rely on the sequence of the entire polymer chain, as a single functionality change can affect the overall properties. Such an example comes from Nature and the placement of a wrong single amino acid residue in hemoglobin.[1] When the sixth glutamic acid is replaced by valine, the local hydrophobic environment of the protein is altered resulting in the collapse of hemoglobin and effectively in ischemia to the carrier organism. Interestingly, the amino acid misplacement is the result of another single building block

misplacement, the mutation of a nucleotide, from a GAG to GTG codon, on the responsible coding DNA strand.[2]

Apart from step-growth-type polymerizations, such as solid-phase peptide synthesis, the introduction of a single functionality within a synthetic polymer mainly relies on the polymer chain end, either the α-, the ω- end, or both, while in some polymerization methods the ability to use a bi-functional initiating group results in a two-arm star polymer, and therefore a single functionality within the polymer chain.[3] Naturally, once a single functionality has been introduced onto a polymer, post-polymerization modifications broaden the range of accessible functional chain end groups.[4]

3.2.1. End group functionalization

End-group functional polymers gain significant properties, although often subtle, from the single end-chain moiety, and thus find various applications.[5-10] Depending on the type of polymerization employed, the chain end can be determined by the functionality of the initiator, the chain transfer agent, or the quencher, while often post-polymerization modification is employed.[11] While this is readily feasible with most common radical and ionic polymerizations, such as ATRP, RAFT, and anionic polymerization,[12-15] the introduction of a single chain end functionality on a polymer synthesized by ROMP has proven challenging.

As mentioned in Chapter 1, with ROMP, chain-end functionalization can be achieved with different pathways that usually result in high yields, but often come with their own challenges. Introduction of a chain transfer agent (CTA) yields high end-group functionalization, however often results in broad molecular weight distributions as such reactions are dominated by chain transfer thus resulting in secondary metathesis products. As ROMP is a living polymerization, the use of a quenching agent is

necessary and, therefore, chain-end functionalization can be achieved by introducing a functional quencher. This method is versatile and allows different functionalities to be introduced; however the efficiency of the quencher is often limited. Higher chain-end functionalization efficiency is achieved by using a purposely-synthesized initiator, which results in the introduction of a single functionality at the α-chain end. Nevertheless, such syntheses are challenging, which is far from ideal given that a new initiator needs to be synthesized for each desired functionality.

3.2.2. Sacrificial copolymerization

A new approach to chain-end functionalization is the "sacrificial copolymerization" approach whereby a removable monomer is copolymerized and is then "sacrificed", removing it from the polymer, while its by-product becomes the chain-end functionality. Grubbs *et al.* introduced the concept of "sacrificial" polymerization in ROMP, whereby the copolymerization of cyclooctadiene and dioxepin, the latter being the sacrificial monomer, is reported. Polymers synthesized from dioxepins have backbones that contain acetal groups which can be hydrolyzed by exposure to acidic conditions. By doing so, the alcohol product remains on the polymer and thus a hydroxyl end-group is obtained (Figure 3.1).[16]

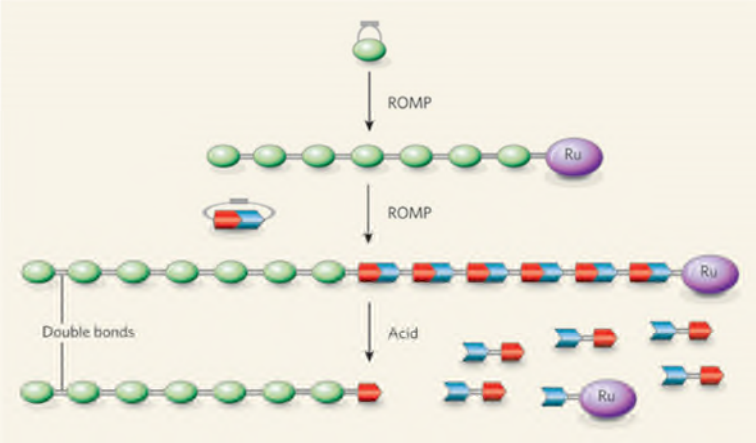

Figure 3.1. Schematic representation of the strategy followed for the sacrificial polymerization of acid-labile monomers in order to afford polymers with a single functionalization.[17]

Kilbinger *et al.* used this concept in the ROMP of norbornenes, synthesizing diblock copolymers whereby dioxepins were used to form the second block that was then sacrificed.[18] This method showed high efficiency and further reaction of the alcohol with a range of functional moieties was demonstrated, indicating the versatility of this method as a single functionality insertion.[19-21] Additionally, by quenching the reaction with vinyl lactones, heterotelechelic poly(norbornene)s were obtained bearing a hydroxyl-functional α-chain end, as a result of the dioxepin acetal hydrolysis, and an aldehyde on the ω-end as a result of the vinyl lactone cross metathesis.[21] Extending their study on the kinetics of the dioxepin ROMP, the efficiency of the dioxepin addition was investigated. Three functional dioxepins were synthesized and used for the chain-extension of poly(norbornene), while monitoring the rate of the reaction. It was found that the poly(norbornene) carbene was quickly substituted by the dioxepin carbene (in under 20 minutes) using Grubbs 1st generation catalyst (**G1**) as the catalyst and isopropyl dioxepin as the monomer. It should be noted that homopolymerization of functional dioxepins was reported impossible, unless the catalyst benzylidene was substituted with an alkylidene, achieved by initiation with norbornene. Interestingly,

although the addition of a large excess of dioxepin was shown (up to 16 times compared to the initiator), the molecular weight of the polymers did not significantly increase.[22] In a later report, the successful homopolymerization of methyl dioxepin was shown, albeit in a non-controlled manner. Further sequential chain extensions with alternating batches of norbornene and dioxepin allowed the synthesis of multiblock copolymers that, upon hydrolysis of the acetals in the backbone, resulted in poly(norbornene)s with both chain ends being hydroxyl-functional.[23]

Kilbinger *et al.* have also shown the use of dithiepins as a sacrificial co-monomer in block copolymerization with norbornenes employing Grubbs 3rd generation catalyst.[24] The resulting backbone thioacetal group could be readily cleaved by hydrogenation, affording the thiol-functional poly(norbornene). However, large excesses of the dithiepin monomers were employed in order to achieve sufficient polymerization, which was attributed to the low k_i/k_p of the monomer under the conditions used. In fact, it was shown that using a single equivalent of the dithiepin monomer with respect to the macroinitiator resulted in less than 50% incorporation. When the catalyst was replaced with **G1**, the initiation efficiency significantly decreased, although the k_i/k_p values were not actually determined.

Additionally, the use of a diazaphosphepine as the sacrificial co-monomer in the chain-extension of a living poly(norbornene) allowed the synthesis of an amine-terminated polymer upon acidic hydrolysis of the resulting backbone phosphoramide.[25] Similarly to previous reports, the ability of the sacrificial monomer to polymerize was limited to the insertion of oligomers.

3.2.3. Single monomer addition

Roberts *et al.* explored the potential single monomer insertion in the ROMP of a peptide-functional norbornene. For the targeted application (to render a protein fluorescent upon conjugation with the poly(norbornene)), a fluorophore was required to be present on the polymer chain. In order to achieve that, an activated ester norbornene was first reacted with an equimolar amount of the ROMP catalyst before the peptide-bearing norbornene was added. The fluorophore was then reacted with the activated ester resulting in highly fluorescent polymer.[26] It should, however, be noted that the success of the single monomer addition is not discussed and a statistical distribution was most likely obtained.

Perhaps one of the few examples of truly sequence-controlled polymers by ROMP was reported by Hillmyer *et al.*. After a multistep synthesis of a cyclooctene bearing three functional groups, its polymerization afforded a polymer with the three functionalities at regular intervals (Scheme 3.1).[27] The high precision of this approach is compromised by the highly demanding monomer synthesis and the resulting broad molecular weight distributions.

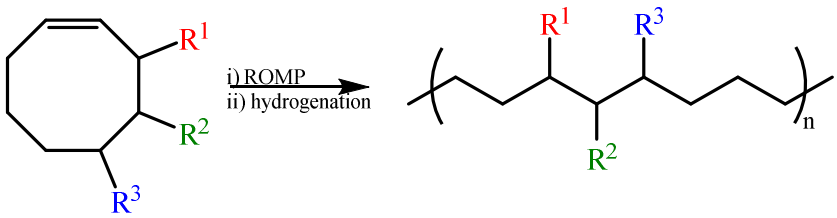

Scheme 3.1. Schematic representation of the approach followed by Hillmyer *et al.* for the synthesis of a sequence-defined polymer by ROMP.[27]

3.2.4. Alternating copolymers

Based on the concept introduced by Lutz *et al.* as discussed in Chapter 2, one would anticipate that sequence control is achievable once a pair of monomers is selected, given

that there is a tendency for alternating copolymerization, but with one monomer still being able to homopolymerize. In ROMP, such monomers are sparse and their alternation seems to be highly dependent on the catalyst used.

Grubbs *et al.* have introduced the concept of ring-opening-insertion-metathesis polymerization (ROIMP) whereby careful selection of catalyst can allow the synthesis of nearly perfectly alternating copolymers, based on the cross-metathesis of unsaturated carbonyl and cyclic olefins (Scheme 3.2). Using this pathway, diacrylates were successfully inserted between the repeat units of a polymer synthesized by ROMP of cycloalkenes.[28] Similarly, Galli *et al.* developed alternating diene metathesis polycondensation (ALTMET), a variation of acyclic diene metathesis (de)polymerization (ADMET). It was shown that the reaction of dienes and diacrylates in the presence of Grubbs 2nd generation catalyst results in nearly perfectly alternating copolymers (Scheme 3.2).[29]

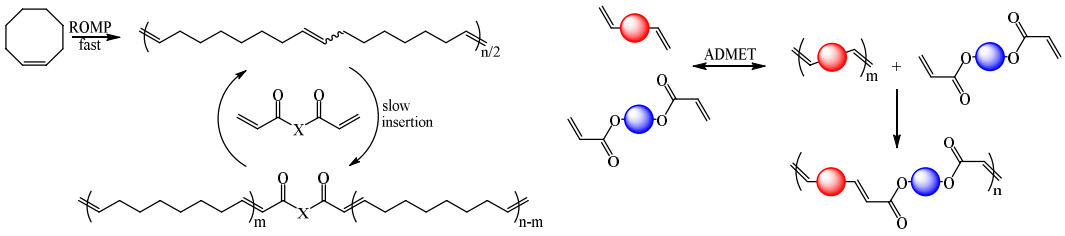

Scheme 3.2. Proposed mechanisms for ROIMP[28] (left) and ALTMET[29] (right).

Additionally, Ilker *et al.* demonstrated the alternating nature of copolymers synthesized by the conventional ROMP of oxanorbornenes and cyclooctene, as well as partial alternation for oxanorbornenes copolymerized with cyclopentene and norbornene.[30] Sampson *et al.* reported the synthesis of perfectly alternating copolymers based on the premise that neither of the monomers employed could form homopolymers. Thus, it was shown that cyclobutene and cyclohexene derivatives could form alternating copolymers

upon reaction with highly reactive catalysts (such as Grubbs 2nd generation catalyst).[31, 32] However, it was also found that backbiting was a significant side-reaction that resulted in cyclic by-products. This effect was later investigated and cyclic alternating copolymers were successfully synthesized by choosing the Grubbs-Hoveyda 2nd generation catalyst.[33] In order to eliminate backbiting, in a later report monomers with bulky, and electron donor-acceptor pair substituents were used. Thus, the synthesis of perfectly alternating linear copolymers by ROMP was successful.[34]

Whilst high precision can be achieved in the sequence of the copolymers, the major drawback of these approaches is the resulting high molecular weight distribution, as well as the limited availability of the monomers explored.

Sutthasupa *et al.* explored the alternating polymerization of amino acid-functional norbornenes with the alternation stemming from the interactions of the pendent moieties. It was found that the protected α-amino group of one amino acid and the carboxylic acid of another could significantly influence the copolymerization resulting in 1:1 ratios in the polymer, thus suggesting alternation.[35]

Al Samak *et al.* observed that the copolymerization of norbornene and cyclopentene, in the presence of purposely synthesized ruthenium catalysts and acidic solvents, results in nearly alternating polymers, based on the ^{13}C NMR signals of the respective olefins.[36, 37]

More recently, it was shown that the use of Mo-based catalysts can also result in the same alternating pattern when norbornene-type and cycloheptene or cyclooctene monomers are employed.[38]

Similar approaches have shown that with the appropriate modifications to the catalyst, norbornene can, in some cases and to a certain extent, copolymerize in an alternating pattern with cyclooctene or cyclopentene.[39-45] This selectivity was attributed to the caging effect introduced by the catalyst ligands. By tuning the size of the metal catalyst

ligands, Chen *et al.* were able to design catalysts that could form perfectly alternating copolymers based on the steric hindrance introduced by each ligand to the incoming monomer.[46, 47]

Grubbs *et al.* studied the alternating copolymerization of cyclooctene and a sterically hindered oxanorbornene. Employing different commercially-available catalysts, different percentages of alternation were observed (up to 73%), however an interesting observation was that exposing a poly(oxanorbornene) to cyclooctene and ROMP catalyst also resulted in a copolymer with alternating oxanorbornene and octene dyads; a phenomenon that was named "sequence editing".[48]

By taking advantage of the ability of dioxepins to participate in the ROMP of norbornenes, it was proposed that if their copolymerization is rapid, they could serve as the functional monomer in a scenario similar to that studied in Chapter 2. Such a system would additionally benefit from the fact that dioxepins are cleavable which would allow indirect determination of the insertion location, by studying the hydrolysis products.

3.3. Results and discussion

Although both dioxepins and dithiepins[24, 21] are capable of undergoing ROMP, because of the added difficulty of the dithiepin synthesis and hydrolysis, the use of dioxepins was instead chosen. Extensive use by the Kilbinger group has shown that dioxepins have high reactivity towards alkylidenes, but suffer from low homopolymerizability. Therefore, their use for single monomer addition is further justified.

3.3.1. Polymerization of functional dioxepins

3.3.1.1. Homopolymerization of DxpPhe

Initially, the homopolymerization of 2-phenyl-4,7-dihydro-2*H*-1,3-dioxepin (DxpPhe) (Scheme 3.3) using Grubbs 1st generation ruthenium catalyst (**G1**) was attempted in order to establish the polymerization rate of dioxepin, but ^{1}H NMR spectra before and after 72 hours of polymerization were found to be identical, suggesting that no polymerization had taken place. This was proposed to be a result of the low reactivity of the alkylidene present on the **G1** catalyst, as well as the fact that DxpPhe was previously shown to be less reactive than other dioxepins.[22]

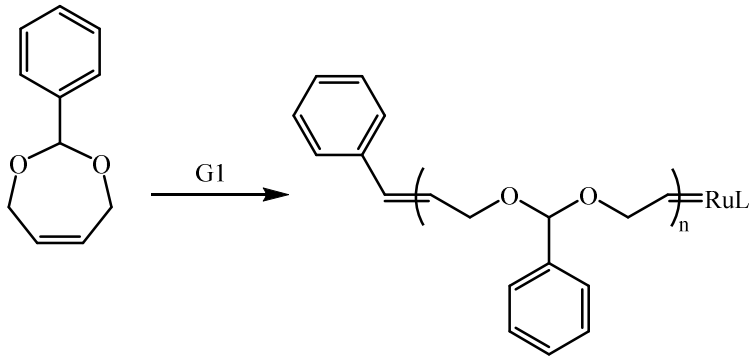

Scheme 3.3. Schematic representation of the homopolymerization of DxpPhe using **G1** as the catalyst.

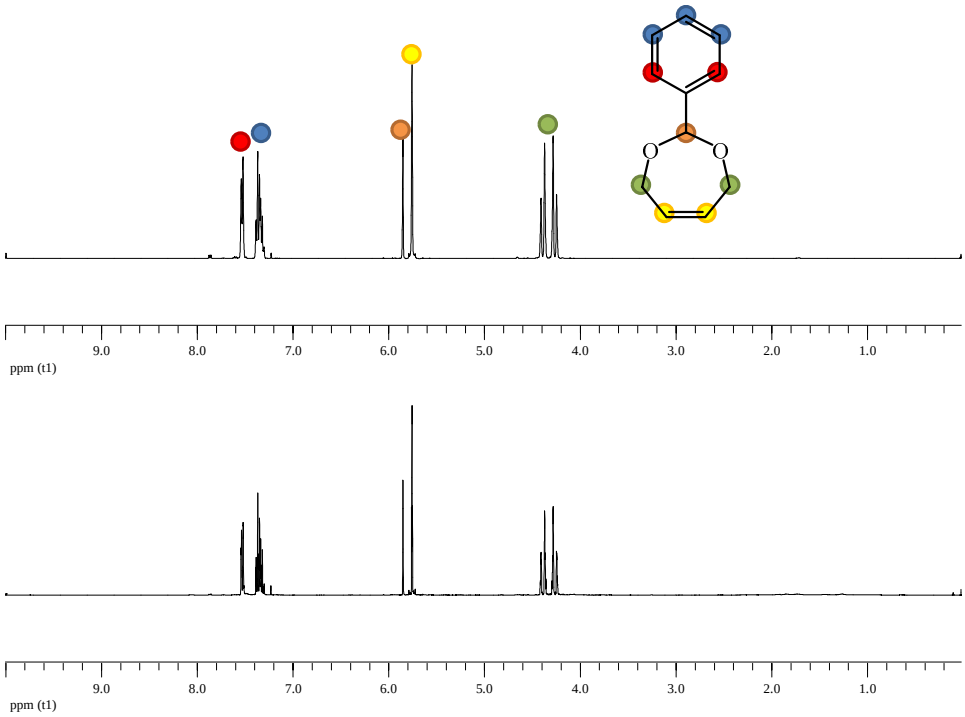

Figure 3.2. ^{1}H NMR spectra of the monomer DxpPhe (top) and an aliquot taken from the polymerization after 72 hours (bottom) ($CDCl_3$, 400 MHz).

3.3.1.2. Polymerization of dioxepin from an activated alkylidene

In order to form a more reactive alkylidene, 2-methyl-4,7-dihydro-2*H*-1,3-dioxepin (DxpMe) was polymerized using a living poly(norbornene) as the macroinitiator. It was previously reported that the methyl-functional dioxepin is more reactive,[22] and was therefore chosen for the chain extension. The *exo* isomer of the norbornene monomer (*N*-hexyl-*exo*-norbornene-5,6-dicarboximide, 10 equivalents) (*exo*NbHex) was used for the synthesis of the first living block as its polymerization reaches high conversions within minutes and therefore very little – if any – unreacted norbornene will remain in the reaction when the second monomer is added (Scheme 3.4).

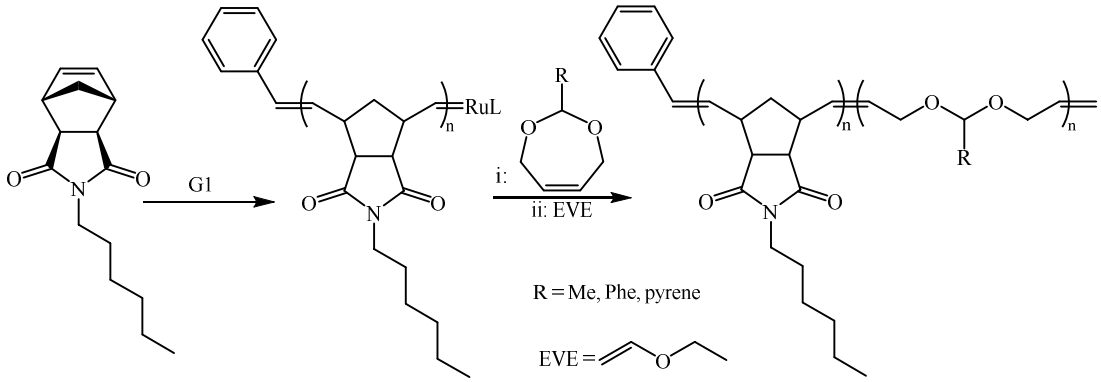

Scheme 3.4. Generic reaction scheme for the chain extension of poly(NbHex) with functional dioxepins.

Two polymers were isolated and analyzed; the quenched first block (**P3.1**) and the resulting block copolymer (**P3.2**). Comparison of the ^{1}H NMR spectra before and after the DxpMe addition shows that its polymerization has only been successful to a certain extent, as characteristic peaks corresponding to protons from the dioxepin polymer backbone are present but the respective integration is low, suggesting low incorporation into the copolymer (Figure 3.3).

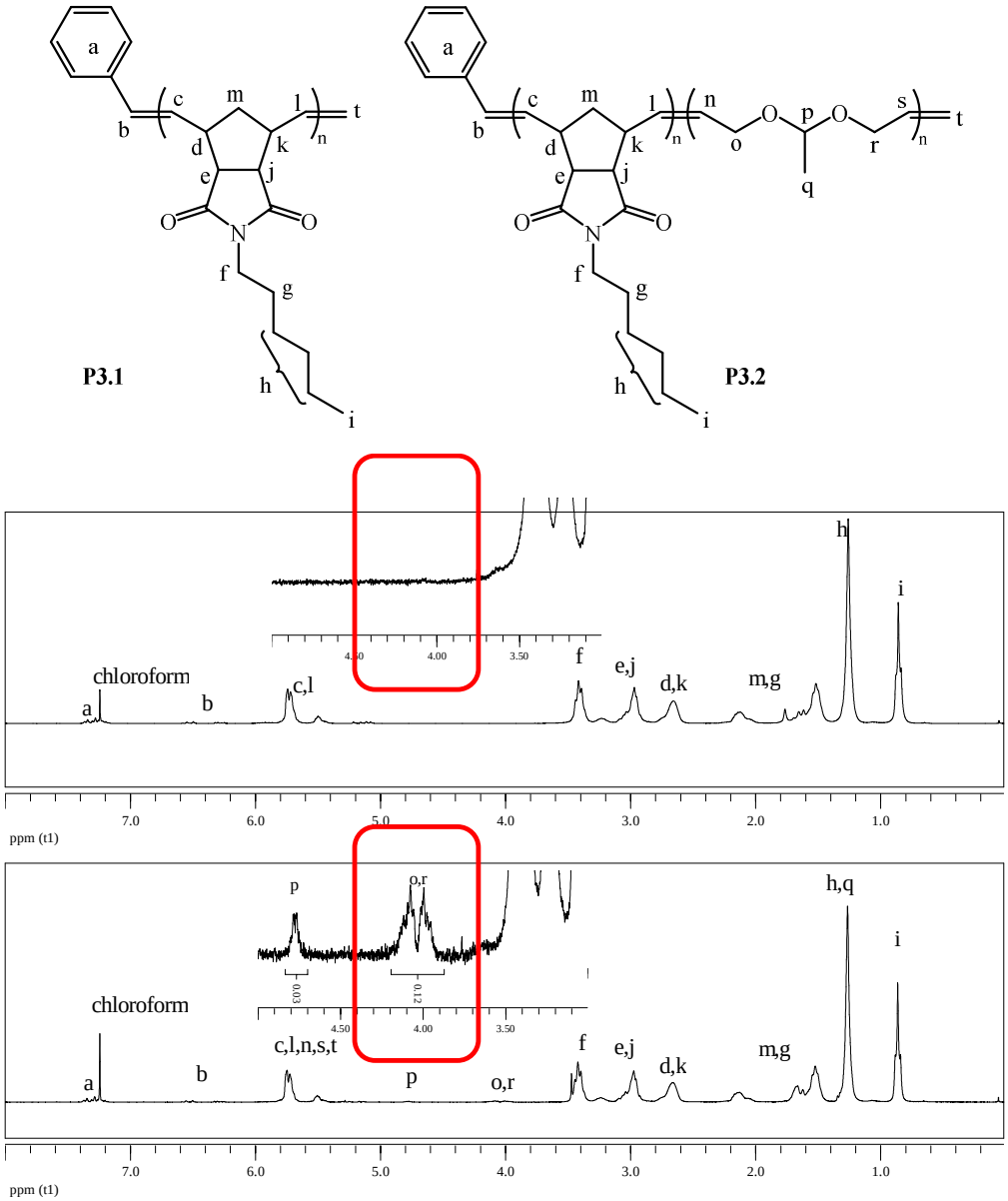

Figure 3.3. Assigned ^{1}H NMR spectra of the isolated polymers **P3.1** before (top) and **P3.2** after (bottom) addition of DxpMe. The insets show the alkoxy proton regions (3-5 ppm) of the respective spectra. ($CDCl_3$, 300 MHz)

The two polymers were also characterized by SEC in order to determine their molecular weight distribution (Figure 3.4).

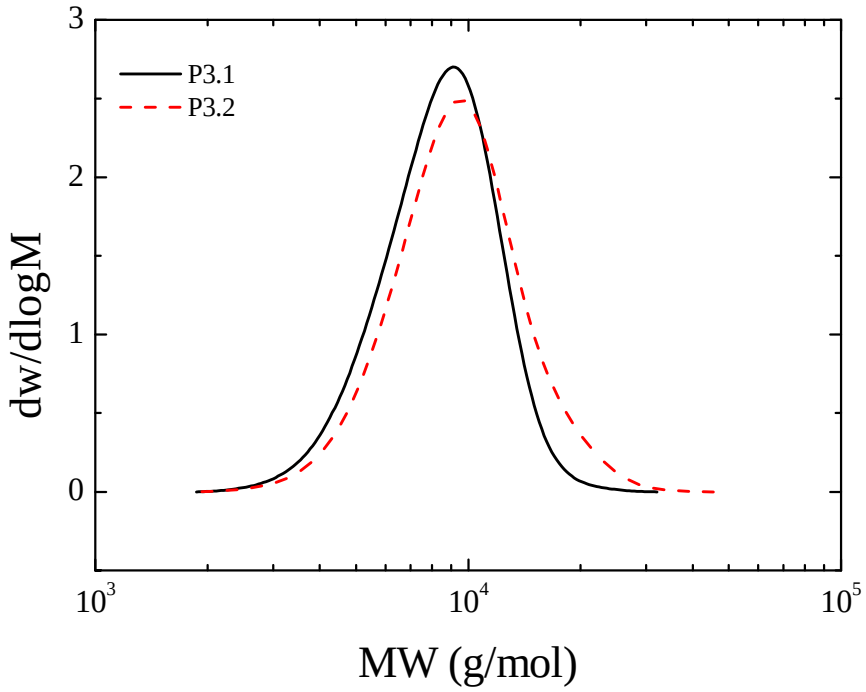

Figure 3.4. Molecular weight distributions obtained by SEC in THF for polymers **P3.1** and **P3.2**.

No significant shift of the polymer distribution was observed, further suggesting the limited success of the chain extension. Additionally, a slight increase of the dispersity (Table 3.1) implies loss of control of the polymerization upon addition of DxpMe.

Table 3.1. Molecular weights and dispersities for the polymers before (**P3.1**) and after (**P3.2**) the addition of DxpMe.

	M_n (g/mol)	M_w (g/mol)	$Đ_M$
P3.1	7,800	8,800	1.13
P3.2	8,600	10,000	1.17

In order to evaluate the degree of chain extension, the polymers were analyzed by MALDI-ToF MS (Figure 3.5).

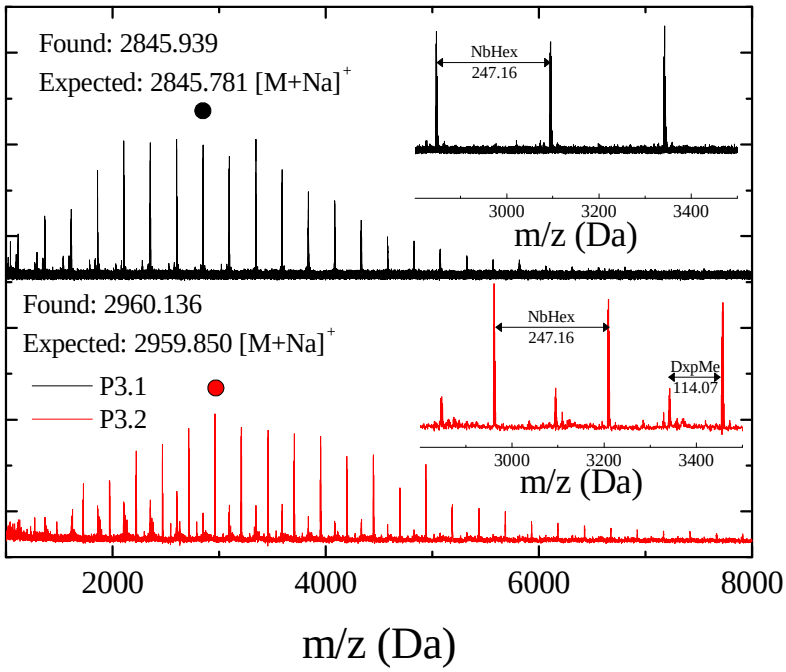

Figure 3.5. MALDI-ToF mass spectra of the two polymers: **P3.1** (top) and **P3.2** (bottom). The inset shows an expanded region of the respective spectra indicating the peak spacing from the monomer additions.

For **P3.1** the mass difference between peaks corresponds to one NbHex unit (247.16 Da) with no other distribution observed however for **P3.2** two distributions are observed. The lower intensity distribution corresponds to the **P3.1** peaks, suggesting no dioxepin was added. The dominant distribution, however, was found to correspond to a polymer with a repeat unit of 247.16 Da and a mass shift of 114.07 Da. This was attributed to the addition of a single DxpMe unit, as corroborated by the good agreement of the expected and measured m/z values. It should also be noted that addition of a second DxpMe unit per polymer chain would result in masses that were not observed (such as 3050.928 Da). These results suggest that homopolymerization of DxpMe, even initiated by the more activated alkylidene presented by the living chain end of a poly(norbornene), is not possible under the conditions employed.

In order to assess whether this is a result of premature termination or steric shielding of the alkylidene, another poly(norbornene) was chain extended with dioxepin before a second norbornene monomer was presented in order to attempt chain extension. Once again, *exo*NbHex was chosen as the first block monomer (Scheme 3.5) and DxpMe as the second block dioxepin, while for the third block *exo*NbPyr was employed as its pyrene functionality has a characteristic UV absorption and can be exploited for further characterization.

Three products were isolated and characterized; the poly(NbHex) homopolymer (**P3.3**), after chain extension with DxpMe (**P3.4**), after chain extension with *exo*NbPyr (**P3.5**), and the product (**P3.5h**) from the exposure of **P3.5** to HCl that is expected to hydrolyze the acetal moiety.

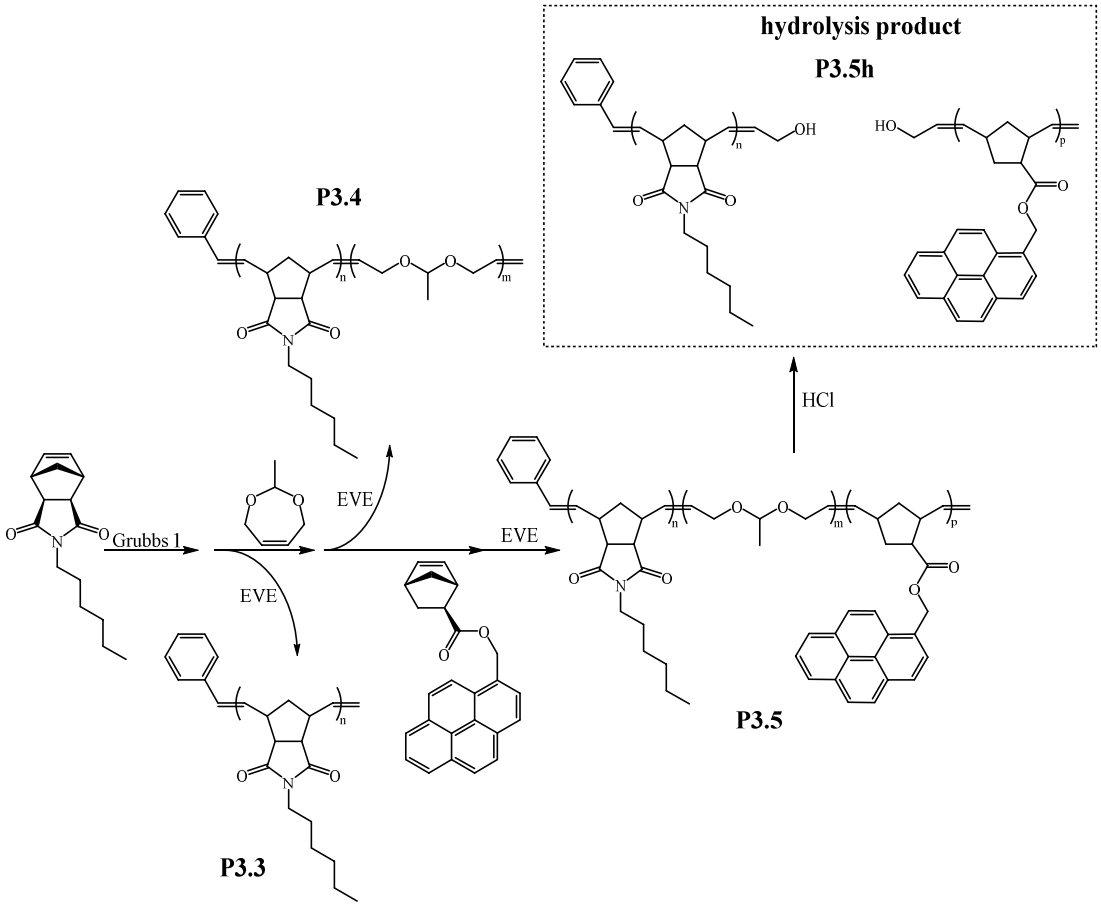

Scheme 3.5. Schematic representation of the synthetic pathway for the synthesis of polymers **P3.3**, **P3.4**, **P3.5**, and the hydrolysis of **P3.5**.

Characterization by SEC (Figure 3.6) revealed, as previously, a controlled polymerization for *exo*NbHex resulting in **P3.3** having a molecular weight of M_n = 3.7 kDa and a $Đ_M$ of 1.17. Addition of DxpMe slightly increased the molecular weight to M_n = 4.0 kDa while further chain extension with *exo*NbPyr resulted in the shifting of the entire molecular weight distribution and increase of the molecular weight to M_n = 5.0 kDa. This demonstrates that addition of DxpMe to the reaction does not result in termination as further chain extension is possible, confirming the expected living nature of the polymerization.

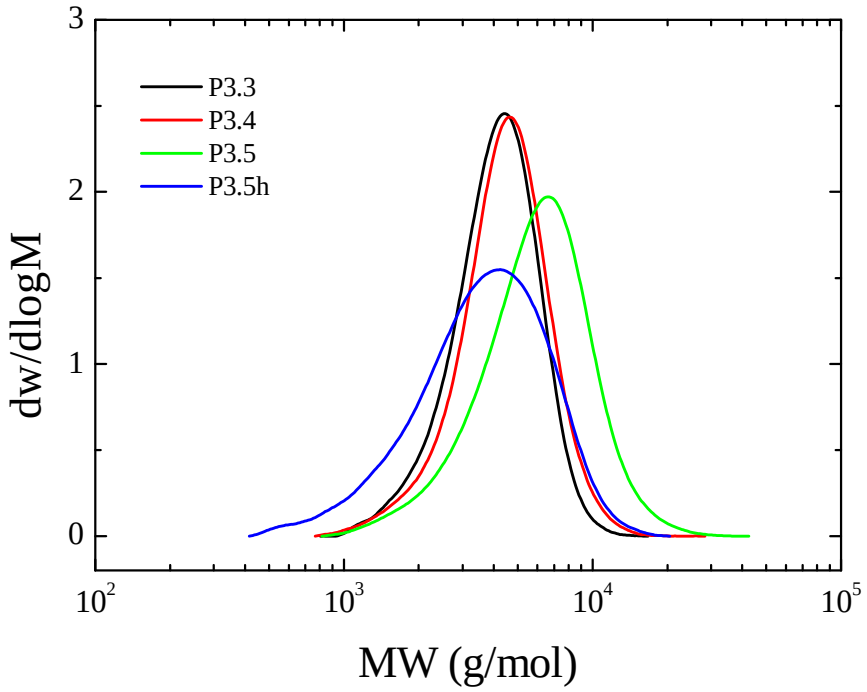

Figure 3.6. Molecular weight distributions of polymers **P3.3**, **P3.4**, **P3.5**, and the hydrolysis product **P3.5h**, obtained by SEC in THF using a DRI detector.

Additionally, using a UV detector (λ = 343 nm) the triblock **P3.5** molecular weight distribution (Figure 3.7) was found to be of similar shape as the distribution from the DRI detector, suggesting homogeneous incorporation of the pyrene moiety on all polymer chains.

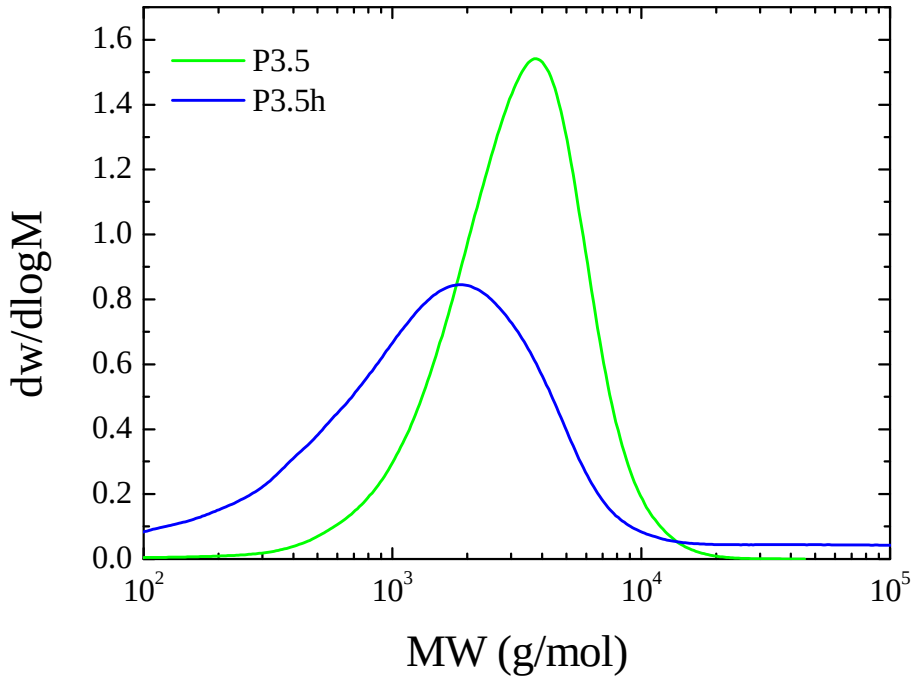

Figure 3.7. SEC (in THF) molecular weight distributions of polymers **P3.5** and the hydrolysis product **P3.5h**, using a UV detector at λ = 343 nm.

Table 3.2. Molecular weights and dispersities for polymers **P3.3**, **3.4**, **3.5**, and the hydrolysis product **P3.5h**.

	M_n (g/mol)	M_w (g/mol)	$Đ_M$
P3.3	3,700	4,400	1.17
P3.4	4,000	4,800	1.20
P3.5	5,000	6,600	1.31
P3.5h	2,900	4,200	1.44

In order to confirm the presence of DxpMe in the polymer, **P3.5** was exposed to acidic conditions (HCl) that would cleave the acetal moiety, resulting in two norbornene homopolymers (Scheme 3.5). The polymer distribution was found by SEC to correspond to a polymer with lower molecular weight than **P3.5** suggesting the successful scission of the polymer backbone (Figure 3.7). Additionally, the increase of the polymer

dispersity compared to either **P3.5** or **P3.3** suggests the presence of two polymer distributions. The separation of the two distributions was attempted *via* chromatography, however as their respective molecular weights were similar, the isolation of either polymer was not possible.

Nevertheless, it was concluded that dioxepins are able to undergo metathesis and add to a living poly(norbornene) maintaining the living nature of the polymerization, as further chain extension is possible, but their homopolymerization is not possible under the studied conditions.

It should be noted that these finding contradict the literature which suggests that ROMP of dioxepins is possible. However, when Kilbinger *et al.* first reported the polymerization of dioxepins as sacrificial monomers to yield hydroxyl-terminal poly(norbornene)s, they justified the shifting of the molecular weight distribution to the successful polymerization of the added dioxepin. Yet, at the time that dioxepin was added, the polymerization of norbornene had only achieved 60% conversion, and therefore the observed increase in the molecular weight was most likely a result of the chain extension of poly(norbornene) with a norbornene-dioxepin copolymer.[18] In a later study, dioxepin was added after the complete consumption of norbornene, however no increase in the molecular weight of the polymer was shown.[22] Additionally, both Kilbinger and Wurm reported the homopolymerization of diazaphosphepine-type monomers only when highly reactive catalysts were employed. When Grubbs 1st generation ruthenium catalyst was used, no polymer was formed.[25, 49] In the original study of Grubbs *et al.* where dioxepin and cyclooctadiene were added in the

polymerization in one pot, dioxepin consumption ranging from 40 to 60% were reported.[16] *

3.3.1.3. Addition to living poly(NbHex)

Previously,[22] Kilbinger *et al.* were able to determine the reactivity of dioxepins towards the living chain end of a poly(norbornene), using DxpPhe, DxpMe, and an isopropyl-functional dioxepin. The study involved kinetic evaluation of the three monomers as a function of equivalents added, employing two different catalysts (**G1** and its triphenyl phosphine derivative). As these results suggest that a large excess of dioxepin is required for the functionalization of a growing poly(norbornene), and taking into account that dioxepin homopolymerization is unlikely, it was proposed that a large excess of dioxepin will rapidly result in single dioxepin-functional poly(norbornene)s. To pursue complete single dioxepin functionalization, *exo*NbHex was polymerized using **G1** as the catalyst (**P3.6**) before the addition of a large excess (100 equivalents) of DxpMe. After quenching the reaction, the polymer **P3.7** was studied by MALDI-ToF MS (Figure 3.8).

* It should be noted that it was later found that dioxepins can undergo homopolymerization under different conditions whereby a Lewis acid was added to the mixture (unpublished data).

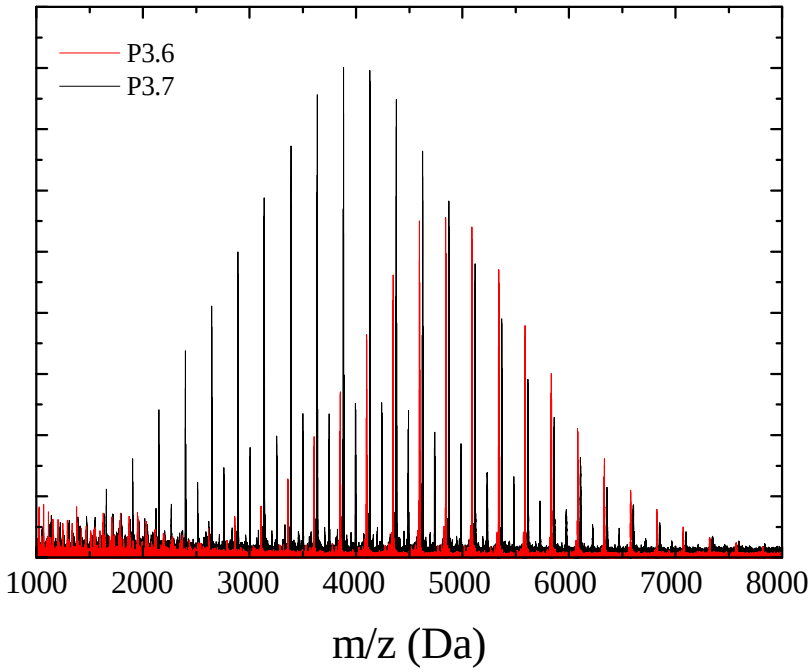

Figure 3.8. MALDI-ToF mass spectra of the polymer before (**P3.6**) and after the addition of 100 eq. DxpMe (**P3.7**).

While the poly(NbHex) homopolymer exhibited a uniform distribution of masses corresponding to the NbHex repeat units, upon addition of DxpMe the distribution appears to shift to lower masses. This was deemed to be an artefact attributed to the decreased ability of higher molecular weight dioxepin-containing polymers to ionize, and thus be detected. To confirm this hypothesis, the two polymers were studied by SEC (Figure 3.9).

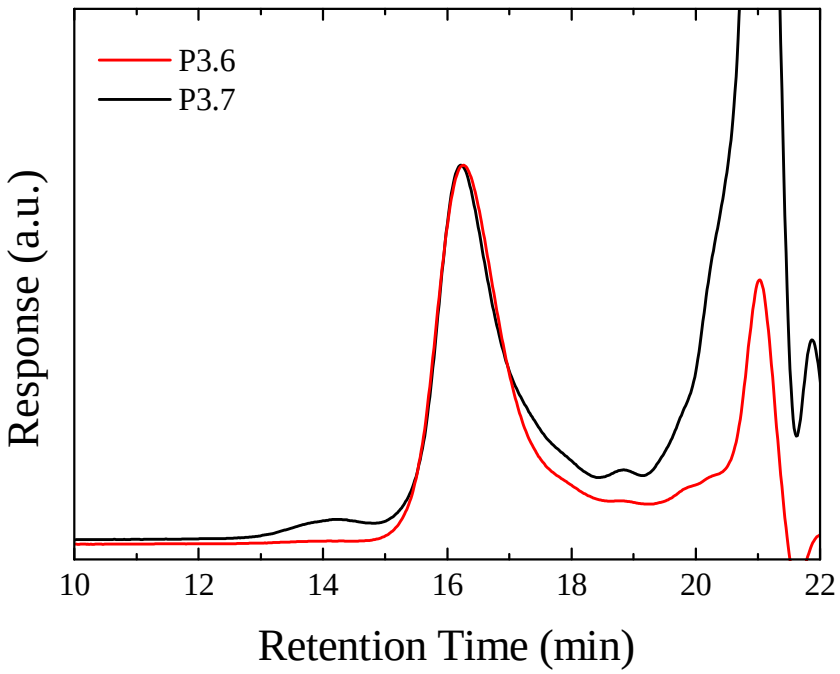

Figure 3.9. Chromatograms of the polymers before (**P3.6**) and after (**P3.7**) addition of DxpMe (SEC in THF).

The chromatograms reveal that the peaks corresponding to the main polymer distribution are similar, however a peak at lower retention times, and thus higher molecular weight, is observed for **P3.7**, as well as tailing towards higher retention times, therefore lower molecular weight, for the main peak. These results suggest that the main polymer distribution was not compromised by the addition of DxpMe, however it has had an effect. Therefore, the MALDI-ToF mass spectra were further studied in an attempt to identify the new polymer populations.

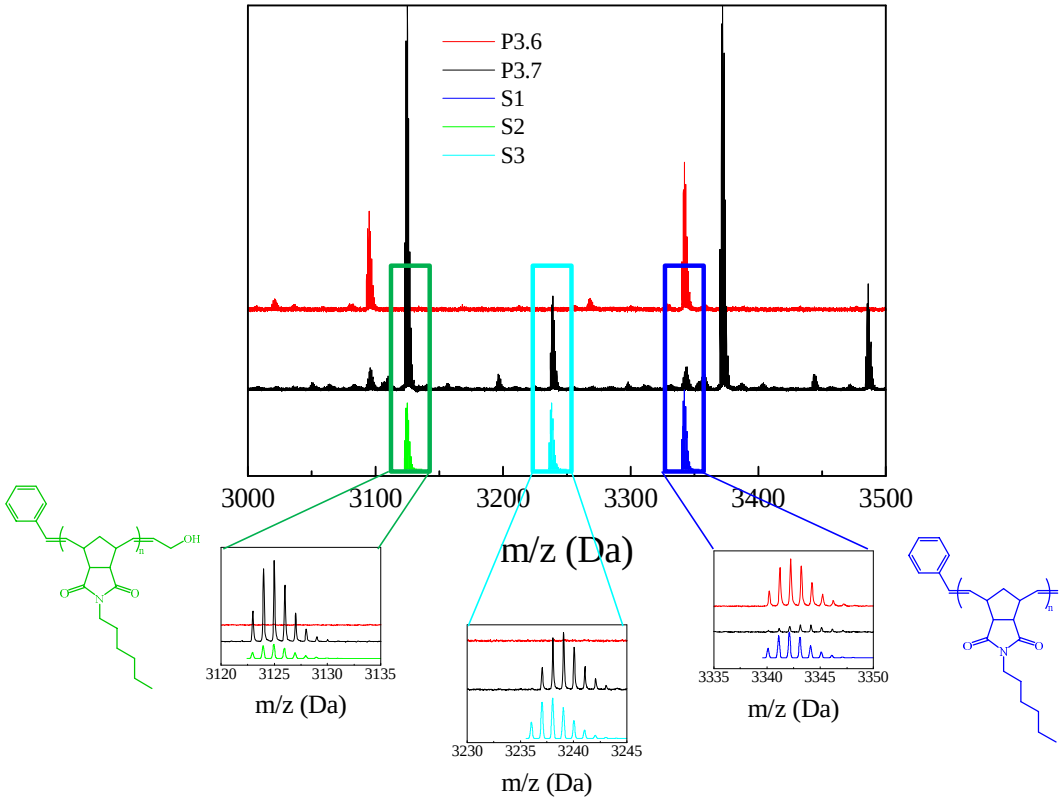

Figure 3.10. Expanded regions of the MALDI-ToF mass spectra of polymers **P3.6** and **P3.7**, and the simulated mass distributions S1-S3. S1 corresponds to the simulated masses of poly(NbHex), S2 to poly(NbHex)-COH, and S3 to cyclized poly(NbHex).

Before addition of DxpMe, the studied masses obtained for **P3.6** correspond to the calculated masses for $C_{203}H_{281}N_{13}O_{26}Na^{+}$, which is the chemical formula for poly(NbHex) with a degree of polymerization (DP) of 13 (sodium adduct). After addition of DxpMe, three of the populations of **P3.7** could be assigned. The primary population was found to correspond to the calculated masses for $C_{189}H_{262}N_{12}O_{25}Na$, which is the chemical formula for poly(NbHex)-COH, that is the product of the hydrolyzed block copolymer of poly(NbHex)-*b*-poly(DxpMe) where the DP of the norbornene block is 12. The secondary population did not correspond to any expected masses, however, since ROMP is prone to backbiting, the simulated peaks correspond to a cyclic poly(NbHex) with a DP of 13 ($C_{195}H_{273}N_{13}O_{26}Na$). While initial comparison

suggests that indeed backbiting has taken place, careful examination shows a difference of 1 Da, therefore the peak cannot be conclusively assigned. Smaller populations were attributed to different adducts, as well as derivatives of the main populations owing to the by-products of the monomer. It should be noted that although **P3.7** was not exposed to acidic conditions, all dioxepin content was found to be hydrolyzed based on the MALDI-ToF MS results. This could be attributed to the higher energy voltage required for the characterization of the polymers that was deemed necessary, as crystallization of the matrix was hindered by the high DxpMe content of the sample. Indeed, upon characterization by ^{1}H NMR spectroscopy (Figure 3.11) the acetal proton peak (δ = 4.7 ppm) was observed, suggesting that the polymer backbone is intact under normal conditions.

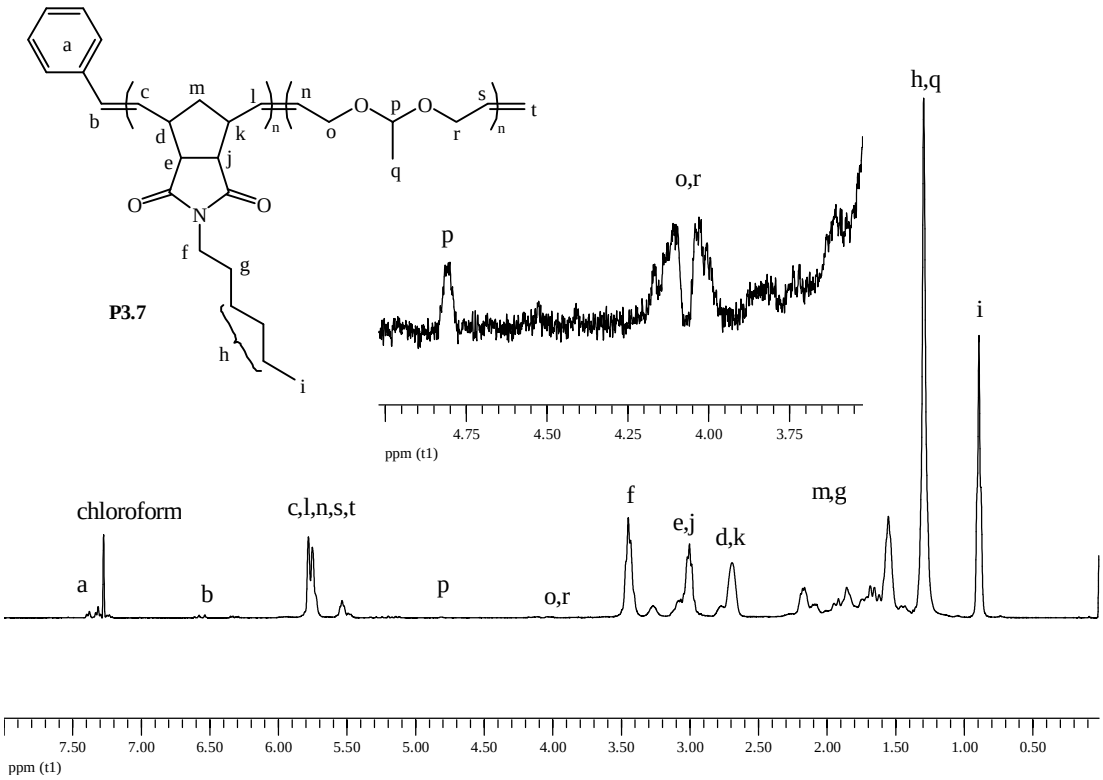

Figure 3.11. Assigned ^{1}H NMR spectrum of the **P3.7** polymer and the acetal region expanded ($CDCl_3$, 300 MHz).

Although no conclusive proof by MALDI-ToF MS was obtained that the dioxepin addition only resulted in a single dioxepin equivalent being added, based on the high chain-end modification and the presence of the acetal in the final polymer (as shown by ^{1}H NMR spectroscopy) strongly implies that this is indeed the case. Nevertheless, while adding large excess of dioxepin can indeed result in the more rapid functionalization with a single DxpMe moiety, it was shown that there is risk of side reactions that will effectively compromise the uniformity of the polymer.

While it was demonstrated that addition of dioxepins onto a pre-formed living poly(norbornene) is possible, and that it results in a single monomer addition, the ability of dioxepins to react with a living poly(norbornene) synthesized by the slower and sterically hindered *endo* isomer is yet undetermined. As such and in an attempt to monitor the rate of the dioxepin addition, 2-(1-pyrenyl)-4,7-dihydro-2*H*-1,3-dioxepin (DxpPyr) was chosen, as the pyrene moiety could be exploited for further characterization of the polymer based on its characteristic UV absorption. The addition of a moderate excess of dioxepin (5 equivalents) to the ROMP of *endo*NbHex (**P3.8**) was evaluated by monitoring the addition by SEC (Figure 3.12) using both a DRI detector and a UV (λ = 343 nm) detector.

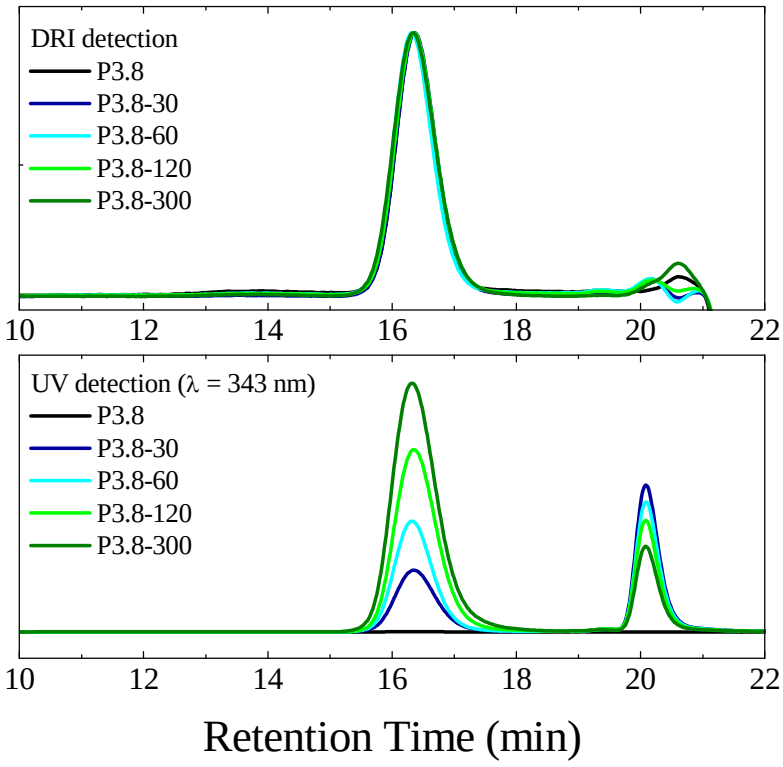

Figure 3.12. Chromatograms of polymer **P3.8** and at different intervals after the addition of DxpPyr, detected by DRI (top) and UV (λ = 343 nm) (bottom) (SEC in THF).

As expected, the parent polymer (**P3.8**) exhibited a Gaussian distribution, indicating control of the polymerization, while no signal was detected by the UV detector because poly(NbHex) does not absorb at λ = 343 nm. After the addition of DxpPyr, a gradual increase of the intensity of the UV signal indicates gradual incorporation of the pyrene moiety. Additionally, no shifting of the retention time of the polymer peak is observed, suggesting that DxpPyr does not significantly change the molecular weight of the polymer (Table 3.3). It can be therefore inferred that once again a single monomer addition is achieved.

Table 3.3. Molecular weights and molecular weight distributions for **P3.8** and the samples after addition of DxpPyr.

	Reaction Time (min)	M_n (kDa)	M_w (kDa)	$Đ_M$
P3.8	0	3.6	4.0	1.11
P3.8-30	30	3.5	4.0	1.14
P3.8-60	60	3.7	4.2	1.13
P3.8-120	120	3.5	4.0	1.14
P3.8-300	300	3.5	4.1	1.17

In order to evaluate the successful functionalization of the poly(NbHex) chain-end, the samples were also studied by MALDI-ToF MS (Figure 3.13).

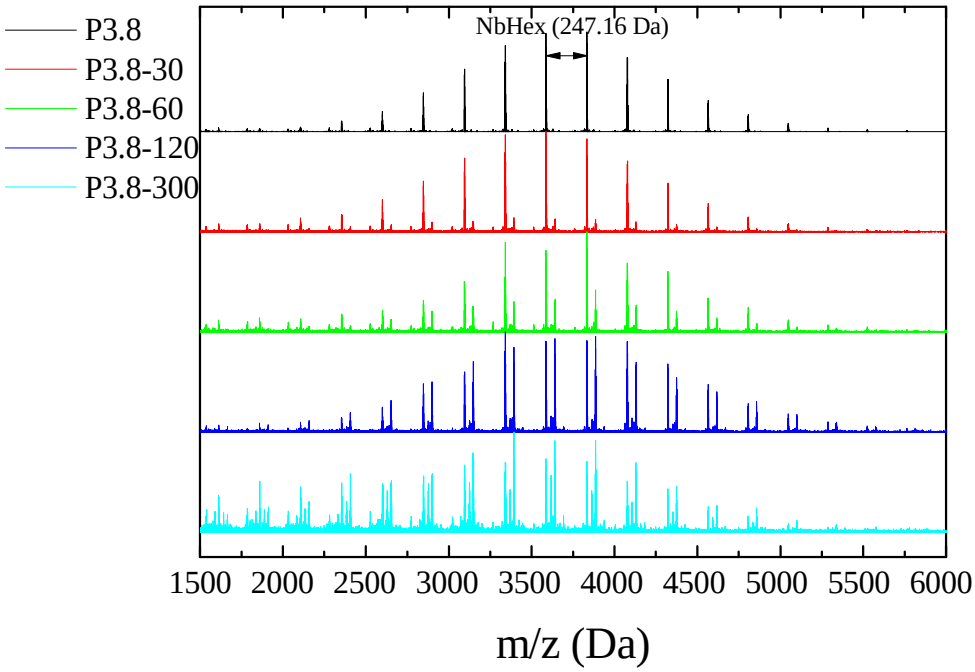

Figure 3.13. MALDI-ToF mass spectra for **P3.8** and after addition of DxpPyr at different time intervals.

Initially, for **P3.8** a uniform distribution was obtained, with the distance between peaks corresponding to the mass of an *endo*NbHex repeat unit. After addition of DxpPyr (**P3.8-30**) a new distribution appears. The relative intensity of the new distribution

further increases with reaction time, although the unfunctionalized polymer distribution is still observed.

Additionally, a third distribution can be seen at longer reaction times (**P3.8-120**, **P3.8-300**). Careful study of an expanded region of the spectra revealed that the second distribution corresponds to the addition of a single DxpPyr moiety (Figure 3.14).

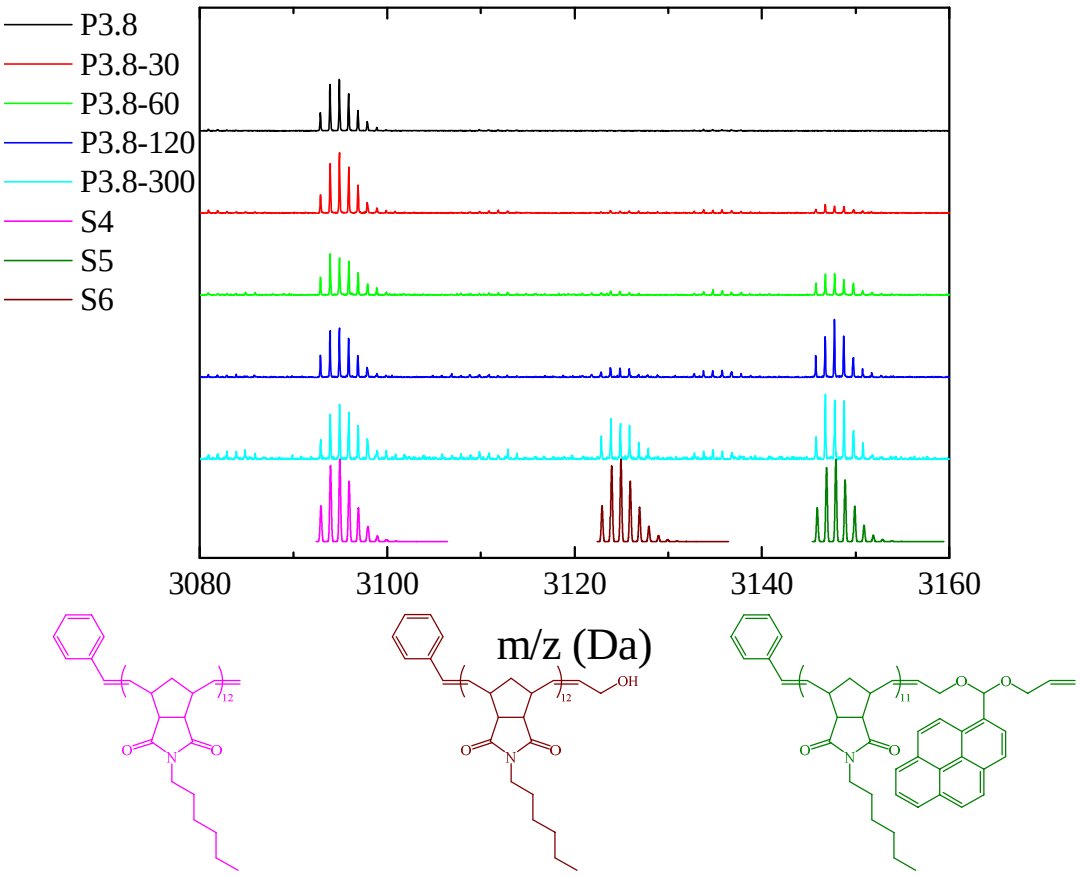

Figure 3.14. Expanded region of the MALDI-ToF mass spectra for **P3.8** and after addition of DxpPyr at different time intervals, as well as the predicted isotopic distributions for poly(NbHex) (S4), poly(NbHex)-DxpPyr (S5), and poly(NbHex)-COH (S6). Structures correspond to the simulated isotopic distributions.

To confirm the single addition of the DxpPyr moiety, the predicted isotopic distribution for $C_{188}H_{260}N_{12}O_{24}Na$, which is the chemical formula for the sodium adduct of

poly(NbHex) with a DP = 12 was plotted (**S4**) and found to overlay with the obtained peaks. Similarly, the predicted isotopic distribution for $C_{194}H_{255}N_{11}O_{24}Na$, which is the chemical formula of the sodium adduct of poly(NbHex)-*co*-poly(DxpPyr) with a DP_{NbHex} = 11 and DP_{DxpPyr} = 1 (**S5**) was found to match the obtained peaks, further confirming the successful single addition of the polymer with DxpPyr. The third distribution was found to agree with the chemical formula $C_{189}H_{262}N_{12}O_{25}Na$, which corresponds to the hydrolyzed product of poly(NbHex)-*co*-poly(DxpPyr), with a DP_{NbHex} = 12 (**S6**). The final copolymer was also characterized by ^{1}H NMR spectroscopy (Figure 3.15).

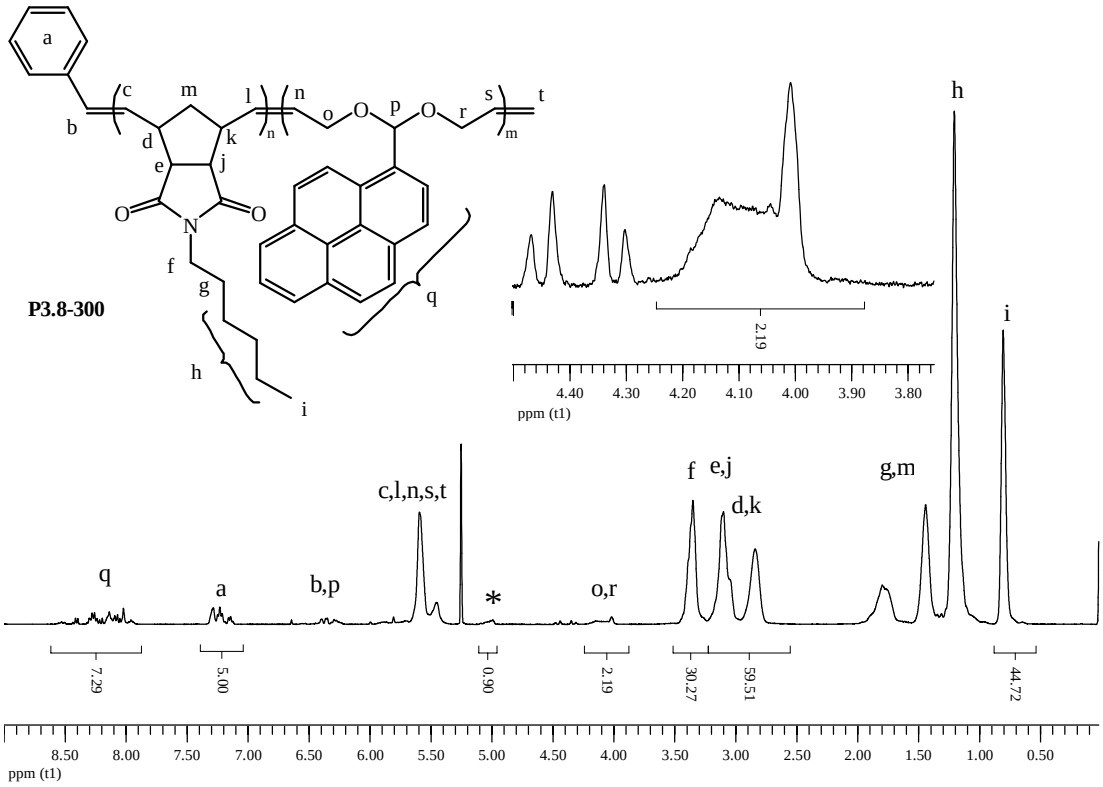

Figure 3.15. Assigned ^{1}H NMR spectrum of the **P3.8-300** polymer and the 4.5-3.8 ppm region expanded. The signal marked with a star corresponds to the unfunctionalized **P3.8** chain-end protons (CD_2Cl_2, 400 MHz).

The presence of a signal that corresponds to the protons of the **P3.8** chain end (δ = 5 ppm) confirms the finding by MALDI that even after five hours, some

poly(NbHex) homopolymer still remains. It should also be noted that signals corresponding to unreacted DxpPyr protons were also observed (δ = 4.4 ppm).

Although complete functionalization was not obtained, even after 5 hours of exposure to DxpPyr, the successful addition of a single equivalent of DxpPyr was obtained, highlighting the potential use of dioxepins for the single functionalization of poly(norbornene)s obtained by ROMP of the *endo* isomer of the monomer. This possibility expands the scope of the precision polymers by ROMP as presented in Chapter 2.

3.3.2. Evaluation of the reactivity of functional dioxepins

3.3.2.1. Reactivity ratios

While the above results demonstrate the reactivity of dioxepins towards an alkylidene presented as a living poly(norbornene), it does not elucidate their reactivity when competing with other norbornenes. Therefore, the determination of their reactivity ratio was sought.[50] The reactivity ratios of two monomers are defined by their relative rates of polymerization (equation 3.1).

$$r_1 = \frac{k_{11}}{k_{12}} \qquad r_2 = \frac{k_{22}}{k_{21}} \tag{3.1}$$

These ratios express the probability of each monomer (namely M_1 and M_2) to react with a polymer chain, if the final monomer on the chain is the same (k_{11} and k_{22} respectively), or the other (k_{12} and k_{21} respectively). In a random copolymerization, r_1 and r_2 are both equal to 1, while in an alternating copolymerization both values are close to zero. Additionally, if r_1 (or r_2) is greater than 1, homopolymerization of M_1 (or M_2

respectively) is favored. It should, however, be noted that these are derivations from the differential Mayo-Lewis model for a copolymer composition (equation 3.2).

$$F_1 = \frac{r_1 f_1^2 + f_1 f_2}{r_1 f_1^2 + 2 f_1 f_2 + r_2 f_2^2} \qquad \textbf{3.2}$$

The assumptions that lead to this equation be used for the determination of the relative reactivity ratios of two monomers do not necessarily apply to ROMP. For example, ROMP is theoretically a reversible process. However, as one of the monomers used here is a bulky norbornene, it can be assumed that de-polymerization, as well as back-biting is negligible.[51] Additionally, it has been postulated that "chain editing" is possible *via* cross-metathesis with a backbone alkene and the incoming monomer.[48] Although such a phenomenon has not been observed in the chain extension of poly(norbornene) with dioxepins (see section 3.3.1.1), it should not be dismissed and should be taken into account when determining the reactivity ratios.

3.3.2.2. Calculation of the reactivity ratios of dioxepins and *exo*NbHex

Previous results suggest that the living chain end of a polymer synthesized using *exo*NbHex as the monomer is readily reactive towards dioxepin, which in turn, upon polymerization, is reactive towards other *exo* norbornenes. It is therefore anticipated that when both *exo* norbornene and dioxepin monomers are present in a polymerization, they will both contribute towards the final copolymer. To evaluate this, the copolymerizations of DxpMe and *exo*NbHex, with monomer feed ratios (f_i) ranging from 0.1 up to 0.9 and a target overall degree of polymerization (DP) of 40 repeat units, were studied by ^{1}H NMR spectroscopy.

In similarity to what was observed in Chapter 2, the polymerization of *exo*NbHex was too fast to monitor the conversion by ^{1}H NMR spectroscopy, with the monomer reaching 100% conversion before a spectrum was obtained. Nevertheless, the copolymer composition (F_1) was assessed with respect to dioxepin incorporation (Figure 3.16).

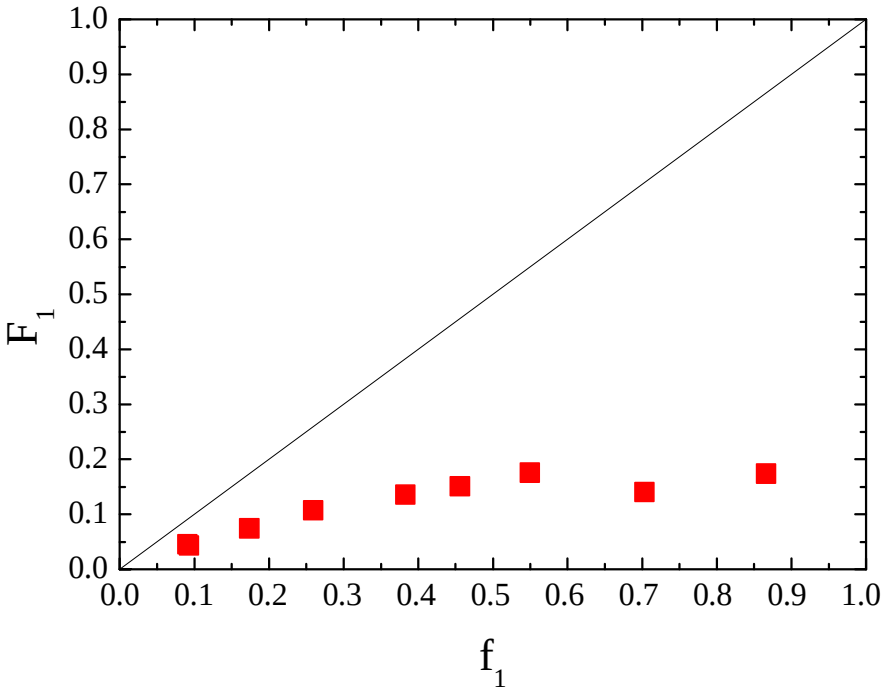

Figure 3.16. Polymer DxpMe content (F_1) with respect to monomer DxpMe feed ratio (f_1) in the copolymerization with *exo*NbHex as determined by ^{1}H NMR spectroscopy. Line shows ideal random copolymerization.

It is apparent that regardless of the dioxepin monomer feed, the copolymer composition never exceeds 20% dioxepin. This is also reflected in the DxpMe monomer conversion which drops with increasing monomer feed. Because of the difference in the conversions of the two monomers, it is impossible to calculate the reactivity ratios, but the conclusion drawn from this series of experiments is that DxpMe is significantly less reactive towards the alkylidene on the poly(NbHex) living end, than the *exo*NbHex is towards the poly(NbHex) chain end.

The same concept was applied to the copolymerization of *exo*NbHex and DxpPhe (Figure 3.17) and the resulting graph was found to be similar to that obtained for the copolymerization of *exo*NbHex with DxpMe.

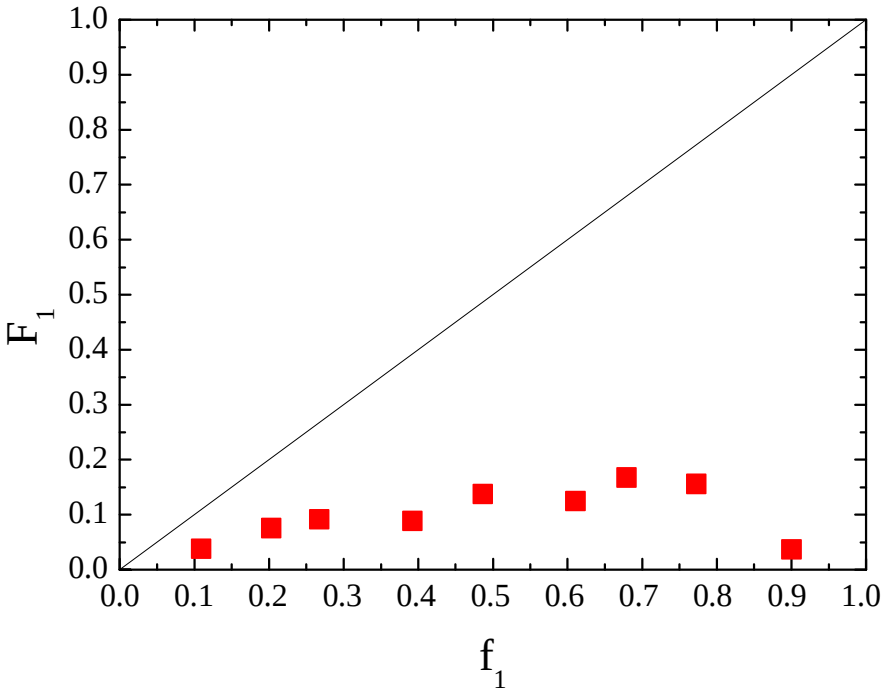

Figure 3.17. Polymer DxpPhe content (F_1) with respect to monomer DxpPhe feed ratio (f_1) in the copolymerization with *exo*NbHex determined by ^{1}H NMR spectroscopy. Line shows ideal random copolymerization.

Once again, the results are skewed by the dissimilar conversions of the two monomers, nevertheless they show the significantly lower reactivity of DxpPhe compared to *exo*NbHex.

It was therefore concluded that dioxepins are significantly less reactive than *exo* norbornenes with the functional group not playing an obvious role to the reactivity.

3.3.2.3. Calculation of the reactivity ratios of dioxepins and *endo*NbHex

While *exo* norbornenes were found to be significantly more reactive than dioxepins, and therefore not applicable for sequence-controlled polymers, it was hypothesized that *endo* norbornenes, that are sterically hindered and result in slower polymerization, would be a better candidate. To evaluate this hypothesis, *endo*NbHex was copolymerized with DxpPhe at different monomer feed ratios in order to calculate their reactivity ratios. Since *endo* norbornenes are less reactive, the polymerizations were monitored by ^{1}H NMR spectroscopy and upon reaching overall monomer conversion of ~10%, the polymer composition in dioxepin was measured and plotted against the dioxepin monomer feed ratio (Figure 3.18).

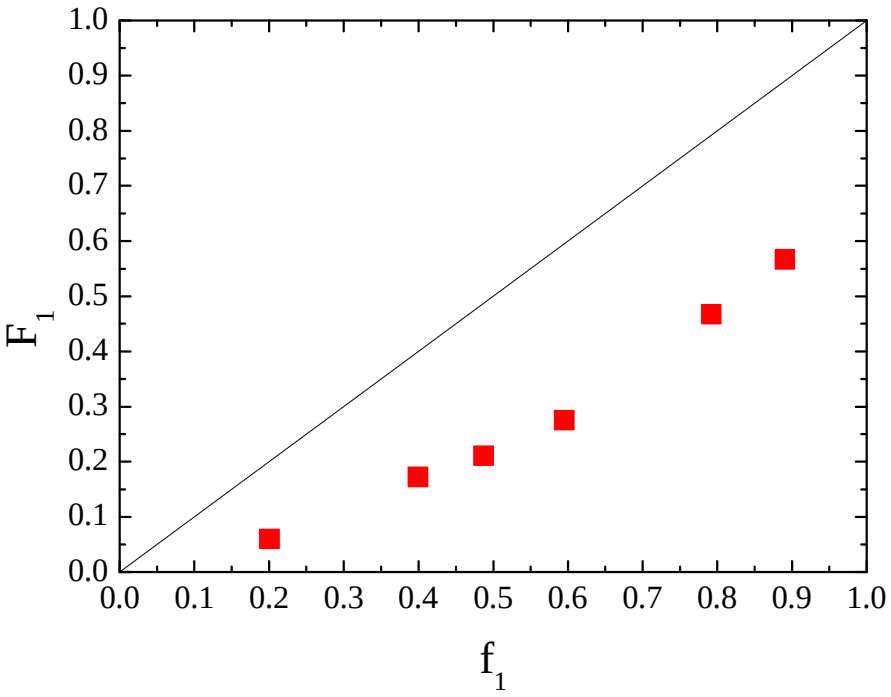

Figure 3.18. Polymer DxpPhe content (F_1) with respect to monomer DxpPhe feed ratio (f_1) in the copolymerization with *endo*NbHex determined by ^{1}H NMR spectroscopy. Line shows ideal random copolymerization.

It is obvious that unlike the copolymerization with the *exo* norbornene isomer, DxpPhe participates in the copolymerization with *endo*NbHex reaching copolymer compositions of up to 55%. From these results, the calculation of the reactivity ratios r_1 and r_2 were possible using Contour, a software developed by van Herk which applies a non-linear least squares (NLLS) method.[52] The reactivity ratios were found to be 0.19 for DxpPhe (r_1) and 3.48 for *endo*NbHex (r_2) with the confidence intervals shown in Figure 3.19.

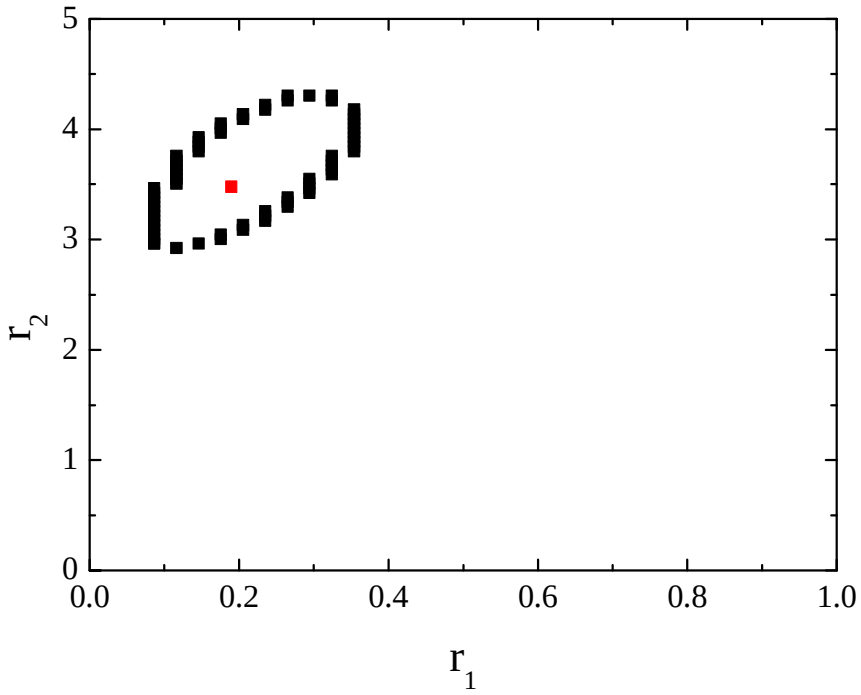

Figure 3.19. Plot of joint confidence intervals (95%) of the reactivity ratios for DxpPhe (r_1) and *endo*NbHex (r_2).

While the margins of error are quite broad, it is concluded that r_2 is significantly larger than unity, and thus based on equation 3.1) k_{22} is greater than k_{21} which further suggests that *endo*NbHex is more likely to react with itself than with DxpPhe. However, r_1 is much smaller than unity which suggests that k_{11} is smaller than k_{12} and therefore DxpPhe is more likely to react with *endo*NbHex than with itself.

These results, combined with previously acquired knowledge (Chapter 2) show that although both *endo*NbHex and DxpPhe struggle to homopolymerize, in a competitive environment *endo*NbHex is proven more reactive.

3.3.3. Sequential polymerization of norbornene

Based on the findings so far, dioxepins cannot homopolymerize but can add a single monomer to a living poly(norbornene), without compromising the living nature of the polymerization, and thus allowing further addition of norbornene. As such, dioxepins could effectively be added in large excess to the ROMP of norbornene-type monomers and yet achieve single additions and, to an extent, sequence control *via* their precise insertion. To test this hypothesis, the polymerization of *endo* and *exo* norbornenes in the presence of large excess of dioxepin was carried out.

3.3.3.1. Polymerization of *endo* norbornenes in the presence of DxpPhe

Initially, the polymerization of *endo* norbornenes in a solution with a high concentration of dioxepin was sought. The strategy (Scheme 3.6) involved the sequential addition of batches of *endo*NbHex in the reaction mixture where large excess of DxpPhe was present, as it is not expected that DxpPhe will polymerize, despite the presence of **G1** catalyst.

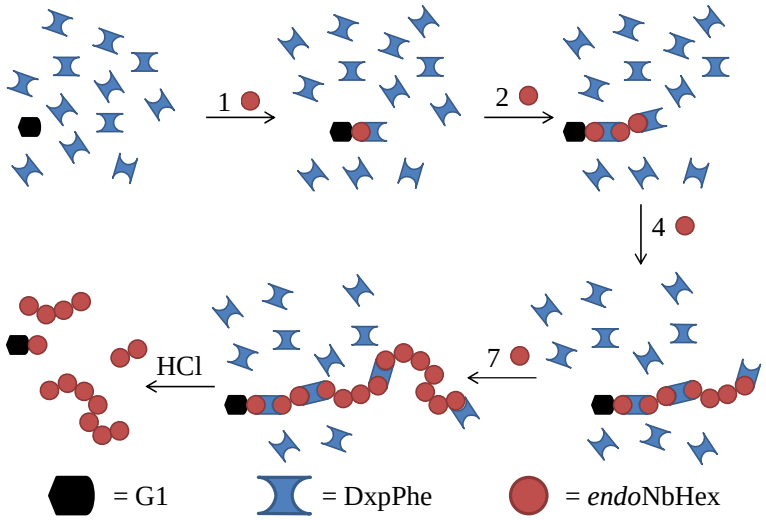

Scheme 3.6. Strategy for the sequential polymerization of *endo*NbHex in the presence of DxpPhe.

As such, DxpPhe (20 eq.) was allowed to react with **G1** before the addition of *endo*NbHex in four batches containing one, two, four, and seven equivalents of the monomer. The duration between each addition was determined by the kinetics of *endo*NbHex homopolymerization, as discussed in Chapter 2. Between additions, a sample was removed from the reaction and characterized by SEC (Figure 3.20) and ^{1}H NMR spectroscopy (**P3.9** after the first batch, **P3.10** after the second batch, **P3.11** after the third batch, and **P3.12** after the fourth batch).

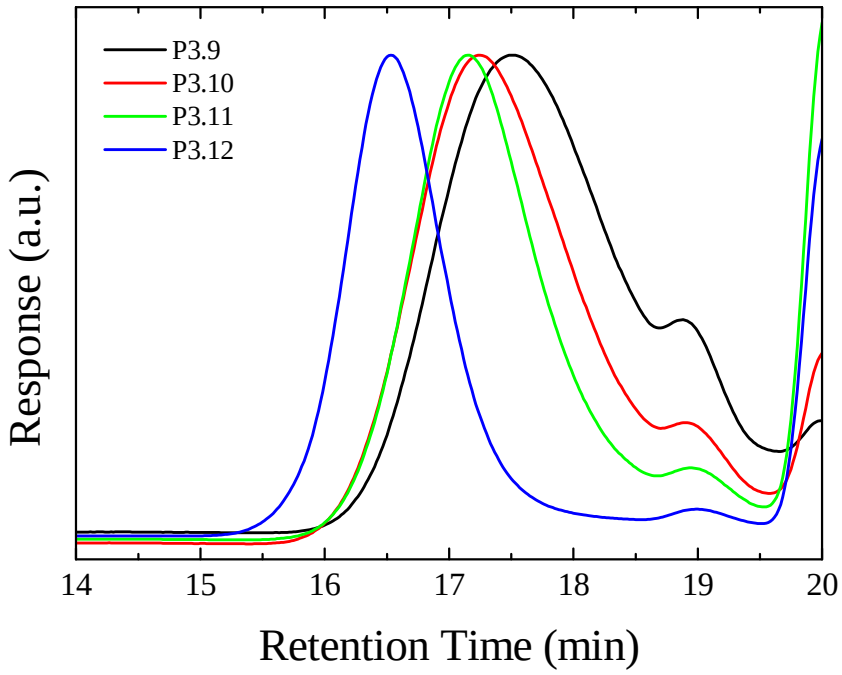

Figure 3.20. Molecular weight distributions of **P3.9**, **P3.10**, **P3.11**, and **P3.12** obtained by SEC.

An apparent shifting to lower retention times, and thus to higher molecular weights with each addition is observed, attributed to the polymerization of *endo*NbHex. A low molecular weight shoulder was also observed and was attributed to termination by-products. Nonetheless, the main polymer distribution peak was used to determine the molecular weights of the polymers (Table 3.4), and the results were plotted against the DP of the poly(NbHex) block (Figure 3.21) determined by ^{1}H NMR spectroscopy.

Table 3.4. Molecular weights and dispersities of **P3.9**, **P3.10**, **P3.11**, and **P3.12**.

	M_n (g/mol)	M_w (g/mol)	$Đ_M$
P3.9	1,600	2,400	1.48
P3.10	2,000	2,900	1.47
P3.11	2,300	3,200	1.39
P3.12	4,400	6,000	1.35

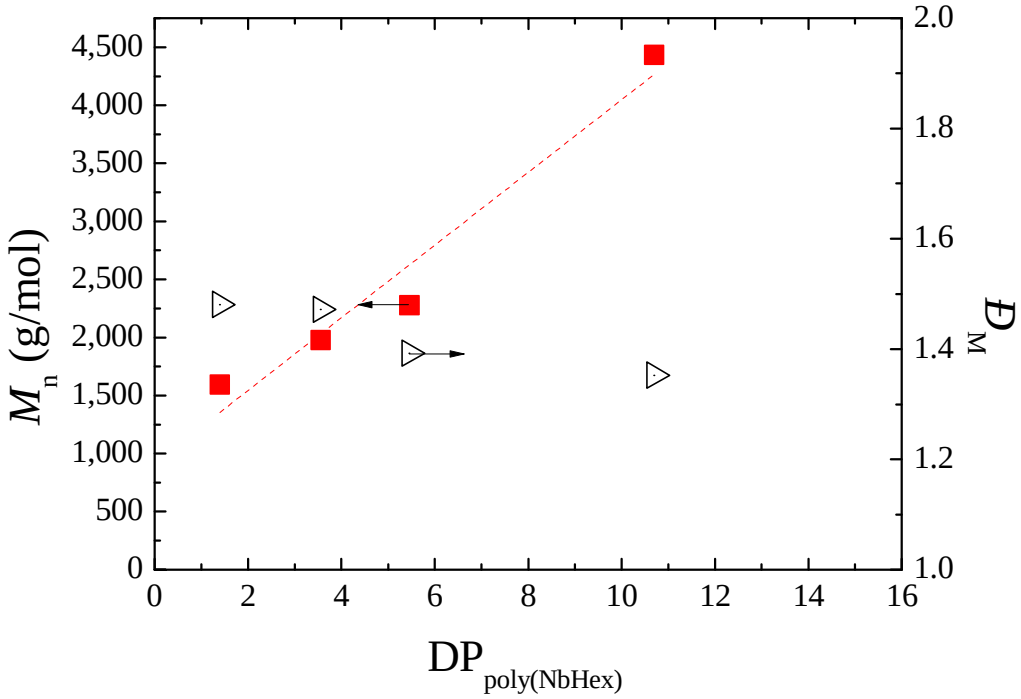

Figure 3.21. Number-average molecular weights and dispersities of **P3.9**, **P3.10**, **P3.11**, and **P3.12** with respect to the DP of the poly(NbHex) blocks, determined by ^{1}H NMR spectroscopy. Dashed line represents the linear fit of the M_n datapoints.

The overall increase in molecular weight of the main population peak with respect to the poly(NbHex) DP, suggests the increase is a result of the addition of *endo*NbHex repeat units with little contribution from the dioxepin monomer. Moreover, decrease of dispersity with each addition indicates the controlled nature of the polymerization.

The polymers were then exposed to acidic conditions in order to hydrolyze the acetal groups in the backbone, subsequently resulting in the corresponding hydroxyl-functional poly(NbHex) oligomers, which were characterized by SEC (Figure 3.22).

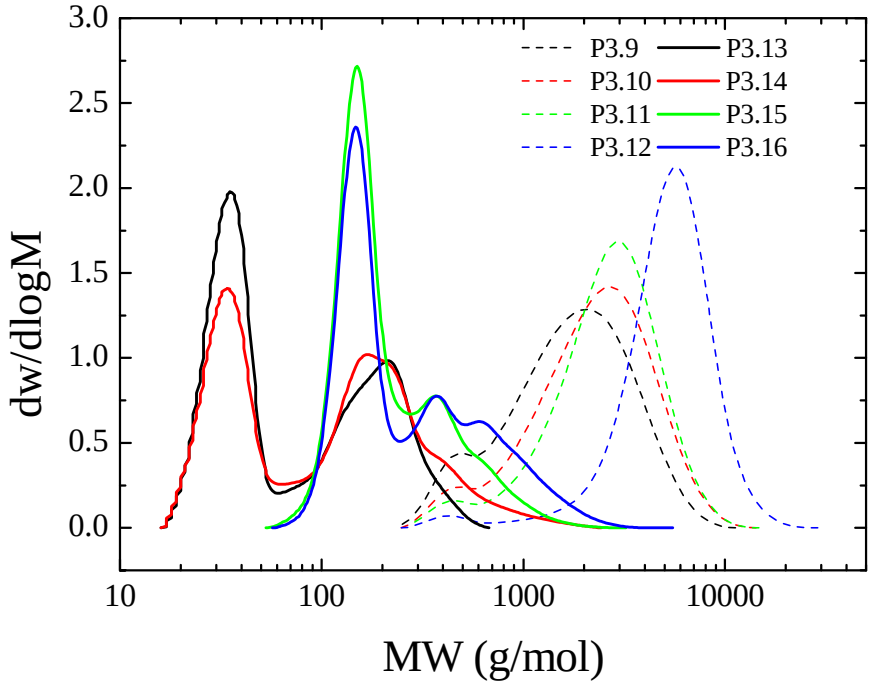

Figure 3.22. SEC molecular weight distributions of the copolymers **P3.9**, **P3.10**, **P3.11**, and **P3.12**, and their hydrolyzed counterparts **P3.13**, **P3.14**, **P3.15**, and **P3.16**.

Shifting of the peaks to lower molecular weights is observed and attributed to the hydrolysis of the acetal moieties in the backbone, while the appearance of multiple distributions suggests that oligomers with different molecular weights were obtained. This indicates that the added equivalents of *endo*NbHex successfully polymerized, before dioxepin could copolymerize, thus resulting in distinct poly(NbHex) blocks connected with a DxpPhe unimer. Nonetheless, it is anticipated that higher molecular weight oligomers would be difficult to obtain as DxpPhe would statistically contribute to the copolymer and thus result in smaller than anticipated poly(NbHex) blocks. This is also supported by the fact that the hydrolysis product from **P3.12**, **P3.16**, does not produce a new peak in the SEC trace, but instead a high molecular weight shoulder, which implies incorporation of DxpPhe within the final poly(NbHex) block.

3.3.3.2. Polymerization of *exo* norbornenes in the presence of DxpMe

Contrary to *endo* norbornenes, based on the higher reactivity of *exo* norbornenes, it was anticipated that their polymerization in the presence of excess dioxepin would proceed with higher precision in the resulting block copolymers. As such, a similar strategy was employed in order to sequentially polymerize *exo* norbornenes in a mixture containing a high concentration of dioxepin. Therefore, in an excess of DxpMe and in the presence of **G1**, *exo*NbHex was added and allowed to polymerize before addition of *exo*NbMorph (Scheme 3.7).

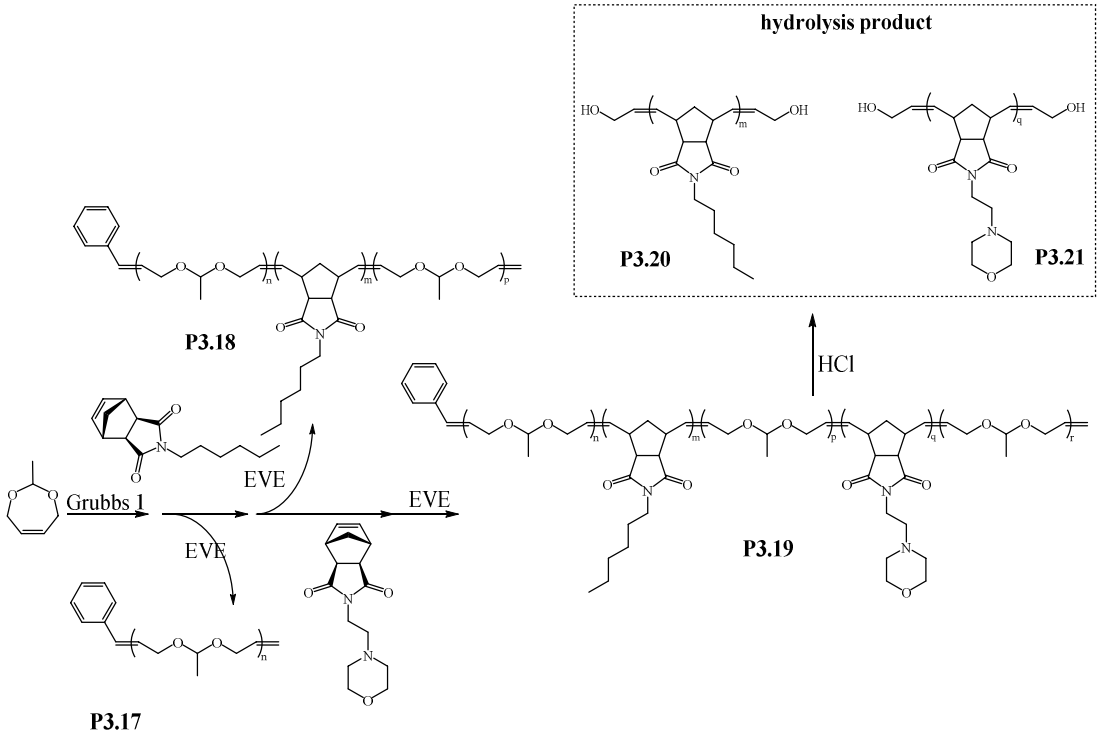

Scheme 3.7. Schematic representation of the procedure followed for the synthesis of **P3.17**, **P3.18**, **P3.19**, **P3.20**, and **P3.21** *via* sequential additions followed by hydrolysis.

After allowing each monomer to react for one hour, three polymer samples were collected: **P3.17** after polymerization of DxpMe, **P3.18** after addition of *exo*NbHex, and **P3.19** after addition of *exo*NbMorph. Additionally, the hydrolysis of **P3.19** should result

in two homopolymers consisting of poly(NbHex) (**P3.20**) and poly(NbMorph) (**P3.21**). All polymers were characterized by SEC and their chromatograms are shown in Figure 3.23.

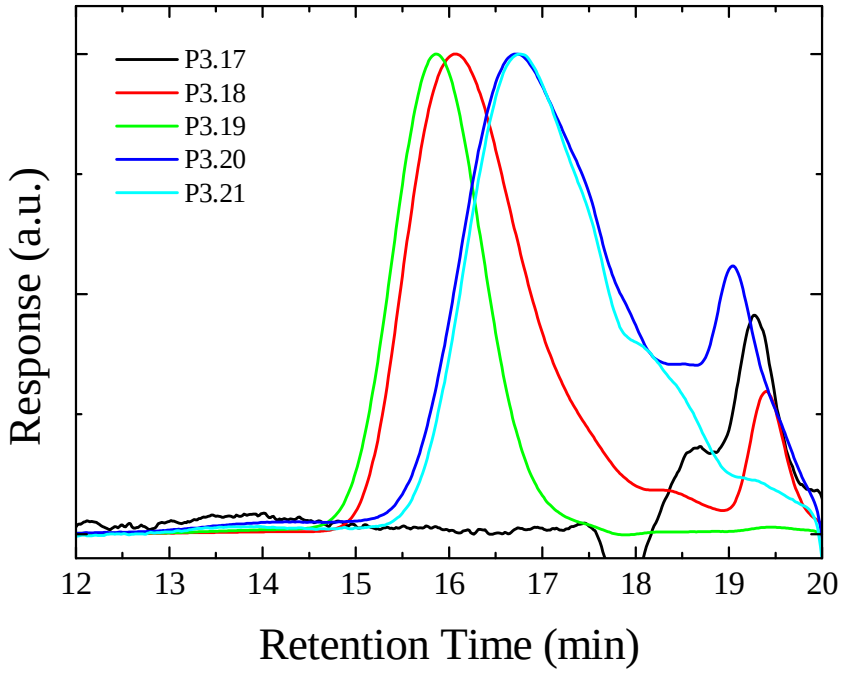

Figure 3.23. Chromatograms of polymers **P3.17**, **P3.18**, **P3.19**, **P3.20**, and **P3.21**.

Unsurprisingly, homopolymerization of DxpMe (**P3.17**) did not produce a peak, as the product would mainly consist of DxpMe unimers and DxpMe monomers. Upon addition of *exo*NbHex, however, a peak appears that corresponds to a polymer with a molecular weight of 3,200 g/mol (Table 3.5). It is noteworthy that although *exo*NbHex generally produces polymers with narrow molecular weight distributions, in this case it was found to be broad ($Đ_M$ = 1.73).

Table 3.5. Molecular weight and molecular weight distributions determined by SEC of polymers **P3.17**, **P3.18**, **P3.19**, **P3.20** and **P3.21**.

	M_n (g/mol)	M_w (g/mol)	$Đ_M$
P3.17	-	-	-
P3.18	3,200	5,600	1.73
P3.19	6,100	8,000	1.32
P3.20	2,100	3,000	1.44
P3.21	1,200	2,500	2.02

Upon addition of *exo*NbMorph the polymer distribution in the SEC shifts to lower retention time, therefore suggesting higher molecular weight polymer. It was found that the molecular weight of **P3.19** was almost double that of **P3.18** indicating successful chain extension with *exo*NbMorph. Additionally, the molecular weight distribution was found to have decreased ($Đ_M$ = 1.32) suggesting no further loss of control of the polymerization. Hydrolysis of **P3.19** should therefore result in two homopolymers consisting of poly(NbHex) (**P3.20**) and poly(NbMorph) (**P3.21**). Upon analysis of the hydrolyzed polymers by SEC, the traces were found to be very similar which was attributed to the difficulty in separating the two macromolecules during the workup of the reaction. Despite the anticipated hydrophilicity of poly(NbMorph) and hydrophobicity of poly(NbHex), following extraction with DCM and water, both polymers were found in both organic and aqueous layers, potentially due to the hydroxyl groups that render poly(NbHex) more hydrophilic and the pH-responsive nature of the morpholine moiety on poly(NbMorph). Nonetheless, the polymer peaks in the chromatogram correspond to polymers with molecular weights lower than that of the parent copolymers indicating that *exo* norbornenes can competitively polymerize in the presence of dioxepins and form homopolymers with dioxepin only contributing towards the end of the norbornene polymerization.

The sample after addition of *exo*NbHex (**P3.18**) was purified and also characterized by ^{1}H NMR spectroscopy (Figure 3.24).

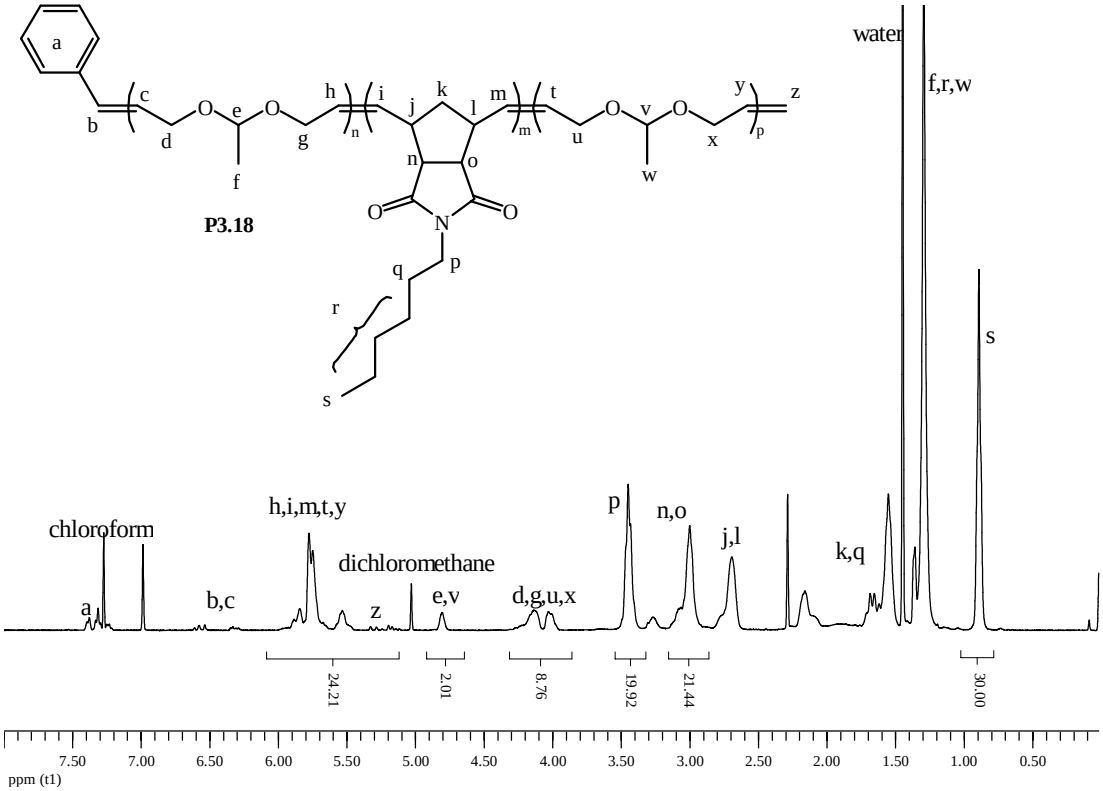

Figure 3.24. Chemical structure and the assigned ^{1}H NMR spectrum of **P3.18**. ($CDCl_3$, 300 MHz)

The signals corresponding to both dioxepin and norbornene repeat units were observed, indicating successful copolymerization of DxpMe and *exo*NbHex. Moreover, with the assumption that *exo*NbHex reached 100% conversion, thus having an average DP = 10, it is found that DxpMe has an average DP = 2. Studying the copolymer after addition of *exo*NbMorph was less revealing as the morpholine signals overlap with the **P3.18** signals (Figure 3.25).

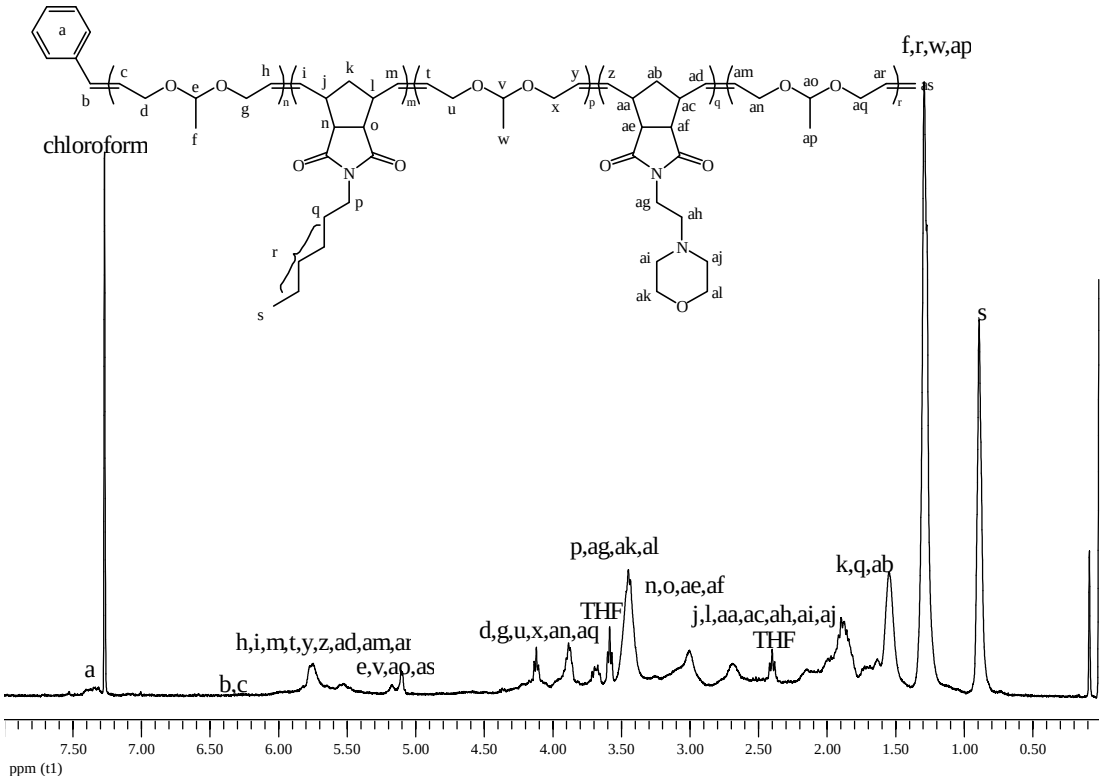

Figure 3.25. ^{1}H NMR spectrum of the **P3.19** copolymer.

Nonetheless, it is proposed that telechelic poly(norbornene)s can be synthesized in a one-pot reaction with the end-groups provided by the dioxepin monomer, either as the monomer unit, or the hydrolysis product.

3.4. Conclusions

This basic study of the reactivity of dioxepins towards ruthenium alkylidenes, and more specifically those produced by Grubbs 1st generation catalyst and its living poly(norbornene)s, demonstrates the practical consequences from the low polymerization rates of dioxepins. While it is not possible to produce homopolymers, or block copolymers, the studied dioxepins showed a tendency to add a single equivalent to a living poly(norbornene) formed by the ROMP of either *endo* or *exo* norbornenes, without compromising the living nature of the polymerization, as further addition of another norbornene resulted in chain extension. When competing with *exo* norbornenes,

dioxepins contribute very little to the final copolymer composition, however when competing with the less reactive *endo* norbornenes, successful copolymerization was observed. Nonetheless, in the presence of a great excess of dioxepin, both *exo* and *endo* norbornenes could be used for the synthesis of a copolymer with relatively known sequence, by simply adding the norbornene monomer in small batches. It is anticipated that with further investigation into the parameters that govern the rate of ROMP of dioxepins, as well as other cycloheptene-based monomers, a more complex precision polymer can be synthesized – as long as the addition always results in one repeat unit.

3.5. Materials and Methods

Benzaldehyde (>99.5%), *cis*-2-butene-1,4-diol (97%), *p*-toluenesulfonic acid monohydrate (99%), acetaldehyde (99%), 1-pyrenecarboxaldehyde (99%), and 4-(2-aminoethyl)morpholine (99%) were purchased from Sigma-Aldrich and used without further purification. Solvents were purchased from Fisher Scientific and used as received. *N*-hexyl-*endo*-norbornene-5,6-dicarboximide (*endo*HexNb), *N*-hexyl-*exo*-norbornene-5,6-dicarboximide (*exo*HexNb), and (1-pyrenyl)methyl-*exo*-5-norbornene-2-carboxylate (*exo*NbPyr) were synthesized as described in Chapter 2.

Nuclear magnetic resonance (^{1}H and ^{13}C NMR) spectra were recorded in $CDCl_3$ or CD_2Cl_2 solutions on a Bruker AC-250, a Bruker DPX-300, a Bruker AV-400 or a Bruker DPX- 400, a DRX-500, and a Bruker AV II-700 spectrometer. Chemical shifts are reported as δ in parts per million (ppm) and referenced to the chemical shift of the residual solvent resonances ($CDCl_3$ ^{1}H: δ=7.26 ppm; ^{13}C: δ=77.16 ppm) and/or internal standards (TMS ^{1}H: δ = 0.00 ppm; ^{13}C: δ = 0.00 ppm). High resolution mass spectra (HRMS) were collected using a Bruker MaXis UHR-ESI TOF. MALDI ToF mass spectra were acquired on a Bruker Daltonics Ultraflex and an Autoflex MALDI-ToF

mass spectrometer in positive ion ToF detection performed using an accelerating voltage of 25 kV. Solutions in THF of dithranol as matrix (30 mg/mL), sodium or potassium trifluoroacetate as ionization agent (2 mg/mL) and analyte (1 mg/mL) were mixed prior to being spotted on the MALDI plate and air-dried. The samples were measured in reflector ion mode and calibrated by comparison to SpheriCal (Polymer Factory) single molecular weight standards (1,200-8,000 Da). Simulated masses were obtained using the software "Molecular weight calculator" Version 6.49 developed by Matthew Monroe. All reported masses are based on the isotopic abundances of the reported chemical formulae. SEC measurements were performed on an Agilent 390-MDS equipped with differential refractive index and UV detectors. The separation was achieved by a guard column (Varian PLGel 5 μm) and two mixed-D columns (Varian PLGel 5 μm) using THF (2% TEA mixture) or chloroform (2% TEA mixture) as the eluent at a flow rate of 1 mL/min. Data analysis was performed using Cirrus v3.3 with calibration curves produced using Varian Polymer laboratories Easi-Vials linear poly(styrene) standards with molecular weights ranging from 162 to 2.4×10^5 g/mol.

3.5.1. Synthesis

3.5.1.1. Synthesis of 2-phenyl-4,7-dihydro-2*H*-1,3-dioxepin (DxpPhe)

For the synthesis of DxpPhe a modified literature procedure[18] was followed. Benzaldehyde (9.8 g, 92.5 mmol, 1 eq.), *cis*-2-butene-1,4-diol (8.6 g, 97.3 mmol, 1.05 eq.), and *p*-toluenesulfonic acid (170 mg, 0.9 mmol, 0.01 eq.) were dissolved in DCM (30 mL). Anhydrous $MgSO_4$ was added until the supernatant was clear and the mixture was stirred overnight at room temperature. The solvent was removed under reduced pressure and the remaining oil was passed through a basic alumina plug to yield

the monomer as a clear oil (10.33 g, 60% isolated yield). ^{1}H NMR (CD_2Cl_2, 500 MHz) δ (ppm): 7.57 (2H, d, ^{3}J = 6.5 Hz, Ar), 7.41 (3H, m, Ar), 5.88 (1H, s, acetal), 5.83 (2H, m, CH=CH), 4.35 (4H, m, -CH_2); ^{13}C NMR (CD_2Cl_2, 125 MHz) δ (ppm): 139.2, 129.9, 128.3, 128.1, 126.4, 102.1, 64.6; HRMS *m/z*: expected: 199.0730, found: 199.0732 $[M+Na]^+$.

3.5.1.2. Synthesis of 2-methyl-4,7-dihydro-2*H*-1,3-dioxepin (DxpMe)

A similar procedure to the synthesis of DxpPhe was followed for the preparation of DxpMe, using acetaldehyde (3.9 g, 89.1 mmol, 1.3 eq.) and *cis*-2-butene-1,4-diol (9.2 g, 86.5 mmol, 1 eq.) in a THF/DCM (1:4) mixture. The product was isolated in 98% yield (9.7 g). ^{1}H NMR (CD_2Cl_2, 500 MHz) δ (ppm): 5.73 (2H, m, CH=CH), 4.99 (1H, q, ^{3}J = 5.2 Hz, acetal), 4.25 (4H, m, -CH_2), 1.32 (3H, d, ^{3}J = 5.2 Hz, -CH_3); ^{13}C NMR (CD_2Cl_2, 125 MHz) δ (ppm): 129.8, 101.1, 64.6, 19.8; HRMS *m/z*: expected: 115.0754, found: 115.0755 $[M+H]^+$.

3.5.1.3. 2-(1-pyrenyl)-4,7-dihydro-2*H*-1,3-dioxepin (DxpPyr)

A similar procedure to the synthesis of DxpPhe was followed for the preparation of DxpPyr, using 1-pyrenecarboxaldehyde (5 g, 21.7 mmol, 1.05 eq.) and *cis*-2-butene-1,4-diol (1.8 g, 20.7 mmol, 1 eq.) in DCM (20 mL). After removal of the volatiles, the product was isolated *via* recrystallization from ethyl acetate as yellow crystals in 17% yield (1 g). ^{1}H NMR (CD_2Cl_2, 500 MHz) δ (ppm): 7.90-8.40 (9H, m, pyrene), 6.61 (1H, s, acetal), 5.78 (2H, m, CH=CH), 4.28-4.45 (4H, m, -CH_2); ^{13}C NMR (CD_2Cl_2, 125 MHz) δ (ppm): 131.8, 131.6, 131.2, 130.6, 128.6, 127.6, 127.5, 127.4, 126.0, 125.4, 125.3, 124.9, 124.6, 124.2, 123.9, 123.6, 101.0, 65.2; HRMS *m/z*: expected: 323.1043, found: 323.1043 $[M+Na]^+$.

3.5.1.4. *N*-(2-morpholinoethyl)-*exo*-norbornene-5,6-dicarboximide (*exo*NbMorph)

Similar to the procedures reported in Chapter 2, for the synthesis of *exo*NbMorph, *cis*-5-norbornene-*exo*-2-dicarboxylic anhydride (1 g, 6.1 mmol, 1 eq.) was dissolved in 20 mL toluene before the addition of 4-(2-aminoethyl)morpholine (1.23 g, 9.44 mmol, 1.55 eq.). The reaction was heated to reflux (120 ºC) overnight. Then, the volatiles were removed under reduced pressure. The product was isolated, after passing through a silica plug and recrystallization from petroleum ether, as off-yellow crystals (60% isolated yield). ^{1}H NMR: ($CDCl_3$, 500 MHz) δ (ppm): 6.30 (2H, m, CH=CH), 3.60 (6H, m, -O-CH_2- and O=C-N-CH_2-), 3.27 (2H, m, O=C-CH-C<u>H</u>-), 2.67 (2H, m, O=C-CH-), 2.54 (2H, t, ^{3}J = 6.1 Hz, -N-CH_2-C<u>H</u>$_2$-N-$(CH_2)_2$-), 2.46 (4H, m, -N-$(CH_2)_2$-), 1.47-1.63 (2H, m, CH_2 bridge); ^{13}C NMR ($CDCl_3$, 125 MHz) δ (ppm): 178.1, 137.8, 67.0, 54.8, 53.3, 47.7, 45.3, 42.6, 35.3; HRMS: *m/z*: expected: 277.1547, found: 277.1548 $[M+H]^+$.

3.5.1.5. Homopolymerization of DxpPhe

In a typical polymerization, DxpPhe (70 mg, 0.398 mmol, 100 eq.) was dissolved in $CDCl_3$ (300 µL) and placed in a dry NMR tube fitted with a Young's tap, while in an ampoule **G1** (3.3 mg, 3.98 µmol, 1 eq.) was also dissolved in $CDCl_3$ (300 µL). The two were degassed *via* three freeze-pump-thaw cycles before the catalyst was added to the NMR tube under N_2. The polymerization was allowed to proceed under a nitrogen blanket at room temperature.

3.5.1.6. Chain extension of poly(NbHex) (**P3.1**) with DxpMe (**P3.2**)

*Exo*NbHex (200 mg, 0.808 mmol, 10 eq.) was dissolved in $CDCl_3$ (1 mL) in a dry ampoule, while **G1** (66.5 mg, 0.081 mmol, 1 eq.) was dissolved in $CDCl_3$ (1 mL) in

another ampoule. Both solutions were degassed *via* three freeze-pump-thaw cycles before their contents were combined with cannula transfer under N_2. The polymerization was allowed to proceed under a nitrogen blanket for one hour, when an aliquot was removed, quenched with 100-fold excess of EVE and used for further characterization (**P3.1**). A solution of DxpMe (23.1 mg, 0.202 mmol, 5 eq.) previously degassed by three freeze-pump-thaw cycles, was added to the reaction mixture. The reaction was allowed to proceed for 16 hours before quenching with EVE.

3.5.1.7. Synthesis of poly(NbHex)-*b*-poly(DxpMe)-*b*-poly(NbPyr) (**3.5**)

Initially, *exo*NbHex (226 mg, 1.075 mmol, 5 eq.) was dissolved in chloroform (1 mL) in a dry ampoule, while in a different ampoule **G1** (177 mg, 0.215 mmol, 1 eq.) was also dissolved in chloroform (1 mL). After degassing *via* three freeze-pump-thaw cycles the contents of the ampoules were combined *via* cannula transfer under N_2 and the reaction was allowed to proceed for two hours under a nitrogen blanket. An aliquot was removed (450 μL) and quenched with 100-fold excess EVE and further characterized (**P3.3**). A solution of DxpMe (95.1 mg, 0.833 mmol, 5 eq.) in chloroform (775 μL), previously degassed by three freeze-pump-thaw cycles, was added to the reaction and the polymerization was allowed to proceed for two hours at room temperature. Then, an aliquot was removed (450 μL), quenched with 100-fold excess EVE, and further characterized (**P3.4**). A previously degassed solution of *exo*NbPyr (237.3 mg, 0.673 mmol, 5 eq.) in chloroform (905 μL) was added to the reaction mixture and the polymerization was allowed to proceed for two hours before quenching with 100-fold excess EVE. The polymer (**P3.5**) was isolated by precipitation in methanol containing potassium 2-isocyanoacetate (5 eq.) to remove insoluble ruthenium species.[53]

3.5.1.8. Hydrolysis of **P3.5**

The polymer **P3.5** (10 mg) was dissolved in THF (5 mL) and HCl (35%, 1 mL) was added. The reaction was stirred for two hours at room temperature before removing volatiles under reduced pressure. The hydrolysis products were characterized without further purification.

3.5.1.9. Addition of DxpMe to a living ROMP of *exo*NbHex

Initially, all reagents were each dissolved in DCM (470 µL) and separately degassed *via* three freeze-pump-thaw cycles. Then, *exo*NbHex (30 mg, 0.122 mmol, 10 eq.) was transferred under N_2 to the ampoule containing **G1** (10 mg, 0.012 mmol, 1 eq.). The reaction was allowed to proceed at room temperature under nitrogen blanket for one hour. An aliquot was removed and quenched (**P3.6**), while to the reaction DxpMe (69.4 mg, 0.608 mmol,100 eq. with respect to the remaining catalyst) was added and allowed to polymerize for 15 hours. The polymerization was quenched (**P3.7**) with 100-fold excess EVE and dried under reduced pressure.

3.5.1.10. Addition of DxpPyr to a living ROMP of *endo*NbHex (**P3.8**)

In a dry ampoule, *endo*NbHex (500 mg, 2.022 mmol, 20 eq.) and **G1** (83.1 mg, 0.101 mmol, 1 eq.) were dissolved in DCM (4 mL) and were then degassed by three freeze-pump-thaw cycles. The polymerization was allowed to proceed at room temperature under N_2 for 18 hours. Then, an aliquot was removed and quenched (**P3.8**) with 100-fold excess EVE. To the polymerization, a previously degassed *via* three freeze-pump-thaw cycles solution of DxpPyr (121.6 mg, 0.405 mmol, 5 eq. with respect to the remaining catalyst) in DCM (1 mL) was added. Aliquots of the reaction were

withdrawn after 0.5 hours (**P3.8-30**), 1 hour (**P3.8-60**), 2 hours (**P3.8-120**), and 5 hours (**P3.8-300**) and quenched.

3.5.1.11. Determination of reactivity ratios

For copolymerizations with *exo*NbHex, the two monomers (see tables below for amounts) were dissolved in DCM (200 µL) and placed in an NMR tube fitted with a Young's tap. The solution was degassed *via* three freeze-pump-thaw cycles before a previously degassed stock solution in CD_2Cl_2 of Grubbs 1st generation catalyst (50 µL, 0.041 M) was added. The mixture was degassed once more and the tube was filled with nitrogen. The reaction was monitored by NMR spectroscopy.

Table 3.6. Quantities of reagents used for the copolymerizations of DxpMe and *exo*NbHex towards the calculation of their reactivity ratios.

	DxpMe		*exo* NbHex		**G1**	
	m (mg)	n (mmol)	m (mg)	n (mmol)	m (mg)	n (nmol)
10:90	1.87	0.016	36.43	0.147	3.37	4.095
20:80	3.74	0.033	32.38	0.131	3.37	4.095
30:70	5.61	0.049	28.33	0.115	3.37	4.095
40:60	7.47	0.065	24.28	0.098	3.37	4.095
50:50	9.34	0.082	20.24	0.082	3.37	4.095
60:40	11.21	0.098	16.19	0.065	3.37	4.095
70:30	13.08	0.115	12.14	0.049	3.37	4.095
80:20	14.95	0.131	8.09	0.033	3.37	4.095
90:10	16.82	0.147	4.05	0.016	3.37	4.095

Table 3.7. Quantities of reagents used for the copolymerizations of DxpPhe and *exo*NbHex towards the calculation of their reactivity ratios.

	DxpPhe		*exo* NbHex		**G1**	
	m (mg)	n (mmol)	m (mg)	n (mmol)	m (mg)	n (nmol)
10:90	2.06	0.012	25.96	0.105	3.37	4.095
20:80	4.11	0.023	23.08	0.093	3.37	4.095
30:70	6.17	0.035	20.19	0.082	3.37	4.095
40:60	8.22	0.047	17.31	0.070	3.37	4.095
50:50	10.28	0.058	14.43	0.058	3.37	4.095
60:40	12.34	0.070	11.54	0.047	3.37	4.095
70:30	14.39	0.082	8.65	0.035	3.37	4.095
80:20	16.45	0.093	5.77	0.023	3.37	4.095
90:10	18.51	0.105	2.88	0.012	3.37	4.095

For copolymerizations with *endo*NbHex, the two monomers (see table below for amounts) were dissolved in CH_2Cl_2 (310 μL) and placed in an NMR tube fitted with a Young's tap. The solution was degassed *via* three freeze-pump-thaw cycles before a previously degassed stock solution in CD_2Cl_2 of **G1** (300 μL, 0.024 M) was added. The mixture was degassed once more and the tube was filled with nitrogen. The reaction was monitored by NMR spectroscopy.

Table 3.8. Quantities of reagents used for the copolymerizations of DxpPhe and *endo*NbHex towards the calculation of their reactivity ratios.

	DxpPhe		*endo* NbHex		**G1**	
	m (mg)	n (mmol)	m (mg)	n (mmol)	m (mg)	n (nmol)
20:80	11.13	0.063	62.48	0.253	6.50	7.898
40:60	22.27	0.126	46.86	0.190	6.50	7.898
50:50	27.84	0.158	39.05	0.158	6.50	7.898
60:40	33.40	0.190	31.24	0.126	6.50	7.898
80:20	44.54	0.253	15.62	0.063	6.50	7.898
90:10	50.11	0.284	7.81	0.032	6.50	7.898

3.5.1.12. Sequential polymerization of *endo* norbornenes

Initially, stock solutions of all reagents were prepared and degassed *via* three freeze-pump-thaw cycles. DxpPhe (214 mg, 1.215 mmol, 20 eq.) was dissolved in DCM (500 μL), *endo*NbHex (250 mg, 1.011 mmol) was dissolved in DCM (2.5 mL), and **G1** (50 mg, 0.061 mmol, 1 eq.) was dissolved in 500 μL DCM. The solutions containing DxpPhe and **G1** were combined *via* cannula transfer under N_2 and stirred for 30 minutes before *endo*NbHex solution (150 μL, 1 eq.) was added under N_2 to the reaction mixture. The polymerization was allowed to proceed for two hours before an aliquot (250 μL) was removed and quenched with 100-fold excess EVE (**P3.9**), while *endo*NbHex solution (235 μL, 2 eq.) was added under N_2 to the reaction mixture. The polymerization was allowed to proceed for four hours before an aliquot (300 μL) was removed and quenched with 100-fold excess EVE (**P3.10**), while *endo*NbHex solution (346 μL, 4 eq.) was added under N_2 to the reaction mixture. The polymerization was allowed to proceed for another ten hours before an aliquot (400 μL) was removed and quenched with 100-fold excess EVE (**P3.11**), while endoNbHex solution (400 μL, 7 eq.) was added under N_2 to the reaction mixture. The polymerization was stirred for another 20 hours before quenching with 100-fold excess EVE (**P3.12**). All samples were dried and characterized without further purification.

3.5.1.13. Hydrolysis of **P3.9**, **P3.10**, **P3.11**, and **P3.12**

To a solution containing the polymer **P3.9** (~10 mg) in THF (1 mL) was added HCl solution (35%, 1 mL). The reaction was stirred for 15 hours before the volatiles were removed under reduced pressure. The resulting polymer (**P3.13**) was characterized without further purification. A similar procedure was followed for the hydrolysis of **P3.10** to afford **P3.14**, **P3.11** to afford **P3.15**, and **P3.12** to afford **P3.16**.

3.5.1.14. Sequential polymerization of *exo* norbornenes

Initially, stock solutions of all reagents were prepared and degassed *via* three freeze-pump-thaw cycles. DxpMe (100 mg, 0.876 mmol, 10 eq.) was dissolved in DCM (200 μL), *exo*NbHex (216.7 mg, 0.876 mmol, 10 eq.) was dissolved in DCM (200 μL), *exo*NbMorph (242.1 mg, 0.876 mmol, 10 eq.) was dissolved in DCM (200 μL), and **G1** (72.1 mg, 0.088 mmol, 1 eq.) was dissolved in 1 mL DCM. The solutions containing DxpMe and **G1** were combined *via* cannula transfer under N_2 and stirred for one hour before removing an aliquot (600 μL) which was quenched with 100-fold excess EVE (**P3.17**), while *exo*NbHex solution (100 μL) was added under N_2 to the reaction mixture. The polymerization was allowed to proceed for an hour before an aliquot (400 μL) was removed and quenched with 100-fold excess EVE (**P3.18**), while *exo*NbMorph solution (50 μL) was added under N_2 to the reaction mixture. The polymerization was allowed to proceed for another hour before quenching with 100-fold excess EVE (**P3.19**). All samples were dried and characterized without further purification.

3.5.1.15. Hydrolysis of **P3.19**

P3.19 (20 mg) was dissolved in a mixture of THF/MeOH (1:1, 5 mL) and HCl (35%, 0.5 mL) was added. The reaction was stirred overnight and then the volatiles were removed under reduced pressure. The precipitate was found to be insoluble in THF (attributed to the protonation of the morpholine group), therefore DCM was first placed in the reaction vessel and stirred for one hour. The solution (**P3.20**) was collected and dried separately from the precipitate (**P3.21**) which was extracted into DCM phase after basic water was added to the mixture.

3.6. References

1. V. M. Ingram, *Nature*, 1957, **180**, 326-328.
2. M. J. Stuart and R. L. Nagel, *The Lancet*, 2004, **364**, 1343-1360.
3. A. B. Mabire, M. P. Robin, H. Willcock, A. Pitto-Barry, N. Kirby and R. K. O'Reilly, *Chem. Commun.*, 2014, **50**, 11492-11495.
4. A. S. Goldmann, M. Glassner, A. J. Inglis and C. Barner-Kowollik, *Macromol. Rapid Commun.*, 2013, **34**, 810-849.
5. D. Albagli, G. C. Bazan, R. R. Schrock and M. S. Wrighton, *J. Am. Chem. Soc.*, 1993, **115**, 7328-7334.
6. R. M. Owen, J. E. Gestwicki, T. Young and L. L. Kiessling, *Org. Lett.*, 2002, **4**, 2293-2296.
7. F. Lo Verso and C. N. Likos, *Polymer*, 2008, **49**, 1425-1434.
8. Y. Xia, R. Verduzco, R. H. Grubbs and J. A. Kornfield, *J. Am. Chem. Soc.*, 2008, **130**, 1735-1740.
9. A. C. Lamanna and L. L. Kiessling, *ACS Chem. Biol.*, 2009, **4**, 828-833.
10. A. E. Madkour, A. H. R. Koch, K. Lienkamp and G. N. Tew, *Macromolecules*, 2010, **43**, 4557-4561.
11. M. A. Tasdelen, M. U. Kahveci and Y. Yagci, *Prog. Polym. Sci.*, 2011, **36**, 455-567.
12. T. Otsu, M. Yoshioka and T. Tanaka, *Eur. Polym. J.*, 1992, **28**, 1325-1329.
13. J. Jagur-Grodzinski, *J. Polym. Sci. Part A: Polym. Chem.*, 2002, **40**, 2116-2133.
14. B. Boutevin, G. David and C. Boyer, in *Oligomers - Polymer Composites - Molecular Imprinting*, Springer Berlin Heidelberg, 2007, vol. 206, pp. 31-135.
15. M. Beija, M.-T. Charreyre and J. M. G. Martinho, *Prog. Polym. Sci.*, 2011, **36**, 568-602.
16. C. Fraser, M. A. Hillmyer, E. Gutierrez and R. H. Grubbs, *Macromolecules*, 1995, **28**, 7256-7261.
17. S. Perrier and X. Wang, *Nature*, 2007, **445**, 271-272.
18. S. Hilf, E. Berger-Nicoletti, R. H. Grubbs and A. F. M. Kilbinger, *Angew. Chem. Int. Ed.*, 2006, **45**, 8045-8048.
19. S. Hilf and A. F. M. Kilbinger, *Macromol. Rapid Commun.*, 2007, **28**, 1225-1230.

20. S. Hilf, N. Hanik and A. F. M. Kilbinger, *J. Polym. Sci. Part A: Polym. Chem.*, 2008, **46**, 2913-2921.
21. S. Hilf and A. F. M. Kilbinger, *Macromolecules*, 2010, **43**, 208-212.
22. S. Hilf, R. H. Grubbs and A. F. M. Kilbinger, *Macromolecules*, 2008, **41**, 6006-6011.
23. S. Hilf and A. F. M. Kilbinger, *Macromolecules*, 2009, **42**, 1099-1106.
24. S. Hilf and A. F. M. Kilbinger, *Macromolecules*, 2009, **42**, 4127-4133.
25. A. A. Nagarkar, A. Crochet, K. M. Fromm and A. F. M. Kilbinger, *Macromolecules*, 2012, **45**, 4447-4453.
26. K. S. Roberts and N. S. Sampson, *Org. Lett.*, 2004, **6**, 3253-3255.
27. J. Zhang, M. E. Matta and M. A. Hillmyer, *ACS Macro Lett.*, 2012, **1**, 1383-1387.
28. T.-L. Choi, I. M. Rutenberg and R. H. Grubbs, *Angew. Chem. Int. Ed.*, 2002, **41**, 3839-3841.
29. S. Demel, C. Slugovc, F. Stelzer, K. Fodor-Csorba and G. Galli, *Macromol. Rapid Commun.*, 2003, **24**, 636-641.
30. M. F. Ilker and E. B. Coughlin, *Macromolecules*, 2002, **35**, 54-58.
31. A. Song, K. A. Parker and N. S. Sampson, *J. Am. Chem. Soc.*, 2009, **131**, 3444-3445.
32. L. Tan, K. A. Parker and N. S. Sampson, *Macromolecules*, 2014, **47**, 6572-6579.
33. A. Song, K. A. Parker and N. S. Sampson, *Org. Lett.*, 2010, **12**, 3729-3731.
34. J. Romulus, L. Tan, M. Weck and N. S. Sampson, *ACS Macro Lett.*, 2013, **2**, 749-752.
35. S. Sutthasupa, M. Shiotsuki, T. Masuda and F. Sanda, *J. Am. Chem. Soc.*, 2009, **131**, 10546-10551.
36. B. Al Samak, A. G. Carvill, J. J. Rooney and J. M. Thompson, *Chem. Commun.*, 1997, 2057-2058.
37. B. Al Samak, V. Amir-Ebrahimi, D. G. Corry, J. G. Hamilton, S. Rigby, J. J. Rooney and J. M. Thompson, *J. Mol. Catal. A: Chem.*, 2000, **160**, 13-21.
38. H. Jeong, J. M. John, R. R. Schrock and A. H. Hoveyda, *J. Am. Chem. Soc.*, 2015, **137**, 2239-2242.
39. V. Amir-Ebrahimi and J. J. Rooney, *J. Mol. Catal. A: Chem.*, 2004, **208**, 115-121.

40. M. Bornand and P. Chen, *Angew. Chem. Int. Ed.*, 2005, **44**, 7909-7911.
41. M. Bornand, S. Torker and P. Chen, *Organometallics*, 2007, **26**, 3585-3596.
42. K. Vehlow, D. Wang, M. R. Buchmeiser and S. Blechert, *Angew. Chem. Int. Ed.*, 2008, **47**, 2615-2618.
43. M. Lichtenheldt, D. Wang, K. Vehlow, I. Reinhardt, C. Kühnel, U. Decker, S. Blechert and M. R. Buchmeiser, *Chem. Eur. J.*, 2009, **15**, 9451-9457.
44. K. Vehlow, M. Lichtenheldt, D. Wang, S. Blechert and M. R. Buchmeiser, *Macromol. Symp.*, 2010, **296**, 44-48.
45. M. R. Buchmeiser, I. Ahmad, V. Gurram and P. S. Kumar, *Macromolecules*, 2011, **44**, 4098-4106.
46. S. Torker, A. Müller and P. Chen, *Angew. Chem. Int. Ed.*, 2010, **49**, 3762-3766.
47. S. Torker, A. Müller, R. Sigrist and P. Chen, *Organometallics*, 2010, **29**, 2735-2751.
48. C. S. Daeffler and R. H. Grubbs, *Macromolecules*, 2013, **46**, 3288-3292.
49. T. Steinbach, E. M. Alexandrino and F. R. Wurm, *Polym. Chem.*, 2013, **4**, 3800-3806.
50. D. M. Haddleton, M. C. Crossman, K. H. Hunt, C. Topping, C. Waterson and K. G. Suddaby, *Macromolecules*, 1997, **30**, 3992-3998.
51. J. B. Matson and R. H. Grubbs, *Macromolecules*, 2010, **43**, 213-221.
52. A. M. van Herk, *J. Chem. Educ.*, 1995, **72**, 138.
53. J. French and S. T. Diver, in *Encyclopedia of Reagents for Organic Synthesis*, John Wiley & Sons, Ltd, 2001.

Chapter 4 - Synthesis of temperature-responsive protein-polymer bioconjugates

4.1. Abstract

In this chapter an example of a protein-polymer bioconjugate is demonstrated. The protein used is a superfolder green fluorescent protein (GFP) that was synthesized by our collaborators at Northwestern University, Chicago, IL, USA. Three different analogues of the sfGFP were provided whereby the incorporation of the non-natural amino acid *p*-azidophenylalanine (*p*AzF) was achieved in different positions on the protein. For the synthesis of the bioconjugate, an alkyne-functional temperature-responsive polymer was synthesized by reversible addition-fragmentation chain transfer (RAFT) polymerization employing an alkyne-bearing chain transfer agent. The polymer was conjugated to the protein and the properties of the resulting bioconjugate were studied as a function of temperature.

All protein syntheses and characterization, and analyses by SDS-PAGE were conducted by Arnaz Ranji and Jian Li from the Jewett group at Northwestern University, USA. Measurement and analysis by SAXS were conducted by Anaïs Pitto-Barry from the O'Reilly group at the University of Warwick, UK.

4.2. Introduction

In the 1970s, Davies *et al.* pioneered the concept polymer-protein bioconjugates by covalently attaching poly(ethylene glycol) (PEG) molecules onto proteins. The observed enhanced properties of the proteins included solubility, electrophoretic mobility, but perhaps more importantly decreased immunogenicity and slower excretion from living organisms.[1, 2] Since then, PEG has been employed in a variety of bioconjugated systems as a result of its biocompatibility, ease of functionalization, and commercial availability, and can be found in a broad range of FDA-approved drugs.[3-11] Noteworthy is also the

use of branched PEG analogues, such as poly[oligo(ethylene glycol) methyl ether methacrylate] (POEGMA), that have been shown to further enhance the biocompatibility of their bioconjugates.[12]

Nevertheless, the use of polymers that endow the protein with more intricate properties has been sought, such as polymers that respond to external stimuli. Stimuli-responsive polymers have the ability to alter their physico-chemical properties as a response to small changes in their environment, such as light, temperature, pH.[13] It is therefore expected that bioconjugates composed of such polymers will inherit these properties, potentially expanding their potential.[14-16] A seminal body of work on the subject was conducted by Hoffman *et al.* who successfully attached stimuli-responsive polymers, mainly poly(*N*-isopropylacrylamide) (poly(NIPAM)), onto enzymes. Upon triggering the response, the polymer was shown to alter the enzyme properties, by effectively altering the local environment of the active site.[14, 17, 18] Additionally, the thermal response of poly(NIPAM)-enzyme bioconjugates was shown to provide the ability to isolate the enzyme from an aqueous solution upon heating, without significantly compromising its activity.[19-22, 18, 23] Nevertheless, the conjugation often results in a drop of the enzyme activity, attributed to the interference of the polymer chain with the enzyme active site.[24] Thus, the careful design of the bioconjugation is imperative, whereby the conjugation site is rationally selected. By doing so, the finely tuned binding efficiency of streptavidin was demonstrated, which was a result of the polymer (poly(NIPAM)) hydration, a temperature-triggered property.[25]

Since then, a large body of work has been dedicated to the study of responsive bioconjugates, whereby the ability of the polymer to reversibly de-hydrate, thus effectively forming an amphiphile is targeted.[26-32] These (frequently referred to as "smart" bioconjugates[26]) are often studied as potential "on/off" systems.[33, 22, 34] In

similar examples, permanently amphiphilic bioconjugates,[35-37, 30, 31] whereby the protein is conjugated with a hydrophobic polymer, have shown potential in improving the protein activity (such as inhibition of tumor cell growth),[38] although in some cases the opposite effect was observed.[39, 40] In addition to the effect on protein activity, bioconjugates with an amphiphilic character (often referred to as "giant amphiphiles") form elaborate nanostructures as a result of their self-assembly in water.[39, 36, 41, 37, 42]

While a large body of literature is dedicated to the attachment of polymer chains onto proteins, noteworthy is the synthesis of protein-polymer bioconjugates whereby the polymerization occurs *in situ* from the surface of the protein (Figure 4.1). This process, often referred to as "grafting from", mainly benefits from easier isolation of the pure product *via* separation from lower molecular weight by-products. Recently, such "grafting from" approaches have become more accessible since the development of reversible deactivation radical polymerizations,[43, 44] such as atom transfer radical polymerization (ATRP), and reversible addition-fragmentation chain transfer (RAFT) polymerization that allow the reaction to occur under conditions suitable for retention of the protein stability.[45] Nonetheless, "grafting from" also often suffers from low initiation efficiencies that result in poor control over the amount of polymer chains grafted onto the protein substrate.[46] Another similar approach, often referred to as "grafting through", requires the immobilization of a polymerizable group onto the surface of the protein which, upon polymerization, is incorporated in a polymer backbone. While *via* this method high conjugation yields are obtained, it does not permit control over the final bioconjugate architecture.[47] Nevertheless, the ability to form a protein-polymer bioconjugate in a few simple steps with little purification required makes "grafting through" and "grafting from" a constantly growing research field.

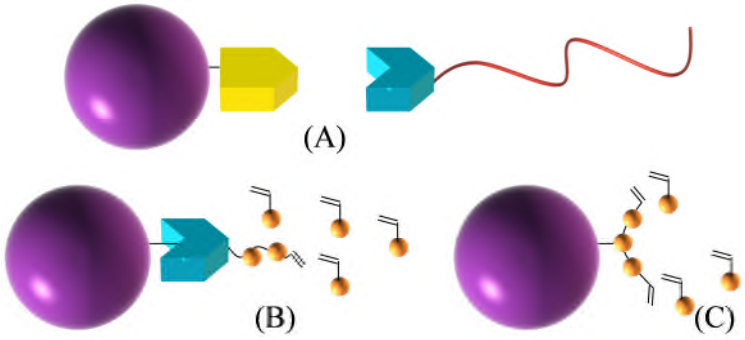

Figure 4.1. Schematic representation of the potential pathways for the formation of a polymer-protein bioconjugate (A) "grafting to", (B) "grafting from", and (C) "grafting through".

As opposed to *in situ* polymerizations, the anchoring of preformed polymers to a protein *via* a mild reaction (also known as "grafting to") permits control of the molecular characteristics of the polymer chains prior to their attachment. Perhaps the most reported and highly efficient conjugation method involves the functionalization of all available natural amino acid target moieties on the protein,[48-51] commonly lysine or cysteine. Other approaches have targeted the *N*-terminus of the protein;[52, 53] while in some examples a single available functional amino acid is targeted.[20, 25, 54, 36] These synthetic pathways have been extensively presented in numerous noteworthy reviews.[4, 5, 55-57, 43, 58, 59, 47, 44, 60-62] Although the vast majority of reports in the literature involve the functionalization of lysine and cysteine residues, the effective change in amine and thiol groups results in alteration of the net charge or the redox potential of the protein, respectively.

To circumvent this limitation, the use of non-natural amino acids as attachment points onto the protein surface provides an elegant alternative. Although Nature takes advantage of only twenty naturally occurring amino acids for the synthesis of proteins, in the case of post-translational modification of some amino acids, the protein exhibits new properties as a result of the functionalities introduced.[63, 64] Inspired by this observation, the synthesis of non-natural amino acids has drawn the attention of the

scientific community[65] and nowadays there are more than 150 synthetic amino acids available that can be genetically encoded in organisms.[66, 67] Applications of synthetic amino acids incorporated into proteins involve protein labelling, protein activity triggering, and probing of the catalytic mechanisms of enzymes.[68-70] In order to achieve the incorporation of non-natural amino acids into functional proteins, one approach involves the replacing of all naturally occurring ones; however this has been shown to affect the protein activity.[71-75] Greater precision has been achieved *via* the amber suppression technique using orthogonal aminoacyl-tRNA synthetase/tRNA pairs, a method extensively used for the synthesis of proteins where the location of the functional handle is important.[76-79, 67] In a few recent reports, the incorporation of non-natural amino acids within functional polymers has been pursued as the first step towards a protein-polymer bioconjugate. Such amino acids include alkynes, azides,[80, 81] maleimides,[82] halides[83] and norbornenes,[84] common handles for "click" reactions, such as copper-catalyzed alkyne-azide cycloaddition (CuAAC).[85-89] In fact, "click" reactions are often used for the synthesis of biomaterials as they offer high yields under benign conditions.[90]

Green fluorescent protein (GFP) is a well-studied and widely exploited protein as a result of its high fluorescence and stability.[91] It is made of 238 amino acids that form a barrel of β-sheets surrounding a central α-helical peptide that forms the fluorophore.[92, 93] In terms of its conjugation with synthetic polymers, it is often used as a model protein, as its luminescence is an excellent indication for its activity. In recent examples, Nolte *et al.* studied the self-assembly of bioconjugates comprised of green fluorescent protein (GFP) and poly[(oligo ethylene glycol) methyl ether acrylate) (POEGA).[94] Following a well-known strategy, the reaction of an alkyne-functional maleimide with a single free cysteine available on the surface of GFP resulted in the formation of an alkyne-

functional GFP. By employing copper-catalyzed azide-alkyne cycloaddition, the protein was successfully attached to an azide-functional POEGA and the resulting bioconjugate exhibited temperature-responsive properties. As such, at elevated temperatures the bioconjugate behaved as a giant amphiphile and spherical aggregates were observed. More recently, Matyjaszewski *et al.* reported the incorporation of the non-natural amino acid *p*-azidophenylalanine (*p*AzF) into a GFP and its subsequent bioconjugation with a PEG containing two alkyne functionalities. Attributed to the tendency of native GFP to dimerize, a "step-growth" formation of micron-sized assemblies was observed.[95]

Based mainly on these two reports, the use of a genetically modified GFP was pursued, whereby one or two *p*AzF residues are introduced within the protein and subsequently bioconjugated with an alkyne-functional temperature-responsive polymer. The protein-polymer bioconjugate is expected to inherit the responsive properties of the polymer and thus an insight on the effect of the conjugation location could be potentially provided.

4.3. Results and Discussion

The Jewett lab (Northwestern University, IL, USA) has been developing a method to obtain superfolder green fluorescent protein (GFP) in a manner that allows the incorporation of non-natural amino acids at different locations in excellent yields (unpublished results). As such, they synthesized three different GFP analogues whereby *p*AzF substituted the residues S2 (**G2-N_3**), T216 (**G216-N_3**), or two residues: S2 and T216 (**G2.216-N_3**) (Scheme 4.1 and Figure 4.2). It should be noted that the expected masses in the MS account for the loss of a serine residue when substituting T216, and the addition of a methionine residue when substituting S2.

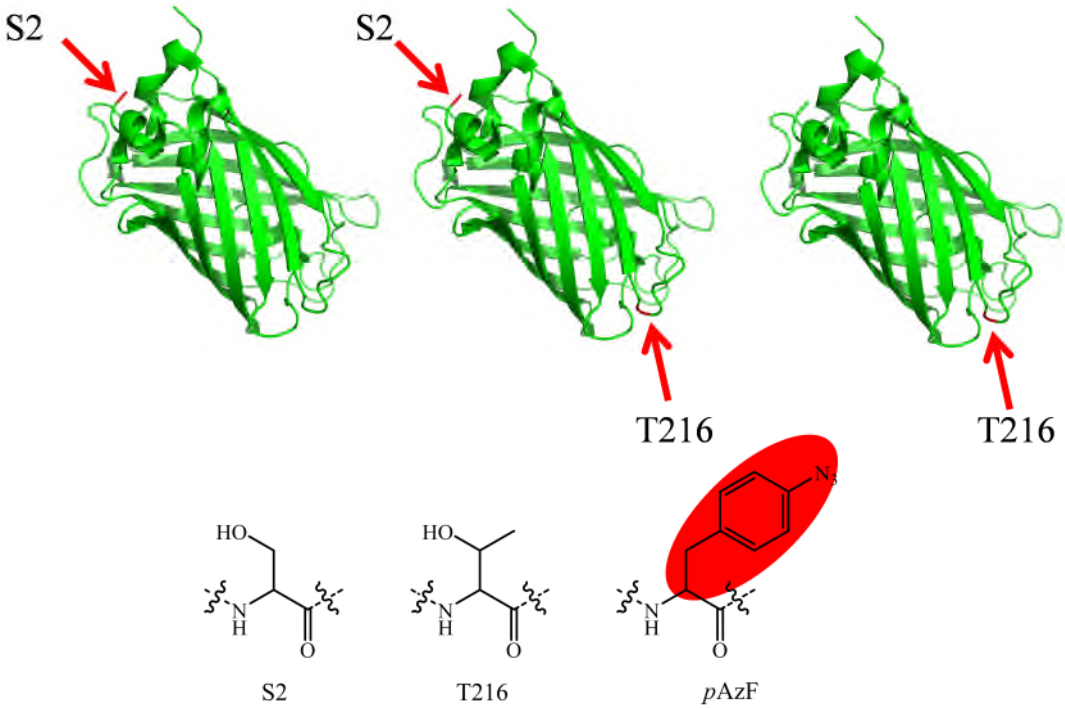

Scheme 4.1. Schematic representation of the three GFP analogues with the modified residues highlighted, and the chemical structure corresponding to the residues.

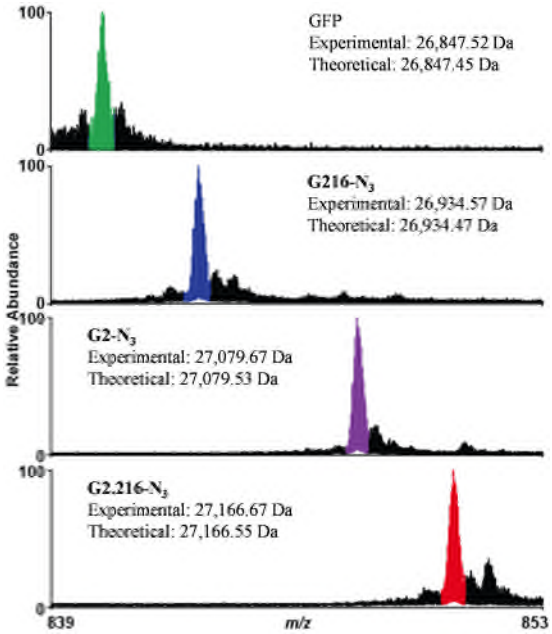

Figure 4.2. Mass spectrum of the 32+ charge state of GFP obtained *via* top-down mass spectrometry illustrating site-specific incorporation of *p*AzF at single and multiple sites. Major peaks in each spectrum coincide with the theoretical peaks for each species and have been highlighted.

4.3.1. GFP-dye conjugation

In order to confirm the accessibility of these sites by a hydrophilic alkyne-functional molecule, an alkyne analogue of the fluorescent dye rhodamine B (**Rhod-alk**) was synthesized and used with the three proteins in a copper-catalyzed alkyne-azide cycloaddition (CuAAC) reaction (Scheme 4.2).

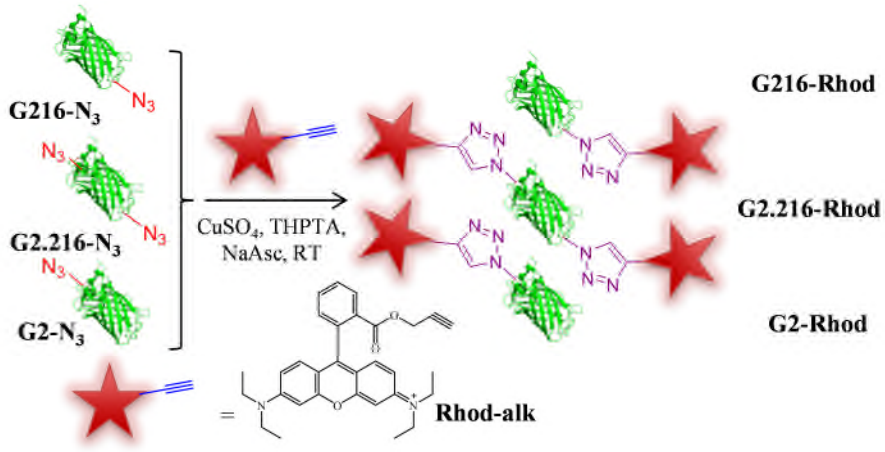

Scheme 4.2. Schematic representation of the CuAAC reaction using the three GFP derivatives **G216-N_3**, **G2.216-N_3**, and **G2-N_3** and **Rhod-alk** to form **G216-Rhod**, **G2.216-Rhod**, and **G2-Rhod** respectively.

After extensive purification by filtration, the samples were characterized by fluorescence spectroscopy in order to confirm the presence of the fluorescent dye **Rhod-alk** as well as the retention of the GFP activity (Figure 4.3).

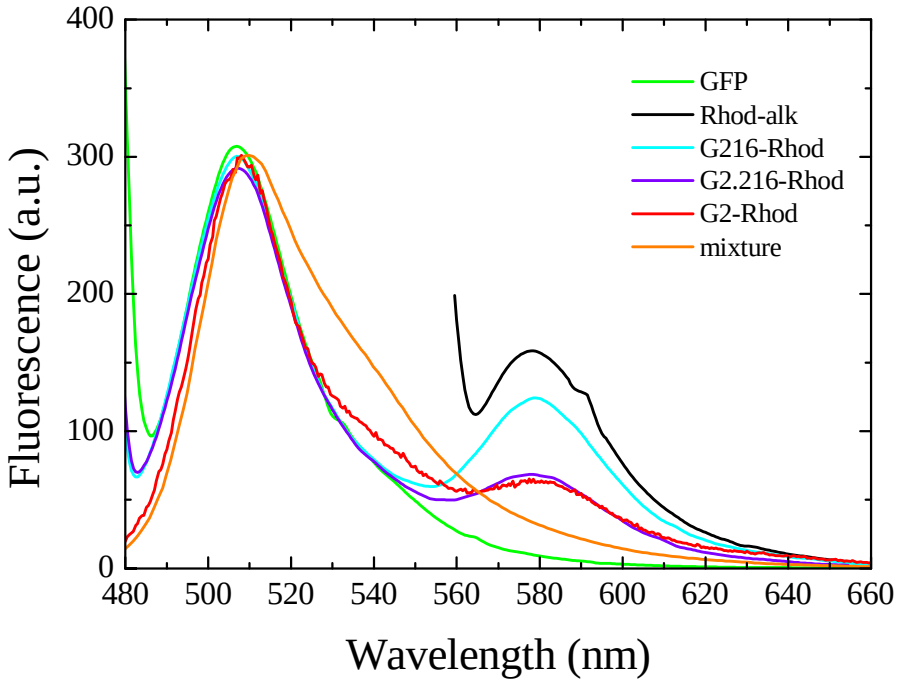

Figure 4.3. Fluorescence emission spectra for the native GFP, the three GFP-dye bioconjugates **G216-Rhod**, **G2.216-Rhod**, and **G2-Rhod**, and a mixture of GFP and **Rhod-alk** excited at 470 nm, as well as the **Rhod-alk** dye excited at 550 nm.

Upon excitation at λ_{ex} = 470 nm, the native GFP sample exhibited an emission maximum at λ_{em} = 507 nm, attributed the GFP fluorophore. Similarly, the GFP-dye bioconjugates all exhibited an emission maximum at λ_{em} = 507 nm attributed to the GFP fluorophore, thus suggesting the retention of the protein activity. Furthermore, an additional peak at λ_{em} = 580 nm was also observed, which was attributed to the conjugated Rhodamine moiety. It should be noted that when excited at λ_{ex} = 470 nm **Rhod-alk** is not significantly emissive at λ_{em} = 580 nm (Figure 4.4), which suggests that in the case of the protein-dye bioconjugates the excited GFP fluorophore transfers energy to the Rhodamine moiety (Förster resonance energy transfer, FRET) resulting in its excitation and subsequent observed emission.[96] An emission at λ_{em} = 580 nm was not observed when the **Rhod-alk** dye was simply mixed with the wild type GFP, suggesting no energy transfer takes place. As such energy transfers are only possible when the

fluorophores are within proximity; this further indicates the successful conjugation of the dye onto the proteins. It should be noted that the relative intensity of the observed emissions at λ_{em} = 580 nm does not correlate to the concentration of fluorophore as the intensity depends on the distance of the two fluorescent groups.

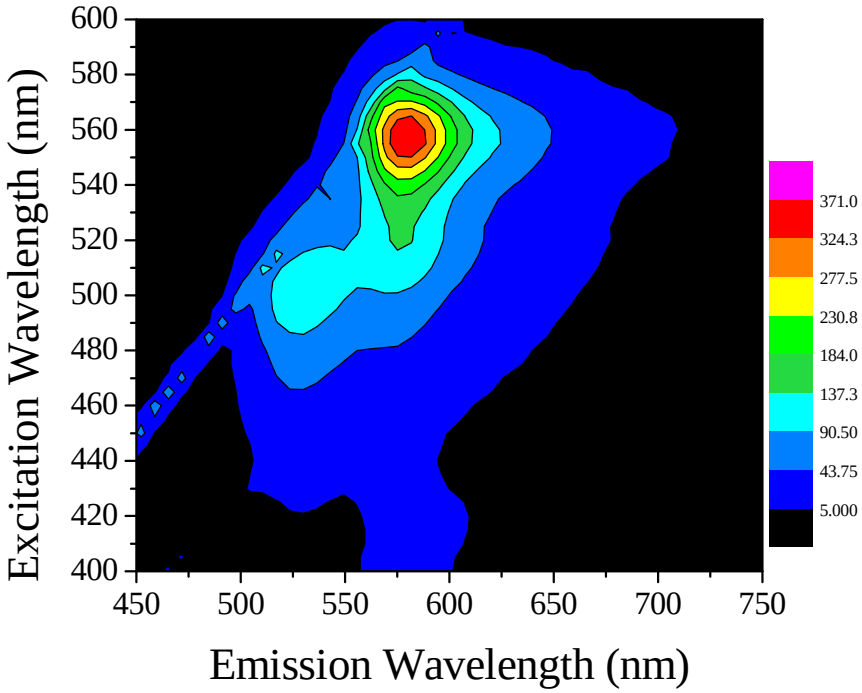

Figure 4.4. Two-dimensional excitation/emission spectrum of **Rhod-alk** in buffer solution.

The bioconjugates were also characterized by poly(acrylamide) gel electrophoresis (PAGE) in order to further confirm the presence of the dye onto the proteins (Figure 4.5). For comparison, the CuAAC conditions were also employed using the unmodified GFP (**G0-Rhod**).

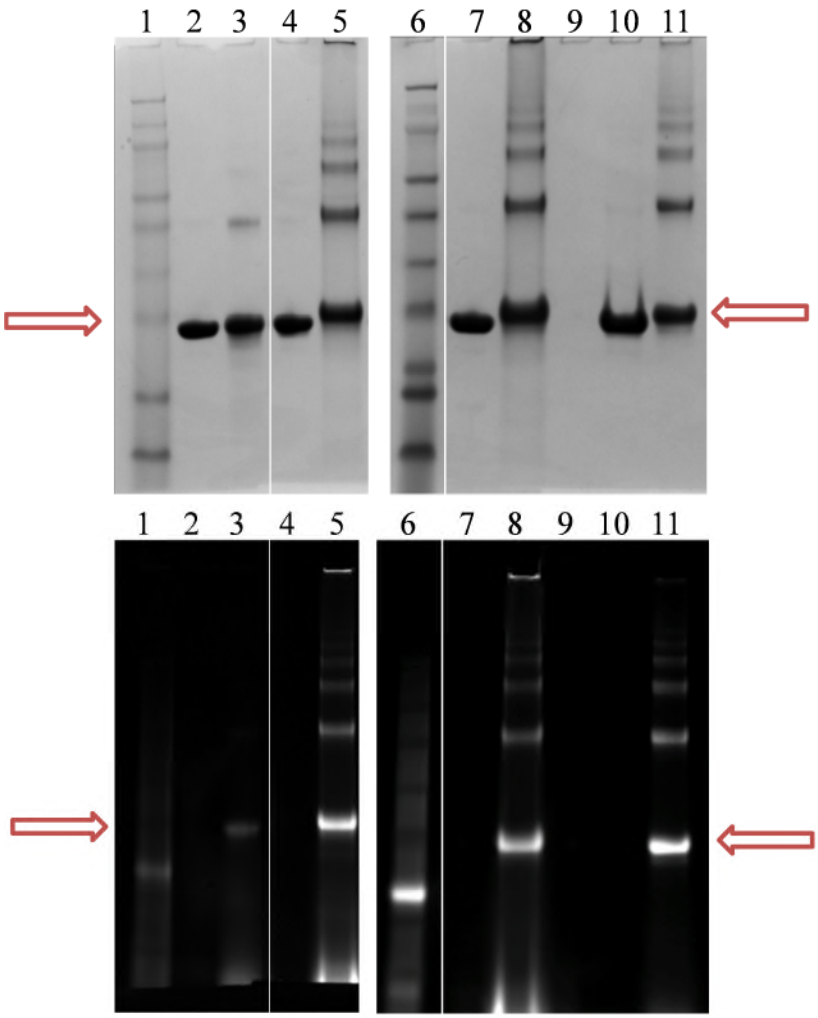

Figure 4.5. PAGE gel of the protein-dye bioconjugates visualized by Coomassie Brilliant Blue (top) and Ruby Red fluorescence (bottom): Left: lane 1: ladder, lane 2: GFP, lane 3: **G0-Rhod**, lane 4: **G216-N_3**, lane 5: **G216-Rhod**; Right: lane 6: ladder, lane 7: **G2-N_3**, lane 8: **G2-Rhod**, lane 9: blank, lane 10: **G2.216-N_3**, lane 11: **G2.216-Rhod**.

Initially the PAGE gels were visualized based on their fluorescence when excited at λ_{ex} = 550 nm and λ_{em} = 630 nm, that would allow observation of the bands containing the Rhodamine-based dye. The resulting images were directly comparable to the ones obtained upon staining of the gels with Coomassie Blue, which is a universal stain. Lanes that were loaded with the parent proteins **G2-N_3**, **G216-N_3**, and **G2.216-N_3** did not produce a band observable by fluorescence, although present when stained by Coomassie Blue, thus confirming that there was no dye conjugated. Their corresponding bioconjugates, **G2-Rhod**, **G216-Rhod**, and **G2.216-Rhod** on the other hand all

produced highly fluorescent bands that were also observable when stained by Coomassie Blue, with mobilities corresponding to GFP. This indicates that indeed the azide-functional GFP molecules have successfully reacted with the alkyne-functional dye. When observed by fluorescence, the non-functional GFP **G0-Rhod** showed a faint band with a mobility corresponding to the unmodified GFP; however the relative intensity suggests that only minimal non-specific incorporation of the **Rhod-alk** has taken place. It should be noted that the bands with lower mobilities observed for all samples exposed to the CuAAC reaction conditions were attributed to aggregates of the protein and the bioconjugates.

Although the successful reaction of **Rhod-alk** with the azide-functional GFP can be inferred based on the fluorescence and PAGE data, liquid chromatography-mass spectrometry (LC-MS) was also employed to confirm that these are not a result of non-covalent interactions (Figure 4.6 and Figure 4.7).

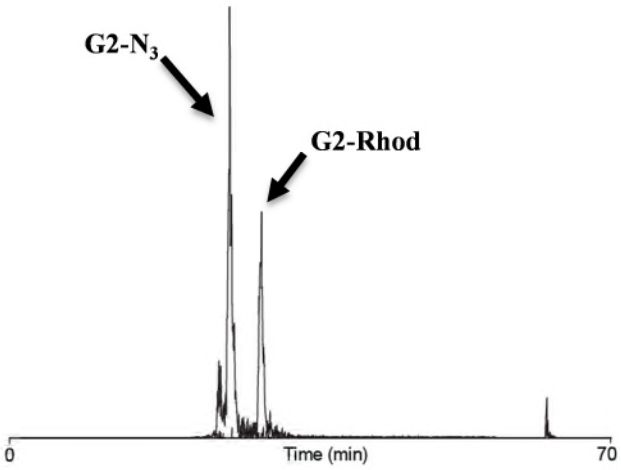

Figure 4.6. Chromatogram obtained from the LC-MS of **G2-Rhod**.

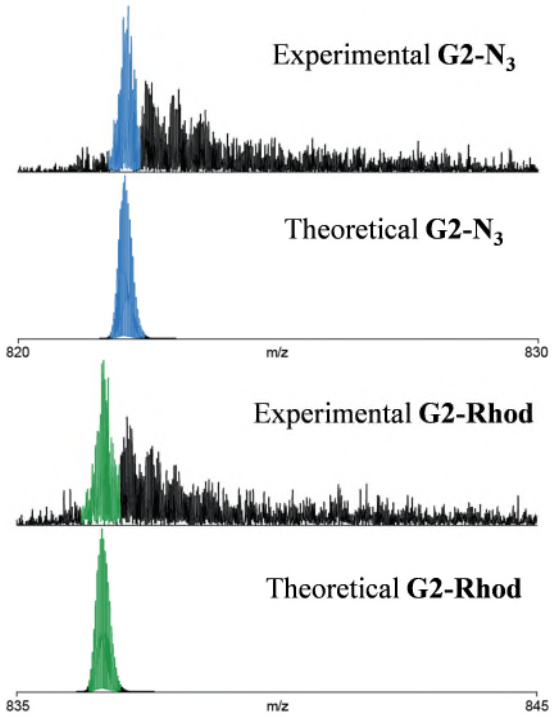

Figure 4.7. Mass spectra of **G2-N_3** and **G2-Rhod**, and the corresponding spectra based on the theoretical isotope distributions. Major peaks in each spectrum coincide with the theoretical peaks for each species and have been highlighted.

While it is apparent from the LC-MS chromatogram that the cycloaddition efficiency is low, the theoretical mass distribution of the functionalized protein matches the experimental, thus confirming the successful CuAAC of **G2-N_3** with **Rhod-alk**. The results from the attempted CuAAC of the alkyne-functional dye **Rhod-alk** and the azide-functional GFP analogues **G2-N_3**, **G216-N_3**, and **G2.216-N_3** indicate that all functional protein residues are indeed – to an extent – accessible for such reactions, and thus conjugation with an alkyne-functional polymer is justified.

4.3.2. Polymerizations

Upon verification of the accessibility of the selected sites on the protein, the synthesis of temperature-responsive polymers of different molecular weights was sought for the formation of the bioconjugates (Scheme 4.3). As such, nine different systems would be obtained (three different proteins and three different polymers) and the effect of the

conjugation site as well as the polymer molecular weight on the temperature-responsive properties of the bioconjugates could be assessed.

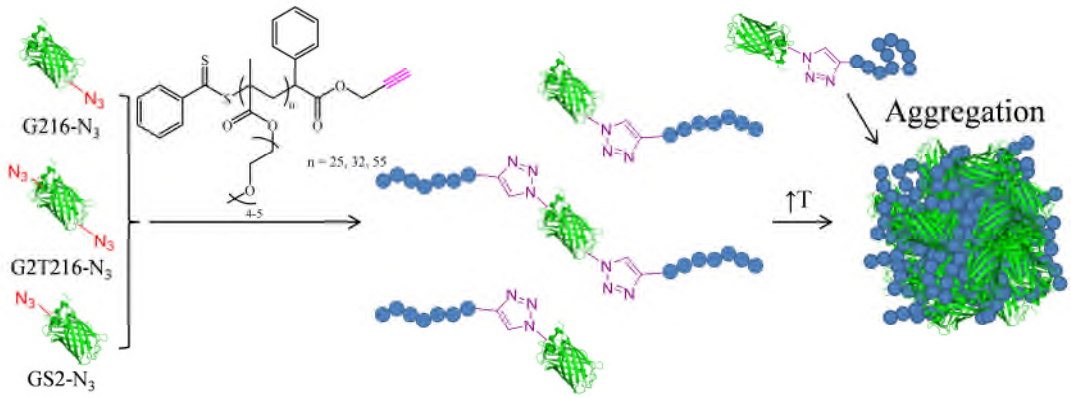

Scheme 4.3. Schematic representation of the strategy followed for the synthesis of the temperature-responsive protein-polymer bioconjugates.

For the synthesis of the polymers, RAFT polymerization was employed as it is an easy process that allows the formation of polymers with an alkyne chain end in a single step. As such, an alkyne-functional dithiobenzoate CTA was synthesized, and used for the polymerization of poly(ethylene glycol) methyl ether methacrylate (OEGMA). Similarly to PEG, as discussed in the introduction (section 4.2), POEGMA has been shown to be biocompatible[38] and additionally, exhibits a lower critical solution temperature (LCST) in water.[97] Therefore, three poly(OEGMA) polymers were synthesized, aiming at different molecular weights. After optimization of the polymerization conditions with regards to the targeted molecular weight, three polymers with different molecular weights were obtained and characterized by SEC (Figure 4.8 and Table 4.1).

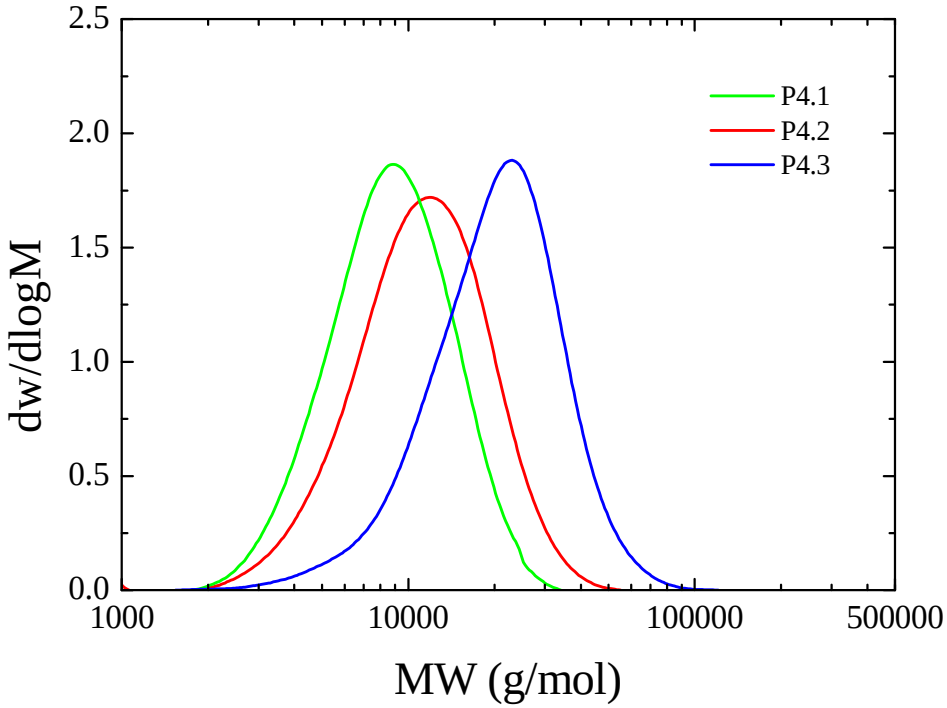

Figure 4.8. Molecular weight distributions of P4.1, P4.2, and P4.3 obtained by SEC in THF (2% Et_3N).

Table 4.1. Molecular weights and dispersities for **P4.1**, **P4.2**, and **P4.3** (determined by SEC in THF against poly(methyl methacrylate) standards).

	M_n (g/mol)	M_w (g/mol)	$Đ_M$
P4.1	7,600	9,600	1.26
P4.2	9,600	12,600	1.32
P4.3	16,700	22,700	1.35

In all cases molecular weight distributions with tailing towards lower molecular weights was observed. This was attributed to potential side reactions taking place and it is suggested that further optimization of the polymerization conditions would eliminate low molecular weight tailing.[98] The chromatograms obtained for the polymers using a differential refractive index detector (DRI) and a UV detector set to λ = 309 nm, a

wavelength at which the dithiobenzoate group absorbs, were compared in order to evaluate the retention of the end-group (Figure 4.9).

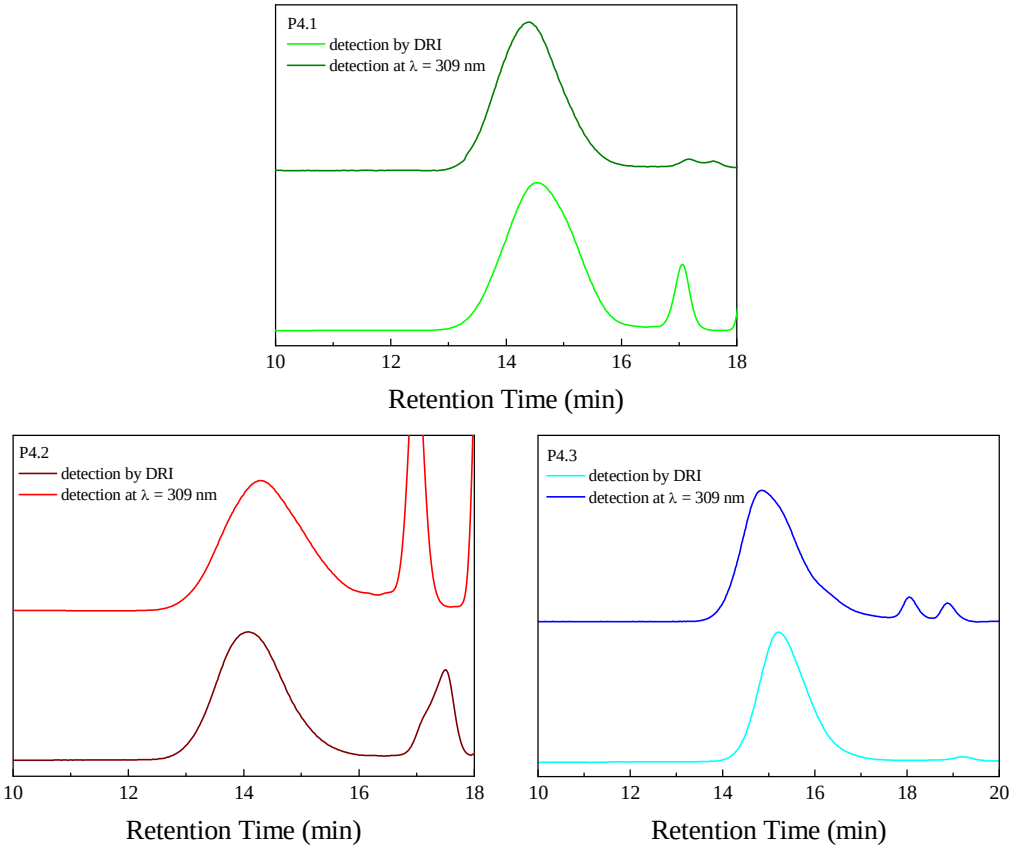

Figure 4.9. Comparison of the chromatograms obtained for **P4.1**, **P4.2**, and **P4.3** using a DRI and a UV detector (SEC in THF, 2% Et_3N).

Although in all cases the distributions corresponding to the polymers are similar for both detection methods, it is observed that at high retention times, and therefore low molecular weights, all polymers exhibit a pronounced shoulder when using the UV detection method. This indicates a higher concentration of the dithiobenzoate group for the lower molecular weight polymers relatively to the non-absorbing repeat unit concentration, which is expected. Therefore, no loss of the end group is indicated. Nevertheless, it should be noted that **CTA1** was chosen as it bears the alkyne

functionality on the R group, thus permitting the bioconjugation regardless of the thiocarbonylthio bond stability.[99]

In order to confirm this hypothesis, **P4.1** was analyzed by ^{1}H NMR spectroscopy (Figure 4.10).

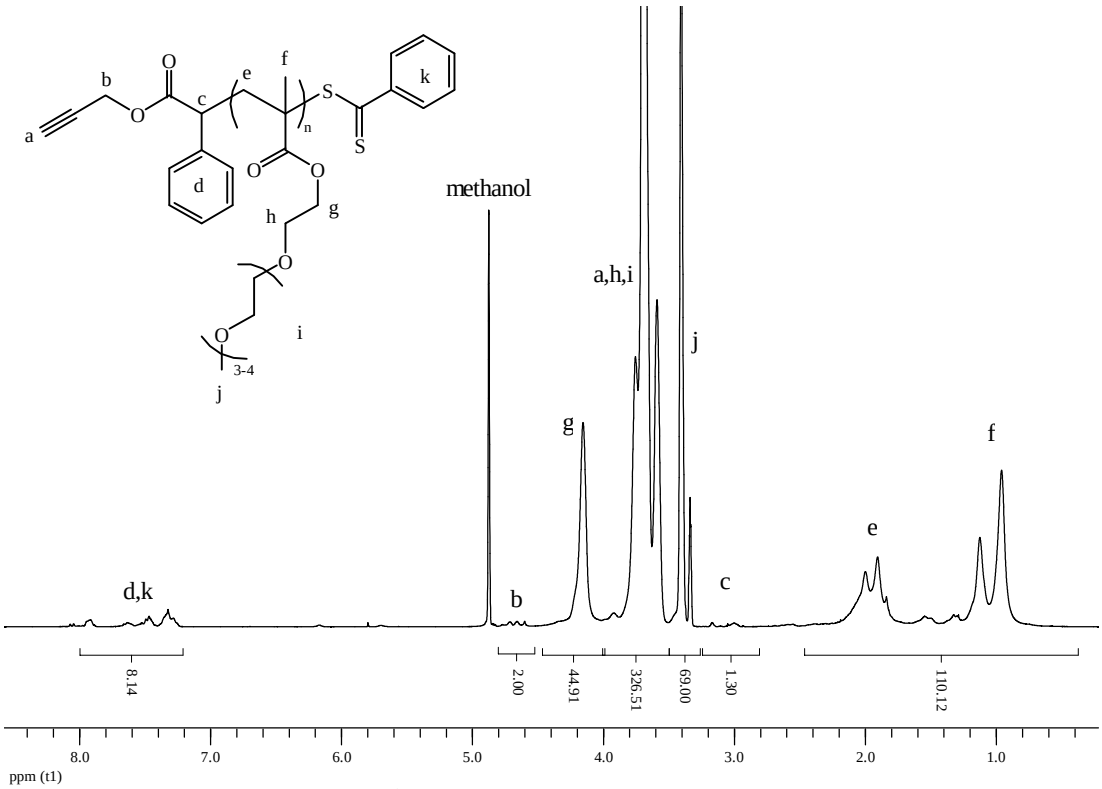

Figure 4.10. Assigned ^{1}H NMR spectrum of polymer **P4.1** showing the characteristic peaks of the end groups (CD_3OD, 500 MHz).

Although the signal corresponding to the alkyne proton was not observed, as it is expected to overlap with the signals from the protons of the pendent PEG groups, the signal corresponding to the CH_2 protons that links the alkyne with the ester was observed at δ = 4.6 ppm. This suggests that the end group is still intact. It should be noted that a small amount of monomer still remains in the sample, in spite of the extensive dialysis, as low intensity signals from the vinyl protons can still be observed at δ = 5.7 and 6.2 ppm. Analysis by ^{1}H NMR spectroscopy was not found suitable for the larger polymers, as the end group signals were significantly weaker as a result of the

greater integration of the repeat unit protons. Additional characterization by infrared spectroscopy was also deemed unsuitable, as the characteristic vibrations of the alkyne group were very weak. Therefore, further proof of the retention of the alkyne end group would be inferred from the efficiency of the CuAAC reaction.

4.3.3. GFP-poly(OEGMA) bioconjugates

The conditions employed for the CuAAC reactions were based on the findings from a comprehensive study on the optimal conditions for CuAAC between polymers and DNA, as that system also suffered from low concentration and high molecular weight components, and further adjusted based on other reports in the literature.[100, 101, 95] As such, each of the three proteins was conjugated with each of the three synthesized polymers, using high excess of the latter, resulting in nine conjugates (Figure 4.11).

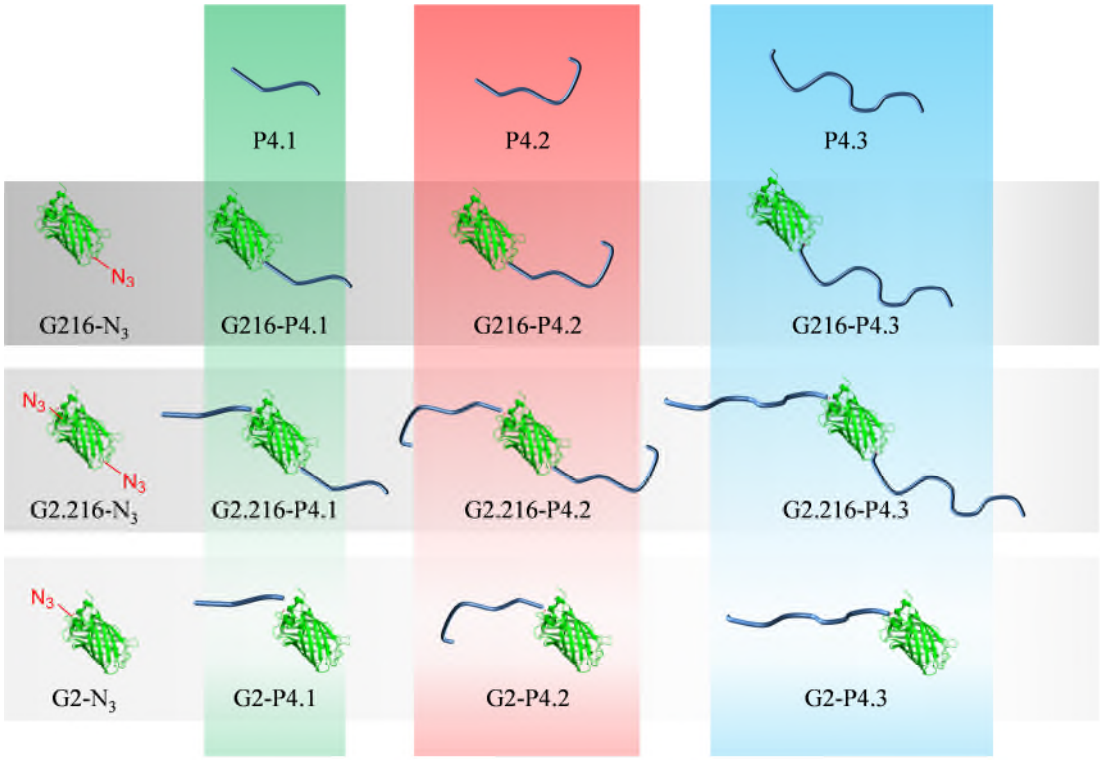

Figure 4.11. Schematic representation of the nine bioconjugates resulting from conjugation of each of the three proteins **G216-N_3**, **G2.216-N_3**, and **G2-N_3** with each of the three polymers **P4.1**, **P4.2**, and **P4.3**.

The crude products from the CuAAC of the proteins and the polymers were purified by size exclusion chromatography in aqueous solution (Figure 4.12).

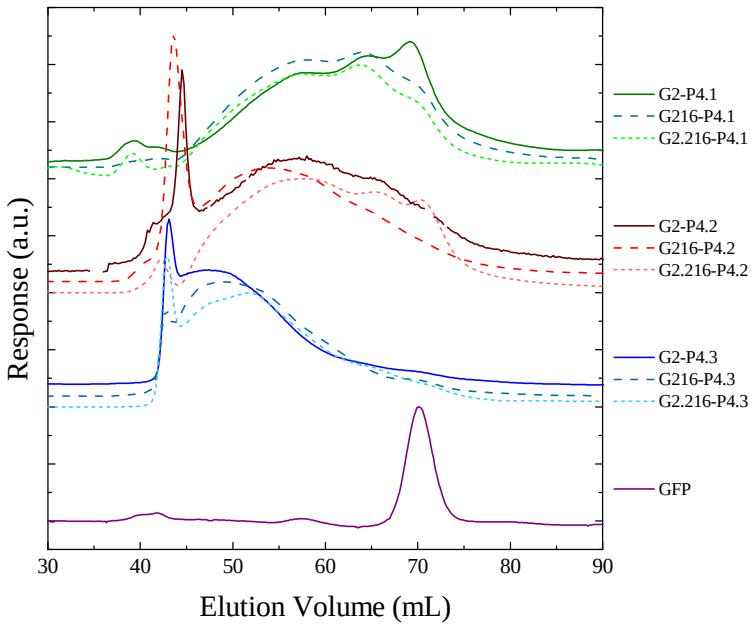

Figure 4.12. Chromatograms from the crude protein-polymer bioconjugates (SEC in Tris buffer).

In all cases a residual GFP peak eluting at ~70 mL was present, suggesting the incomplete reaction between the alkyne-functional polymer and the azide-containing protein. Nonetheless, in all cases the main population was found to elute at lower volumes, thus corresponding to higher effective molecular weights, and were attributed to the successful conjugation. Additionally, the shifting of the main peak to lower retention volumes with increasing polymer molecular weight indicates the increasing molecular weight of the bioconjugates. It should be noted that the peak at ~45 mL corresponds to the exclusion limit of the SEC column. The samples eluting between 45-65 mL were collected and concentrated before further characterization by PAGE analysis (Figure 4.13).

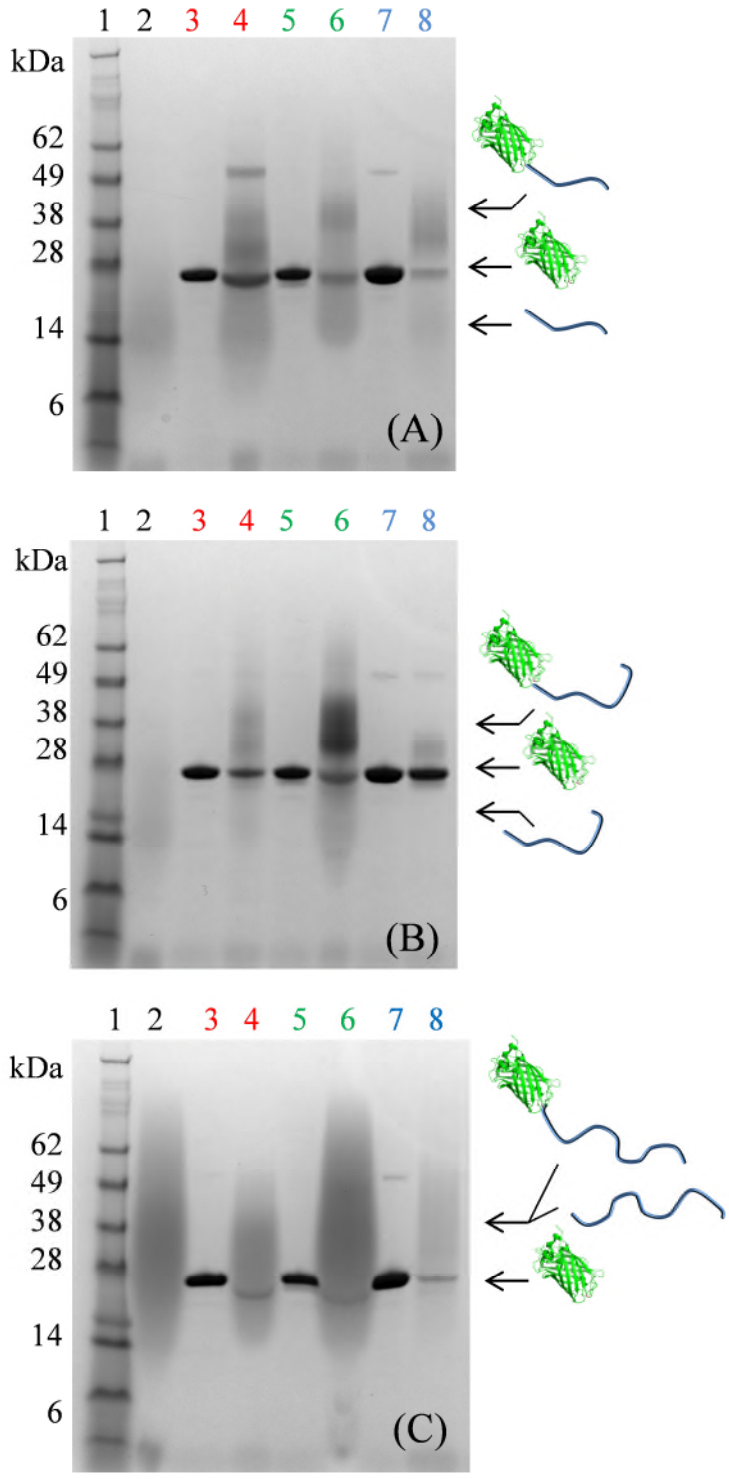

Figure 4.13. PAGE gels of the proteins upon conjugation with **P4.1** (A) lane 1: ladder, lane 2: **P4.1**, lane 3: **G2-N_3**, lane 4: **G2-P4.1**, lane 5: **G216-N_3**, lane 6: **G216-P4.1**, lane 7: **G2.216-N_3**, lane 8: **G2.216-P4.1**, upon conjugation with **P4.2** (B) lane 1: ladder, lane 2: **P4.2**, lane 3: **G2-N_3**, lane 4: **G2-P4.2**, lane 5: **G216-N_3**, lane 6: **G216-P4.2**, lane 7: **G2.216-N_3**, lane 8: **G2.216-P4.2**, and upon conjugation with **P4.3** (C) lane 1: ladder, lane 2: **P4.3**, lane 3: **G2-N_3**, lane 4: **G2-P4.3**, lane 5: **G216-N_3**, lane 6: **G216-P4.3**, lane 7: **G2.216-N_3**, lane 8: **G2.216-P4.3**.

While the bands corresponding to the neat proteins (lanes 3, 5, and 7 in all cases) appear to be narrow and dark, the bands corresponding to the bioconjugates were found to be significantly broader. This was attributed to the greater dispersity of the polymer that is also inherited by the bioconjugates. Indeed, the bands corresponding to the neat polymers (lane 2 in all cases) were broad. Additionally, the lanes loaded with the protein-polymer bioconjugates contained more than one band, suggesting insufficient purification. In order to quantify the relative concentration of the impurities densitometric analysis of the lanes was carried out and the resulting trace was fitted with Gaussian peaks, corresponding to the polymer, the protein, and the bioconjugate. The relative concentration was determined by the relative integration of the Gaussian peaks (Figure 4.14).

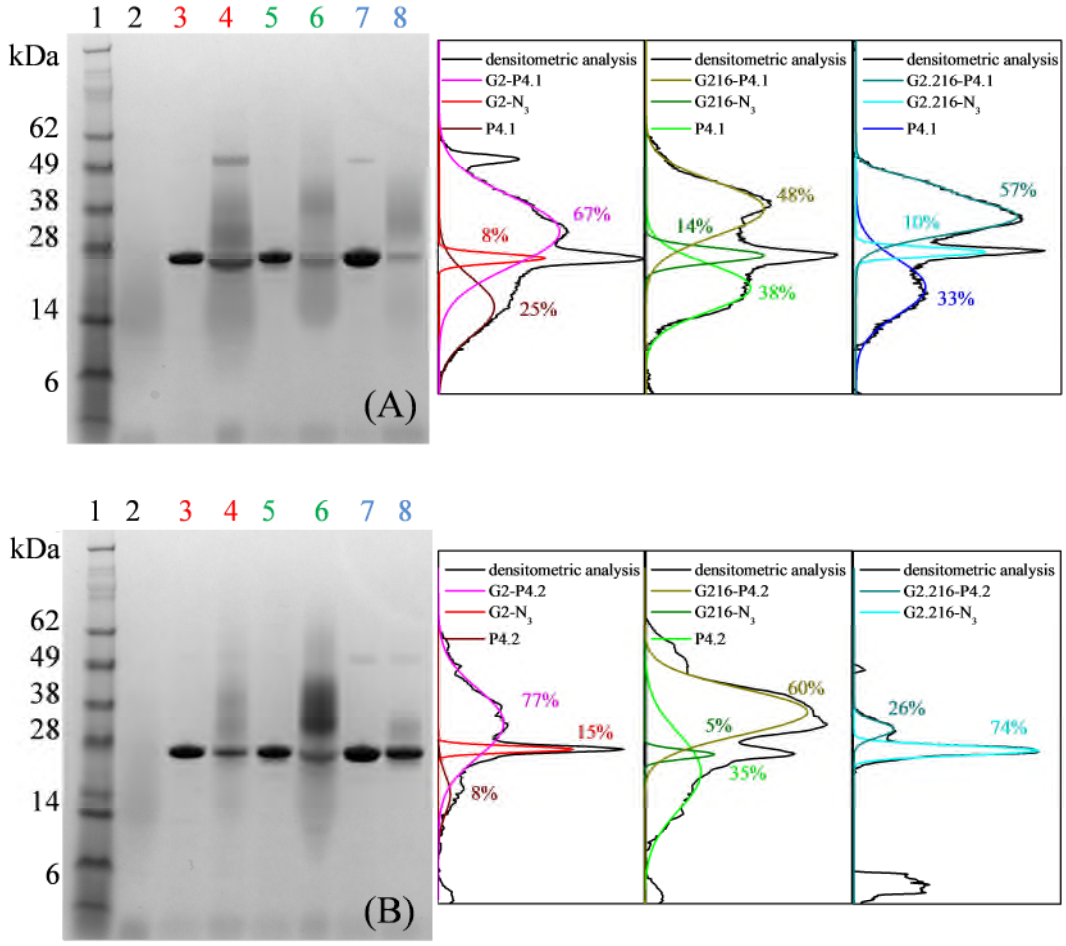

Figure 4.14. PAGE gels of the proteins and densitometric analysis upon conjugation with **P4.1** (A) lane 1: ladder, lane 2: **P4.1**, lane 3: **G2-N_3**, lane 4: **G2-P4.1**, lane 5: **G216-N_3**, lane 6: **G216-P4.1**, lane 7: **G2.216-N_3**, lane 8: **G2.216-P4.1**, upon conjugation with **P4.2** (B) lane 1: ladder, lane 2: **P4.2**, lane 3: **G2-N_3**, lane 4: **G2-P4.2**, lane 5: **G216-N_3**, lane 6: **G216-P4.2**, lane 7: **G2.216-N_3**, lane 8: **G2.216-P4.2**

With the exception of **G2.216-P4.2** whereby the residual unconjugated **G2.216-N_3** was found to be 74% of the sample, in all cases the remaining unconjugated protein was under 15%. However, in all cases unconjugated polymer was found to remain in the sample. It should be noted that densitometric analysis was not carried out for the proteins conjugated with **P4.3** as the polymer band was found to overlap with the bands corresponding to the protein and the bioconjugates, however the bands corresponding to

the unreacted proteins are less intense compared to the other PAGE gels, thus suggesting small amount of un-conjugate protein remaining in the solution.

4.3.4. Thermo-responsive properties

As mentioned previously, PEGMA is a temperature-responsive polymer and thus it is expected that the bioconjugates will inherit this property by exhibiting a cloud point upon heating of the solution. In order to study this, the absorption at λ = 600 nm of the samples was examined as a function of the solution temperature. However, upon heating for the first time a pink precipitate was observed while the solution was cloudy. The supernatant was separated from the precipitate which was characterized by ^{1}H NMR spectroscopy (Figure 4.15).

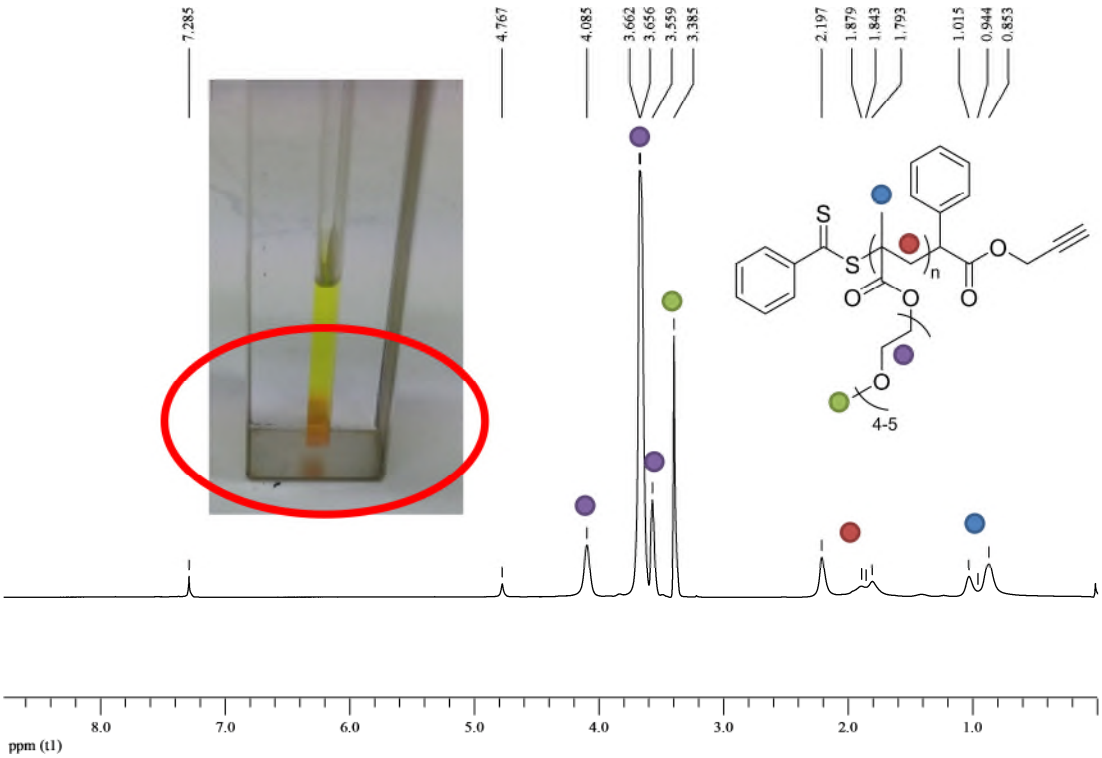

Figure 4.15. Photograph showing the observed pink precipitate and its corresponding assigned ^{1}H NMR spectrum, showing the characteristic signals from the POEGMA homopolymer ($CDCl_3$, 400 MHz)

Upon removal of the precipitate the efficiency of the purification was assessed by PAGE of **G216-P4.2** (Figure 4.16).

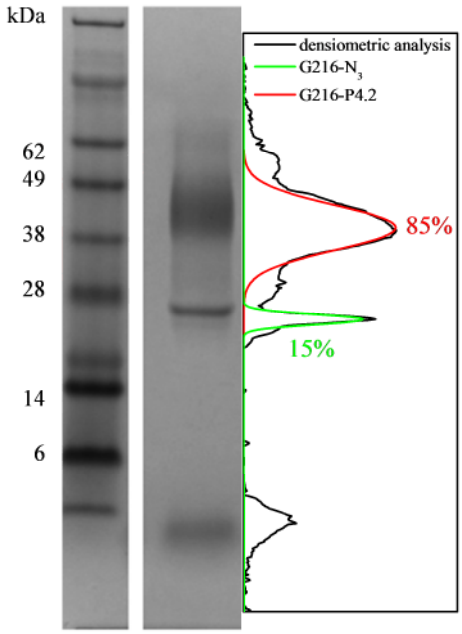

Figure 4.16. PAGE gel and densitometric analysis of the **G216-P4.2** bioconjugate upon purification by the thermal precipitation of excess polymer.

Although some unreacted protein still remains in the solution, the higher mobility band corresponding to the unconjugated polymer has been removed, suggesting the successful purification of the sample. As such, this procedure was repeated for all samples before studying their cloud point as a function of the solution temperature.

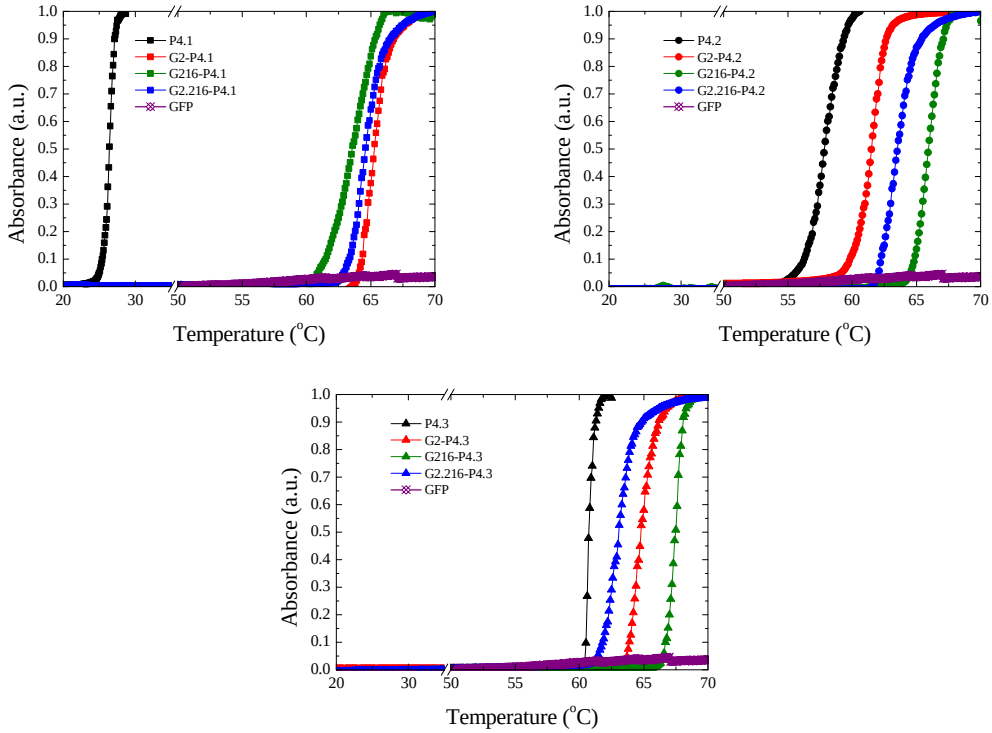

Figure 4.17. Cloud point curves for GFP (purple line), **P4.1**, **P4.2**, and **P4.3** (black lines) and the corresponding bioconjugates after CuAAC with **G2-N$_3$** (red lines), **G216-N$_3$** (green lines), and **G2.216-N$_3$** (blue lines). All lines are averages of three measurements.

In the case of the proteins conjugated with **P4.1**, the cloud point was found to be significantly higher than the neat polymer alone, which was attributed to the fact that the protein provides better water-solubility than the end group of the polymer itself, thus rendering it more hydrophilic. For the **P4.2** and **P4.3** bioconjugates, the cloud point was slightly higher than that of the homopolymers. While the transition temperature of the bioconjugates varied from 61 to 67 °C, there is a distinct effect of the polymer molecular weight and the conjugation site. As such, the shorter polymer (**P4.1**) results in bioconjugates that, regardless of the conjugation site, become insoluble almost at the same temperature (63-65 °C). Increasing the molecular weight of the conjugated polymer (**P4.2**) results in the **G2-P4.2** cloud point to be *ca.* 4 °C lower compared to that of **G216-P4.2**. Although both conjugation sites are located in the flexible loops of the GFP barrel, the local environment appears to affect the ability of the PEGMA chains to

collapse above their cloud point. This is again observed when comparing the two conjugation sites for the larger (**P4.3**) polymers. Interestingly, the transition temperature for the double-conjugated protein **G2.216-P4.2** occurs at a temperature intermediate to the observed transition of the **G2-P4.2** and **G216-P4.2**. Nevertheless, the transition temperature for the higher molecular weight polymer (**P4.3**) conjugated in two positions, as is the case for **G2.216-P4.3**, is lower than either of the two single-functionalized proteins by *ca*. 1 ºC (compared to **G2-P4.3**) and 3 ºC (compared to **G216-P4.3**). This can be attributed to the two polymer chains reaching a critical molecular weight that allows them to interact and thus decrease the effective transition temperature, as seen in other bioconjugate systems.[102] While these conclusions are justified by the observed trends, they are essentially based on three datapoints for each set of measurements, thus are not irrefutable. Further investigations on the effect of the polymer molecular weight on the cloud point of the respective bioconjugates would elucidate the behavior of such systems. It should be noted that none of the cloud points of the bioconjugates showed hysteresis between heating and cooling cycles.

The observations from the cloud point measurements were also confirmed by small-angle X-ray scattering (SAXS) analysis of the samples (measured and analyzed by Anaïs Pitto-Barry). Obtaining a dimensionless Kratky plot for all samples at room temperature (Figure 4.18) and at elevated temperatures (Figure 4.19) was pursued in order to study the morphology of the bioconjugates as particles. As such, the intensity I(q) was normalized to the forward scattering intensity I(0), thus eliminating the molecular weight parameter, while normalization of the scattering wavenumber, q, to the radius of gyration (R_g) of the protein renders the angular scale independent of the protein size.[103]

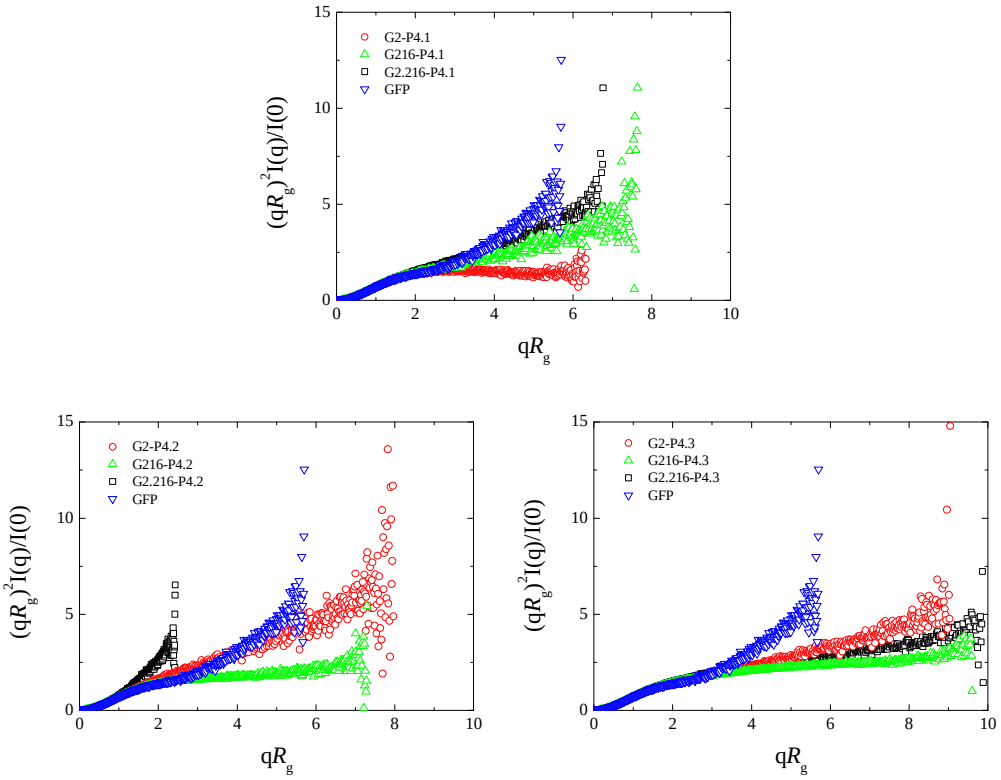

Figure 4.18. Dimensionless Kratky plot for the protein-polymer bioconjugates at room temperature.

Comparison of the obtained graphs suggests that at low qR_g values the structured domains of the bioconjugates are similar to that of the protein in all cases. However, at high qR_g values the gradient of the datapoints for the bioconjugates is smaller than that of the protein, suggesting a more compact structure. Notably, the proteins conjugated with **P4.3** exhibit a significantly more compact structure than any other bioconjugate (or the protein), indicating that the polymer has a greater ability to wrap around the protein compared to the lower molecular weight ones. Nonetheless it should be noted that all graphs obtained at room temperature deviate from the typical bell-shaped curve obtained for folded proteins. However, at elevated temperatures (65 ºC) more compact structures are observed (Figure 4.19).

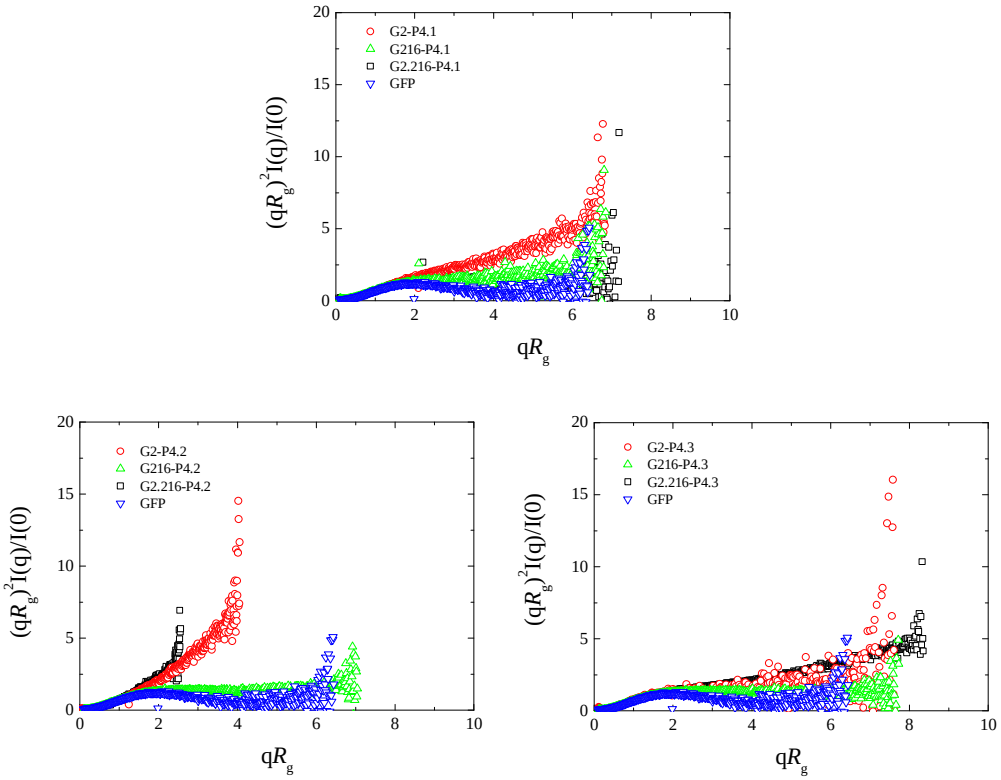

Figure 4.19. Dimensionless Kratky plot for the protein-polymer bioconjugates at 65 ºC.

Interestingly, the native GFP shows a more compact structure, as suggested by the bell-like shape, at elevated temperatures when compared to room temperature. Additionally, at 65 ºC it appears more compact than all the bioconjugates, suggesting contribution of the collapsed polymer chains to the unstructured domains observed. Noteworthy is that regardless of the polymer molecular weight, conjugation with **G216-N_3** results in a more compact structure at elevated temperatures, compared to the bioconjugates obtained from the **G2-N_3** protein. These results further indicate the different behavior of the polymers when conjugated to different sites on a protein.

As discussed previously, the solutions of the bioconjugates exhibit a cloud point upon heating without macroscopic precipitation. This indicates the self-assembly of the amphiphilic bioconjugates, whereby the hydrophilic part is the protein and the

hydrophobic the polymer. As such, the determination of the size of the **G216-P4.2** bioconjugate was sought by dynamic light scattering (DLS) (Figure 4.20).

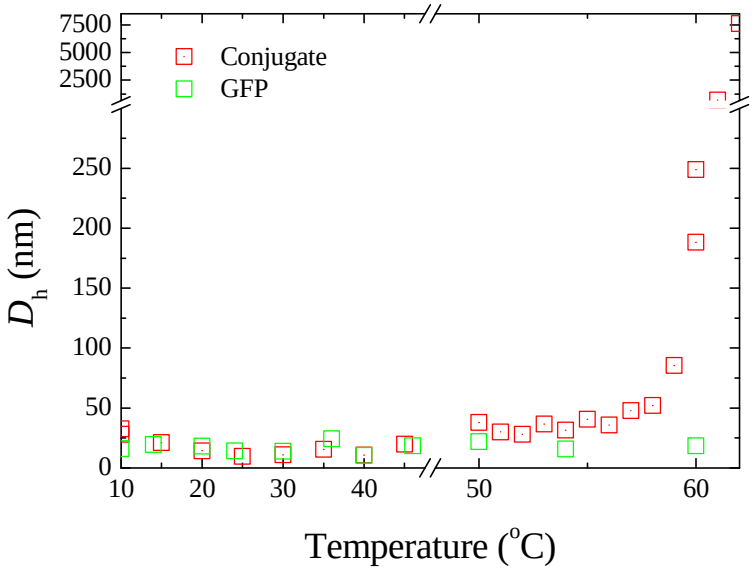

Figure 4.20. Dependence of the hydrodynamic diameter of the **G216-P4.2** bioconjugate and GFP on temperature, measured in buffer.

Upon heating, the hydrodynamic size of the bioconjugates dramatically increases, whereas the unfunctionalized GFP is found to retain its original size. It should be however noted that larger populations were also observed – regardless of the measuring temperature, which were attributed to aggregates also observed in neat buffer.

In order to further confirm that the increase in size is attributed to the assembly of the bioconjugates as opposed to aggregation of buffer solutes, the sample was dissolved in water and the measurement was repeated (Figure 4.21).

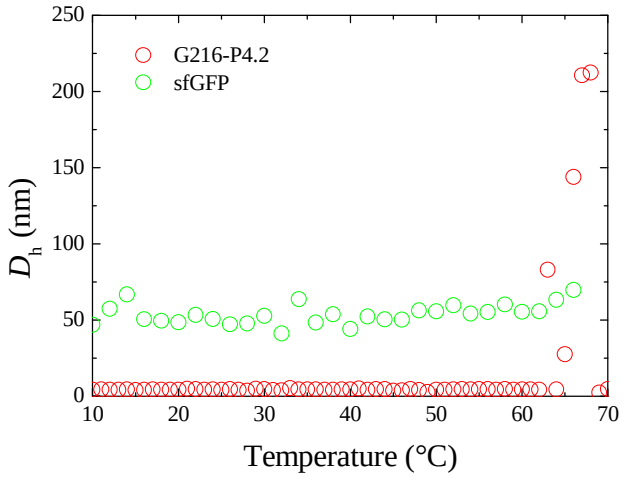

Figure 4.21. Determination of the hydrodynamic sizes of sfGFP and **G216-P4.2** at different temperatures in water.

The size of the particles in the water was found to increase when the solution temperature was above 62 ºC. While in pure water (as opposed to buffer solution) the protein is expected to partially denature and hence aggregate, as suggested by the large sizes obtained for the sfGFP in water, the results obtained for the bioconjugate show a similar temperature-responsive trend in the aggregation of the bioconjugates as the trend seen in the buffer solution. Therefore, the larger particles observed at elevated temperatures in buffer are not an artefact produced by the buffer itself, but a result of the bioconjugate aggregation.

It was hypothesized that the bioconjugates will self-assemble into higher-order structures, in a fashion similar to amphiphilic copolymers. To further examine the size and shape of the aggregates, a small sample was deposited on a graphene oxide grid at elevated temperature in order for the structures to retain their formation (Figure 4.22) and were then observed by transmission electron microscopy (TEM).

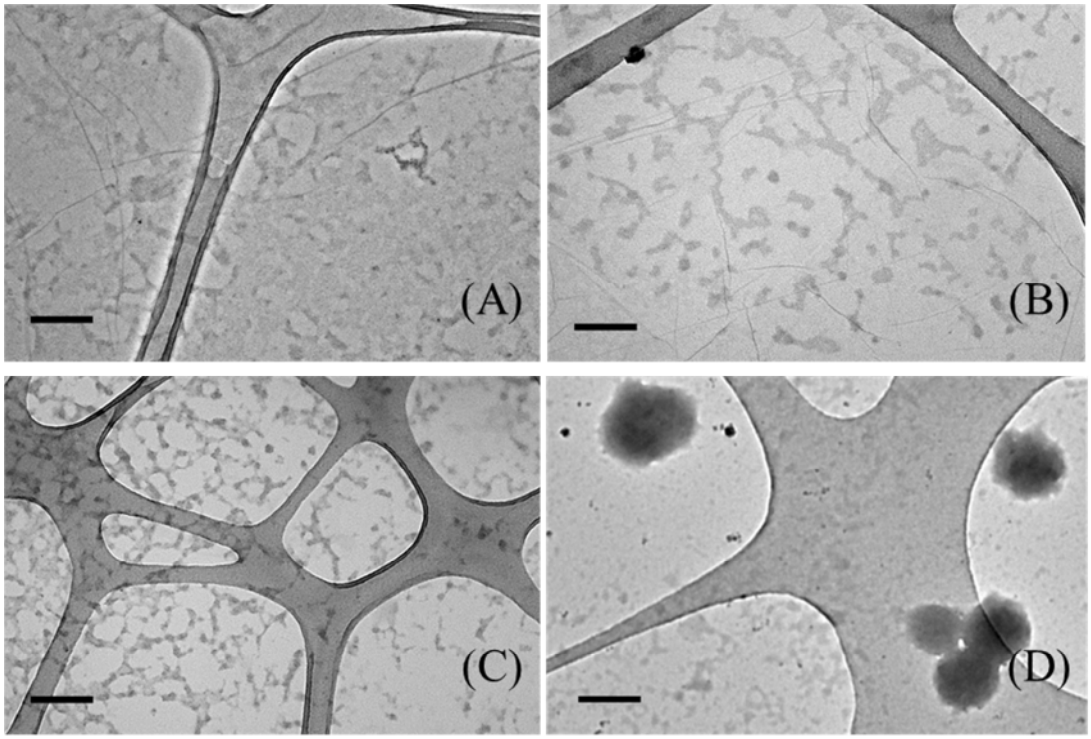

Figure 4.22. Representative TEM images of the **G2-P4.1** (A), **G2-P4.2** (B), **G2-P4.3** (C), and **G2.216-P4.2** (D) prepared at temperatures above the cloud point of the bioconjugates (Scale bars: 200 nm; graphene oxide grids, unstained).

The obtained images from the polymers conjugated with **G2-N_3** show aggregates of sizes varying from 20-200 nm, further confirming the amphiphilic character of the bioconjugates that self-assemble at elevated temperatures. In addition to that, the bioconjugate **G2.216-P4.2** is shown where larger particles (up to 400 nm) as well as smaller aggregates are observed. This can be a result of the higher polymer, and thus hydrophobic, content of the bioconjugates. While the shape of the aggregates varies from spherical to lamellar, the reproducibility of the images was inconsistent and, at this point, it is hypothesized that the heating rate affects the resulting morphology and further investigation is therefore deemed necessary in order to obtain more well-defined structures.

4.3.5. Activity of the bioconjugates

As mentioned in the introduction of this Chapter, it is often the case that conjugation of a protein with a polymer results in loss in activity. In order to elucidate this, the fluorescence quantum yield of the **G216-P4.2** bioconjugate was determined and compared to that calculated for GFP. This was achieved by recording the absorption and fluorescence spectra of the two samples (Figure 4.23), as well as a 0.1 μM solution of fluorescein free acid in 0.1 M NaOH, as the standard sample.[104]

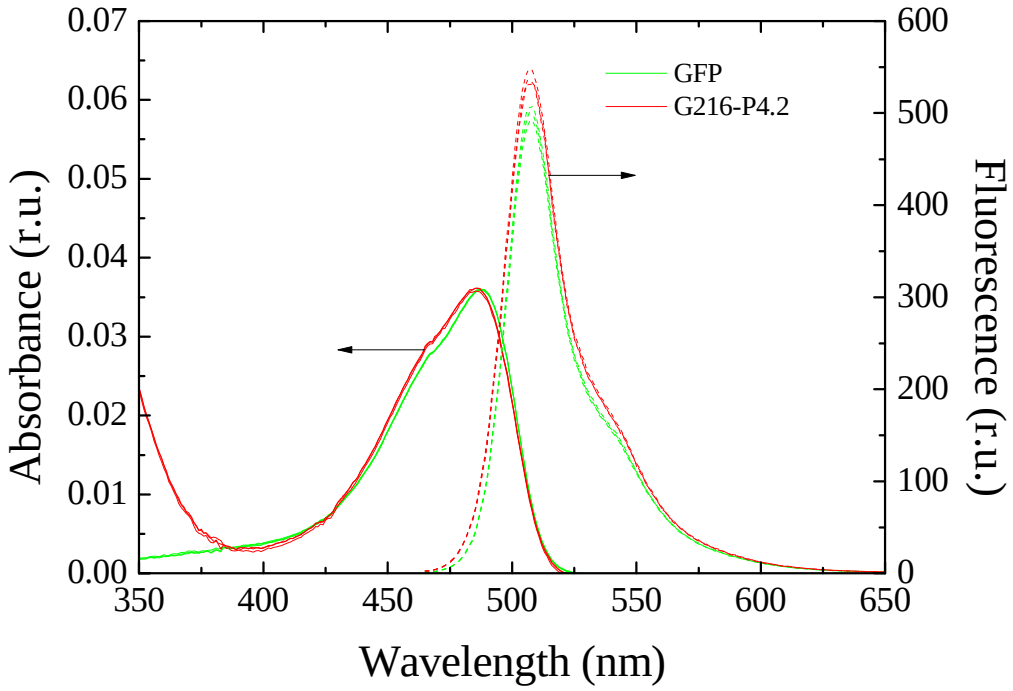

Figure 4.23. Normalized absorption and fluorescence emission spectra in relative units (r.u.) for GFP and **G216-P4.2**, showing retention of the protein fluorescence upon functionalization.

From the absorption spectra, the absorption factors, f, were determined for each sample using equation **(4.1)**, where λ_{ex} = 460 nm.

$$f_{sample} = 1 - 10^{-A(\lambda_{ex})} \quad \textbf{(4.1)}$$

Then, the quantum yield (Φ) was determined based on the fluorescence spectra and the known quantum yield of fluorescein Φ_{st} = 0.89, based on equation **(4.2)** (F is the fluorescence emission peak integration and n is the solvent refractive index).

$$\Phi_{sample} = \Phi_{st} \frac{F_{sample}}{F_{st}} \frac{f_{st}}{f_{sample}} \frac{n_{sample}^2}{n_{st}^2} \quad \textbf{(4.2)}$$

As such, GFP was found to have a quantum yield of 0.613 (±0.016) while the quantum yield of the bioconjugate **G216-P4.2** was found to be 0.638 (±0.014). This suggests that the fluorescence of the protein is indeed not affected by the conjugated polymer.

The effect of the conjugation on the protein activity was also assessed by multiple heating-cooling cycles between 25 and 70 ºC and measuring the fluorescence intensity (Figure 4.24).

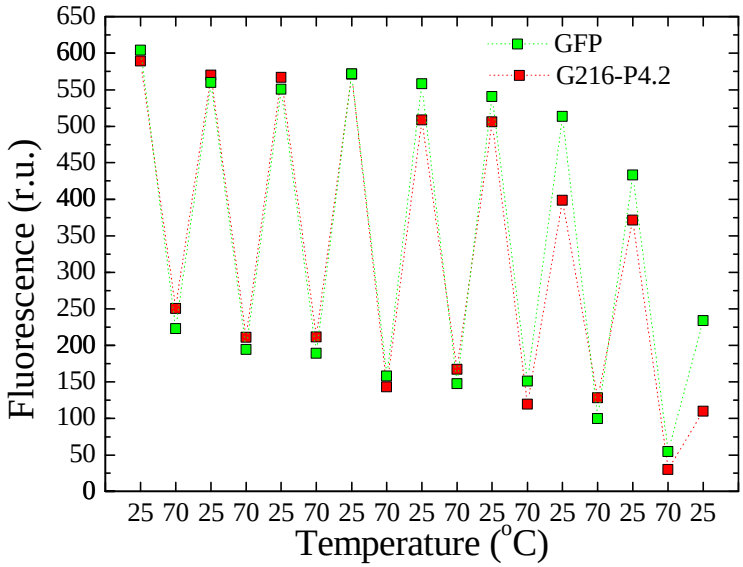

Figure 4.24. Fluorescence maxima (λ_{ex} = 470 nm, λ_{em} = 507 nm) of the un-functionalized GFP and the **G216-P4.2** bioconjugate as a function of temperature upon multiple heating-cooling cycles.

Although the initial fluorescence at room temperature for both samples was similar, upon heating to 75 ºC it had significantly decreased. However, upon cooling the

fluorescence was almost completely regained for both samples. After repeating the heating-cooling cycles six times, a drop in the fluorescence is observed for both samples, although it is more prominent for the protein-polymer bioconjugate. Only after eight cycles the fluorescence intensity drops to less than half the initial intensity at room temperature for both samples, as a result of the repeated heating cycles. It was hypothesized that the more prominent loss of activity of the bioconjugate is attributed to the fact that as upon heating the polymer is dehydrated, creating a hydrophobic environment on the surface of the protein that was previously hydrophilic, thus disrupting the protein folding and resulting in the loss of fluorescence. It is noteworthy that the drop in activity is only observed after the sixth cycle that corresponds to ~ 1 hour of heating in total.

4.4. Conclusions

To conclude, the conjugation of a temperature-responsive polymer onto selected sites on a protein was successfully achieved by CuAAC reaction. The selected sites were introduced *via* engineering of GFP resulting in the substitution of selected natural amino acids with the non-natural azide functional *p*AzF. The azide moiety was orthogonally functionalized with an alkyne-bearing fluorescent dye in order to prove the accessibility of the sites for such reactions. This was successfully shown by the appearance of the dye fluorescence emission, even when excited at the excitation wavelength of the protein, suggesting energy transfer, and thus proximity. Three polymers were synthesized by RAFT polymerization using an alkyne-bearing CTA and were then used for the CuAAC reaction with the azide moieties on the proteins. The nine obtained bioconjugates all exhibited temperature-responsive properties that were found to be affected by the molecular weight of the polymer as well as the conjugation site onto the protein.

Although increasing the solution temperature resulted in the formation of aggregates, further studies on the parameters that affect the morphology of the structure are necessary.

4.5. Materials and Methods

2,2′-Azobis(2-methylpropionitrile) (AIBN) was recrystallized from methanol. Poly(ethylene glycol) methyl ether methacrylate ($OEGMA_{300}$) was purchased from Sigma-Aldrich and was passed through a basic alumina plug before use. Rhodamine B (>95%), propargyl alcohol (99%), *tris*-(3-hydroxypropyltriazolylmethyl)amine (95%), (+)-sodium L-ascorbate (>98%), copper sulfate pentahydrate (>98%), 4-bromophenylacetic acid (98%), and carbon disulfide (>99%) were purchased from Sigma-Aldrich and used without further purification.

Nuclear magnetic resonance (^{1}H and ^{13}C NMR) spectra were recorded on a Bruker AC-250, a Bruker DPX-300, a Bruker AV-400 or a Bruker DPX- 400, a Bruker AV-500, and a Bruker AV II-700 spectrometer. Chemical shifts are reported as δ in parts per million (ppm) and referenced to the chemical shift of the residual solvent resonances ($CDCl_3$ ^{1}H: δ = 7.26 ppm; ^{13}C: δ = 77.2 ppm; CD_3OD ^{1}H: δ = 4.78 ppm, ^{13}C: 49.3 ppm). High resolution mass spectra (HRMS) were collected using a Bruker MaXis UHR-ESITOF. Dynamic light scattering measurements were conducted on a Malvern Zetasizer equipped with a 632 nm laser source and a fixed angle detector (172 ^{o}). Aqueous size exclusion chromatography was performed on a GE Healthcare AKTA-Purifier equipped with a HiLoad Superdex 75 PG column and a fraction collector, operating at 4 ºC. SEC measurements were carried out on an Agilent 390-MDS equipped with differential refractive index and UV detectors. The separation was achieved by a guard column (Varian PLGel 5 μm) and two mixed-D columns

(Varian PLGel 5 μm) using THF (2% Et_3N mixture) as the eluent at a flow rate of 1 mL/min. Data analysis was performed using Cirrus v3.3 with calibration curves produced using Varian Polymer laboratories Easi-Vials linear poly(methyl methacrylate) standards. Transmission electron microscopy was performed on a JEOL 2000FX in bright field mode. Sample preparation is as follows: the bioconjugates were diluted x100 and heated to 70 ºC. A graphene oxide-coated TEM grid was also heated to 75 ºC before deposition of the sample droplet. After the drop dried, the grid was rinsed with pre-heated deionized water to remove buffer salts. The buffer used in all experiments is a pH 8 Tris-Cl buffer. Fluorescence spectra were recorded on a single beam Perkin Elmer LS55 fluorometer. PAGE gel analysis was carried out using 4-12 % NuPAGE SDS-PAGE gel kits (Invitrogen). Densiometric analysis was performed using ImageJ software and determining the grayscale profile of the lane length. UV/vis spectroscopy was carried out on a Perkin Elmer Lambda 35 UV/vis spectrometer, equipped with a PTP-1+1 Peltier temperature programmer. For the cloud point measurements the absorbance of the samples at λ = 600 nm was measured as a function of the solution temperature.

4.5.1.1. Synthesis of *N*-(6-(diethylamino)-9-(2-((prop-2-yn-1-yloxy) carbonyl)phenyl)-3*H*-xanthen-3-ylidene)-*N*-ethylethanaminium (**Rhod-alk**)

In an ice cold round-bottom flask propargyl alcohol (81 μL, 1.392 mmol, 1 eq.), Rhodamine B (1g, 2.088 mmol, 1.5 eq.), *N*,*N*'-dicyclohexylcarbodiimide (310.2 mg, 1.503 mmol, 1.08 eq.) were dissolved in 50 mL dichloromethane (CH_2Cl_2) before the addition of 4-(dimethylamino)pyridine (11.1 mg, 0.090 mmol, 0.065 eq.). The reaction was allowed to warm to room temperature and was stirred overnight. The precipitates were removed by filtration and the solvent was removed under reduced pressure. The

product was isolated as a dark purple-green solid after purification by column chromatography (382 mg, 57% isolated yield). TLC (CH_2Cl_2:methanol 9:1): R_f = 0.43; ^{1}H NMR ($CDCl_3$, 300 MHz) δ (ppm): 8.29 (1H, m, Ar), 7.80 (1H, m, Ar), 7.72 (1H, m, Ar), 7.31 (1H, m, Ar), 7.03 (2H, d, ^3J = 9.5 Hz, Ar), 6.87 (2H, dd, ^3J = 2.4, 9.5 Hz, Ar), 6.80 (2H, d, ^3J = 2.4 Hz, Ar), 4.59 (1H, d, ^3J = 2.4, -OCH_2-), 3.57-3.65 (8H, q, ^3J = 7.1 Hz, C**H**$_2$-CH_3), 2.39 (1H, t, ^3J = 2.4 Hz, C≡CH), 1.29 (12H, t, ^3J = 7.1 Hz, CH_3); ^{13}C NMR (CD_3OD, 125 MHz) δ (ppm): 113.7, 112.9, 95.8, 76.3, 75.3, 52.3, 45.55, 12.1; HRMS (*m/z*): expected: 481.2486; found: 481.2492 $[M]^+$.

4.5.1.2. CuAAC reaction of azide-functional GFP and **Rhod-alk**

In a typical reaction (see Table 4.2 for exact quantities), freshly prepared solutions (in buffer) of **Rhod-alk** (40 µL, 5.455 mM), *tris*-(hydroxypropyltriazolylmethyl)amine (THPTA) (80 µL, 0.013 M), (+)-sodium L-ascorbate (NaAsc) (90 µL, 0.113 M), and copper sulfate pentahydrate (40 µL, 0.005 M) were added to a protein solution (250 µL, 0.081 mM). The reaction was stirred at room temperature overnight. Excess dye was then removed by consecutive spin filtration and addition of fresh buffer cycles until the filtrate was clear.

Table 4.2. Calculated quantities for the CuAAC reaction of the azide functional proteins and the alkyne functional dye **Rhod-alk**.

	protein	**Rhod-alk**	THPTA	NaAsc	$CuSO_4 \cdot 5H_2O$
G2-Rhod	1.125 mg 41.7 nmol 1 eq.	0.216 mg 0.42 μmol 10 eq.	0.905 mg 2.08 μmol 50 eq.	4.13 mg 20.83 μmol 500 eq.	0.104 mg 0.42 μmol 10 eq.
G216-Rhod	1.125 mg 41.7 nmol 1 eq.	0.216 mg 0.416 μmol 10 eq.	0.905 mg 2.08 μmol 50 eq.	4.13 mg 20.83 μmol 500 eq.	0.104 mg 0.42 μmol 10 eq.
G2.216-Rhod	1.125 mg 41.7 nmol 1 eq.	0.432 mg 0.832 μmol 20 eq.	1.810 mg 4.16 μmol 100 eq.	8.26 mg 41.66 μmol 1000 eq.	0.208 mg 0.84 μmol 20 eq.

4.5.1.3. Synthesis of prop-2-yn-1-yl 2-phenyl-2-((phenylcarbonothioyl) thio)acetate (**CTA1**)

The synthesis of the alkyne CTA was concluded in 3 steps, based on procedures from the literature.[105-107] For the first step, α-bromophenyl acetic acid (5g, 23.25 mmol, 1 eq.) was added to freshly distilled thionyl chloride (12.6 mL, 172.81 mmol, 7.4 eq.) and the mixture was refluxed under nitrogen for 2.5 hours. Excess reagents and by-products were removed by distillation at room temperature to yield a brown oil that was used without further purification.

For the second step, in a dry round bottom flask, propargyl alcohol (6.77 mL, 116.21 mmol, 5 eq.) and triethylamine (6.48 mL, 46.5 mmol, 2 eq.) were dissolved in dry dichloromethane (25 mL) and purged with nitrogen before the brown oil was added drop-wise. The mixture was stirred overnight before washing with 0.1M HCl, water, saturated $HNaCO_3$, and water. The organic layer was then dried over $MgSO_4$ and dried under reduced pressure. The pure product (prop-2-yn-1-yl 2-bromo-2-phenylacetate) was isolated by flash chromatography (2.8 g, 48% isolated yield). TLC ($CHCl_2$:Petroleum Ether): $R_f = 0.73$; ^{1}H NMR ($CDCl_3$, 300 MHz) δ (ppm) 7.39 (2H, m,

Ar), 7.24 (3H, m, Ar), 5.25 (1H, d, ^{3}J = 2.5 Hz, -CH-Br), 4.61 (2H, m, -O-CH_2-), 2.36 (1H, m, ≡CH); ^{13}C NMR ($CDCl_3$, 75 MHz) δ (ppm): 167.6, 135.3, 129.5, 128.7, 128.0, 76.5, 75.9, 53.7, 45.9.

For the third step, 2-phenyl magnesium bromide (3M solution in diethyl ether, 2.95 mL, 8.84 mmol, 1 eq.) was added to a dry round bottom flask containing dry THF (9 mL). The mixture was heated to 40 ºC before the slow addition of carbon disulfide (532 µL, 8.84 mmol, 1 eq.). Then, the previously synthesized prop-2-yn-1-yl 2-bromo-2-phenylacetate was added (2.35 g, 9.29 mmol, 1.05 eq.) and the reaction was allowed to proceed overnight at 80 ºC. Upon cooling, 20 mL of ice-cold water were added and the organic layer was extracted with diethyl ether three times. The combined ether phases were washed with water and dried over $MgSO_4$. The product was purified by flash chromatography (1.33 g, 46% isolated yield). TLC (Et_2O:Petroleum ether 1:2): *R*f = 0.54; ^{1}H NMR ($CDCl_3$, 300 MHz) δ (ppm): 7.98 (2H, dd, ^{3}J = 1.1, 8.4 Hz, Ar), 7.44 (8H, m, Ar), 5.71 (1H, s, -S-CH-), 4.74 (2H, m, CH_2), 2.47 (1H, d, ^{3}J = 2.5, ≡CH); ^{13}C NMR (CD_3OD, 125 MHz) δ (ppm): 226.3, 168.1, 143.9, 132.7, 132.6, 129.0, 128.9, 128.6, 128.5, 128.3, 76.6, 45.5, 58.5, 53.0; HRMS (*m/z*): expected: 349.0327; found: 349.0325 $[M+Na]^{+}$.

4.5.1.4. RAFT polymerizations – Synthesis of **P4.1**, **P4.2**, and **P4.3**

For a typical synthesis (see Table 4.3 for exact quantities), AIBN (1.2 mg, 7 µmol, 0.1 eq.), **CTA1** (22.8 mg, 70µmol, 1 eq.), and the monomer $OEGMA_{300}$ (2 mL, 7 mmol, 100 eq.) were dissolved in 1,4-dioxane (4 mL) and degassed by three freeze-pump-thaw cycles. The ampoule was then charged with nitrogen and the reaction was stirred for three hours at 65 ºC. The polymer was isolated *via* precipitation in cold hexane, followed by dialysis against pure water to remove excess monomer.

Table 4.3. Reagent quantities and conditions used for the synthesis of the alkyne-functional polymers

		P4.1	**P4.2**	**P4.3**
$OEGMA_{300}$	m (g)	2.0	1.0	2.0
	n (mmol)	6.670	3.334	6.670
	eq.	50	50	100
CTA1	m (mg)	43.2	21.6	22.8
	n (mmol)	0.132	0.066	0.070
	eq.	1	1	1
AIBN	m (mg)	2.2	1.1	1.2
	n (mmol)	0.013	0.007	0.007
	eq.	0.1	0.1	0.1
dioxane	V (mL)	4	2	4
time	(h)	2	2.5	3

4.5.1.5. CuAAC reaction of azide-functional GFP and polymers **P4.1**, **P4.2**, and **P4.3**

In a typical reaction (see Table 4.4 for exact quantities), freshly prepared solutions (in buffer) of the polymer, THPTA (80 µL, 0.013 M), NaAsc (90 µL, 0.113 M), and copper sulfate pentahydrate (40 µL, 0.005 M) were added to a protein solution (250 µL, 0.081 mM). The reaction was stirred at room temperature overnight. The bioconjugates were purified initially by SEC in order to remove low molecular weight impurities and excess GFP. Excess polymer was further removed by thermal precipitation (see section 4.3.4).

Table 4.4. Quantities calculated for the CuAAC of **P4.1**, **P4.2**, and **P4.3** to the three different proteins **G2-N_3**, **G216-N_3**, and **G2.216-N_3.**

	protein	polymer	THPTA	NaAsc	$CuSO_4 \cdot 5H_2O$
G2-P4.1	1.125 mg 40 nmol 1 eq.	31.8 mg 4.17 µmol 100 eq.	0.905 mg 2.08 µmol 50 eq.	4.13 mg 20.85 µmol 500 eq.	0.104 mg 0.42 µmol 10 eq.
G216-P4.1	0.88 mg 30 nmol 1 eq.	24.8 mg 3.25 µmol 100 eq.	0.706 mg 1.62 µmol 50 eq.	3.22 mg 16.25 µmol 499 eq.	0.081 mg 0.32 µmol 10 eq.
G2.216-P4.1	0.563 mg 20 nmol 1 eq.	31.8 mg 4.17 µmol 200 eq.	0.906 mg 2.09 µmol 100 eq.	4.13 mg 20.85 µmol 1001 eq.	0.104 mg 0.42 µmol 20 eq.
G2-P4.2	1.302 mg 50 nmol 1 eq.	46.3 mg 4.82 µmol 100 eq.	1.042 mg 2.4 µmol 50 eq.	4.771 mg 24.08 µmol 500 eq.	0.12 mg 0.48 µmol 10 eq.
G216-P4.2	2.604 mg 100 nmol 1 eq.	92.6 mg 9.64 µmol 100 eq.	2.084 mg 4.8 µmol 50 eq.	9.542 mg 48.16 µol 500 eq.	0.24 mg 0.96 µmol 10 eq.
G2.216-P4.2	1.324 mg 50 nmol 1 eq.	94 mg 9.79 µmol 200 eq.	2.14 mg 4.93 µmol 100 eq.	9.71 mg 49.01 µmol 1000 eq.	0.24 mg 0.96 µmol 20 eq.
G2-P4.3	1.125 mg 40 nmol 1 eq.	69.6 mg 4.17 µmol 100 eq.	0.9 mg 2.07 µmol 50 eq.	4.12 mg 20.8 µmol 499 eq.	0.104 mg 0.42 µmol 10 eq.
G216-P4.3	1.125 mg 40 nmol 1 eq.	69.6 mg 4.17 µmol 100 eq.	0.9 mg 2.07 µmol 50 eq.	4.12 mg 20.8 µmol 499 eq.	0.104 mg 0.42 µmol 10 eq.
G2.216-P4.3	1.35 mg 50 nmol 1 eq.	167 mg 10 µmol 200 eq.	2.17 mg 4.99 µmol 100 eq.	9.91 mg 50.02 µmol 1000 eq.	0.25 mg 1 µmol 20 eq.

4.6. References

1. A. Abuchowski, J. R. McCoy, N. C. Palczuk, T. van Es and F. F. Davis, *J. Biol. Chem.*, 1977, **252**, 3582-3586.
2. A. Abuchowski, T. van Es, N. C. Palczuk and F. F. Davis, *J. Biol. Chem.*, 1977, **252**, 3578-3581.
3. F. Fuertges and A. Abuchowski, *J. Control. Release*, 1990, **11**, 139-148.
4. F. M. Veronese, *Biomaterials*, 2001, **22**, 405-417.
5. M. J. Roberts, M. D. Bentley and J. M. Harris, *Adv. Drug Deliv. Rev.*, 2002, **54**, 459-476.
6. P. Caliceti and F. M. Veronese, *Adv. Drug Deliv. Rev.*, 2003, **55**, 1261-1277.
7. J. M. Harris and R. B. Chess, *Nat. Rev. Drug Discov.*, 2003, **2**, 214-221.
8. F. M. Veronese and G. Pasut, *Drug Discov. Today*, 2005, **10**, 1451-1458.
9. M. J. Joralemon, S. McRae and T. Emrick, *Chem. Commun.*, 2010, **46**, 1377-1393.
10. K. Knop, R. Hoogenboom, D. Fischer and U. S. Schubert, *Angew. Chem. Int. Ed.*, 2010, **49**, 6288-6308.
11. S. N. S. Alconcel, A. S. Baas and H. D. Maynard, *Polym. Chem.*, 2011, **2**, 1442-1448.
12. F. M. Veronese, P. Caliceti and O. Schiavon, *J. Bioact. Compat. Polym.*, 1997, **12**, 196-207.
13. M. A. C. Stuart, W. T. S. Huck, J. Genzer, M. Muller, C. Ober, M. Stamm, G. B. Sukhorukov, I. Szleifer, V. V. Tsukruk, M. Urban, F. Winnik, S. Zauscher, I. Luzinov and S. Minko, *Nat. Mater.*, 2010, **9**, 101-113.
14. P. S. Stayton, T. Shimoboji, C. Long, A. Chilkoti, G. Ghen, J. M. Harris and A. S. Hoffman, *Nature*, 1995, **378**, 472-474.
15. E. S. Gil and S. M. Hudson, *Prog. Polym. Sci.*, 2004, **29**, 1173-1222.
16. O. D. Krishna and K. L. Kiick, *Biopolymers*, 2010, **94**, 32-48.
17. V. Bulmus, Z. Ding, C. J. Long, P. S. Stayton and A. S. Hoffman, *Bioconjugate Chem.*, 1999, **11**, 78-83.
18. Z. Ding, C. J. Long, Y. Hayashi, E. V. Bulmus, A. S. Hoffman and P. S. Stayton, *Bioconjugate Chem.*, 1999, **10**, 395-400.
19. G. Chen and A. S. Hoffman, *Bioconjugate Chem.*, 1993, **4**, 509-514.

20. A. Chilkoti, G. Chen, P. S. Stayton and A. S. Hoffman, *Bioconjugate Chem.*, 1994, **5**, 504-507.
21. Z. Ding, G. Chen and A. S. Hoffman, *Bioconjugate Chem.*, 1996, **7**, 121-125.
22. Z. Ding, G. Chen and A. S. Hoffman, *J. Biomed. Mater. Res.*, 1998, **39**, 498-505.
23. R. B. Fong, Z. Ding, C. J. Long, A. S. Hoffman and P. S. Stayton, *Bioconjugate Chem.*, 1999, **10**, 720-725.
24. P. Tae Gwan and A. S. Hoffman, *J. Biomater. Sci., Polym. Ed.*, 1993, **4**, 493-504.
25. Z. Ding, R. B. Fong, C. J. Long, P. S. Stayton and A. S. Hoffman, *Nature*, 2001, **411**, 59-62.
26. A. S. Hoffman and P. S. Stayton, *Macromol. Symp.*, 2004, **207**, 139-152.
27. H. G. Borner and H. Schlaad, *Soft Matter*, 2007, **3**, 394-408.
28. C. Boyer, V. Bulmus, J. Liu, T. P. Davis, M. H. Stenzel and C. Barner-Kowollik, *J. Am. Chem. Soc.*, 2007, **129**, 7145-7154.
29. A. S. Hoffman and P. S. Stayton, *Prog. Polym. Sci.*, 2007, **32**, 922-932.
30. A. J. Dirks, R. J. M. Nolte and J. J. L. M. Cornelissen, *Adv. Mater.*, 2008, **20**, 3953-3957.
31. K. Velonia, *Polym. Chem.*, 2010, **1**, 944-952.
32. H. Li, M. Li, X. Yu, A. P. Bapat and B. S. Sumerlin, *Polym. Chem.*, 2011, **2**, 1531-1535.
33. M. Taniguchi, M. Kobayashi and M. Fujii, *Biotechnol. Bioeng.*, 1989, **34**, 1092-1097.
34. T. Shimoboji, E. Larenas, T. Fowler, S. Kulkarni, A. S. Hoffman and P. S. Stayton, *Proc. Natl. Acad. Sci. U.S.A.*, 2002, **99**, 16592-16596.
35. J. M. Hannink, J. J. L. M. Cornelissen, J. A. Farrera, P. Foubert, F. C. De Schryver, N. A. J. M. Sommerdijk and R. J. M. Nolte, *Angew. Chem. Int. Ed.*, 2001, **40**, 4732-4734.
36. A. J. Dirks, S. S. van Berkel, N. S. Hatzakis, J. A. Opsteen, F. L. van Delft, J. J. L. M. Cornelissen, A. E. Rowan, J. C. M. van Hest, F. P. J. T. Rutjes and R. J. M. Nolte, *Chem. Commun.*, 2005, 4172-4174.
37. B. Le Droumaguet, G. Mantovani, D. M. Haddleton and K. Velonia, *J. Mater. Chem.*, 2007, **17**, 1916-1922.

38. H. Maeda, *Adv. Drug Deliv. Rev.*, 2001, **46**, 169-185.
39. M. J. Boerakker, J. M. Hannink, P. H. H. Bomans, P. M. Frederik, R. J. M. Nolte, E. M. Meijer and N. A. J. M. Sommerdijk, *Angew. Chem. Int. Ed.*, 2002, **41**, 4239-4241.
40. K. Velonia, A. E. Rowan and R. J. M. Nolte, *J. Am. Chem. Soc.*, 2002, **124**, 4224-4225.
41. M. J. Boerakker, N. E. Botterhuis, P. H. H. Bomans, P. M. Frederik, E. M. Meijer, R. J. M. Nolte and N. A. J. M. Sommerdijk, *Chem. Eur. J.*, 2006, **12**, 6071-6080.
42. I. C. Reynhout, J. J. L. M. Cornelissen and R. J. M. Nolte, *J. Am. Chem. Soc.*, 2007, **129**, 2327-2332.
43. J. Nicolas, G. Mantovani and D. M. Haddleton, *Macromol. Rapid Commun.*, 2007, **28**, 1083-1111.
44. B. Le Droumaguet and J. Nicolas, *Polym. Chem.*, 2010, **1**, 563-598.
45. V. Bulmus, *Polym. Chem.*, 2011, **2**, 1463-1472.
46. G. N. Grover and H. D. Maynard, *Curr. Opin. Chem. Biol.*, 2010, **14**, 818-827.
47. L. A. Canalle, D. W. P. M. Lowik and J. C. M. van Hest, *Chem. Soc. Rev.*, 2010, **39**, 329-353.
48. F. Lecolley, L. Tao, G. Mantovani, I. Durkin, S. Lautru and D. M. Haddleton, *Chem. Commun.*, 2004, 2026-2027.
49. L. Tao, G. Mantovani, F. Lecolley and D. M. Haddleton, *J. Am. Chem. Soc.*, 2004, **126**, 13220-13221.
50. K. L. Heredia, D. Bontempo, T. Ly, J. T. Byers, S. Halstenberg and H. D. Maynard, *J. Am. Chem. Soc.*, 2005, **127**, 16955-16960.
51. M. Li, P. De, S. R. Gondi and B. S. Sumerlin, *Macromol. Rapid Commun.*, 2008, **29**, 1172-1176.
52. H. B. F. Dixon, *J. Protein Chem.*, 1984, **3**, 99-108.
53. J. M. Gilmore, R. A. Scheck, A. P. Esser-Kahn, N. S. Joshi and M. B. Francis, *Angew. Chem. Int. Ed.*, 2006, **45**, 5307-5311.
54. T. Shimoboji, Z. Ding, P. S. Stayton and A. S. Hoffman, *Bioconjugate Chem.*, 2001, **12**, 314-319.
55. H.-A. Klok, *J. Polym. Sci. Part A: Polym. Chem.*, 2005, **43**, 1-17.

56. P. Thordarson, B. Le Droumaguet and K. Velonia, *Appl. Microbiol. Biotechnol.*, 2006, **73**, 243-254.
57. K. L. Heredia and H. D. Maynard, *Org. Biomol. Chem.*, 2007, **5**, 45-53.
58. M. A. Gauthier and H.-A. Klok, *Chem. Commun.*, 2008, 2591-2611.
59. J.-F. Lutz and H. G. Börner, *Prog. Polym. Sci.*, 2008, **33**, 1-39.
60. C. Boyer, X. Huang, M. R. Whittaker, V. Bulmus and T. P. Davis, *Soft Matter*, 2011, **7**, 1599-1614.
61. R. M. Broyer, G. N. Grover and H. D. Maynard, *Chem. Commun.*, 2011, **47**, 2212-2226.
62. R. P. Johnson, J. V. John and I. Kim, *Eur. Polym. J.*, 2013, **49**, 2925-2948.
63. C. T. Walsh, S. Garneau-Tsodikova and G. J. Gatto, *Angew. Chem. Int. Ed.*, 2005, **44**, 7342-7372.
64. G. A. Khoury, R. C. Baliban and C. A. Floudas, *Sci. Rep.*, 2011, **1**, 1-5.
65. C. Noren, S. Anthony-Cahill, M. Griffith and P. Schultz, *Science*, 1989, **244**, 182-188.
66. L. Wang, J. Xie and P. G. Schultz, *Annu. Rev. Biophys. Biomol. Struct.*, 2006, **35**, 225-249.
67. A. Dumas, L. Lercher, C. D. Spicer and B. G. Davis, *Chem. Sci.*, 2015, **6**, 50-69.
68. D. Mendel, J. A. Ellman and P. G. Schultz, *J. Am. Chem. Soc.*, 1991, **113**, 2758-2760.
69. D. J. Weber, A. K. Meeker and A. S. Mildvan, *Biochemistry*, 1991, **30**, 6103-6114.
70. D. Summerer, S. Chen, N. Wu, A. Deiters, J. W. Chin and P. G. Schultz, *Proc. Natl. Acad. Sci. U.S.A.*, 2006, **103**, 9785-9789.
71. K. L. Kiick, E. Saxon, D. A. Tirrell and C. R. Bertozzi, *Proc. Natl. Acad. Sci. U.S.A.*, 2002, **99**, 19-24.
72. Y. Tang and D. A. Tirrell, *Biochemistry*, 2002, **41**, 10635-10645.
73. P. Wang, Y. Tang and D. A. Tirrell, *J. Am. Chem. Soc.*, 2003, **125**, 6900-6906.
74. Y. Tang, P. Wang, J. A. Van Deventer, A. J. Link and D. A. Tirrell, *ChemBioChem*, 2009, **10**, 2188-2190.
75. J. A. Johnson, Y. Y. Lu, J. A. Van Deventer and D. A. Tirrell, *Curr. Opin. Chem. Biol.*, 2010, **14**, 774-780.
76. C. C. Liu and P. G. Schultz, *Annu. Rev. Biochem.*, 2010, **79**, 413-444.

77. P. O'Donoghue, J. Ling, Y.-S. Wang and D. Soll, *Nat. Chem. Biol.*, 2013, **9**, 594-598.
78. J. W. Chin, *Annu. Rev. Biochem.*, 2014, **83**, 379-408.
79. S. H. Hong, Y.-C. Kwon and M. C. Jewett, *Front. Chem.*, 2014, **2**.
80. A. Deiters, T. A. Cropp, M. Mukherji, J. W. Chin, J. C. Anderson and P. G. Schultz, *J. Am. Chem. Soc.*, 2003, **125**, 11782-11783.
81. H. Neumann, K. Wang, L. Davis, M. Garcia-Alai and J. W. Chin, *Nature*, 2010, **464**, 441-444.
82. S. Marburg, A. C. Neckers and P. R. Griffin, *Bioconjugate Chem.*, 1996, **7**, 612-616.
83. M. J. O'Donnell, C. W. Lugar, R. S. Pottorf, C. Zhou, W. L. Scott and C. L. Cwi, *Tetrahedron Lett.*, 1997, **38**, 7163-7166.
84. K. Lang, L. Davis, J. Torres-Kolbus, C. Chou, A. Deiters and J. W. Chin, *Nature Chem.*, 2012, **4**, 298-304.
85. R. Huisgen, *Angew. Chem. Int. Ed.*, 1963, **2**, 565-598.
86. R. Huisgen, *Angew. Chem. Int. Ed.*, 1963, **2**, 633-645.
87. H. C. Kolb, M. G. Finn and K. B. Sharpless, *Angew. Chem. Int. Ed.*, 2001, **40**, 2004-2021.
88. V. V. Rostovtsev, L. G. Green, V. V. Fokin and K. B. Sharpless, *Angew. Chem. Int. Ed.*, 2002, **41**, 2596-2599.
89. S. Schoffelen, M. H. L. Lambermon, M. B. v. Eldijk and J. C. M. van Hest, *Bioconjugate Chem.*, 2008, **19**, 1127-1131.
90. W. Tang and M. L. Becker, *Chem. Soc. Rev.*, 2014, **43**, 7013-7039.
91. R. Y. Tsien, *Annu. Rev. Biochem.*, 1998, **67**, 509-544.
92. G. N. Phillips Jr, *Curr. Opin. Struct. Biol.*, 1997, **7**, 821-827.
93. J. M. Kendall and M. N. Badminton, *Trends Biotechnol.*, 1998, **16**, 216-224.
94. C. Lavigueur, J. G. Garcia, L. Hendriks, R. Hoogenboom, J. J. L. M. Cornelissen and R. J. M. Nolte, *Polym. Chem.*, 2011, **2**, 333-340.
95. S. Averick, O. Karácsony, J. Mohin, X. Yong, N. M. Moellers, B. F. Woodman, W. Zhu, R. A. Mehl, A. C. Balazs, T. Kowalewski and K. Matyjaszewski, *Angew. Chem. Int. Ed.*, 2014, **53**, 8050-8055.
96. B. Valeur and M. N. Berberan-Santos, in *Molecular Fluorescence*, Wiley-VCH Verlag GmbH & Co. KGaA, 2012, pp. 213-261.

97. J.-F. Lutz, *J. Polym. Sci. Part A: Polym. Chem.*, 2008, **46**, 3459-3470.

98. G. Moad, *Macromol. Chem. Phys.*, 2014, **215**, 9-26.

99. P. De, M. Li, S. R. Gondi and B. S. Sumerlin, *J. Am. Chem. Soc.*, 2008, **130**, 11288-11289.

100. S. I. Presolski, V. P. Hong and M. G. Finn, *Curr. Protoc. Chem. Biol.*, 2011, **3**, 153-162.

101. T. R. Wilks, J. Bath, J. W. de Vries, J. E. Raymond, A. Herrmann, A. J. Turberfield and R. K. O'Reilly, *ACS Nano*, 2013, **7**, 8561-8572.

102. M. Liu, P. Tirino, M. Radivojevic, D. J. Phillips, M. I. Gibson, J.-C. Leroux and M. A. Gauthier, *Adv. Funct. Mater.*, 2013, **23**, 2007-2015.

103. D. Durand, C. Vivès, D. Cannella, J. Pérez, E. Pebay-Peyroula, P. Vachette and F. Fieschi, *J. Struct. Biol.*, 2010, **169**, 45-53.

104. C. Würth, M. Grabolle, J. Pauli, M. Spieles and U. Resch-Genger, *Nat. Protoc.*, 2013, **8**, 1535-1550.

105. S. Perrier, P. Takolpuckdee, J. Westwood and D. M. Lewis, *Macromolecules*, 2004, **37**, 2709-2717.

106. R. K. O'Reilly, M. J. Joralemon, C. J. Hawker and K. L. Wooley, *J. Polym. Sci. Part A: Polym. Chem.*, 2006, **44**, 5203-5217.

107. I. Blakey, T. L. Schiller, Z. Merican and P. M. Fredericks, *Langmuir*, 2009, **26**, 692-701.

Chapter 5 - Catalytic nanogels: study of the effect of structural properties

5.1. Abstract

In this Chapter, the use of cross-linked polymer particles, hereinto referred to as "nanogels", as catalytic nanoreactors is assessed as a function of their structural properties. Employing biphasic polymerizations, L-proline-loaded nano-sized particles were synthesized in an attempt to create aldolase mimics. The fine tuning of the hydrophobicity of the catalyst nanoenvironment was initially studied by employing different co-monomers in the emulsion polymerization process. Additionally, the catalytic nanoparticles were rendered recyclable by creating a core-shell morphology whereby the hydrophilic shell provided steric stabilization to the hydrophilic catalytic core. Finally, the increase of cross-linking density in an attempt to "switch off" the catalytic properties of the nanogels is shown. In all experiments, the catalytic efficiency of the particles is used as a mean of characterization of the nanogels properties.

This work was carried out in collaboration with Annhelen Lu from Rachel O'Reilly's group at the University of Warwick.

5.2. Introduction

5.2.1. Aldolase mimics: L-Proline

5.2.1.1. Catalytic activity

Enantioselective carbon-carbon forming reactions in Nature are carried out by enzymes such as aldolases.[1] While enzymes are globally used for their catalytic properties, from small scale reactions up to industrial scale reactions, simplified catalysts that rely on small organic molecules – organocatalysts – are more desirable. As opposed to enzymes that suffer from loss of activity when stored for long periods of time (due to fluctuations

in temperature and pH and degradation) small molecule catalysts offer a simple pathway to a broad range of reactions at low cost. Additionally, organocatalysts are generally more stable under normal conditions than the typically used metal catalysts, they are generally non-toxic, more environmentally-friendly, and are easier to obtain.[2]

To this end, L-proline has been proven to be an efficient organocatalyst for various reactions and has been used mainly for Robinson annulations,[3, 4] Michael additions[5, 6] Mannich reactions,[7, 8] and aldol additions (Scheme 5.1).[9-11]

In the original publication of List *et al.*, it was proposed that L-proline functions as a micro-aldolase with the formation of an enamine intermediate.[9] Aldolases, and more specifically class I aldolases, have complex active centers where the aldehyde substrate initially reacts with lysine to form a Schiff base. Then, the corresponding enamine is formed that then reacts with the carbonyl of the second aldehyde substrate and, after proton shuffling with the participation of a water molecule, the aldol product is obtained with high enantioselectivity.[12] While enzymes are most efficient in water, where their 3D structure is obtained, their catalytic centers tend to be hydrophobic. Nonetheless, as shown by the reaction mechanism, water plays an important role in the catalytic cycle. Loh *et al.* reported the use of L-proline in imidazolium-based ionic liquids where high catalyst loading (30 mol%) was deemed necessary to obtain yields between 50-60% with reasonable enantiomeric excess (~ 70%).[13] In a similar manner, Kotrusz *et al.* reported the successful aldol reaction of different substrates in an ionic liquid environment.[14] In this case, the reported yields and enantioselectivity were superior, even with decreased catalyst loading, although a limitation in the range of reactive substrates was also reported. Chan *et al.* also exploited ionic liquids, this time anchoring the L-proline moiety onto one. The aldol reaction took place in DMSO with reasonable yields (~ 70%) and enantiomerically enriched products, but more importantly the

catalyst was readily recyclable and reusable.[15] Hayashi *et al.* observed that when used in the presence of water, L-proline can catalyze the aldol reaction with high yields and excellent diastereo- and enantio-selectivities, however this was found to be dependent on the substrates used.[16]

5.2.1.2. Effect of water

Torii *et al.* synthesized a tetrazole derivative of proline that efficiently catalyzed aldol reactions of different substrates in acetonitrile in excellent yields. More importantly, the acceleration of the reaction was reported when water was added to the reaction mixture.[17] To that end, Pikho *et al.* demonstrated the effect of water in the reactions catalyzed by L-proline in DMF, whereby increasing the water content resulted in acceleration of the aldol reaction.[18] Chimni *et al.* also synthesized a hydrophobic derivative of L-proline and studied its catalytic efficiency in organic solvents with high quantities of water (up to 1:1).[19] Although high yields were obtained, low enantioselectivities were reported, presumably due to the alteration of the proline carboxylic acid.

When L-proline is employed as the catalyst in 100% water however, the reaction halts at low yields (<5%). Barbas III *et al.* obtained high activity from L-proline in a phosphate buffer, which was attributed to the presence of the surfactant sodium dodecyl sulfate (SDS) in the buffer, thus offering the hydrophobic environment required for the catalysis to work.[20] Aratake *et al.* showed that by modifying L-proline with a hydrophobic group, such as siloxy-group, the catalysis can be performed in water. In fact, surprisingly high yields, enantio- and diastereo-selectivities were obtained.[21] Similarly, Hayashi *et al.* also used a hydrophobic derivative of L-proline in water, and also reported the successful reaction of two hydrophobic reagents, with surprisingly high enantio- and stereo-

selectivities.[22] More importantly, when the same catalysts were used in the absence of water, a drop in both enantio- and stereo-selectivity was reported. This was a significant breakthrough, as the synthesis of the catalyst is simple and scalable, but also loadings as low as 1 mol% were found to efficiently catalyze aldol reactions.

It was therefore suggested that a hydrophobic nanoenvironment is necessary for the efficient catalytic cycle of L-proline, with the presence of *some* water enhancing the reaction rates and overall selectivities.

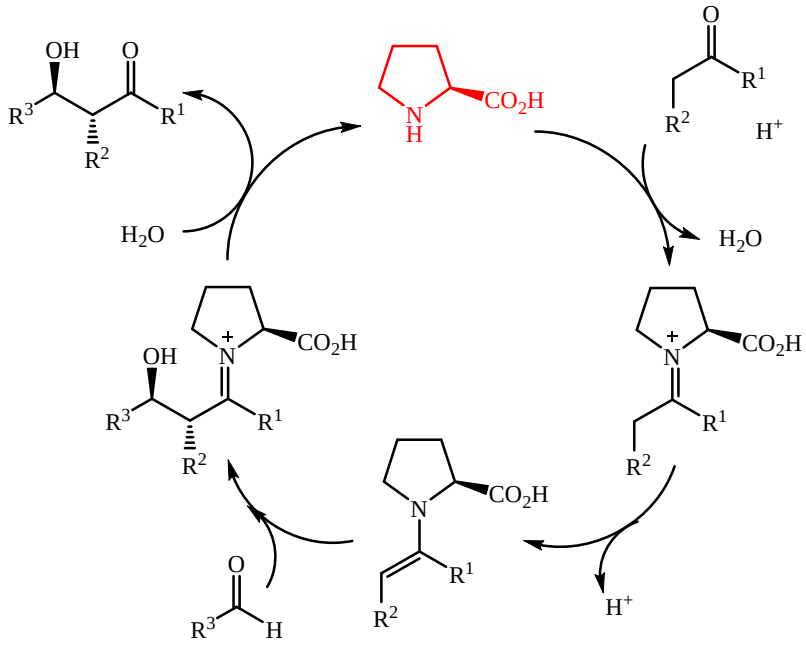

Scheme 5.1. Generally accepted mechanism for the catalytic cycle of L-proline in the aldol reaction between a ketone and an aldehyde.

With this rationale, a few reports in the literature have proposed ways of introducing L-proline in a hydrophobic environment, while in the presence of water. Peng *et al.* employed a biphasic reaction, used a micellar system formed by SDS, achieving high yields, however at the price of prolonged reaction times and high catalyst loading (40 mol%).[23]

Mase *et al.* modified L-proline in order to obtain the catalyst with long alkyl chains. When it was used in water, it effectively acted both as a surfactant and the catalyst and high yields and selectivities were obtained.[24] This was shown for a range of substrates, thus highlighting the broad applicability of the approach. In a similar fashion, Hayashi *et al.* also attached a long alkyl chain onto the hydroxyl group of L-4-hydroxyproline. The cross-aldol reaction in water was carried out in the absence of co-solvent, yet the formation of an emulsion was observed and high yields and selectivities were obtained.[25] More recently, Ghorai *et al.* synthesized an elaborate amphiphilic molecule with L-proline bound between the hydrophilic and the hydrophobic ends of the surfactant. When the aldol reaction was carried out in water, high activity and selectivity was reported, with the additional benefit of an "in-flask" recovery of the catalyst.[26]

5.2.1.3. Polymer-supported L-proline

Kokotos *et al.* utilized commercially available dendrimers to functionalize the surface with L-proline moieties. Despite the accelerated reaction in DMF compared to the small molecule catalyst, enantio-selectivities did not exceed 50%.[27] Benaglia *et al.* immobilized the proline moiety onto a poly(ethylene glycol) (PEG) in order to enhance its solubility and potentially be able to recycle the catalyst. Reactions were performed in DMF and DMSO and the products were obtained in reasonable yields (~ 60%) while high enantiomeric excess was also reported.[28, 29] Similarly, Tao *et al.* attached L-proline onto a linear poly(styrene). Aldol reactions with significantly decreased catalyst loadings were carried out in DMF/water mixtures with excellent yields and selectivities. Additionally, the ability to re-use the catalytic system was reported without an effect in the obtained yields.[30, 31] Using reversible-addition chain-transfer (RAFT) polymerization, O'Reilly *et al.* also synthesized L-proline-containing poly(styrene) that

self-assembled in water-containing DMF. Once again, high yields and enantio- and stereo-selectivities were obtained, while the catalyst was recyclable and re-useable.[32]

Noto *et al.* used commercially available poly(styrene) resins bearing thiol moieties to immobilize an alkene-functional L-proline. The beads were subsequently used in the catalysis of a variety of substrates in water obtaining in most cases excellent yields and selectivities, outperforming the homogeneous catalysis systems.[33, 34] In a similar approach, Pericàs *et al.* utilized an azide-functional Merrifield resin and employed copper-catalyzed azide-alkyne cycloaddition to attach an alkyne-bearing proline.[35, 36]

While immobilization of organocatalysts onto polymeric supports, such as Merrifield resins, is easy, efficient, and scalable, it lacks in terms of accurately determining the catalyst loading and distribution.[37] To address this, Kristensen *et al.* envisioned a bottom-up approach for the synthesis of (meth)acrylate micron-sized beads that would allow the incorporation of known amounts of L-proline. This was achieved *via* the suspension polymerization of a methacrylate proline derivative and benzyl methacrylate, resulting in 100 micron-sized particles with tuneable loadings. The efficiency of the beads in the aldol reaction in water was found to be comparable to that obtained from Merrifield-type resins, even when the catalyst loading was as low as 1 mol%.[38] Similarly, Gallardo *et al.* attempted the synthesis of cross-linked polymers consisting solely of proline-functional monomers, however their catalytic activity was found to be low.[39]

Palmans *et al.* synthesized linear copolymers composed of a hydrophobic moiety that has the tendency to stack at room temperature, a hydrophilic block, and an L-proline-functional monomer. The polymers would form single-molecule particles in water and, when used for the catalysis of aldol reactions, high yields were obtained. The success of the system was attributed to its similarity to the structural properties of enzymes.[40]

Recently, O'Reilly *et al.* reported the incorporation of L-proline in a diblock copolymer comprising of a hydrophobic and a hydrophilic block.[41] In water, the copolymer self-assembled into micelles with the proline moieties residing in the hydrophobic core. These micelles efficiently catalyzed the aldol reaction of 4-nitrobenzaldehyde and cyclohexanone as a result of the formation of a hydrophobic nano-environment able to sequester the hydrophobic reagents.

In a similar manner, Monteiro *et al.* copolymerized an L-proline-functional monomer with *N*-isopropyl acrylamide (NIPAM) using poly(dimethyl acrylamide) as the macroinitiator, resulting in a copolymer that could form micelles at temperatures above the lower critical solution temperature of poly(NIPAM). The micelles could efficiently catalyze the aldol reaction with high selectivities. Upon cooling the poly(NIPAM) block became hydrophilic resulting in the disassembly of the micelles and the release of the aldol product, which would subsequently precipitate as a consequence of its hydrophobicity. This approach also showed the recycling potential of the system, as the polymer solution could be re-used with little loss in catalytic properties.[42]

5.2.2. Nanogels

It is apparent from the existing literature that there is a tendency to seek a catalytic system that can easily be obtained albeit maintaining high efficiency, while the ability to recycle is an additional benefit. Nanogels (and microgels) are a potential platform as they are complex systems that are synthesized in industrial scale reactions.[43-45]

Although microscopic gels were synthesized as early as in 1935,[46] an increased interest on the subject rekindled in 1949 when the rubber crisis of the war dictated the introduction of alternative methods to produce "synthetic rubber".[47] Since then, a vast amount of publications where nanogels (or microgels) are synthesized and studied for

their properties and applications have appeared, which are summarized in numerous excellent reviews.[48-53]

Perhaps the most intriguing of such systems are those that change their physico-chemical properties as a response to external stimuli, such as changes in the solution temperature.[49, 54, 55] A typical temperature-responsive system is nanogels composed of poly(NIPAM); a polymer that undergoes hydrophilic-to-hydrophobic transition in water, when the solution temperature increases. This is a result of the disruption of the hydrogen bonding between the NIPAM amide and water molecules when the temperature increases, and it is a reversible process. The properties of linear poly(NIPAM) and its copolymers have been extensively studied.[56] Chibante *et al.* were the first to report the synthesis of NIPAM-based nanogels and demonstrated their thermoresponsive properties.[57] Since then, NIPAM has become one of the most widely used monomers for the synthesis of nanogels.[58, 49, 59, 60, 52, 61]

Cross-linked NIPAM-based nanogels have also been used as intelligent microreactors where the reversible hydrophobic nature of poly(NIPAM) as a response to temperature has been used to control access of substrates into the catalytic core. In some cases, enhanced catalytic activity is observed at elevated temperatures as the hydrophobic nature of PNIPAM enhances substrate uptake.[62, 63] In other cases, the opposite effect has been reported where the collapse of PNIPAM instead blocks the catalytic sites and thus reduces nanoreactor activity.[64, 65]Several groups have successfully taken advantage of both the hydrophilic and hydrophobic properties of PNIPAM, allowing catalysis of both hydrophilic and hydrophobic substrates by simply tuning the temperature of the system.[66, 67]

In the 1950s, Beaman *et al.* intrigued by the "idealized model for polymer molecules" that microgels represent, studied the properties of styrenic, acrylamide, and acrylate

cross-linked particles synthesized by emulsion polymerization. They were able to demonstrate that the amount of cross-linking agent in the microgels can alter the solution properties of the dispersion such as the intrinsic viscosity.[68] The effect of cross-linking density on the properties of the microgels, mainly with respect to their potential loading, has been the center of attention of a few studies.[69] It is generally accepted that nanogel particles follow Flory's theory of network swelling whereby increased cross-linking results in the decrease of the ability of the network to swell.[70] Fréchet *et al.* have also noticed an effect of the cross-linking density of hydrophobic nanogels on the accessibility of reactive moieties within the core by added reagents.[71] More specifically, they reported the synthesis of poly(styrene)-based core cross-linked star polymers *via* emulsion polymerization, bearing azide functionalities within the core. The arms of the star were then "clicked" on by copper-catalyzed cycloaddition that partially consumed the azide moieties. The remaining ones were then reacted with a variety of water-incompatible catalysts to afford the catalytic nanoparticle. The success of the catalyzed reactions was attributed to the hydrophobic nanoenvironment.

In an attempt to combine the properties of two different materials, core-shell particles were developed employing a variety of techniques to achieve this higher order morphology. A variety of possible combinations has been reported in the literature[72, 73] as such particles can be obtained from block copolymers, two-step heterogeneous polymerizations, and controlled radical polymerizations.[74] Controversially, the first example of a core-shell system consisting of a poly(styrene) core and a poly(NIPAM) shell was synthesized in a one-pot emulsion polymerization procedure, and the resulting morphology was attributed to the microphasic separation of the polymers, as well as the different kinetic profile of the two monomers.[75] Nevertheless, the vast majority of reports on core-shell nanogels involve a two-step process whereby the formation of the

shell is achieved by the seeded emulsion polymerization of the shell monomer.[76-81] Interestingly, the segregated polymer layers provide the nanoparticles with properties different to those obtained when the two components are simply mixed.[76]

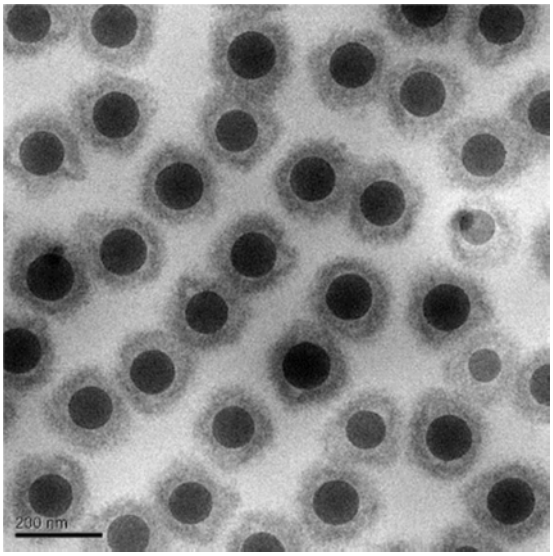

Figure 5.1. Cryo-TEM image of poly(styrene)-*co*-poly(NIPAM) core-shell particles.[82]

5.3. Results and discussion

5.3.1. Nanogel synthesis

The synthesis of the nanogels was pursued *via* emulsion polymerization of hydrophobic methacrylates as it is an easy and scalable method that allows the formation of spherical particles with uniform sizes in water. Furthermore, due to the high monomer conversions commonly obtained by such processes, crucial parameters such as degree of functionalization with catalytic moieties (DoF) can be determined by the ratio of reagents in the synthesis step. Additionally, although for the accurate determination of cross-linking density (CLD) the swelling ratio of the cross-linked polymer network in a good solvent is required, CLD is here defined by the relative concentration of the cross-linker ethylene glycol dimethacrylate (EGDMA) in the polymerization mixture. For the

functionalization of the nanogels with the catalytic moiety L-proline, a methacrylate monomer was coupled with 4-hydroxyproline to afford *O*-methacryloyl-*trans*-4-hydroxy-L-proline hydrochloride (ProMA) and used in the emulsion copolymerization (Figure 5.2).

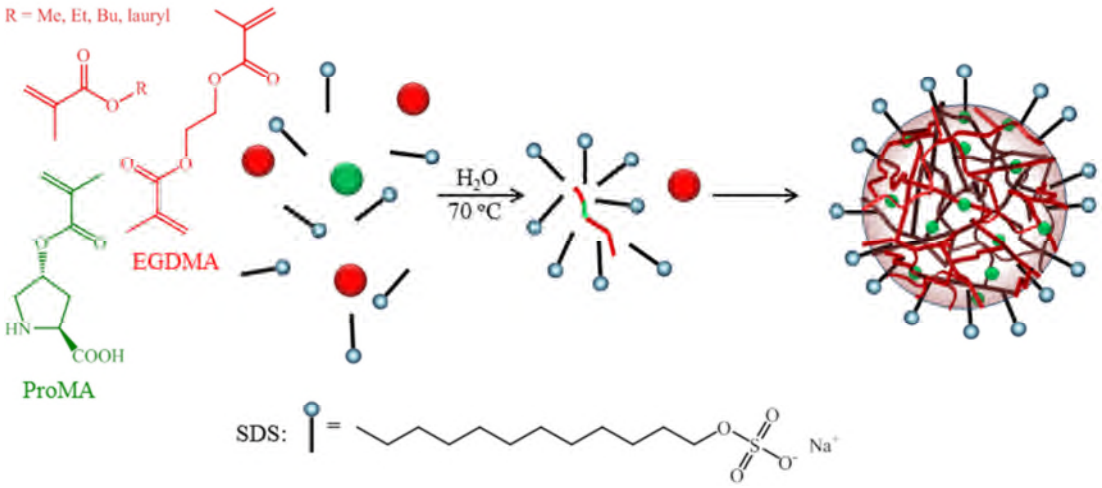

Figure 5.2. Schematic representation of the synthesis of the L-proline functional hydrophobic nanogels.

5.3.2. L-Proline-containing nanogels: Tuning the hydrophobicity

5.3.2.1. Tuning the co-monomer

From the literature, it is apparent that the hydrophobicity of the L-proline nanoenvironment requires fine balancing in order to obtain high catalytic activity without compromising the selectivities. To assess this, nanogels with different compositions were synthesized, changing the monomer with which ProMA was copolymerized (Table 5.1). The co-monomers methyl methacrylate (MMA), ethyl methacrylate (EMA), *n*-butyl methacrylate (BuMA), and lauryl methacrylate (LMA) were chosen for their increasing hydrophobicity that would permit evaluation of the nanoenvironment surrounding the catalyst. In all cases the nanogels concentration was 10 mg/mL and the cross-linking density was 0.5 wt%, based on the EGDMA feed ratio.

Table 5.1. Names of synthesized nanogels with respect to their co-monomer and the degree of functionalization (DoF).*

	Degree of Functionalization (DoF, wt%)			
co-monomer	**2**	**5**	**9**	**15**
MMA	N5.M0.5-2	N5.M0.5-5	N5.M0.5-9	N5.M0.5-15
EMA	N5.E0.5-2	N5.E0.5-5	N5.E0.5-9	N5.E0.5-15
BuMA	N5.B0.5-2	N5.B0.5-5	N5.B0.5-9	N5.B0.5-15
LMA	N5.L0.5-2	N5.L0.5-5	N5.L0.5-9	N5.L0.5-15

The obtained nanogels were characterized by dynamic light scattering (DLS) (Figure 5.3 and Figure 5.4) and transmission electron microscopy (TEM) (Figure 5.5) to verify their uniformity and shape.

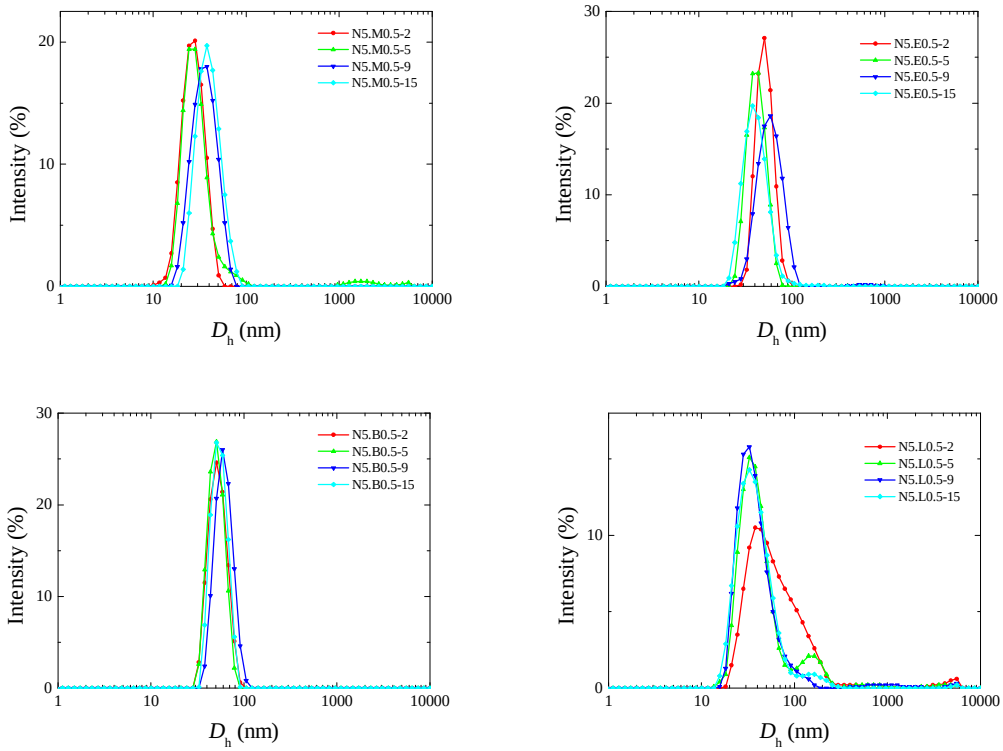

Figure 5.3. Size distributions averaged by intensity for the hydrophobic nanogels in water at 25 °C.

* Note that the name of each nanogels follows the generic format: **N5.**(monomer)(CLD)-(DoF)

The distributions obtained by DLS indicate that overall uniform sized particles were synthesized, although a broadening of the peaks for the LMA-based nanogels suggests that some larger particles were also present. Nonetheless, all synthesized particles were found to have comparable hydrodynamic sizes (Figure 5.4).

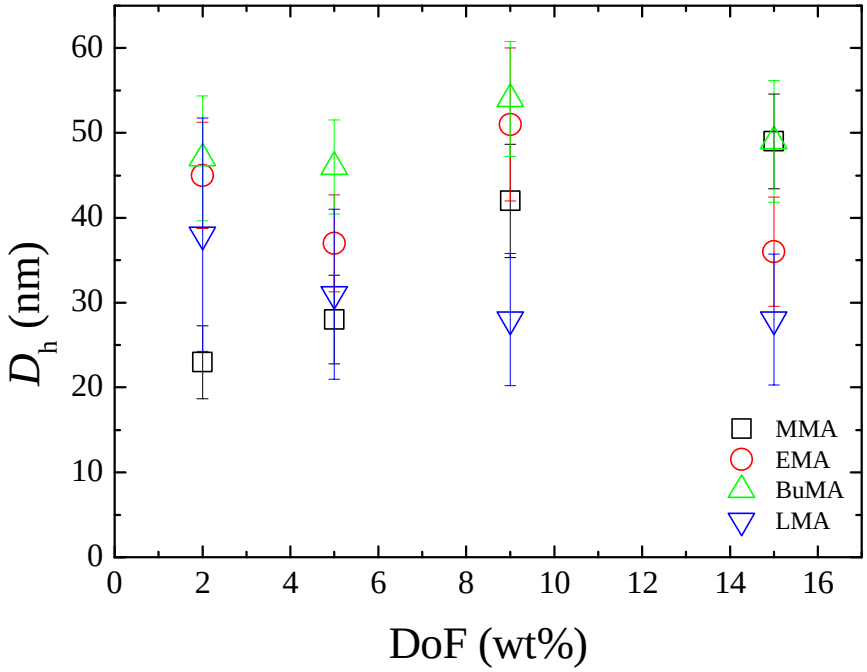

Figure 5.4. Hydrodynamic diameters of the hydrophobic nanogels with respect to the co-monomer (MMA: squares, EMA: circles, BuMA: triangles, LMA: diamonds) and the degree of functionalization (DoF, wt%). Error bars show size dispersity.

Figure 5.5 shows representative TEM images of the nanogels with 2% DoF and the different co-monomers used. For the MMA-based **N5.M0.5-2** nanogels, particles with uniform sizes and no aggregation are observed, while the shape is nearly spherical. Similarly, the EMA-based nanogels **N5.E0.5-2** were found to be slightly larger, however no aggregates are observed. The BuMA-based nanogels **N5.B0.5-2** were found to deviate the most from the targeted spherical shape; however this may be attributed to the low T_g of the BuMA polymer that results in the collapse of the structure in the dry state,

such as in the case of the TEM samples. As expected from the DLS results, the LMA-based nanogels **N5.L0.5-2** were found to have more ill-defined shapes, although small spherical particles were also observed.

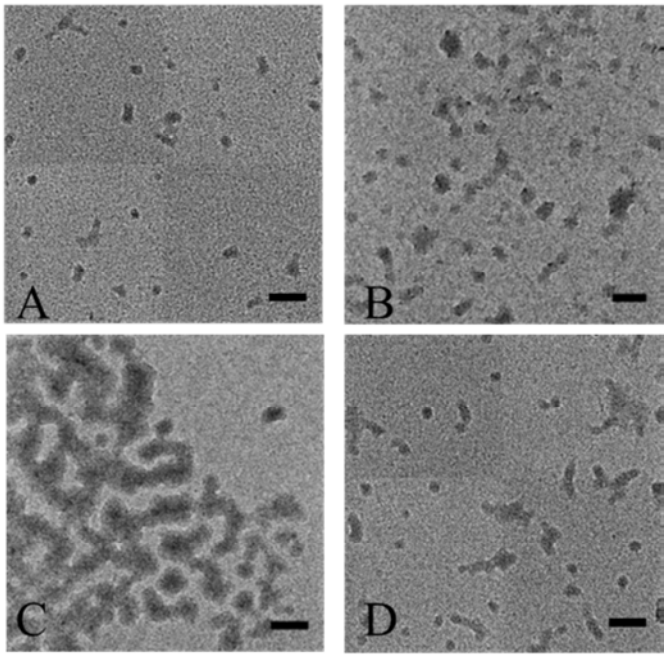

Figure 5.5. Representative TEM images of the hydrophobic nanogels **N5.M0.5-2** (A), **N5.E0.5-2** (B), **N5.B0.5-2** (C), and **N5.L0.5-2** (D). Formvar-coated grid (Scale bar: 100 nm)

The nanogels were then used as catalytic nanoreactors in the aldol reaction between cyclohexanone and 4-nitrobenzaldehyde, a benchmark reaction in the assessment of the catalyst activity and selectivity (Scheme 5.2).[83, 34, 36, 32] In order to evaluate the effect of the catalyst environment hydrophobicity, the reaction was carried out (in triplicate) for each DoF and each co-monomer.

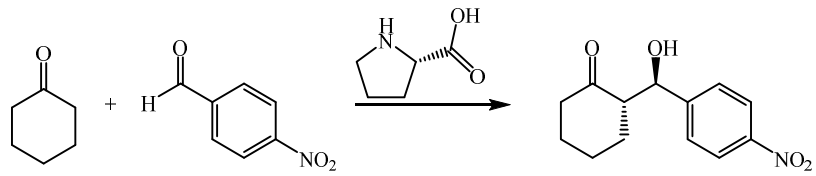

Scheme 5.2. Schematic representation of the benchmark aldol reaction catalyzed by L-proline.

The results of the catalysis reactions are summarized in Table 5.2. In terms of conversion, the highest activity is obtained by the EMA-based nanogels whereby nearly all aldehyde moieties were consumed. Reasonable conversions are also obtained from the MMA- and the BuMA-based nanogels, despite the higher and lower hydrophilicity, respectively, compared to the EMA-based nanogels. However, it was proposed that this may be a result of the steric hindrance presented by the pendent alkyl chains of the respective polymer repeat units.

Table 5.2. Catalytic activity of the hydrophobic nanogels after 24 hours, based on the hydrophobic co-monomer and the DoF. Conversion and diastereomeric ratio determined by ^{1}H NMR spectroscopy. Enantiomeric excess determined by HPLC using a chiral stationary phase.[†]

	DoF (%)	Conversion (%)	*anti/syn*	*ee* (%)
N5.M0.5-2	2	73	97/3	99
N5.M0.5-5	5	51	97/3	88
N5.M0.5-9	9	57	97/3	81
N5.M0.5-15	15	53	98/2	67
N5.E0.5-2	2	99	99/1	99
N5.E0.5-5	5	97	98/2	99
N5.E0.5-9	9	95	98/2	99
N5.E0.5-15	15	95	98/2	97
N5.B0.5-2	2	78	99/1	99
N5.B0.5-5	5	63	99/1	99
N5.B0.5-9	9	79	97/3	99
N5.B0.5-15	15	78	98/2	99
N5.L0.5-2	2	16	95/5	99
N5.L0.5-5	5	19	96/4	98
N5.L0.5-9	9	13	95/5	97
N5.L0.5-15	15	14	98/2	89

To probe the relative hydrophobicity of the nanogels, Nile Red – a hydrophobic fluorescent dye – was introduced to the dispersions and its uptake into the nanogels was assessed by fluorescence spectroscopy (Figure 5.6).

[†] All catalyses and their analyses performed by Annhelen Lu.

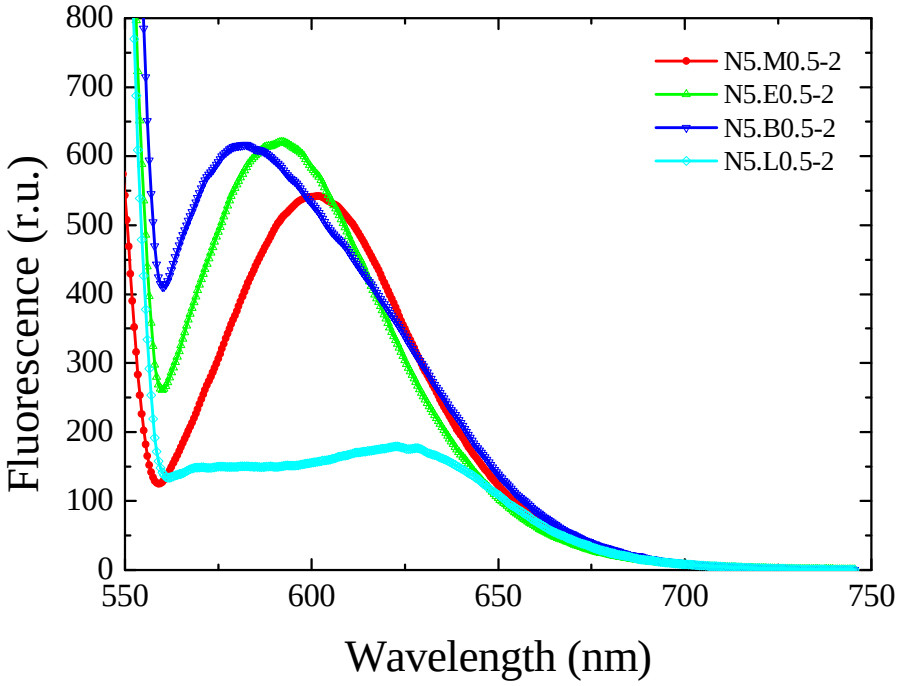

Figure 5.6. Fluorescence emission spectra of the nanogels loaded with Nile Red (λ_{ex} = 550 nm).

The difference in intensity of the excitation peaks (in relative units, r.u.) was attributed to the relative ability of the nanogels to sequester the hydrophobic dye, while the wavelength at which the maximum emission is observed indicates the hydrophobicity of the nanoenvironment, with longer wavelength emission indicating a more hydrophilic environment.[84] As expected, it was therefore found that the methyl methacrylate-based nanogels **N5.M0.5-2** presented the most hydrophilic environment with the λ_{max} = 602 nm, followed by the ethyl methacrylate-based **N5.E0.5-2** with λ_{max} = 592 nm, and *n*-butyl-methacrylate-based **N5.B0.5-2** with λ_{max} = 582 nm. The lauryl methacrylate-based nanogels **N5.L0.5-2** were found to exhibit two emission maxima, although based on the fact that redshift is a result of a hydrophilic environment for Nile Red, the peak with λ_{max} = 623 nm was attributed to dye aggregates present in the water phase. The dye encapsulated by the nanogels was assigned to the peak with λ_{max} = 571 nm. Under the

hypothesis that the relative intensity of the emission peak is an indication of the dye uptake by the nanogels, it can be assumed that the ethyl methacrylate-based **N5.E0.5-2** and the *n*-butyl methacrylate-based **N5.B0.5-2** have the greatest sequestering potential, followed by the methyl methacrylate-based **N5.M0.5-2**, while the lauryl methacrylate-based **N5.L0.5-2** has significantly lower dye uptake. Nevertheless, it should be taken into account that due to the shifting of the emission maxima, the relative intensities can be misleading.[84]

The results from the dye uptake experiment indicate that the low catalytic activity observed for the LMA-based nanogels may be a result of poorer ability to uptake the hydrophobic reagents. However, direct comparison of the BuMA- and the EMA-based nanogels suggests that although they have similar ability to sequester hydrophobic reagents, EMA-based nanogels are significantly more reactive. Furthermore, looking into the obtained enantio-selectivities, EMA- and BuMA-based nanogels were similarly efficient, regardless of the catalyst loading. This is not the case for the MMA-based nanogels where a drop in enantiomeric excess is observed with increasing DoF. While this could be an effect of decreasing isolation of the catalytic moieties hindering the formation of their transition states, this effect was not observed for any of the other sets of nanogels. Additionally, since the L-proline moiety is hydrophilic, it is proposed that increasing the DoF effectively increases the water content within the nanogels and thus affects the selectivities. Once again, the uptake of Nile Red from the lowest and the highest DoF MMA-based nanogels was assessed by fluorescence spectroscopy (Figure 5.7). The higher DoF nanogel **N5.M0.5-15** was found to exhibit a λ_{max} = 608 nm which is at a longer wavelength than that of **N5.M0.5-2** (λ_{max} = 600 nm), thus confirming the more hydrophilic environment within the particles.

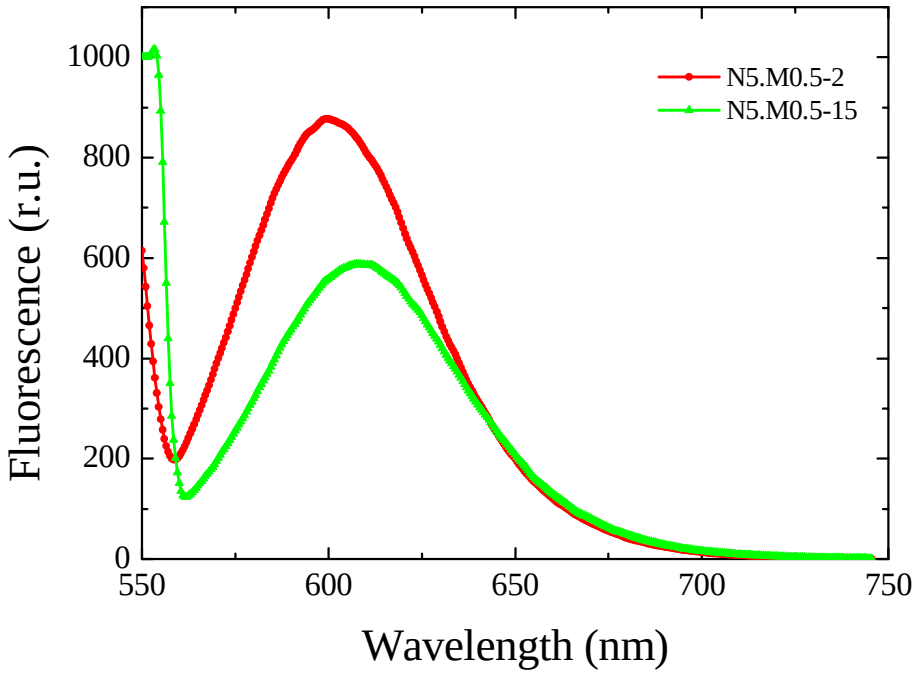

Figure 5.7. Fluorescence emission spectra of Nile Red loaded in the **N5.M0.5-2** and the **N5.M0.5-15** nanogels (λ_{ex} = 550 nm).

It can be therefore concluded that the hydrophobic/hydrophilic balance in a confined environment such as that of a hydrophobic cross-linked polymer particle can be tuned by the careful selection of the monomer. Additionally, when such nanoparticles are employed as nanoreactors, one cannot dismiss the hydrophobic/hydrophilic character of the introduced catalyst as it can significantly alter the local environment. Nevertheless, nanogels are excellent platforms for such systems as these parameters can easily be altered in the synthesis process, which is an industrially-applicable reaction.

5.3.2.2. Core-shell nanogels

Cost-efficient systems are not only defined by their synthesis, but also from their output.[85] Therefore, a method to recycle catalytic nanogels was pursued. As discussed in Chapter 1, hydrophobic nanogels dispersed in water require stabilization. In this case,

this is provided by the SDS which is physisorbed on the surface of the nanogels with the alkyl chain oriented towards the polymer, while the charged sulfate is exposed to the aqueous phase. As such, when the particles are destabilized, they form irreversible aggregates. In the case of the catalytic nanogels, destabilization occurs in the product isolation process, as addition of excess organic solvent disrupts the ionic interactions of SDS with the solvent. It was therefore proposed that a hydrophilic layer chemisorbed onto the particles would allow their re-dispersion once re-introduced to an aqueous medium.

To achieve this, a coating of cross-linked polymer layer was targeted. As discussed in the introduction (Section 5.2.2) there is a precedent of using pre-formed polymer particles as seeds for the emulsion polymerization of a second monomer, thus resulting in core-shell morphologies. However, typical emulsion polymerizations in water require the resulting polymer to be insoluble in the dispersion medium, and therefore hydrophobic, which opposes what is hereinto pursued (Figure 5.8). Nonetheless, the polymer needs to be insoluble only under the polymerization conditions, and therefore the use of *N*-isopropylacrylamide (NIPAM) as the monomer for the shell layer was deemed to be an excellent candidate. This is because poly(NIPAM) is a temperature-responsive polymer exhibiting a lower critical solution temperature (LCST) in water, above which water is a non-solvent.[56] The LCST of poly(NIPAM) is typically below 35 ºC, temperature that is significantly lower than the temperature at which the emulsion polymerization takes place (70 ºC).

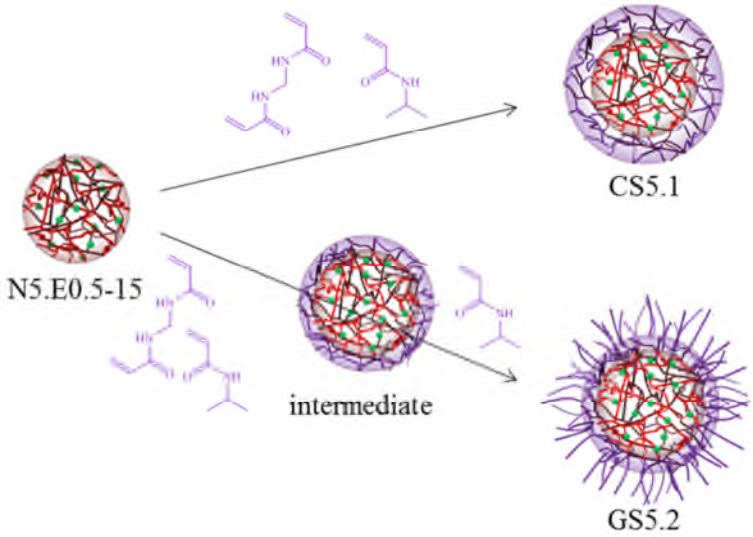

Figure 5.8. Schematic representation of the synthetic procedure followed for the synthesis of the core-shell nanogels (**CS5.1**), and the core-gradient shell nanogels (**GS5.2**), employing EMA-based nanogels (**N5.E0.5-15**) as seeds.

Using EMA-based nanogels as seeds, since these gave the best results in terms of catalytic efficiency, NIPAM and cross-linker were slowly added to the polymerization mixture and the successful formation of a hydrophilic shell was verified by DLS (Figure 5.9).[‡]

[‡] Note that the names of the nanogels represent the particle morphology: CS for core-shell and GS for core-gradient shell

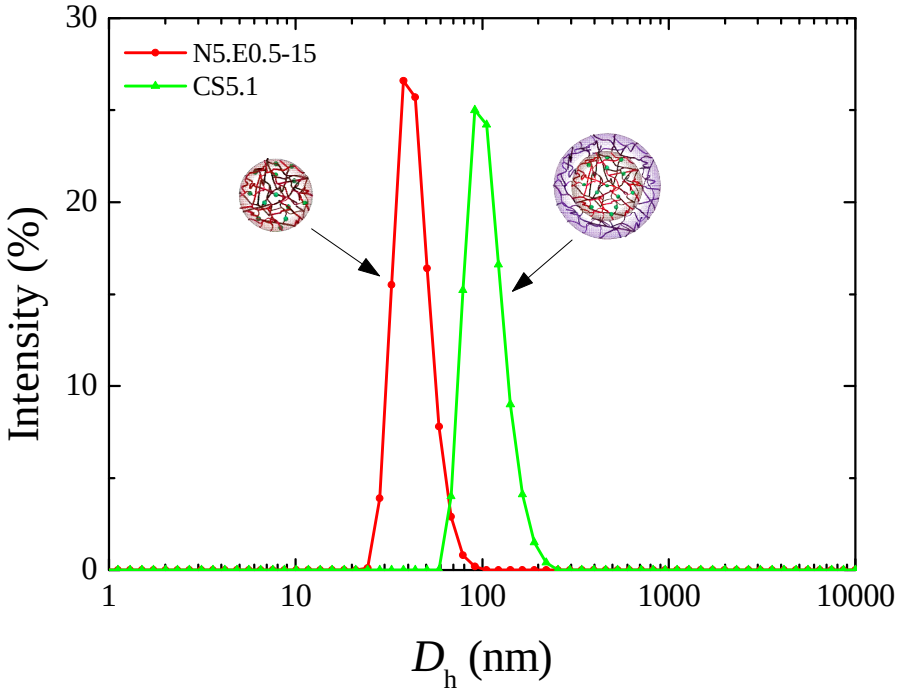

Figure 5.9. Size distributions of the **N5.E0.5-15** core and **CS5.1** core-shell nanogels determined by DLS at 5 ºC.

The core nanogels **N5.E0.5-15** (0.5 wt% CLD, 15 wt% DoF) were found to have a hydrodynamic diameter of 35 nm whereas after the seeded polymerization of the NIPAM gel, the size increased to 132 nm, suggesting the successful growth of the **CS5.1** nanoparticles. It should be noted that the measurements were conducted at 5 ºC to eliminate potential shrinking of the poly(NIPAM) shell.

In a similar manner, the formation of a shell whereby the cross-linking is not consistent was also pursued. It was hypothesized that by creating a shell with gradually decreasing cross-linking density, the transition temperature of the poly(NIPAM) layer could assist in the "shut-down" of the catalytic nanoreactor. Instead of forming, yet another, hydrophobic layer on the surface of the already hydrophobic nanogels, at elevated temperatures the more mobile shell would penetrate into the nanoparticle reducing the mobility of hydrophobic reagents into the core. To achieve the formation of the

"gradient shell" particles, during the seeded polymerization NIPAM and cross-linker quantities were reduced to half the amount added for the **CS5.1** core-shell nanogels, and upon completion of the addition a second batch of monomer containing only NIPAM was added (Figure 5.8). Despite a similar procedure being previously reported,[86] the feasibility of the two-step reaction was assessed by determining the size of the particles before addition of the monomers, after addition of NIPAM and the cross-linker, and after the addition of the final NIPAM batch (**GS5.2**), by DLS (Figure 5.10).

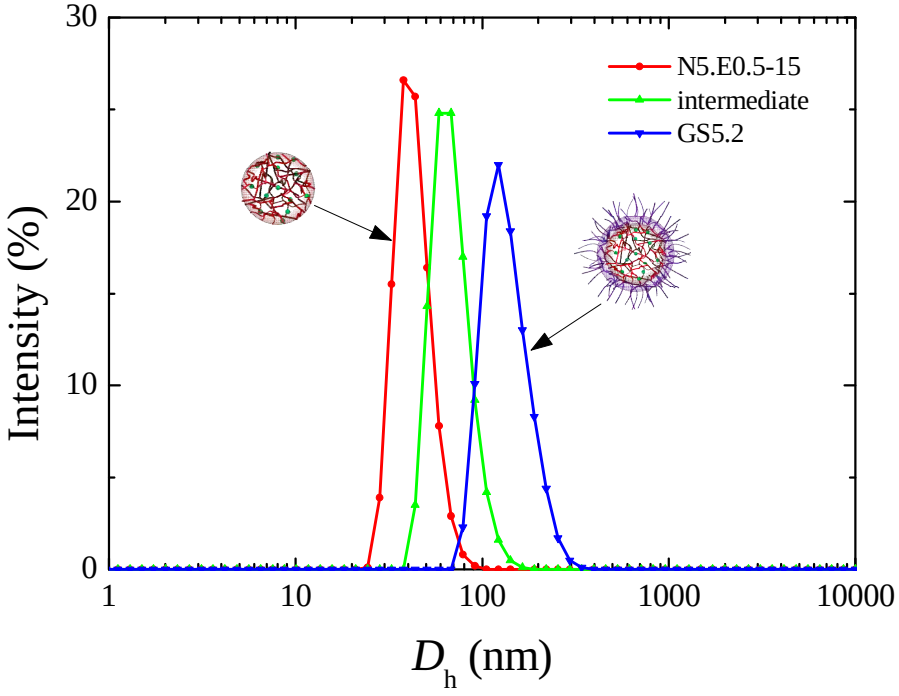

Figure 5.10. Size distributions of the **N5.E0.5-15** core (red line), the intermediate nanogels containing half the amount of NIPAM (green) and **GS5.2** core-gradient shell nanogels, measured by DLS at 5 ºC.

The increase of the size of the nanogels from 35 nm (**N5.E0.5-15**) to 55 nm suggests that at the intermediate stage a shell layer has already formed. Further addition of NIPAM resulted in the increase of the size of the nanogels to 142 nm, thus confirming

that the polymerization proceeds towards the formation of the shell in the absence of cross-linker. Comparison of the nanogels by dry state TEM imaging was less revealing (Figure 5.11).

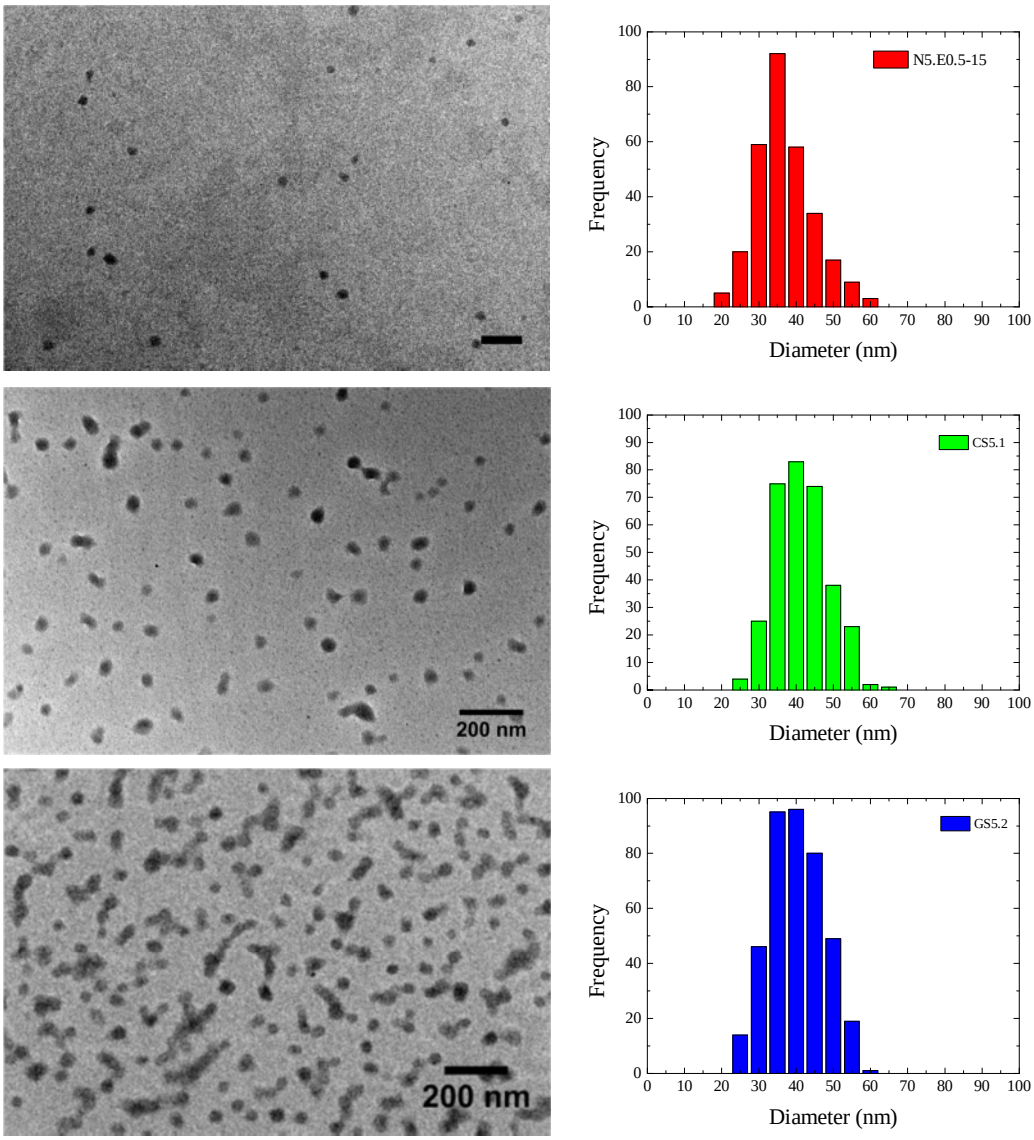

Figure 5.11. TEM images of the **N5.E0.5-15** nanogels (top), the **CS5.1** core-shell nanogels (middle), and the **GS5.2** core-gradient shell nanogels (bottom), and their respective size histograms. (Scale bars: 200 nm)

In all three cases, the nanogels were found to be of comparable sizes whereby the **N5.E0.5-15** nanogels were measured to be 35±8 nm, the **CS5.1** core-shell nanogels were 39±7 nm, and the **GS5.2** core-gradient shell nanogels were 38±7 nm. The absence of a

significant difference was attributed to the fact that the samples are imaged in their dry state, and therefore all water content that would otherwise swell the shell has been removed. As such, the successful formation of a shell cannot be confirmed by dry-state TEM.

To overcome this, the samples were also imaged *via* cryogenic TEM (cryo-TEM) that provides more representative images of the particles in solution (Figure 5.12 and Figure 5.13).

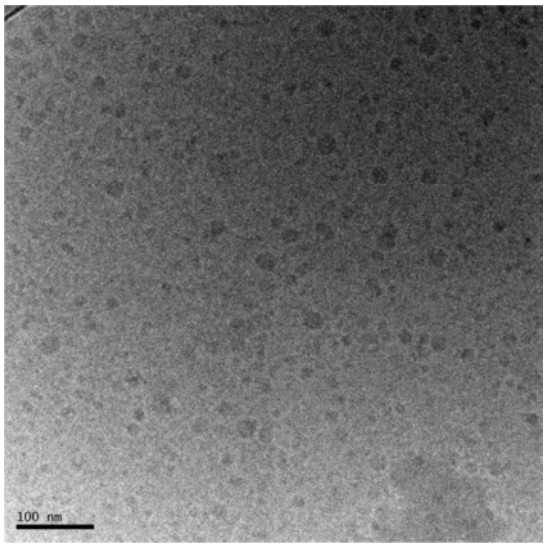

Figure 5.12. Cryo-TEM image of the **N5.E0.5-15** hydrophobic nanogels (scale bar: 100 nm)

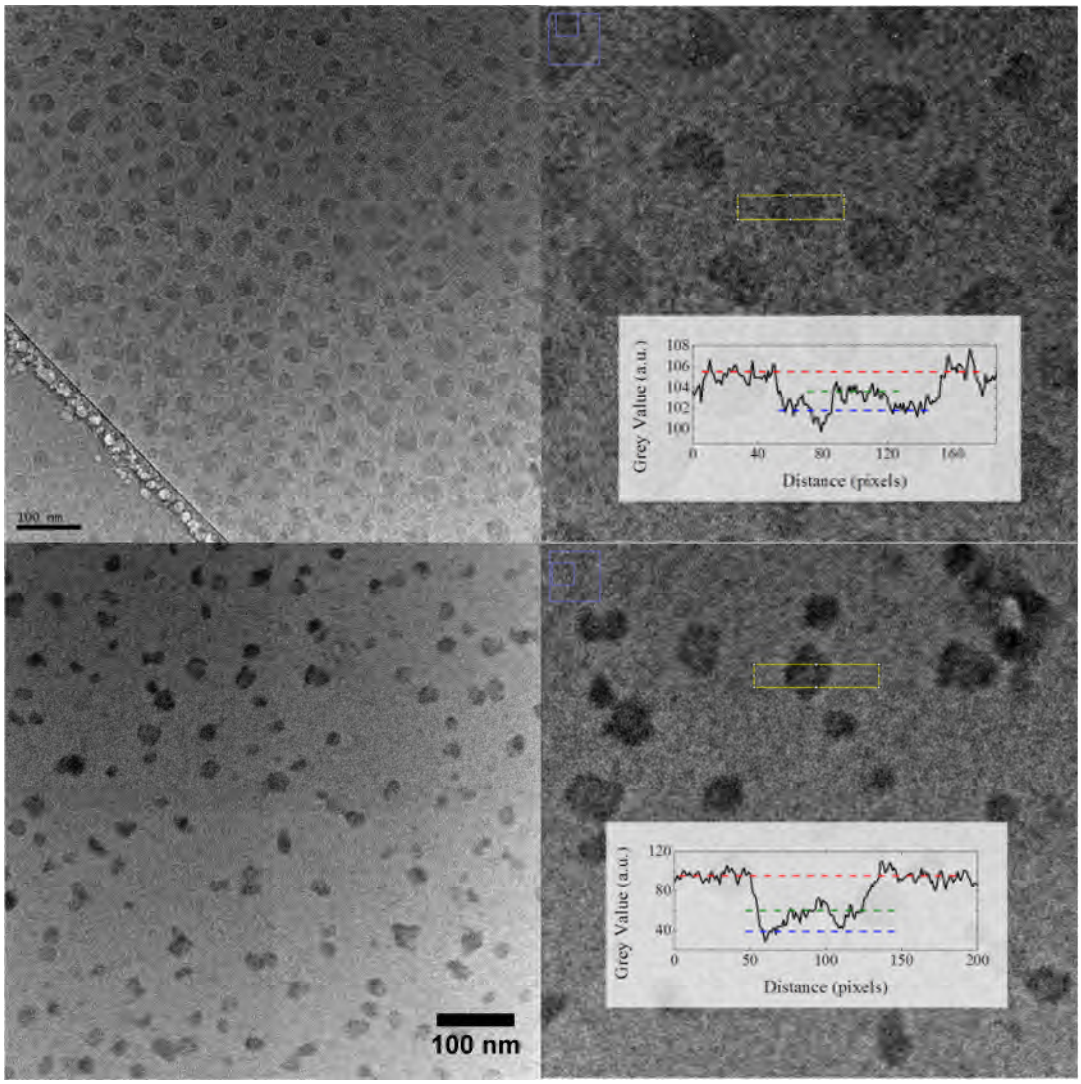

Figure 5.13. Cryo-TEM images of the **CS5.1** core-shell (top) and the **GS5.2** core-gradient shell (bottom) nanogels (Scale bars: 100 nm). The insets show the contrast profile of the highlighted areas.

When compared to the low-contrast **N5.E0.5-15** seed nanogels, both the **CS5.1** core-shell, and more so the **GS5.2** core-gradient shell nanogels were found to have a darker outline. This is highlighted when measuring the contrast profile of the images where three distinct levels can be observed. The upper (brightest) layer was attributed to the background grey value, while the intermediate layer was attributed to the contrast from the nanogel core. The third (darkest) layer was subsequently attributed to the

poly(NIPAM) corona, suggesting the successful formation of the hydrophilic polymer layer on the surface of the hydrophobic nanogels. An additional imaging technique was also employed to confirm the morphology of the nanogels, whereby copper sulfate was employed to selectively stain the poly(NIPAM) content of the nanogels (Figure 5.14).[87]

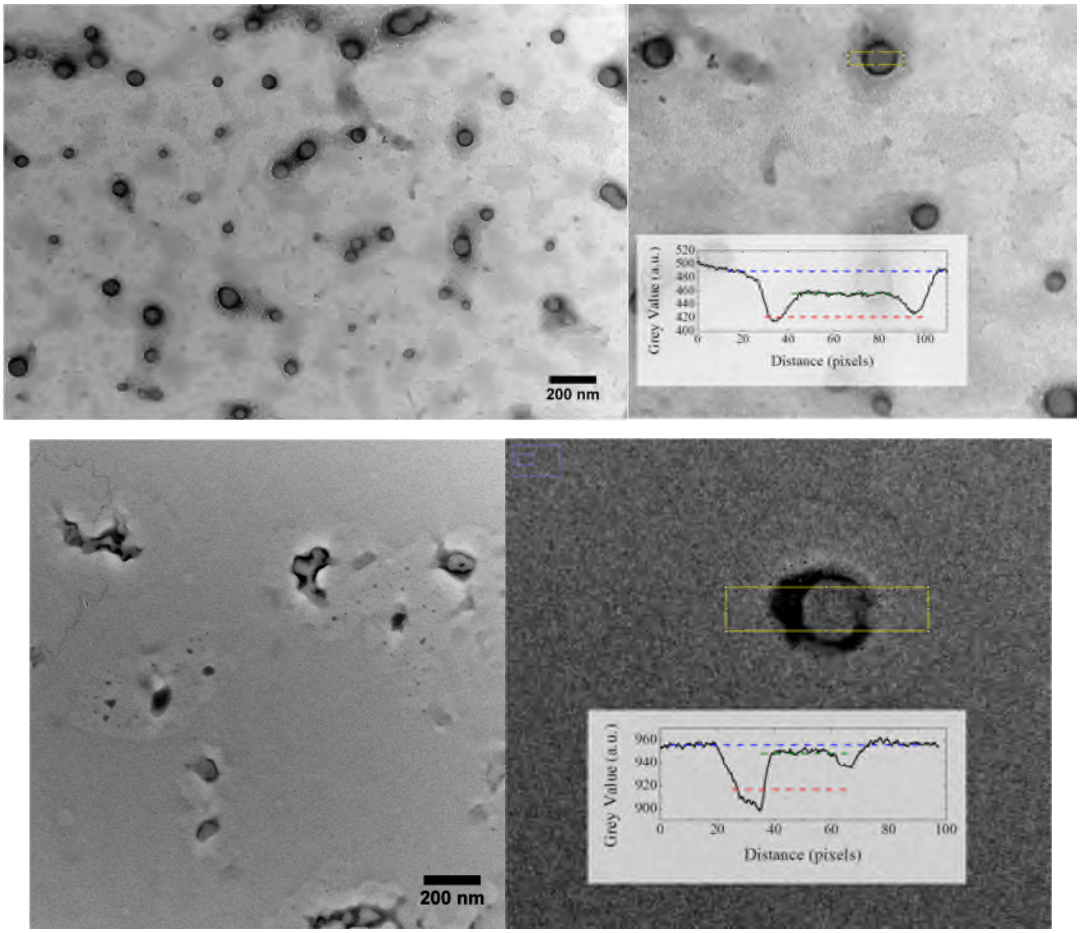

Figure 5.14. Dry-state TEM images of the **CS5.1** core-shell nanogels (top) and the **GS5.2** core-gradient shell nanogels (bottom) stained with copper.

Although the sample preparation procedure is likely to deform the nanogels, as the copper salt interacts with the NIPAM units rendering them water-insoluble while the added acetone solvates the core, a distinct dark halo is observed both for the **CS5.1** and the **GS5.2** nanogels, suggesting that the NIPAM moieties reside on the outer layer of the particles, further confirming the core-shell morphology.

When comparing the core-shell and the core-gradient shell morphologies, no observable differences were obtained to confirm that addition of the NIPAM shell in two steps can result in a gradient shell as opposed to a cross-linked shell. One possible reasoning for the increase in hydrodynamic size would be that it is a result of polymerization of the added NIPAM within the existing poly(NIPAM) shell. In order to evaluate this possibility, two new sets of nanogels were synthesized. Initially, for the synthesis of the **CS5.3** nanogels the cross-linking density of the hydrophilic shell was increased to 50 wt%, as it was hypothesized that if polymerization of NIPAM within the poly(NIPAM) shell had indeed taken place during the synthesis of **GS5.2** a highly dense shell would be obtained, and therefore comparable to **CS5.3**. In terms of size and shape, the **CS5.3** nanogels were found to be very similar to **CS5.1** and **GS5.2** nanogels (Figure 5.16). [§]

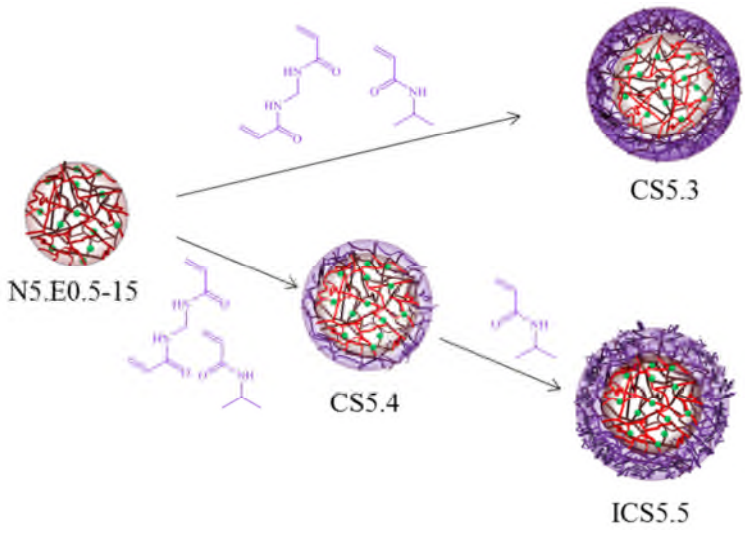

Figure 5.15. Schematic representation of the procedure followed for the synthesis of the highly cross-linked shell **CS5.3** nanogels, and the "impregnated" core-shell **ICS5.5** nanogels *via* the intermediate **CS5.4** core-shell nanogels.

[§] Note that the name of the nanogels represents their morphology: CS for core-shell and ICS for "impregnated" core-shell

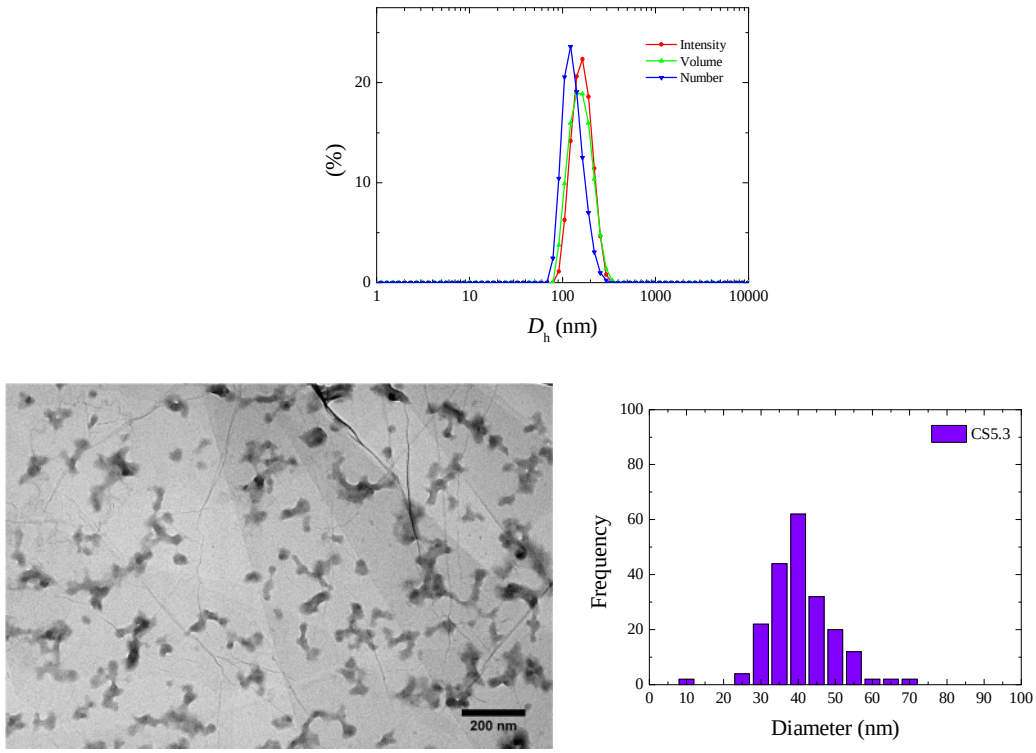

Figure 5.16. DLS characterization at 5 ºC in water (top) and TEM image (bottom left) with the respective size histogram (bottom right) for the **CS5.3** core-shell nanogels.

The hydrodynamic diameter of the **CS5.3** core-shell nanogels was found to be 166 nm in water, while by dry-state TEM imaging particles of an average size of 39±8 nm were observed.

Additionally, the same procedure followed for the synthesis of **GS5.2** was repeated, but in this case the polymerization was stopped at the intermediate stage and the nanogels were purified before the second addition of NIPAM. It was anticipated to demonstrate that in this case the polymerization of the added NIPAM would take place in solution and not affect the nanogels (**ICS5.5**). Once again, the particles were characterized by DLS at each stage to determine their hydrodynamic size (Figure 5.17).

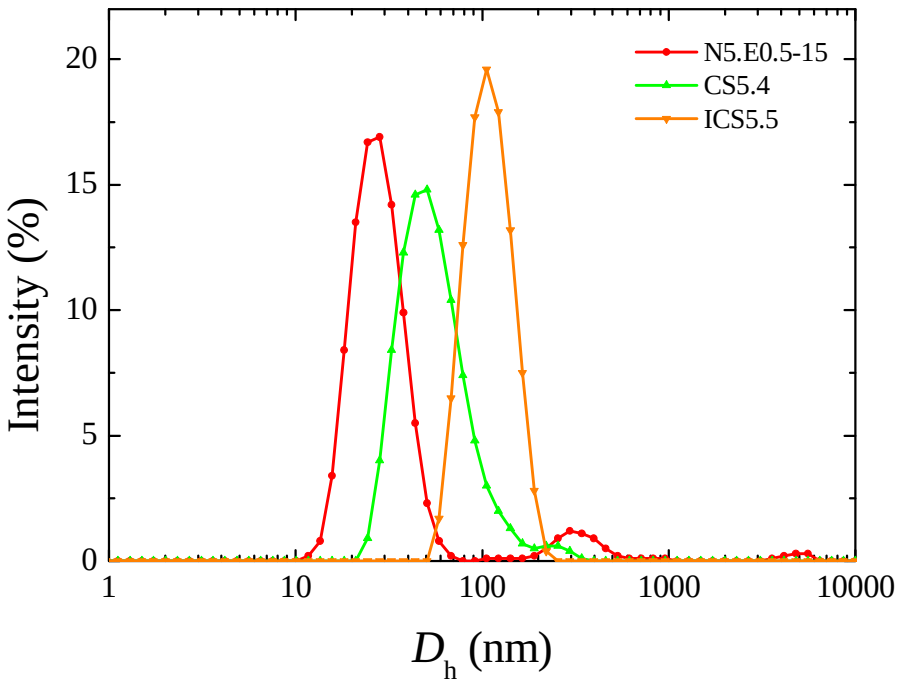

Figure 5.17. Evolution of size distributions towards the synthesis of **ICS5.5** nanogels using **N5.E0.5-15** as the hydrophobic nanogels in the seeded polymerization of the **CS5.4** core-shell nanogels, measured in water at 5 ºC.

Similar to the synthesis of the core-gradient shell particles, the increase of the nanogel size upon addition of the poly(NIPAM) shell is apparent. The seed hydrophobic nanogels **N5.E0.5-15** were found to have a hydrodynamic diameter of 29 nm, while the core-shell **CS5.4** nanogels had a hydrodynamic diameter of 52 nm. Despite the quenching of the reaction, further addition of NIPAM and initiator also resulted in the further increase of the size of the **ICS5.5** nanogels to 102 nm. Although unexpected, this was attributed to the diffusion of the newly formed hydrophobic poly(NIPAM) oligomers into the nanoparticles where the remainder of the polymerization took place, thus resulting in "impregnated" core-shell nanogels.

The thermoresponsive properties of the nanogels were studied by variable temperature DLS (Figure 5.18). As poly(NIPAM) is a temperature-responsive polymer, the particles are expected to expel their water content above that temperature, thus revealing their

original level of hydration. This is anticipated to demonstrate the relative density of the shell of each synthesized particle system.

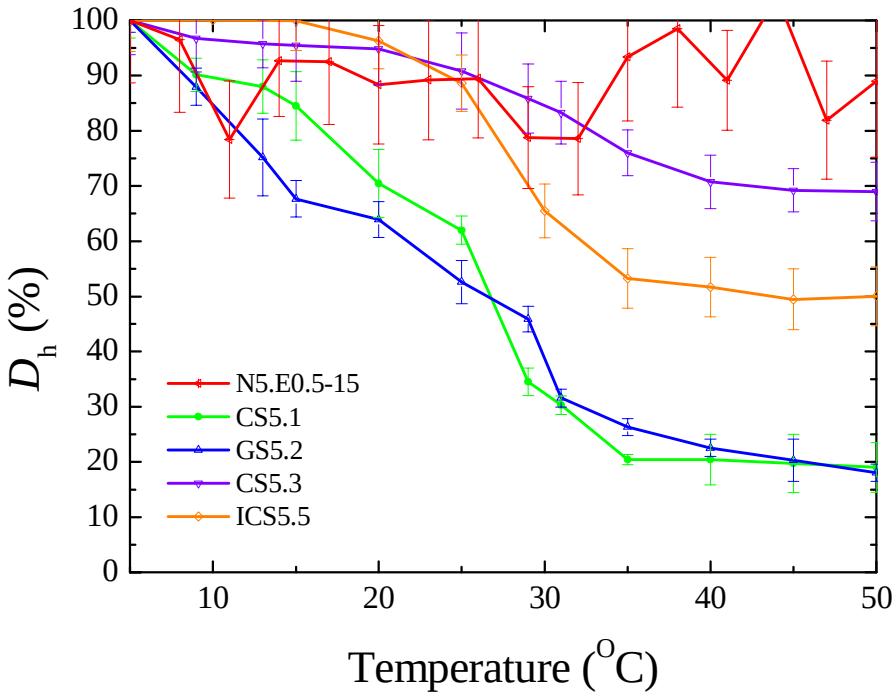

Figure 5.18. Effect of temperature on the relative size of the particles determined by DLS in water. Error bars indicate size dispersities.

The relative size of the particles defined by equation **5.1**, where D_{100} is the relative size of the particles, D_h (T_i) is the hydrodynamic size at a temperature T_i, and D_h (T_5) is the hydrodynamic diameter at 5 ºC.

$$D_{100} = \frac{D_h(T_i)}{D_h(T_5)} \times 100\% \qquad \textbf{5.1}$$

The relative size of the **N5.E0.5-15** hydrophobic core nanogels was found to fluctuate slightly with temperature, however this can be attributed to their small size (32 nm) resulting in greater error in the calculation. Nevertheless, it can be assumed that the overall size is constant suggesting little effect of the temperature on the nanoparticles

size. This is not surprising, as within the measured range of temperatures EMA-based polymers are expected to remain hydrophobic and therefore collapsed. The greatest impact of temperature on the size of the nanogels is observed for the core-shell **CS5.1** and the core-gradient shell **GS5.2** nanogels. Both systems were found to shrink to similar relative sizes, suggesting that the degree of hydration at 5 ºC is comparable. When comparing the core-gradient shell **GS5.2** and the "impregnated" core-shell **ICS5.5** curves, however, the "impregnated" **ICS5.5** nanogels were found to have a much greater relative size at elevated temperatures. This was attributed to the dense "impregnated" shell that effectively allows less amount of water to reside within it, and as a result less water is expelled when the transition takes place. This assumption is further confirmed by comparing the "impregnated" core-shell **ICS5.5** curve with that of the core-highly cross-linked shell **CS5.3** nanogels, which were intentionally designed to have a dense shell. As a result, their relative size only decreases to 68%.

This experiment demonstrates that although "impregnation" of the poly(NIPAM) shell of hydrophobic nanogels is possible *via* a two-step polymerization, when the addition of the second batch of NIPAM is done before termination takes place in the polymerization of the initial shell, the obtained morphology is different.

In order to confirm whether the core-shell **CS5.1** and the core-gradient shell **GS5.2** nanogels are effectively different, the benchmark aldol reaction (Scheme 5.2) was carried out using the two nanogels as the catalytic nanoreactors. These were conducted at three different temperatures (5, 25, and 40 ºC) in order to elucidate the role of the temperature-responsive poly(NIPAM) shell (Figure 5.19).

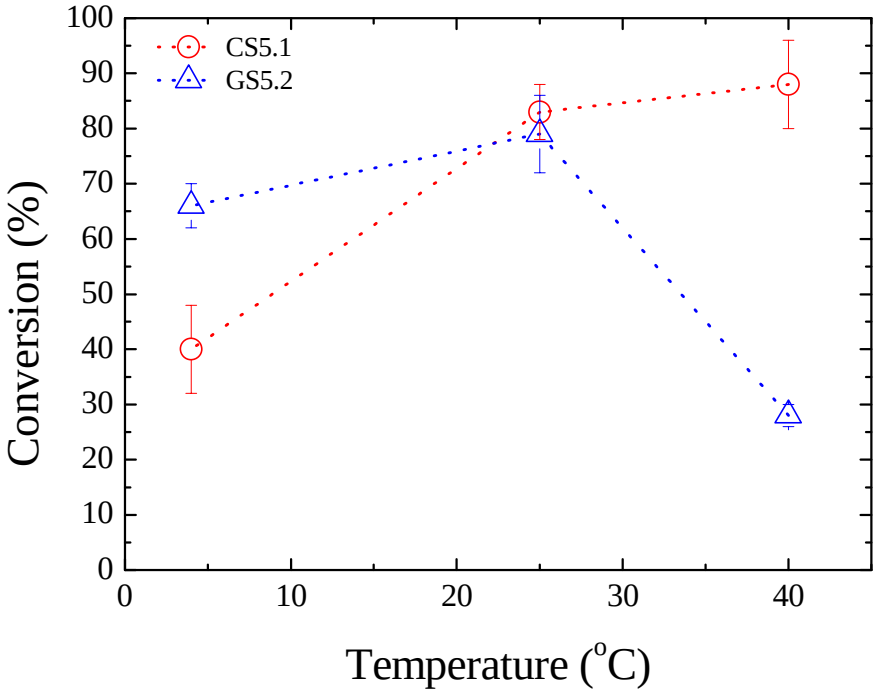

Figure 5.19. Catalytic activity of the **CS5.1** and the **GS5.2** nanogels at three different temperatures: 4 ºC where the poly(NIPAM) shell is fully hydrated, 40 ºC where the poly(NIPAM) shell is fully dehydrated, and an intermediate temperature (25 ºC), after 24 hours of reaction.[**]

Table 5.3. Catalytic efficiency of the **CS5.1** and the **GS5.2** nanogels at different temperatures after 24 hours. Conversion and diastereomeric ratio determined by ^{1}H NMR spectroscopy. Enantiomeric excess determined by HPLC using a chiral stationary phase.

Catalyst	Temperature (°C)	D_h (nm)	Conversion (%)	*anti/syn* ratio	*ee* (%)
CS5.1	4	133	40 ±8	98/2 ±1	86 ±2
	25	70	83 ±5	97/3 ±1	93 ±2
	40	30	88 ±8	96/4 ±1	96 ±1
GS5.2	4	142	66 ±4	96/4 ±2	95 ±1
	25	88	79 ±7	97/3 ±1	95 ±1
	40	28	28 ±2	95/5 ±3	97 ±1

The catalysis results suggest that although at room temperature both the **CS5.1** core-shell and the **GS5.2** core-gradient shell nanogels efficiently catalyze the aldol reaction,

[**] All catalyses and their analyses were carried out by Annhelen Lu.

with yields around 80%, their catalytic efficiency is different at lower and higher temperatures. When the reaction was carried out at 4 ºC, a significant drop in catalytic activity was observed for the **CS5.1** core-shell nanogels, accompanied by a slight drop in enantioselectivity (Table 5.3), compared to the **GS5.2** core-gradient shell nanogels that carried out the reaction in reasonable yield (66%). This can be attributed to the overall lower cross-linking density of the gradient shell, where half the amount of cross-linker, compared to the core-shell nanogels, was used. At elevated temperatures, and more specifically 40 ºC, where the shell of both types of nanogels was completely dehydrated, the yield of the nanogel-catalyzed reaction is significantly higher for the **CS5.1** core-shell nanogels, reaching 88% after 24 hours, as opposed to a dramatic drop in the activity of the **GS5.2** nanogels that only resulted in 28% conversion. This was deemed to be indicative of the different morphologies obtained for the two types of nanogels whereby the cross-linked shell of the **CS5.1** core-shell nanogels becomes hydrophobic and collapses onto the surface of the core, while in the case of **GS5.2** core-gradient shell nanogels the less cross-linked outer layer of the shell can penetrate into the hydrophobic shell sterically blocking the incoming substrates.

The ability to recycle the nanogels by exploiting the hydrophilic character of their shell in water was also demonstrated by studying their catalytic efficiency after six isolation-re-dispersion cycles. Each cycle consists of addition of the reaction substrates into the nanogel dispersion and allowing them to react for 24 hours at room temperature (Figure 5.20), followed by extraction of the reagents and the products into diethyl ether for characterization, drying of the aqueous phase, and re-dispersion of the nanogels in water at 4 ºC.

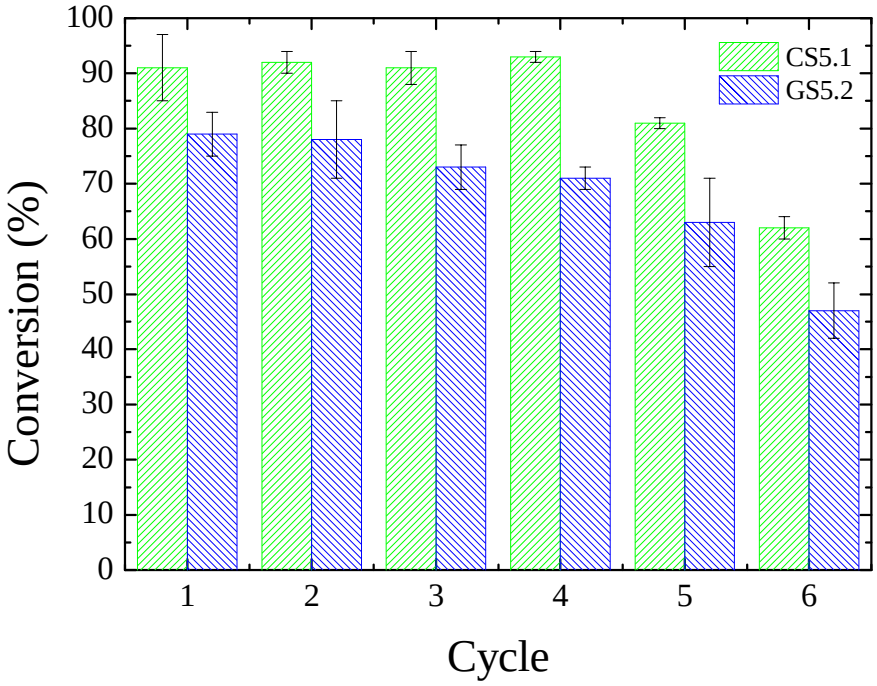

Figure 5.20. Catalytic efficiency of the **CS5.1** and the **GS5.2** nanogels over six cycles, determined by ^{1}H NMR spectroscopy after 24 h. Error bars represent standard deviation as experiments were done in triplicate.[††]

For the **CS5.1** core-shell nanogels the catalytic efficiency remains high for four cycles before a gradual drop that is observed for the following two cycles. For the **GS5.2** core-gradient shell nanogels a gradual drop in the catalytic efficiency is observed from the second cycle. In both cases the decrease in the observed conversion can be attributed to loss of a proportion of the nanogels after each cycle, as the recycling process involves extraction and drying of the aqueous phase before the re-dispersion of the nanogels in water. While optimization of the recycling protocol is necessary, the ability to maintain high activity and selectivity of the catalytic nanogels for both the **CS5.1** and the **GS5.2** nanoparticles, suggests that this methodology is viable for the synthesis of recyclable nanoreactors, and was therefore used in other nanogel systems as well.[88, 89]

[††] All catalyses and their analyses were carried out by Annhelen Lu.

Overall, the results from the core-shell and the core-gradient shell nanogels show that by simple synthetic procedures, different morphologies can be obtained that have slightly different, yet crucially different properties. Core-shell nanogels have shown greater catalytic efficiency at temperatures were the shell is not fully hydrated, while their recycling is possible and viable for at least four cycles. Core-gradient shell nanogels have exhibited good catalytic activity at temperatures were the shell is relatively hydrated. When the shell is fully dehydrated, a significant drop in catalytic activity is observed suggesting that such morphologies can be further studied to optimize the conditions at which complete shut-down of the reaction can be obtained.

5.3.2.3. Tuning the cross-linking density

Another parameter that can easily be tuned in the synthesis of polymeric cross-linked nanoparticles is the degree of cross-linking (hereinto referred to as cross-linking density, CLD). Cross-linked polymers have shown great dependency of their swelling on their cross-linking density and it is hypothesized that this can also affect the catalytic efficiency of catalyst-bearing nanogels. As such, hydrophobic MMA-based nanogels were synthesized with cross-linking densities (hereinto determined by the bifunctional monomer feed ratio) ranging from 0 wt% to 50 wt%, in order to accentuate the catalysis characteristics (Table 5.4).

Table 5.4. Overview of the synthesized hydrophobic MMA-based nanogels with different cross-linking densities.[‡‡]

	CLD (wt%)	DoF (wt%)
N5.M0-2	0.0	2
N5.M0.5-2	0.5	2
N5.M2-2	2.0	2
N5.M5-2	5.0	2
N5.M10-2	10.0	2
N5.M25-2	25.0	2
N5.M50-2	50.0	2

The hydrodynamic size of the particles was determined by DLS (Figure 5.21) and in all cases a uniform size distribution was obtained.

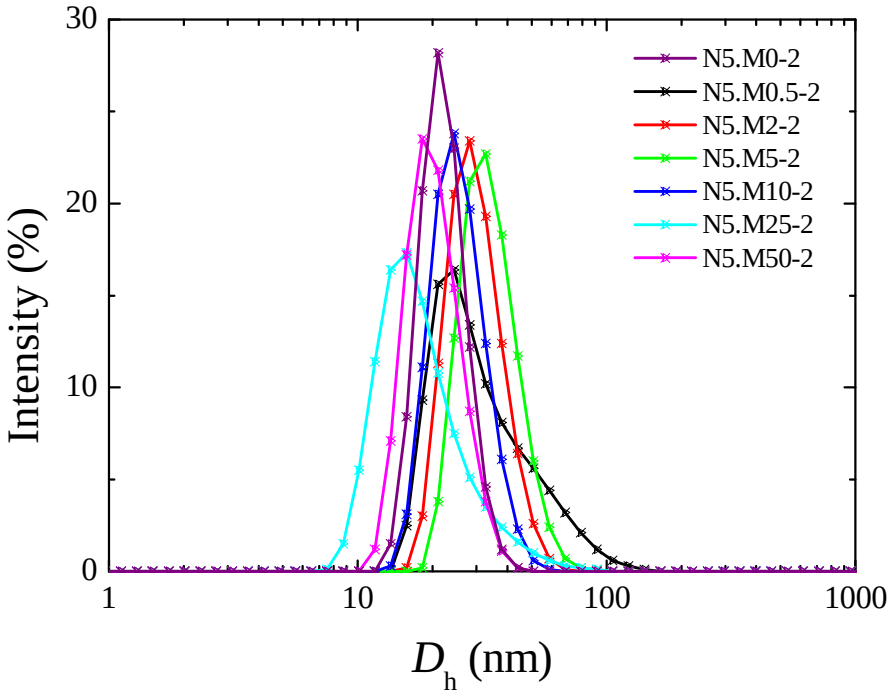

Figure 5.21. Size distributions of the hydrophobic methyl methacrylate-based nanogels with different CLD (0-50 wt%) and 2 wt% DoF, determined by DLS at 25 ºC.

[‡‡] Note that the names of the nanogels follow the format: **N5.M**(CLD)-(DoF) with M indicating the MMA co-monomer.

While overall the sizes of the nanogels are between 10-100 nm, a slight dependence of the hydrodynamic diameter on the CLD is observed (Figure 5.22). Although poly(MMA) is hydrophobic, because of the presence of the hydrophilic proline moieties within the core some water is expected to reside within the particles. As a result, when increasing the CLD, the swelling of the particles is more limited, thus resulting in smaller particles. In a simplified interpretation of the internal structure of the nanogels, one can expect that by increasing the amount of cross-linker the pores into which water can be found become smaller, therefore affecting the overall size of the particles.

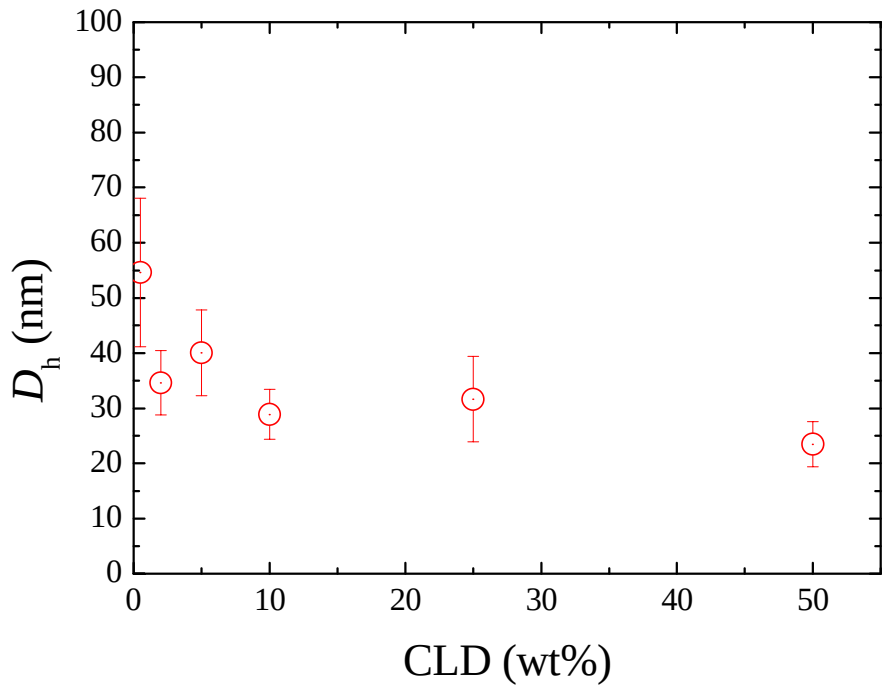

Figure 5.22. Effect of cross-linking density on hydrodynamic size of the MMA-based hydrophobic nanogels in water.

The ultimate effect of the CLD on the catalytic efficiency of the nanogels was again determined by the benchmark aldol reaction between 4-nitrobenzaldehyde and cyclohexanone in water (Scheme 5.2) (Table 5.5).

Table 5.5. Catalytic efficiency of the MMA-based hydrophobic nanogels based on their CLD. Conversions and diastereomeric ratios were determined by ^{1}H NMR spectroscopy after 24 hours. Enantiomeric excess was determined by HPLC using a chiral stationary phase.

	CLD (%)	**Conversion (%)**	***anti/syn* ratio**	***ee* (%)**
N5.M0-2	0	41	98/2	94
N5.M0.5-2	0.5	73	97/3	99
N5.M2-2	2	69	95/5	98
N5.M5-2	5	75	97/3	86
N5.M10-2	10	49	96/4	95
N5.M25-2	25	31	97/3	95
N5.M50-2	50	14	95/5	95

Despite of the fact that all nanogels had the same DoF (2 wt%), a significant effect of the CLD on their catalytic efficiency is observed. At CLD ranging between 0.5 and 5 wt%, all the nanogels were found to perform very similarly with conversions ranging between 69 and 75%. Further increase of the CLD results in the gradual drop of the activity with the highest CLD nanogels, **N5.M50-2** only resulting in 14% conversion after 24 hours. Perhaps the most important observation is that the reaction catalyzed by the **N5.M0-2** nanogels where no cross-linker was present, only resulted in 41% conversion after 24 hours, deviating from the observed trend (Figure 5.23). This highlights the importance of cross-linking which potentially confines the hydrophilic catalyst within the hydrophobic core of the nanogels, thus in this case its absence allows the L-proline moieties to re-arrange in order to be in a more hydrophilic environment.

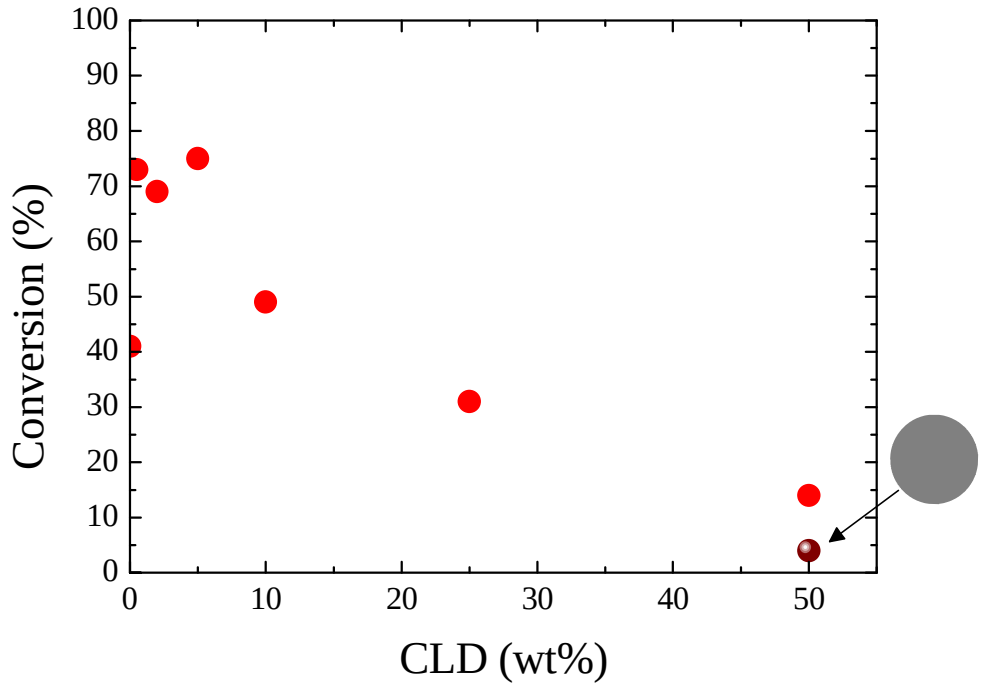

Figure 5.23. Catalytic efficiency of the MMA-based hydrophobic nanogels as a function of their CLD. Conversions were determined by ^{1}H NMR spectroscopy after 24 hours.

Once again, the complete shut-down of the catalytic activity of the nanogels was not successful, even when the CLD was increased to 50 wt%. It was hypothesized that the little activity observed for the heavily cross-linked **N5.M50-2** nanogels was a result of the L-proline moieties residing close to the surface of the particles, where the substrates are able to diffuse. In order to confirm this, the formation of a hydrophobic shell, using **N5.M50-2** as the seed nanogels was pursued (Figure 5.24). The hydrophobic shell was composed of heavily cross-linked poly(*tert*-butyl methacrylate) and the resulting core-shell nanogels (**CS5.6**) were characterized by DLS (Figure 5.25).

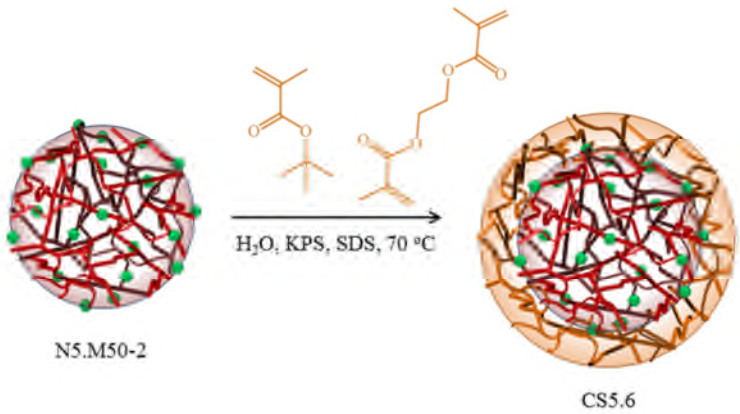

Figure 5.24. Schematic representation of the synthesis of a hydrophobic shell to encapsulate surface L-proline moieties into a heavily cross-linked hydrophobic environment.

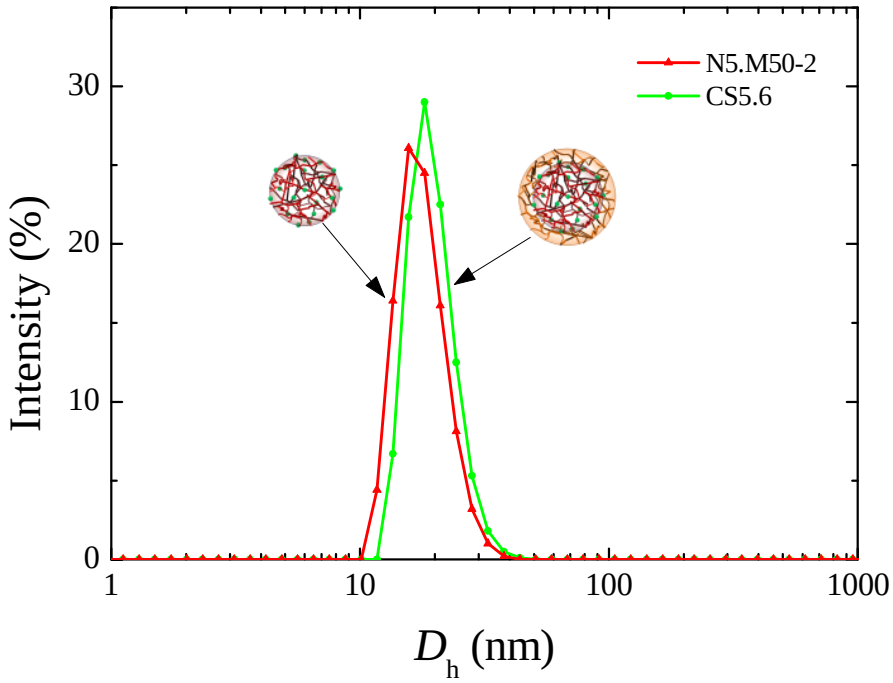

Figure 5.25. Size distributions of the **N5.M50-2** and the **CS5.6** hydrophobic nanogels at 25 ºC.

When compared to the **N5.M50-2** seed nanogels, the size distribution of the **CS5.6** core-shell hydrophobic nanogels does not reveal a great change in the particle size. The shell was however expected to be in the collapsed state, thus a significant change in size was not expected. Additionally, this is in agreement with what was observed in the case

of the hydrophilic shell (section 5.3.2.2) where upon de-solvation, the shell completely collapsed onto the nanogel core.

Nevertheless the catalysis of the aldol reaction was carried out using the core-shell **CS5.6** nanogels as the catalyst support and the measured conversion after 24 hours was under 5%, thus confirming the hypothesis that when all L-proline moieties are confined within a heavily cross-linked hydrophobic environment their catalytic activity is effectively shut-down.

The results from the study on the effect of the CLD on the catalytic activity of L-proline-containing nanogels demonstrate that it is possible to fine-tune the properties of such particles in yet another way. While some cross-linking is necessary in order to maintain the nanogel structure integrity that effectively ensures that the hydrophilic catalytic moiety resides within the hydrophobic core, increasing the CLD of the nanogels above 5 wt% results in a drop in catalytic efficiency. Additionally, when the CLD reaches 50 wt% a dramatic drop in the yield of the catalyzed reaction is observed which is further reduced upon addition of a hydrophobic layer onto the surface of the nanogels.

5.4. Conclusions

Crucial parameters that determine the properties of functional nanogels can be tuned during their synthesis. These parameters were shown to affect the catalytic properties of nanogels that were functionalized with L-proline as a paradigm catalytic moiety. With L-proline being hydrophilic, the co-monomer used in the synthesis of hydrophilic nanogels was found to greatly impact the catalytic activity of the nanogels, attributed to the local environment hydrophilicity. Nevertheless, an optimal balance was achieved by copolymerization of the L-proline functional monomer with ethyl methacrylate, with the

nanogels catalyzing in excellent yields in the benchmark aldol reaction while achieving high enantio- and stereo-selectivity.

The catalytic nanogels were also used as seeds in the seeded emulsion polymerization of a hydrophilic shell consisting of the temperature-responsive poly(NIPAM). Two different morphologies were readily obtained by tuning the shell monomer feed, whereby adding the NIPAM/cross-linker slowly resulted in a core-shell structure, while adding a smaller amount of NIPAM/cross-linker, followed by the addition of NIPAM resulted in a core-gradient shell morphology. The two were found to be very similar by TEM, DLS, and in terms of their temperature-responsive properties. Nonetheless, their ability to effectively catalyze the benchmark aldol reaction was different at a range of temperatures. Both nanogel systems were also shown to be readily recyclable with minimal loss of their catalytic activity after four cycles, while retaining some activity after six cycles.

An investigation of the effect of the cross-linking density of the hydrophobic nanogels on their catalytic efficiency suggested that highly cross-linked nanogels can shut-down the catalytic cycle of L-proline.

5.5. Materials and Methods

Trans-4-hydroxy-L-proline (>99%), methacryloyl chloride (>97%), sodium dodecyl sulfate (>99%), and potassium persulfate (>99%) were purchased from Sigma-Aldrich and were used without further purification. All monomers were purchased from Sigma-Aldrich at the highest available purity and used without further purification. Solvents were purchased from Fisher Scientific and used as received. Water was purified using an ion exchange cartridge (18.2 MΩ·cm). SpectraPor dialysis tubing was purchased from Spectrum Labs, with a molecular weight cut-off of 10 kDa.

Nuclear magnetic resonance (^{1}H and ^{13}C NMR) spectra were recorded in $CDCl_3$, C_3D_7NO, CD_3OD, or $(CD_3)_2SO$ solutions on a Bruker AC-250, a Bruker DPX-300, a Bruker AV-400 or a Bruker DPX- 400, a DRX-500, and a Bruker AV II-700 spectrometer. Chemical shifts are reported as δ in parts per million (ppm) and referenced to the chemical shift of the residual solvent resonances and/or internal standards (TMS ^{1}H: δ = 0.00 ppm; ^{13}C: δ = 0.0 ppm). High resolution mass spectra (HRMS) were collected using a Bruker MaXis UHR-ESI TOF. Dynamic light scattering (DLS) measurements were conducted on a Malvern Zetasizer Nano ZS instrument equipped with a 4 mW He-Ne 633 nm laser module and a detector at 173^{o}. When required, the temperature of the solution was altered using the software built-in temperature scan mode, set to allow equilibration at each temperature interval for 60 s. All data were analyzed using Malvern DTS 6.32 software. TEM samples were prepared by drop deposition of an aqueous solution (unless otherwise stated) onto a copper/carbon grid coated with Formvar or graphene oxide sheets. The droplet was allowed to stand for one minute before excess liquid was blotted off. Images were obtained on a JEOL 2011, or a JEOL 2000FX transmission electron microscope operating at 200 kV and analyzed using ImageJ software. Cryo-TEM samples were prepared by drop-deposition onto lacey carbon grids that were subsequently plunged into liquid ethane. Fluorescence spectra were obtained using a single-beam Perkin-Elmer LS55 fluorometer, using a slit width of 5.0 nm and exciting at 550 nm. Emission spectra were collected between 550 and 750 nm.

5.5.1.1. Synthesis of *O*-methacryloyl-*trans*-4-hydroxy-L-proline hydrochloride (ProMA)

The L-proline-functional monomer was synthesized according to the literature.[38] In a dry round-bottom flask *trans*-4-hydroxy-L-proline (5g, 38 mmol, 1 eq.) was slowly added into trifluoroacetic acid (TFA) (21.8 g, 191 mmol, 5 eq.) over an ice bath. Then, *p*-toluenesulfonic acid (1.31 g, 7.6 mmol, 0.2 eq.) was added followed by the addition of methacryloyl chloride (7.9 g, 76 mmol, 2 eq.). The reaction was stirred initially at 0 ºC and let to warm up to room temperature over three hours. Then, it was cooled again and diethyl ether was slowly added until a white precipitate was formed. The precipitate was collected and recrystallized over isopropanol/water (90:10 v/v) to afford a white powder (3.8g, isolated yield 50%). ^{1}H NMR (CD_3OD, 400 MHz): δ (ppm): 6.22 (1H, m, vinyl), 5.75 (1H, m, vinyl), 5.52 (1H, m, -O-CH), 4.64 (1H, m, -N-CH), 3.56-3.73 (2H, m, -N-CH_2), 2.49-2.68 (2H, m, CH_2), 1.98 (3H, s, CH_3); ^{13}C NMR (CD_3OD, 125 MHz) δ (ppm): 169.2, 166.2, 135.7, 126.1, 72.9, 58.4, 53.5, 34.4, 16.8; HRMS *m/z*: 222.0734 expected: 222.0737 $[M+Na]^+$.

5.5.1.2. Hydrophobic nanogel synthesis

For a typical nanogel synthesis, SDS (135.0 mg, 0.468 mmol, 27 wt%) was dissolved in water. While degassing by bubbling N_2 into the solution, a mixture of the monomers (see Table 5.6 for the quantities) was added, followed by potassium persulfate (5.0 mg, 0.018 mmol, 1 wt%). The reaction mixture was degassed for ten minutes before immersing into a pre-heated oil bath at 70 ºC. The reaction was stirred at 800 rpm under a nitrogen blanket for 12 hours, before quenching by cooling and exposure to air. The polymerization mixture was then extensively dialyzed against water (10,000 Da

MWCO) to remove excess solutes. Note that all wt% quantities are with respect to the total monomer content.

Table 5.6. Amounts of reagents used for the synthesis of the hydrophobic nanogels.

	Hydrophobic monomer		EGDMA	ProMA	CLD (wt%)	DoF (wt%)
N5.M0.5-2	MMA	470 mg	2.63 mg	10 mg	0.5	2
N5.M0.5-5	MMA	470 mg	2.63 mg	25 mg	0.5	5
N5.M0.5-10	MMA	470 mg	2.63 mg	50 mg	0.5	10
N5.M0.5-15	MMA	470 mg	2.63 mg	85 mg	0.5	15
N5.E0.5-2	EMA	458.5 mg	2.42 mg	10 mg	0.5	2
N5.E0.5-5	EMA	458.5 mg	2.42 mg	25 mg	0.5	5
N5.E0.5-10	EMA	458.5 mg	2.42 mg	50 mg	0.5	10
N5.E0.5-15	EMA	458.5 mg	2.63 mg	80 mg	0.5	15
N5.B0.5-2	BuMA	437.5 mg	2.42 mg	10 mg	0.5	2
N5.B0.5-5	BuMA	437.5 mg	2.42 mg	25 mg	0.5	5
N5.B0.5-9	BuMA	437.5 mg	2.42 mg	43 mg	0.5	9
N5.B0.5-15	BuMA	437.5 mg	2.42 mg	80 mg	0.5	15
N5.L0.5-2	LMA	434 mg	2.42 mg	10 mg	0.5	2
N5.L0.5-5	LMA	434 mg	2.42 mg	23 mg	0.5	5
N5.L0.5-9	LMA	434 mg	2.42 mg	45 mg	0.5	9
N5.L0.5-15	LMA	434 mg	2.42 mg	75 mg	0.5	15

5.5.1.3. Representative catalytic aldol reaction

All catalysis experiments were carried out by Annhelen Lu.

4-Nitrobenzaldehyde (0.038 g, 0.25 mmol, 1 eq.) was dissolved in cyclohexanone (0.104 mL, 1 mmol, 4 eq.) and mixed with the functionalized nanogel (0.005 mmol, 2 mol%) in water (2.5 mL). The reaction mixture was homogenized by vigorous shaking and allowed to stir at the desired temperature for 24 hours. THF/acetone (1:5, 10 mL) was then added to induce swelling of the pores and the reagents/product extracted into the organic fraction. The solvent was then removed *in vacuo* and the crude product analyzed by spectroscopy, determining the reaction conversion and product diastereomeric *anti/syn* ratio. The crude product was then filtered through a short plug of

silica and the enantiomeric excess (*ee*) determined by chiral HPLC (ChiralPak IA, 80:10:10 hexane:propan-2-ol:ethanol, 1.0 $mL \cdot min^{-1}$). Chiral HPLC: minor enantiomer t_R = 12.4 min, major enantiomer t_R = 18.3 min.

5.5.1.4. Recycling of the catalytic nanogels

All catalysis experiments were realized by Annhelen Lu.

The first catalytic cycle was carried out as previously described. The reaction was quenched *via* addition of Et_2O (15 mL) and the biphasic mixture was shaken to extract the aldol product from the nanogel core. Further extraction into Et_2O (3 × 15 mL) was then carried out until the organic phase was no longer yellow. The organic phases were then combined, dried ($MgSO_4$), the solvent removed *in vacuo* and the crude product characterized by ^1H NMR spectroscopy and chiral HPLC. The remaining aqueous phase was completely dried under vacuum and re-dispersed into fresh nanopure water (2.5 mL) at 5 ˚C, after which the nanogels were stirred in the fridge overnight. Prior to the start of a new catalytic cycle, the nanogels were allowed to equilibrate in room temperature with constant stirring. In a second cycle, 4-nitrobenzaldehyde (0.038 g, 0.25 mmol, 1 eq.) was dissolved in cyclohexanone (0.104 mL, 1 mmol, 4 eq.) and added to the recovered and re-dispersed nanogel solution, then homogenized by vigorous shaking. After 24 hours, the same work-up/recovery procedure was applied.

5.5.1.5. Evaluation of the nanogel hydrophobicity with Nile Red

Nile red (1.0 mg, 3.14 nmol) was dissolved in cyclohexanone (208 µL, 2.65 mmol) and split into 5 separate vials. To each vial a dispersion of nanogels in water (1.0 mL each) was added. The nanogel dispersions were sonicated for 5 minutes, prior to stirring for 24 hours. Then, a small aliquot (0.05 mL) was taken and diluted with water (0.5 mL).

Prior to analysis by fluorescence spectroscopy, each sample was filtered through a 0.45 µm syringe filter to remove any non-dissolved dye.

5.5.1.6. Synthesis of the core-shell nanogels (**CS5.1**)

First, hydrophobic nanogels (**N5.E0.5-15**) were synthesized using the procedure described in section 5.5.1.2 using EMA and EGDMA (0.5 wt%) as the co-monomer while the DoF was 15 wt%. After purification, the dispersion of **N5.E0.5-15** (25 mL) was submerged in a pre-heated oil bath at 70 °C under nitrogen. In a separate vessel, SDS (0.018 g) was dissolved in water (25 mL) and stirred under nitrogen. NIPAM (0.220 g, 1.944 mmol), NMBA (1.3 mg, 0.008 mmol, CLD 0.5 wt%), and KPS (2.5 mg, 0.009 mmol) were then added to the SDS/water solution and this polymerization mixture was then slowly added to the heated seed solution, at a rate of 25 $mL{\cdot}h^{-1}$ using a syringe pump. Once the addition was complete, nitrogen was bubbled through the polymerization reaction for an additional 10 minutes and the polymerization was then left to stir at 70 °C for 12 hours. The resulting **CS5.1** nanogels were purified *via* dialysis against nanopure water. *In lieu* of conversion, the dialysate was collected, dried and analyzed by ^{1}H NMR spectroscopy, however only SDS was observed, suggesting high monomer conversions.

5.5.1.7. Synthesis of the core-gradient shell nanogels (**GS5.2**)

The first step was carried out following the procedure explained above for synthesis of **CS5.1** nanogels. In a similar fashion, the seed nanogel particles (25 mL) were heated at 70 °C with nitrogen bubbling. However, instead of making a single pot containing all the NIPAM monomer and cross-linker, the monomer was separated into two addition vessels. The first mixture, used to synthesize the cross-linked shell consisted of NIPAM

(0.110 g, 0.972 mmol), NMBA (0.65 mg, 0.5 wt%, 0.004 mmol), SDS (0.009 g), KPS (2.5 mg, 0.009 mmol) and water (12.5 mL). This solution was added drop-wise to the heated seed particles using a syringe pump at a rate of 25 $mL \cdot h^{-1}$ under nitrogen and then allowed to proceed for 20 minutes. The second pot of polymerization mixture consisted of the remaining NIPAM monomer (0.110 g, 0.972 mmol), SDS (0.009 g) and water (12.5 mL). No additional initiator was added, in order to allow NIPAM to react with the active radicals present in the shell from the first polymerization process and form the corona layer. The **GS5.2** nanogels were purified via dialysis against nanopure water. The dialysate was collected, dried and analyzed by ^{1}H NMR spectroscopy, however only SDS was observed; suggesting high monomer conversion and absence of low molecular weight free PNIPAM.

5.5.1.8. Copper-stained nanogels for TEM imaging

PNIPAM domains in the nanoparticles were selectively stained[87] by incubating the solutions with $CuSO_4$ overnight and subsequently removing excess copper by three consecutive washing cycles *via* ultrafiltration and addition of fresh water. The samples were then dissolved in acetone and deposited onto the TEM grids as described above.

5.5.1.9. Synthesis of the core-heavily cross-linked shell **CS5.3** nanogels

The **CS5.3** nanogels were synthesized in a similar procedure as that followed for the synthesis of **CS5.1** with the exception of the NIPAM and NMBA quantities were both adjusted to 110 mg in order to achieve the 50 wt% CLD.

5.5.1.10. Synthesis of the "impregnated" core-shell nanogels (**ICS5.5**)

In a similar procedure as that followed for the synthesis of the **GS5.2** nanogels, the **ICS5.5** nanogels were obtained with the only difference being that the intermediate particles were purified before the addition of the second monomer batch with the addition of more initiator. The seed nanogel particles **N5.E0.5-15** (25 mL) were synthesized as described previously and were subsequently heated at 70 °C and degassed *via* nitrogen bubbling. Then, a solution of NIPAM (0.110 g, 0.972 mmol), NMBA (0.65 mg, 0.5 wt%, 0.004 mmol), SDS (0.009 g), KPS (2.5 mg, 0.009 mmol), and water (12.5 mL) were added drop-wise to the heated seed particles using a syringe pump at a rate of 25 $mL \cdot h^{-1}$, under nitrogen and allowed to proceed overnight. After purification by dialysis against water, the mixture was reheated to 70 ºC and degassed *via* nitrogen bubbling before the addition of a solution of NIPAM (0.110 g, 0.972 mmol), KPS (2.5 mg, 0.009 mmol) and water (12.5 mL). The **ICS5.5** nanogels were purified *via* dialysis against nanopure water. The dialysate was collected, dried and analyzed by ^{1}H NMR, however only SDS was observed, suggesting high monomer conversions and absence of low molecular weight free PNIPAM.

5.5.1.11. Synthesis of hydrophobic MMA-based nanogels with different CLD

For a typical nanogel synthesis, SDS (135.0 mg, 0.468 mmol, 27 wt%) was dissolved in water. While degassing by bubbling N_2 into the solution, a mixture of the monomers (see Table 5.7 for the quantities) was added, followed by potassium persulfate (5.0 mg, 0.018 mmol, 1 wt%). The reaction mixture was degassed for ten minutes before immersing into a pre-heated oil bath at 70 ºC. The reaction was stirred at 800 rpm under a nitrogen blanket for 12 hours, before quenching by cooling and exposure to air. The polymerization mixture was then extensively dialyzed against water

(10,000 Da MWCO) to remove excess solutes. Note that all wt% quantities are with respect to the total monomer content.

Table 5.7. Amounts of reagents used for the synthesis of the hydrophobic nanogels.

	Hydrophobic monomer		EGDMA	ProMA	CLD (wt%)	DoF (wt%)
N5.M0-2	MMA	470 mg	0 mg	10 mg	0.0	2
N5.M0.5-2	MMA	470 mg	2.63 mg	10 mg	0.5	2
N5.M2-2	MMA	470 mg	10.51 mg	10 mg	2.0	2
N5.M5-2	MMA	470 mg	26.28 mg	10 mg	5.0	2
N5.M10-2	MMA	458.5 mg	52.55 mg	11 mg	10.0	2
N5.M25-2	MMA	458.5 mg	158.7 mg	10 mg	25.0	2
N5.M50-2	MMA	229.3 mg	242.8 mg	10 mg	50.0	2

5.5.1.12. Synthesis of the **CS5.6** core-shell nanogels

A 25 mL dispersion of the **N5.M50-2** nanogels was heated to 70 ºC and a degassed mixture of water (25 mL), SDS (0.063 g, 0.218 mmol), *tert*-butyl methacrylate (0.125 g, 0.879 mmol), EGDMA (0.125 g, 0.631 mmol) and KPS (2.5 mg, 0.009 mmol) were added under nitrogen using an automated syringe pump, at a rate of 25 $mL \cdot h^{-1}$. The polymerization was allowed to proceed for 12 hours at 70 °C before purification by dialysis against water to remove excess SDS.

5.6. References

1. T. D. Machajewski and C.-H. Wong, *Angew. Chem. Int. Ed.*, 2000, **39**, 1352-1375.
2. D. W. C. MacMillan, *Nature*, 2008, **455**, 304-308.
3. K. Kondo, T. Yamano and K. Takemoto, *Die Makromolekulare Chemie*, 1985, **186**, 1781-1785.
4. T. Bui and C. F. Barbas III, *Tetrahedron Lett.*, 2000, **41**, 6951-6954.

5. B. List, P. Pojarliev and H. J. Martin, *Org. Lett.*, 2001, **3**, 2423-2425.
6. M. S. Rasalkar, M. K. Potdar, S. S. Mohile and M. M. Salunkhe, *J. Mol. Catal. A: Chem.*, 2005, **235**, 267-270.
7. B. List, *J. Am. Chem. Soc.*, 2000, **122**, 9336-9337.
8. B. List, P. Pojarliev, W. T. Biller and H. J. Martin, *J. Am. Chem. Soc.*, 2002, **124**, 827-833.
9. B. List, R. A. Lerner and C. F. Barbas III, *J. Am. Chem. Soc.*, 2000, **122**, 2395-2396.
10. K. Sakthivel, W. Notz, T. Bui and C. F. Barbas III, *J. Am. Chem. Soc.*, 2001, **123**, 5260-5267.
11. B. List, *Tetrahedron*, 2002, **58**, 5573-5590.
12. A. Heine, G. DeSantis, J. G. Luz, M. Mitchell, C.-H. Wong and I. A. Wilson, *Science*, 2001, **294**, 369-374.
13. T.-P. Loh, L.-C. Feng, H.-Y. Yang and J.-Y. Yang, *Tetrahedron Lett.*, 2002, **43**, 8741-8743.
14. P. Kotrusz, I. Kmentova, B. Gotov, S. Toma and E. Solcaniova, *Chem. Commun.*, 2002, 2510-2511.
15. W. Miao and T. H. Chan, *Adv. Synth. Catal.*, 2006, **348**, 1711-1718.
16. Y. Hayashi, S. Aratake, T. Itoh, T. Okano, T. Sumiya and M. Shoji, *Chem. Commun.*, 2007, 957-959.
17. H. Torii, M. Nakadai, K. Ishihara, S. Saito and H. Yamamoto, *Angew. Chem. Int. Ed.*, 2004, **43**, 1983-1986.
18. P. M. Pihko, K. M. Laurikainen, A. Usano, A. I. Nyberg and J. A. Kaavi, *Tetrahedron*, 2006, **62**, 317-328.
19. S. S. Chimni, D. Mahajan and V. V. Suresh Babu, *Tetrahedron Lett.*, 2005, **46**, 5617-5619.
20. A. Cordova, W. Notz and C. F. Barbas III, *Chem. Commun.*, 2002, 3024-3025.
21. S. Aratake, T. Itoh, T. Okano, N. Nagae, T. Sumiya, M. Shoji and Y. Hayashi, *Chem. Eur. J.*, 2007, **13**, 10246-10256.
22. Y. Hayashi, T. Sumiya, J. Takahashi, H. Gotoh, T. Urushima and M. Shoji, *Angew. Chem. Int. Ed.*, 2006, **45**, 958-961.
23. Y.-Y. Peng, Q.-P. Ding, Z. Li, P. G. Wang and J.-P. Cheng, *Tetrahedron Lett.*, 2003, **44**, 3871-3875.

24. N. Mase, Y. Nakai, N. Ohara, H. Yoda, K. Takabe, F. Tanaka and C. F. Barbas III, *J. Am. Chem. Soc.*, 2005, **128**, 734-735.
25. Y. Hayashi, S. Aratake, T. Okano, J. Takahashi, T. Sumiya and M. Shoji, *Angew. Chem. Int. Ed.*, 2006, **45**, 5527-5529.
26. B. H. Lipshutz and S. Ghorai, *Org. Lett.*, 2012, **14**, 422-425.
27. E. Bellis and G. Kokotos, *J. Mol. Catal. A: Chem.*, 2005, **241**, 166-174.
28. M. Benaglia, G. Celentano and F. Cozzi, *Adv. Synth. Catal.*, 2001, **343**, 171-173.
29. M. Benaglia, M. Cinquini, F. Cozzi, A. Puglisi and G. Celentano, *Adv. Synth. Catal.*, 2002, **344**, 533-542.
30. Y.-X. Liu, Y.-N. Sun, H.-H. Tan, W. Liu and J.-C. Tao, *Tetrahedron: Asymmetry*, 2007, **18**, 2649-2656.
31. Y.-X. Liu, Y.-N. Sun, H.-H. Tan and J.-C. Tao, *Catal. Lett.*, 2008, **120**, 281-287.
32. A. Lu, T. P. Smart, T. H. Epps III, D. A. Longbottom and R. K. O'Reilly, *Macromolecules*, 2011, **44**, 7233-7241.
33. F. Giacalone, M. Gruttadauria, A. M. Marculescu and R. Noto, *Tetrahedron Lett.*, 2007, **48**, 255-259.
34. M. Gruttadauria, F. Giacalone, A. Mossuto Marculescu, P. Lo Meo, S. Riela and R. Noto, *Eur. J. Org. Chem.*, 2007, **2007**, 4688-4698.
35. D. Font, C. Jimeno and M. A. Pericàs, *Org. Lett.*, 2006, **8**, 4653-4655.
36. D. Font, S. Sayalero, A. Bastero, C. Jimeno and M. A. Pericàs, *Org. Lett.*, 2008, **10**, 337-340.
37. C. A. McNamara, M. J. Dixon and M. Bradley, *Chem. Rev.*, 2002, **102**, 3275-3300.
38. T. E. Kristensen, K. Vestli, K. A. Fredriksen, F. K. Hansen and T. Hansen, *Org. Lett.*, 2009, **11**, 2968-2971.
39. E. G. Doyagüez, F. Parra, G. Corrales, A. Fernández-Mayoralas and A. Gallardo, *Polymer*, 2009, **50**, 4438-4446.
40. E. Huerta, P. J. M. Stals, E. W. Meijer and A. R. A. Palmans, *Angew. Chem. Int. Ed.*, 2013, **52**, 2906-2910.
41. A. Lu, P. Cotanda, J. P. Patterson, D. A. Longbottom and R. K. O'Reilly, *Chem. Commun.*, 2012, **48**, 9699-9701.
42. H. A. Zayas, A. Lu, D. Valade, F. Amir, Z. Jia, R. K. O'Reilly and M. J. Monteiro, *ACS Macro Lett.*, 2013, **2**, 327-331.

43. S. Grandhee, in *Polymer Dispersions and Their Industrial Applications*, Wiley-VCH Verlag GmbH & Co. KGaA, 2003, pp. 163-189.
44. B. Richey and M. Burch, in *Polymer Dispersions and Their Industrial Applications*, Wiley-VCH Verlag GmbH & Co. KGaA, 2003, pp. 123-161.
45. B. Szabo, in *Polymer Dispersions and Their Industrial Applications*, Wiley-VCH Verlag GmbH & Co. KGaA, 2003, pp. 103-122.
46. H. Staudinger and E. Husemann, *Ber. dtsch. Chem. Ges. A/B*, 1935, **68**, 1618-1634.
47. W. O. Baker, *Ind. Eng. Chem.*, 1949, **41**, 511-520.
48. B. R. Saunders and B. Vincent, *Adv. Colloid Interface Sci.*, 1999, **80**, 1-25.
49. R. Pelton, *Adv. Colloid Interface Sci.*, 2000, **85**, 1-33.
50. M. Ballauff and Y. Lu, *Polymer*, 2007, **48**, 1815-1823.
51. N. Sanson and J. Rieger, *Polym. Chem.*, 2010, **1**, 965-977.
52. L. Hu, A. K. Sarker, M. R. Islam, X. Li, Z. Lu and M. J. Serpe, *J. Polym. Sci. Part A: Polym. Chem.*, 2013, **51**, 3004-3020.
53. S. Seiffert, *J. Polym. Sci. Part A: Polym. Chem.*, 2014, **52**, 435-449.
54. Z. Hu, T. Cai and C. Chi, *Soft Matter*, 2010, **6**, 2115-2123.
55. Y. Hertle and T. Hellweg, *J. Mater. Chem. B*, 2013, **1**, 5874-5885.
56. H. G. Schild, *Prog. Polym. Sci.*, 1992, **17**, 163-249.
57. R. H. Pelton and P. Chibante, *Colloids Surf.*, 1986, **20**, 247-256.
58. R. H. Pelton, H. M. Pelton, A. Morphesis and R. L. Rowell, *Langmuir*, 1989, **5**, 816-818.
59. S. Meyer and W. Richtering, *Macromolecules*, 2005, **38**, 1517-1519.
60. Y. Guan and Y. Zhang, *Soft Matter*, 2011, **7**, 6375-6384.
61. B. Sierra-Martin, J. R. Retama, M. Laurenti, A. Fernández Barbero and E. López Cabarcos, *Adv. Colloid Interface Sci.*, 2014, **205**, 113-123.
62. Z. Ge, D. Xie, D. Chen, X. Jiang, Y. Zhang, H. Liu and S. Liu, *Macromolecules*, 2007, **40**, 3538-3546.
63. Y. Lu, S. Proch, M. Schrinner, M. Drechsler, R. Kempe and M. Ballauff, *J. Mater. Chem.*, 2009, **19**, 3955-3961.
64. S. Carregal-Romero, N. J. Buurma, J. Pérez-Juste, L. M. Liz-Marzán and P. Hervés, *Chem. Mater.*, 2010, **22**, 3051-3059.

65. Y. Lu, J. Yuan, F. Polzer, M. Drechsler and J. Preussner, *ACS Nano*, 2010, **4**, 7078-7086.
66. G. Wei, W. Zhang, F. Wen, Y. Wang and M. Zhang, *J. Phys. Chem. C*, 2008, **112**, 10827-10832.
67. D. Valade, Y. Jeon, S. Kessel and M. J. Monteiro, *J. Polym. Sci. A Polym. Chem.*, 2012, **50**, 4762-4771.
68. V. E. Shashoua and R. G. Beaman, *J. Polym. Sci.*, 1958, **33**, 101-117.
69. G. M. Eichenbaum, P. F. Kiser, A. V. Dobrynin, S. A. Simon and D. Needham, *Macromolecules*, 1999, **32**, 4867-4878.
70. P. J. Flory, *Principles of Polymer Chemistry*, First edn., Cornell University Press, Ithaca, United States, 1953.
71. V. Rodionov, H. Gao, S. Scroggins, D. A. Unruh, A.-J. Avestro and J. M. J. Fréchet, *J. Am. Chem. Soc.*, 2010, **132**, 2570-2572.
72. T. Hellweg, *J. Polym. Sci. B Polym. Phys.*, 2013, **51**, 1073-1083.
73. R. A. Ramli, W. A. Laftah and S. Hashim, *RSC Adv.*, 2013, **3**, 15543-15565.
74. Z. An, Q. Qiu and G. Liu, *Chem. Commun.*, 2011, **47**, 12424-12440.
75. D. Duracher, F. Sauzedde, A. Elaissari, A. Perrin and C. Pichot, *Colloid Polym. Sci.*, 1998, **276**, 219-231.
76. C. D. Jones and L. A. Lyon, *Macromolecules*, 2000, **33**, 8301-8306.
77. D. Gan and L. A. Lyon, *J. Am. Chem. Soc.*, 2001, **123**, 7511-7517.
78. I. Berndt and W. Richtering, *Macromolecules*, 2003, **36**, 8780-8785.
79. X. Li, J. Zuo, Y. Guo and X. Yuan, *Macromolecules*, 2004, **37**, 10042-10046.
80. I. Berndt, J. S. Pedersen and W. Richtering, *J. Am. Chem. Soc.*, 2005, **127**, 9372-9373.
81. K. E. Christodoulakis and M. Vamvakaki, *Langmuir*, 2010, **26**, 639-647.
82. J. J. Crassous, M. Ballauff, M. Drechsler, J. Schmidt and Y. Talmon, *Langmuir*, 2006, **22**, 2403-2406.
83. D. Font, A. Bastero, S. Sayalero, C. Jimeno and M. A. Pericàs, *Org. Lett.*, 2007, **9**, 1943-1946.
84. P. Greenspan and S. D. Fowler, *J. Lipid Res.*, 1985, **26**, 781-789.
85. T. E. Kristensen and T. Hansen, *Eur. J. Org. Chem.*, 2010, **2010**, 3179-3204.
86. Y. Lu, A. Wittemann, M. Ballauff and M. Drechsler, *Macromol. Rapid Commun.*, 2006, **27**, 1137-1141.

87. S. Sinha-Ray, Y. Zhang, D. Placke, C. M. Megaridis and A. L. Yarin, *Langmuir*, 2010, **26**, 10243-10249.

88. B. L. Moore, D. Moatsou, A. Lu and R. K. O'Reilly, *Polym. Chem.*, 2014, **5**, 3487-3494.

89. B. L. Moore, A. Lu, D. Moatsou and R. K. O'Reilly, *Eur. Polym. J.*, 2015, **62**, 380-385.

Chapter 6 - Photo-induced cross-linking of thymine-functional nanogels

6.1. Abstract

As a continuation of the work presented in Chapter 5, and the results of the catalyses, a reversible cross-linking agent was employed for the synthesis of hydrophobic and hydrophilic nanogels. A thymine-functional monomer was introduced in the emulsion polymerization of styrene and *N*-isopropylacrylamide, using different monomer loadings, and the ability of the resulting nanogels to photo cross-link, as a result of thymine photo-dimerization, was studied.

This work was carried out in collaboration with Dominic Gray from Rachel O'Reilly's group at the University of Warwick. Dominic Gray synthesized the 30% VBT-functional nanogels and performed the ^{1}H NMR spectroscopy of the thymine-containing polymer particles.

6.2. Introduction

6.2.1. Thymine dimerization

In nature, UV-irradiated DNA forms a mutagenic photoproduct that disrupts the normal cellular processing due to the cyclobutane pyrimidine dimer between adjacent thymine bases.[1, 2]

This is achieved *via* a [2+2] cycloaddition reaction (Scheme 6.1) that proceeds *via* a cyclic transition state, without the involvement of intermediates. While the reaction requires significant heating to overcome the high activation barrier, by photo-activation only small amounts of energy are required to induce the formation of the cyclobutane dimer.[3, 4]

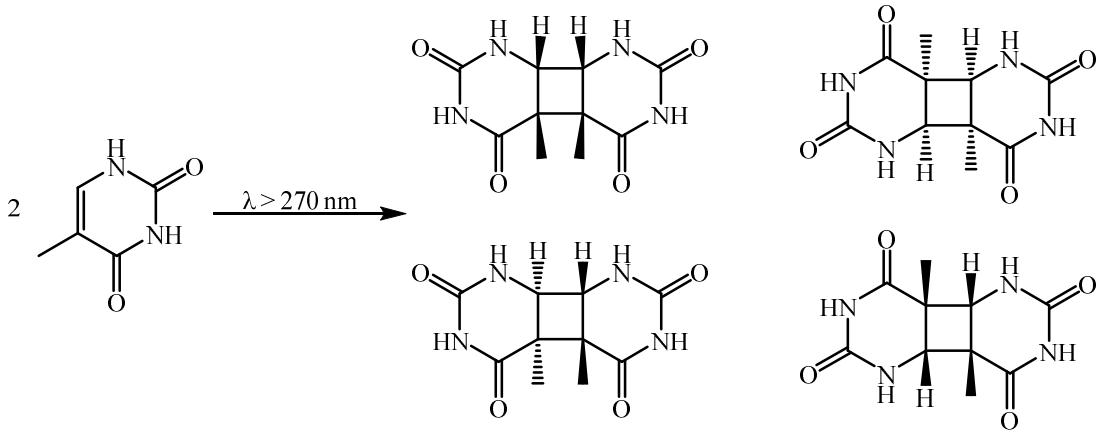

Scheme 6.1. Schematic representation of the [2+2] photo-induced cycloaddition of thymine and the possible products.

Organisms possess repair pathways that render the dimerization reversible,[5] however recent reports suggest that the thymine moieties can be retrieved by irradiation of the cyclobutane pyrimidine dimer at $\lambda < 249$ nm.[6, 4, 7]

As such, incorporation of thymine into polymeric systems has generated a few interesting systems, most of which involve the study of the interaction with other moieties, such as adenine, as briefly described in Chapter 3. With regards to thymine-functional polymer particles, Margaritis *et al.* envisioned the use of thymine-functional poly(styrene) microspheres for biotechnological applications, such as affinity chromatography.[8] Similarly, Taylor *et al.* had previously described the synthesis of thymine-containing polymers and nanoparticles, as well as their UV irradiation-induced dimerization. However, the properties of the synthesized materials were not shown.[9]

Warner *et al.* employed the thymine-functional monomer 1-(vinylbenzyl)thymine (VBT) for the formation of hydrophilic copolymers *via* free-radical polymerization. The thymine moiety was subsequently dimerized by UV irradiation resulting in the formation of water-insoluble films that were used in a variety of applications.[10-13] Similarly, Martino *et al.* have studied the kinetics of the photo-induced cross-linking of a hydrophilic copolymer of VBT with a charged styrenic derivative.[14, 15]

Reversible-deactivation radical polymerization processes have also been employed to form well-defined thymine-containing block copolymers that were self-assembled into micelles. Upon irradiation, the micelles were found to permanently cross-link, attributed to the dimerization of thymine contained in different polymer chains.[16, 17] These micelles were further studied for their ability to release hydrogen-bonding payloads.[18, 19]

Saito *et al.* have reported the synthesis of di-thymine functional molecules that undergo photo-polymerization *via* the dimerization of thymine moieties from different molecules.[4, 7, 20-22] Further irradiation of the new polymers with shorter wavelength, resulted in their de-polymerization.

6.3. Results and discussion

6.3.1. Photo-cross-linked nanogels

From the previous results presented in Chapter 5, it is apparent that by careful consideration of the procedure and components during the synthesis of catalyst-containing nanogels, the properties of the nanoreactor can be fine-tuned. Although this can easily be achieved, a more desirable system would involve the tuning of these parameters post-synthesis. As such, the use of a cross-linker that is triggered by external stimuli was pursued and hence, thymine functional nanogels were chosen. It was proposed that by incorporating a thymine-containing monomer in the synthesis of hydrophobic nanogels, the cross-linking density (CLD) of the resulting nanogels could be then tuned by UV irradiation (Figure 6.1). Additionally, as discussed in the introduction (section 6.2.1), thymine-containing polymers have shown potential for reversible light-induced cross-linking, thus making such a system extremely attractive for its use as an “on-off” catalytic nanoreactor, tuned by the CLD.

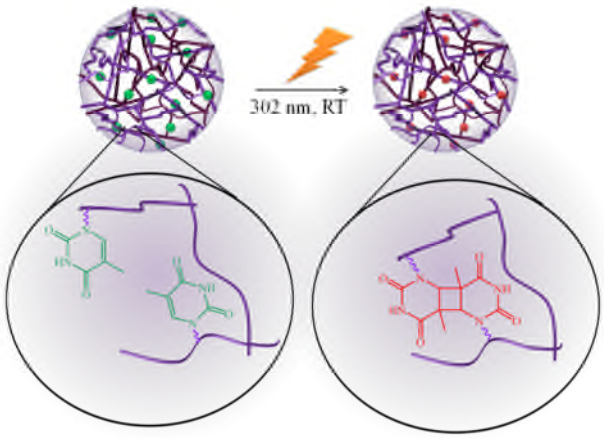

Figure 6.1. Schematic representation of the irradiation-induced dimerization of thymine, and thus cross-linking of the nanogels.

6.3.1.1. Styrene-based nanogels for UV-induced cross-linking

The thymine-containing monomer synthesized for this purpose was 1-(vinylbenzyl)thymine (VBT), which has been previously shown in the literature to successfully polymerize under free-radical polymerization conditions.[8, 23] As it is a styrenic monomer; the co-monomer selected for the emulsion co-polymerization was styrene. Hydrophobic nanogels with different loadings of VBT monomer were synthesized, with the VBT feeding ratio being 2, 10, 20, and 30 wt%, thus resulting in nanogels **N6.ST2**, **N6.ST10**, **N6.ST20**, and **N6.ST30** respectively, and their hydrodynamic diameters were determined by DLS (Figure 6.3).[*]

[*] Note that the naming of the particles follows the generic format: **N6.ST**(VBT loading), whereby S denotes the use of styrene as the co-monomer and T stands for thymine.

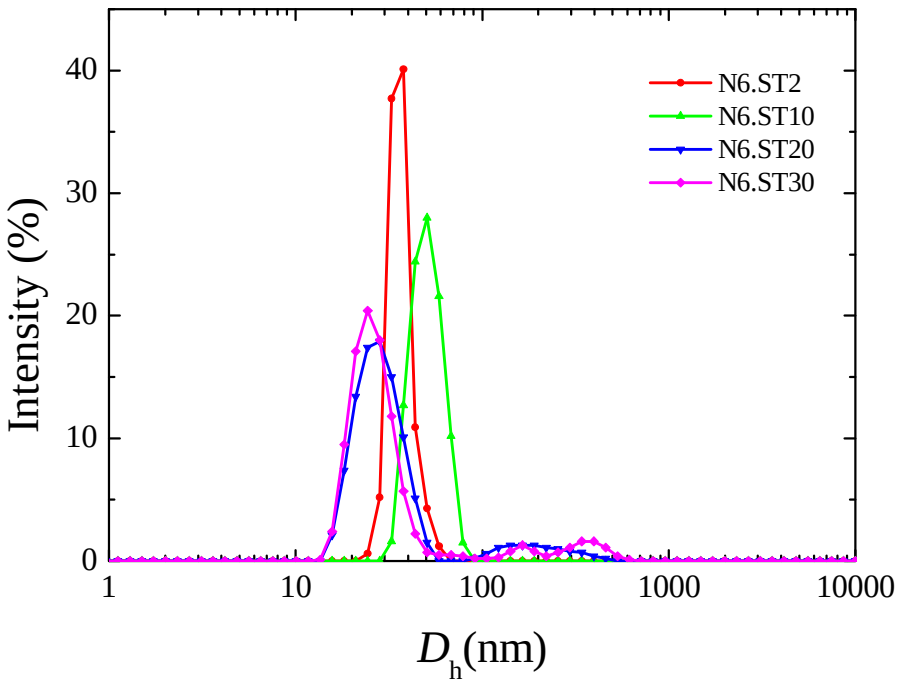

Figure 6.2. Size distributions for the VBT-containing styrene-based nanogels determined by DLS in water.

For the nanogels with the lower VBT loading, **N6.ST2** and **N6.ST10**, uniform distributions were obtained, while the particles containing greater amounts of VBT, **N6.ST20** and **N6.ST30**, produced secondary peaks corresponding to larger size particles. These were attributed to aggregates and were not considered to significantly affect the behavior of the nanogels, as their contribution to the scattered intensity was low. Comparison of the sizes of the particles (Figure 6.3) indicated little effect of the VBT loading on the size of the nanogels.

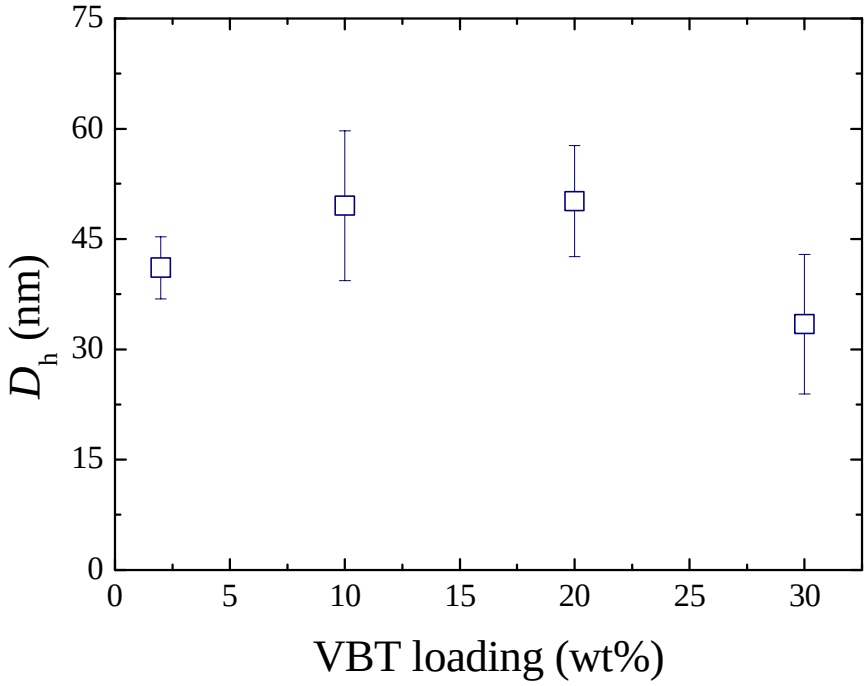

Figure 6.3. Hydrodynamic diameters of the VBT-functional styrene-based nanogels determined by DLS in water at 25 ºC. Error bars indicate size dispersity.

The **N6.ST10** and the **N6.ST30** nanogels were also observed by TEM in order to compare the morphology of the nanoparticles (Figure 6.4 and Figure 6.5).

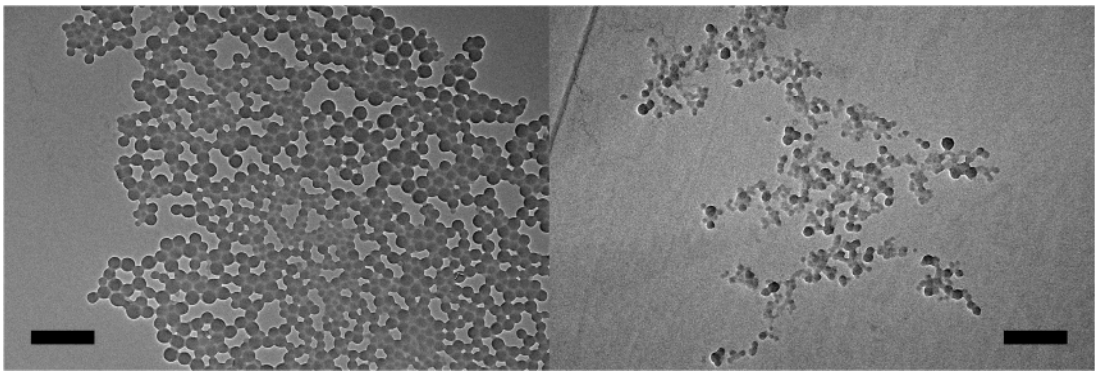

Figure 6.4. Representative TEM images of the **N6.ST10** (left) and the **N6.ST30** (right) nanogels (Scale bars: 200 nm).

Although the TEM images from the **N6.ST10** nanogels show spherical particles of fairly uniform sizes (31±6 nm), the **N6.ST30** nanogels were found to be of less well-defined

shape, although the size was relatively uniform (26±4 nm). The variation in shapes and the broader distribution obtained for the **N6.ST30** nanogels by DLS can potentially be attributed to the poor ability of VBT to polymerize under the employed conditions for emulsion polymerization, potentially as a result of its low solubility in both the aqueous and the organic phase.

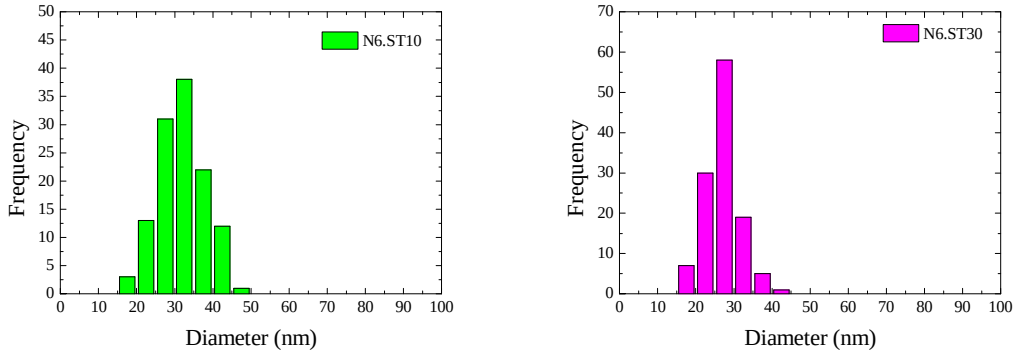

Figure 6.5. Size histograms from the **N6.ST10** and **N6.ST30** particles measured by TEM.

In order to confirm that the nanogels contained both polymerized styrene and VBT moieties, **N6.ST30** was dried and dissolved in deuterated *N*,*N*'-dimethylformamide (DMF), a good solvent for both poly(styrene) and poly(VBT), and analyzed by diffusion-ordered spectroscopy (DOSY) (Figure 6.6).

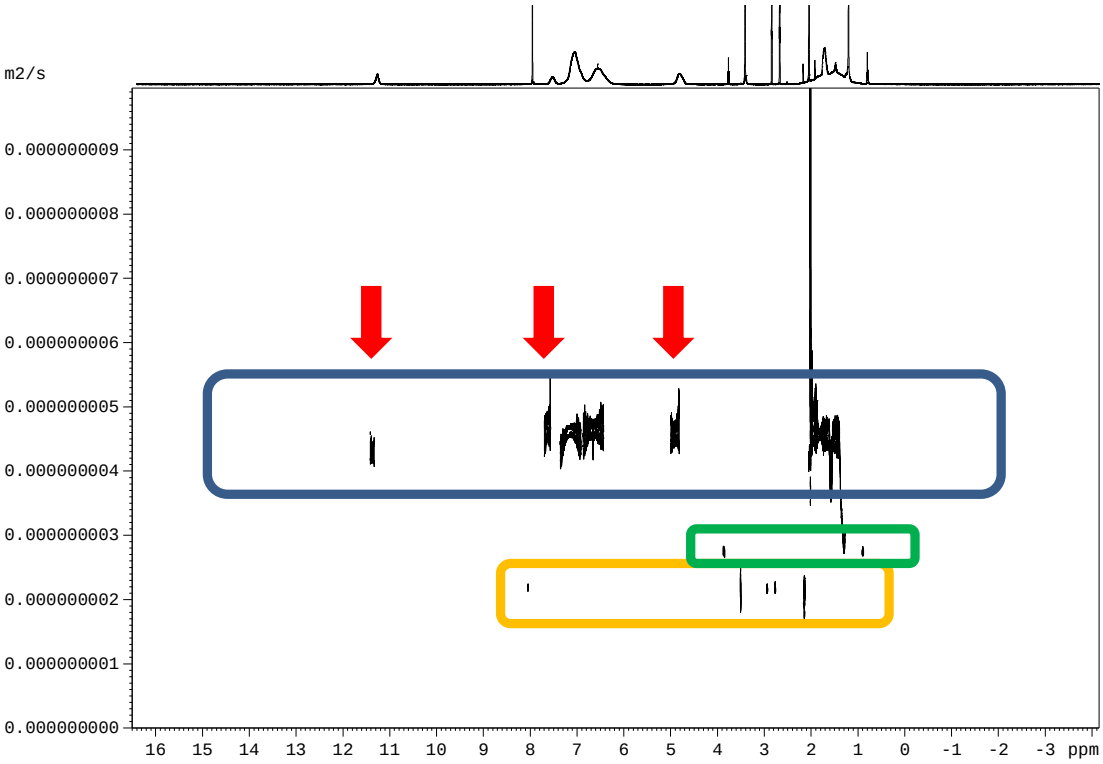

Figure 6.6. DOSY NMR spectrum of **N6.ST30** (500 MHz, C_3D_7NO). The polymer (blue rectangle), the solvent (yellow rectangle), and the surfactant (green rectangle) are highlighted, as well as the signals that correspond solely to the VBT moiety (red arrows).

Signals corresponding to three distinct diffusion coefficients were obtained. The fastest population with a diffusion coefficient 2.2×10^{-9} m^2s^{-1} was attributed to the solvent and the added 3-(trimethylsilyl)propanesulfonic acid (TMS-PSA, used further for quantification purposes), while the second population with an apparent diffusion of 2.8×10^{-9} m^2s^{-1} to the excess SDS. The slowest population with an apparent diffusion of 4.5×10^{-9} m^2s^{-1} was attributed to the copolymer and the presence of the signals corresponding solely to the VBT moieties at the same diffusion indicates the successful incorporation of the functional monomer in the copolymer, and thus in the nanogels.

The nanogels were also characterized by UV-Vis spectroscopy, as thymine exhibits a characteristic absorption peak at λ = 265-270 nm (Figure 6.7) [14]. As a comparison, a sample containing poly(styrene) nanogels with no VBT was also prepared (**N6.ST0**).

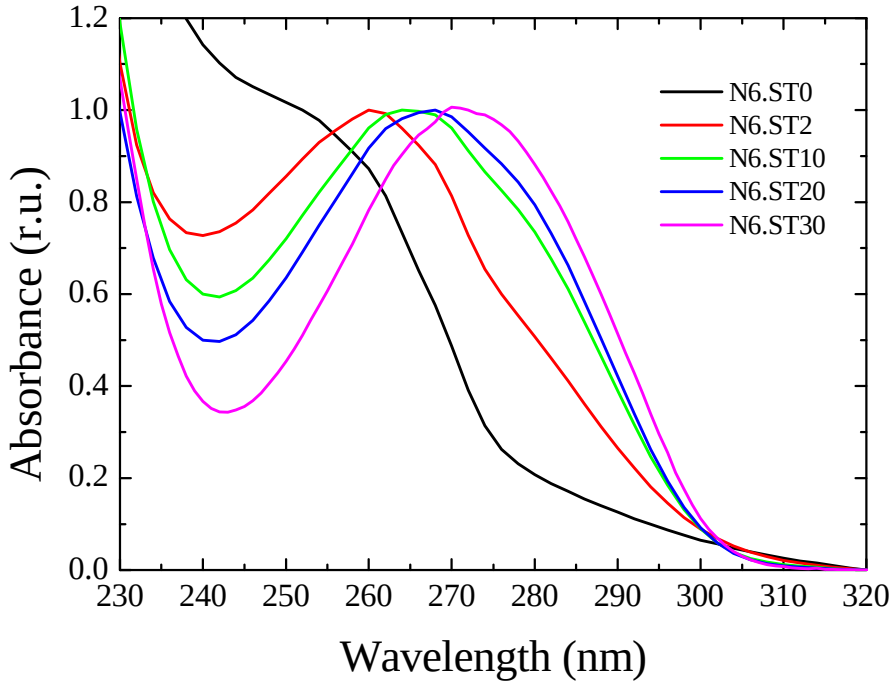

Figure 6.7. Normalized absorption spectra of **N6.ST0** poly(styrene) nanogels and the VBT-containing nanogels **N6.ST2**, **N6.ST10**, **N6.ST20**, and **N6.ST30** in water.

The nanogels containing no VBT (**N6.ST0**) were found to strongly absorb at λ = 254 nm, which was attributed to the styrene moieties absorption. Upon increase of the VBT content of the nanogels, the main absorption peak shifts to higher wavelengths, with the **N6.ST30** nanogels exhibiting an absorption maximum at λ = 272 nm. This shift is attributed to the increase of the VBT content, thus further confirming its successful incorporation into the nanogels.

The nanogel dispersions were then irradiated using a UV chamber where the light source emits within the midrange of the UV spectrum with the maximum intensity at 302 nm. As mentioned in the introduction of this Chapter (section 6.2.1), irradiation of thymine results in the [2+2] cycloaddition reaction between two species and the formation of a cyclobutane cross-link. The progress of the reaction was monitored by UV-vis spectroscopy (Figure 6.8). Note that each nanogel sample was named after the name of

the parent nanogel followed by the duration of the irradiation in hours (*i.e.*, **N6.ST10-12** is the **N6.ST10** nanogels after irradiation for 12 hours).

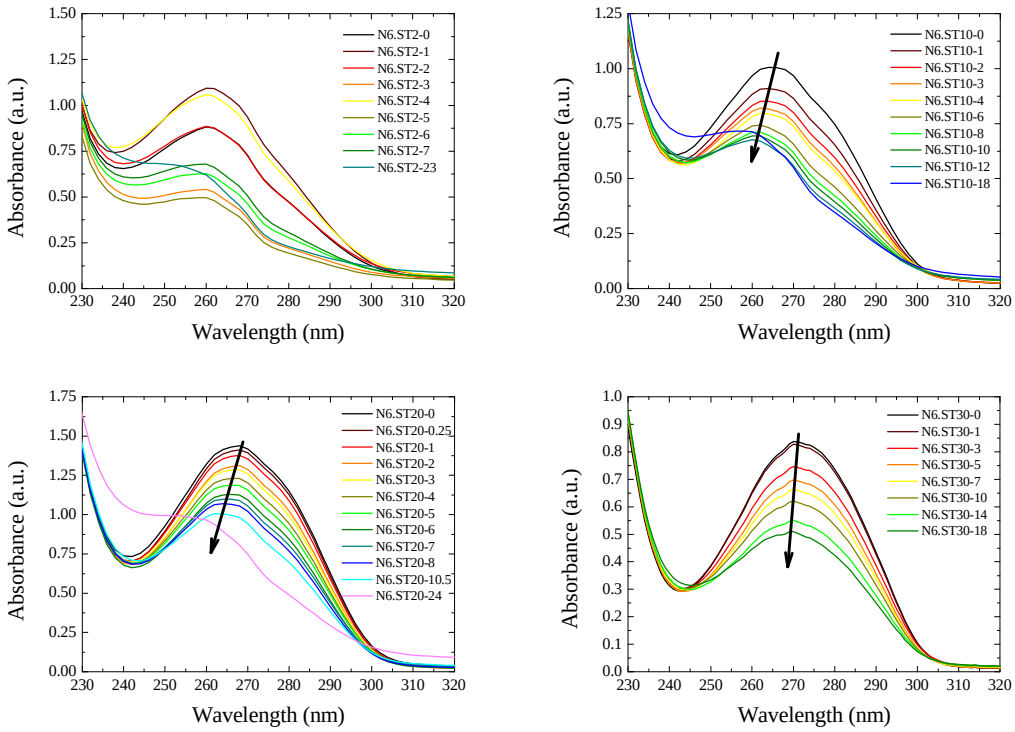

Figure 6.8. Absorption spectra for the styrene-based nanogels with different VBT loadings (2,10, 20, and 30 wt%) upon irradiation.

Upon irradiation of the **N6.ST2** nanogels, the obtained absorption spectra change with irradiation duration, however it does not consistently decrease, possibly because of the low thymine content. In all three other cases, absorption maxima of **N6.ST10**, **N6.ST20**, and **N6.ST30** in the 260-280 nm region are found to gradually decrease with irradiation time, while a slight shift to shorter wavelengths is also observed. This change is attributed to the successful dimerization of the thymine moieties, and subsequently the formation of cross-linking points within the nanogel. It should also be noted that prolonged exposure to UV irradiation caused discoloration of the nanogel dispersions

and macroscopic aggregation (Figure 6.9). Thus, irradiation times varied, with the maximum irradiation time being that upon which the sample aggregation was observed.

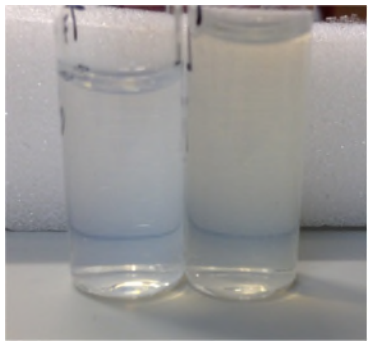

Figure 6.9. Digital photograph of the **N6.ST2** (left) and the **N6.ST2-15** (right) nanogel dispersions, showing the discoloration after prolonged irradiation.

In order to confirm that the cross-linking has taken place within the particles, rather than amongst particles, the size of the particles was monitored by DLS in water (Figure 6.10).

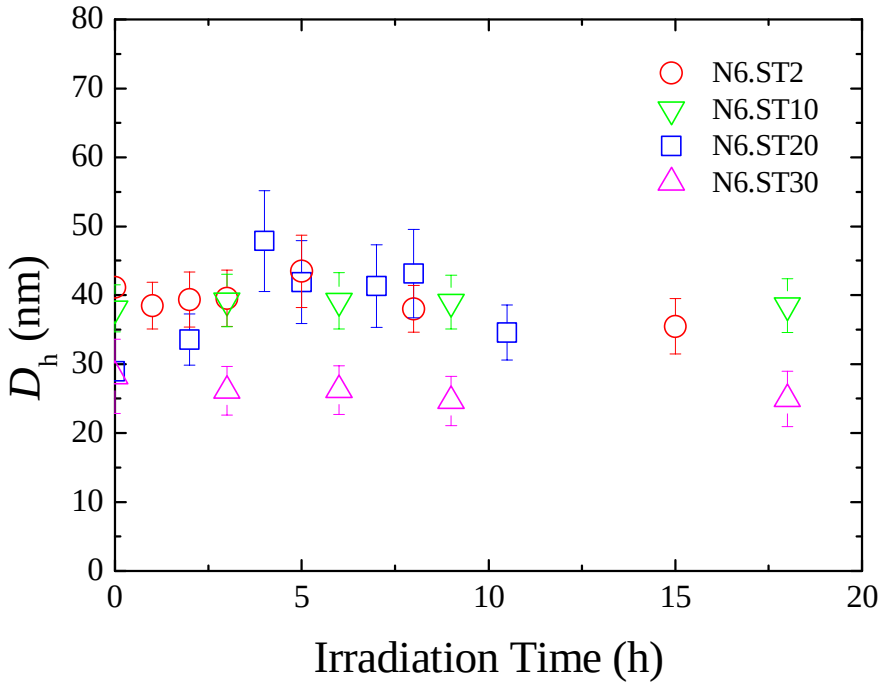

Figure 6.10. Hydrodynamic diameters of the styrene-based VBT-loaded nanogels at different irradiation times, determined by DLS in water at 25 ºC. Error bars correspond to size distributions.

Overall, no significant change of the overall size of the particles was observed with irradiation time, suggesting that indeed no aggregation has taken place as a result of inter-particle cross-linking. Comparison of the size distributions of the nanogels before and after prolonged irradiation times (Figure 6.11) also indicates the retention of the uniform sizes. It is therefore confirmed that the overall size of the nanogels had not been affected. Nevertheless, some broadening in the main distribution peak was observed, suggesting that the morphology of the nanogels may have been affected, potentially as a result of inter-particle cross-linking.

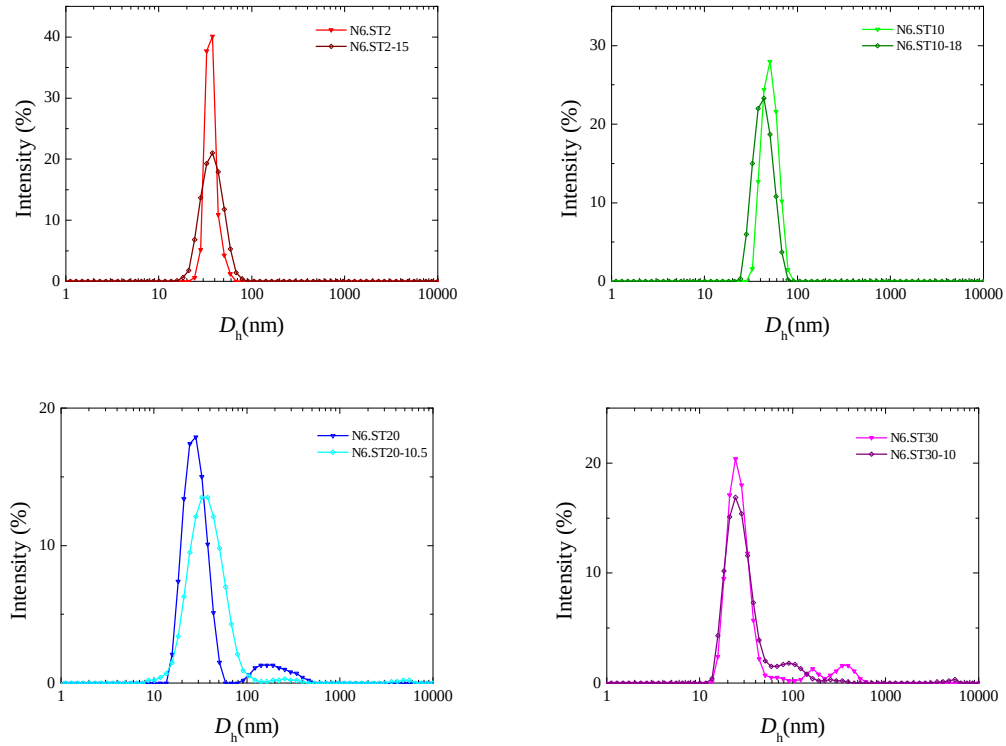

Figure 6.11. Size distributions for the styrene-based nanogels with different VBT loadings, before and after irradiation, determined by DLS in water at 25 ºC.

To investigate the possibility of UV irradiation affecting the morphology of the styrene-based nanogels, **N6.ST10-18** and **N6.ST30-18** were observed by TEM and compared to the parent nanogels (Figure 6.12).

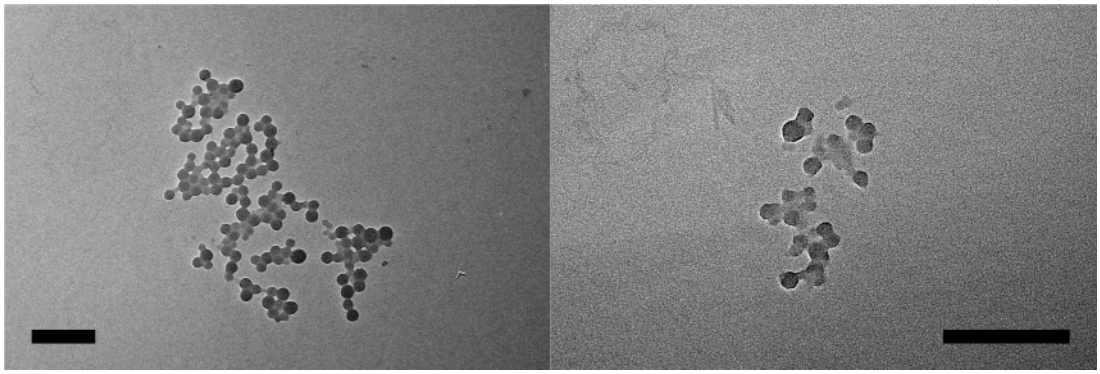

Figure 6.12. TEM images of the **N6.ST10-18** (left) and the **N6.ST30-18** (right) nanogels showing the morphology of the nanogel after irradiation. (Scale bars: 200 nm)

Similarly to the images obtained before irradiation, for **N6.ST10-18** spherical particles of fairly uniform sizes were obtained, while for **N6.ST30-18** no significant change in the size or shape of the particles was observed. The absence of coalesced spherical particles (more apparent in the case of **N6.ST10-18**) further confirms the absence of inter-particle cross-linking.

Results so far indicate that no significant change is observed upon irradiation of the styrene-based nanogels. The only indication that the irradiation-induced cross-linking has occurred is the decrease of the UV absorption of the particles at the wavelength where thymine absorbs. As such, in an attempt to elucidate the efficiency of cross-linking and potentially quantify it, the high VBT-loading nanogels **N6.ST30** were irradiated in water and aliquots were removed, dried, and re-dissolved in deuterated DMF containing a known amount of TMS-PSA, in order to monitor the cross-linking by ^{1}H NMR spectroscopy (Figure 6.13).

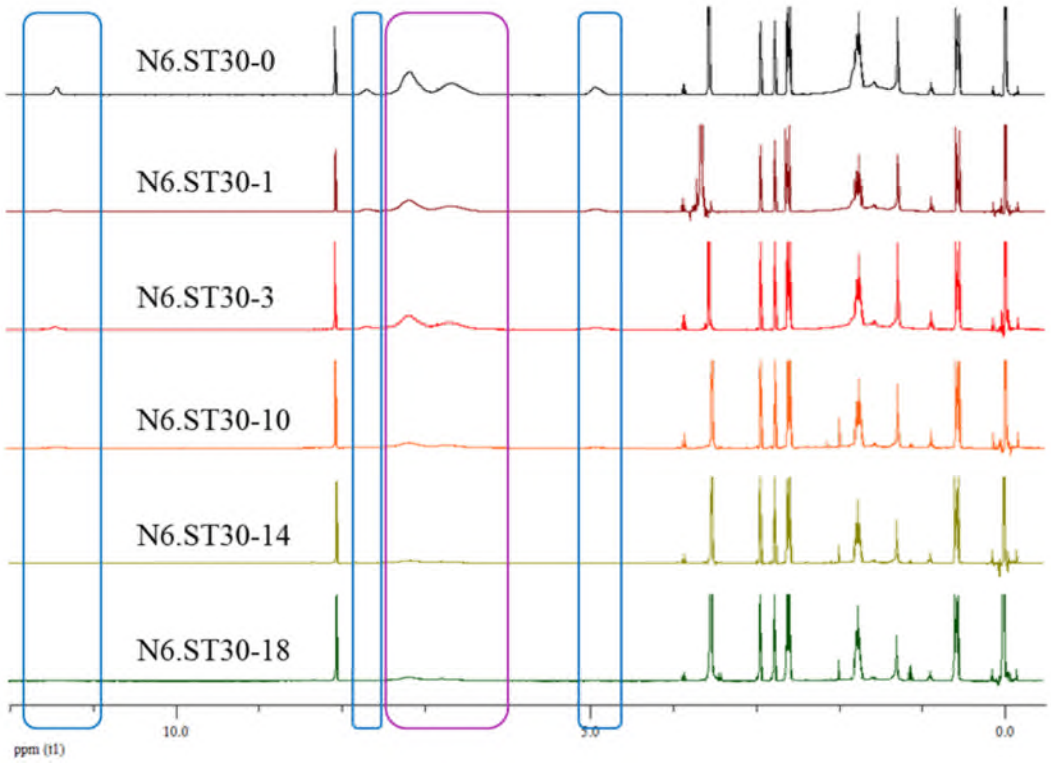

Figure 6.13. ^{1}H NMR spectra of the **N6.ST30** nanogels at different irradiation times, dissolved in C_3D_7NO containing TMS-PSA (400 MHz). Highlighted regions show the characteristic signals from VBT (blue) and styrene and VBT (purple).

In the spectrum from the initial nanogel (**N6.ST30-0**) that has been dried and dissolved in C_3D_7NO the characteristic signals from both the VBT and the styrene moieties are observed, such as the signals corresponding to the aromatic protons at δ = 6.5 – 7.5 ppm. However, as the irradiation time increases the intensity of the polymer signals decreases. This can also be confirmed from the relative integration of the peaks corresponding to the aromatic proton signals of the polymer and the signals from the methyl proton signals of TMS-PSA at δ = 0 ppm (Figure 6.14).

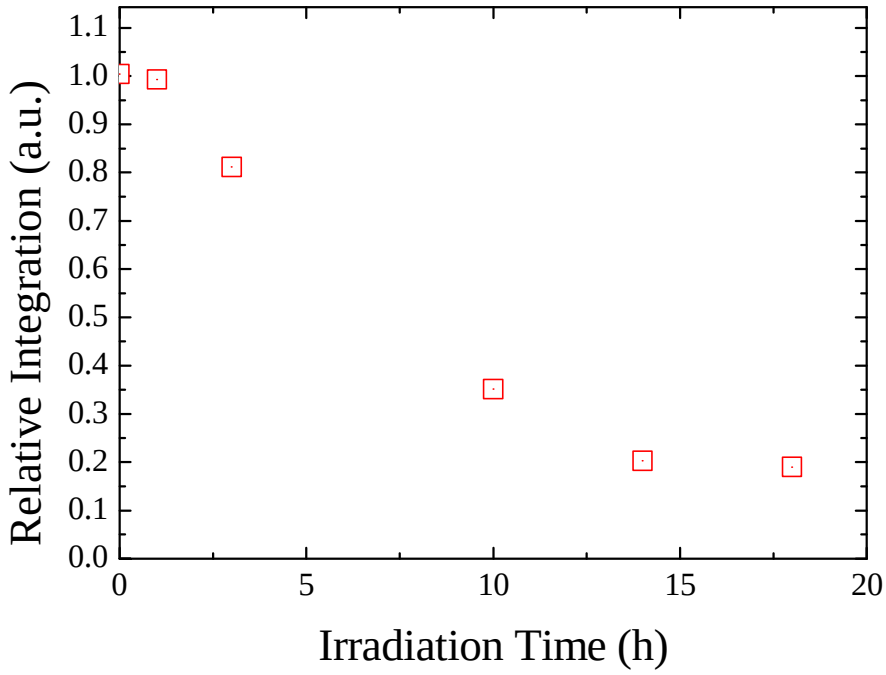

Figure 6.14. Integration of the peaks corresponding to the aromatic proton signals from the VBT and the styrene moieties of the polymer at δ = 6.5 – 7.5 ppm, using TMS-PSA methyl protons (δ = 0 ppm) as the reference, as a function of irradiation time.

Although these results do not conclusively show the cross-linking of the nanogels *i.e.*, *via* the appearance of the cyclobutane signals and the disappearance of the thymine signals, the fact that all the polymer signals disappear with irradiation time suggest that its solvation has changed, therefore it can be inferred that successful cross-linking of the polymer has taken place.[24]

6.3.1.2. *N*-isopropylacrylamide-based nanogels for UV-induced cross-linking

In addition to styrene-based nanogels, the potential use of VBT as a cross-linker in hydrophilic nanogels was also deemed interesting. Unlike hydrophobic nanogels, changing the cross-linking density of hydrophilic nanogels would have a greater impact on their size, as the amount of swelling is directly affected.[25] While hydrophilic styrenic

monomers (such as 4-styrenesulfonic acid) can be easily obtained, their ability to polymerize under emulsion polymerization conditions is not possible because of the requirement of the technique that the polymer is not soluble in the aqueous medium. Therefore, the use of *N*-isopropylacrylamide (NIPAM) as the monomer that would allow the direct synthesis of a hydrophilic nanogel was suggested, as discussed in Chapter 5. Because of the hydrophilicity of poly(NIPAM) at room temperature, a small amount of permanent cross-linker (*N*-*N*'-methylenebis(acrylamide), NMBA) was also used in all polymerizations, to prevent the dissolution of the polymer and thus the deformation of the nanoparticles (Figure 6.15).

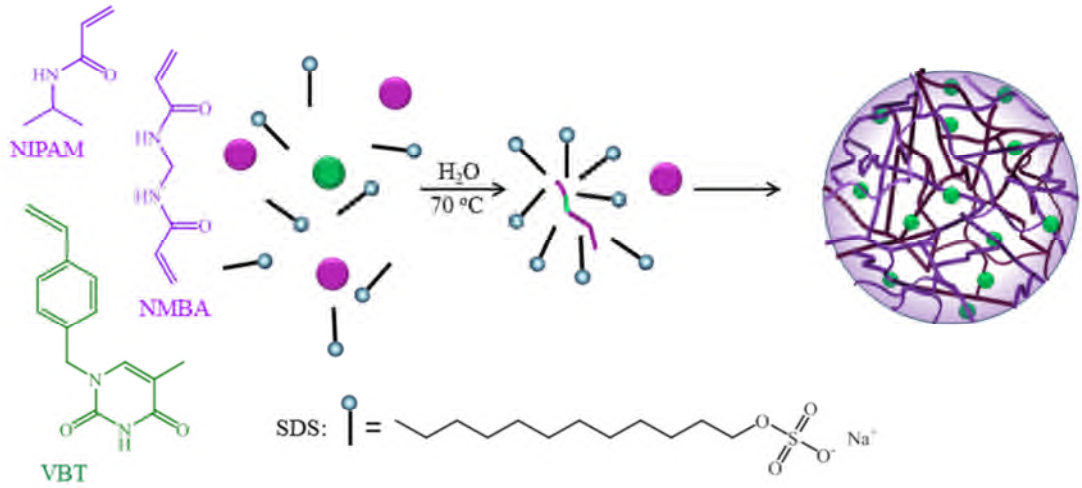

Figure 6.15. Schematic representation of the synthesis of the NIPAM-based VBT-loaded nanogels, in the presence of a permanent cross-linker, NMBA.

In order to confirm that copolymerization of NIPAM and VBT is possible under emulsion polymerization conditions, the two were initially copolymerized without the permanent cross-linker and the resulting polymer was studied by ^{1}H NMR spectroscopy (Figure 6.16 and Figure 6.17).

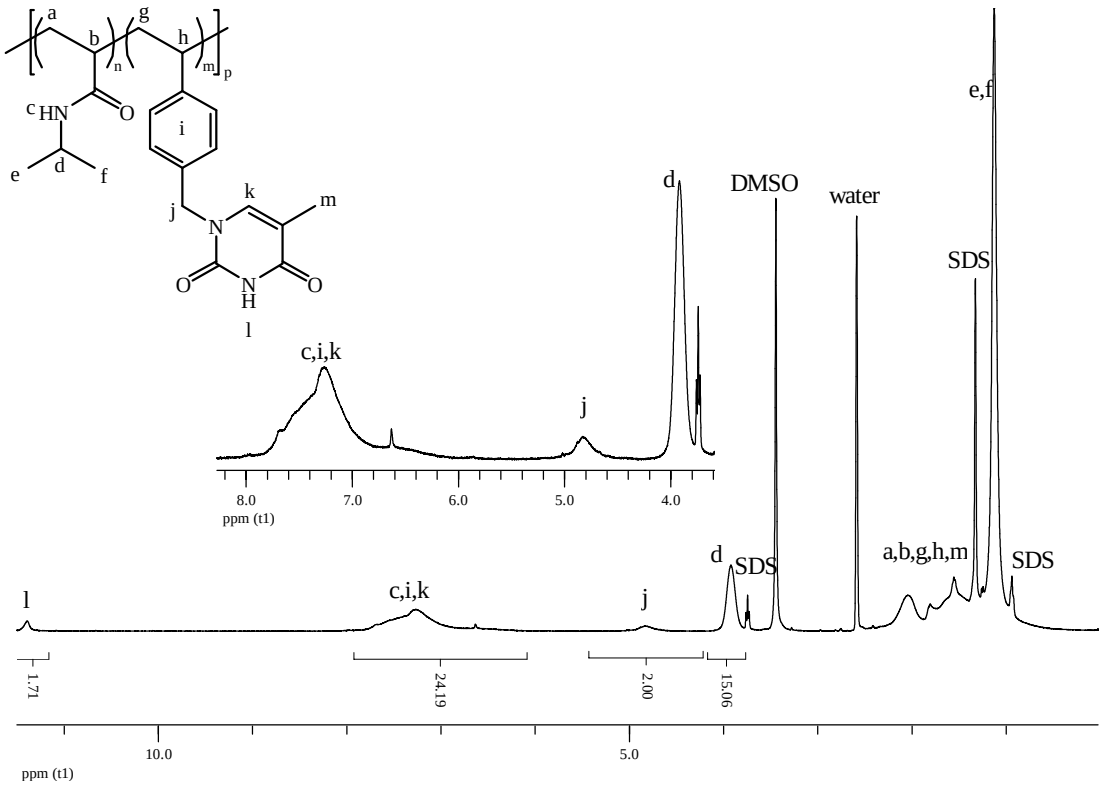

Figure 6.16. Assigned ^{1}H NMR spectrum of poly(NIPAM)-*co*-poly(VBT) synthesized by emulsion copolymerization and an expanded area of the spectrum showing the signals corresponding to the d and j protons of the VBT and NIPAM polymers, respectively ($(CD_3)_2SO$, 400 MHz).

The monomer feed was 20 wt% for VBT (1 eq.) and 80 wt% for NIPAM (8.56 eq.) however in the obtained ^{1}H NMR spectrum, the relative integration of the signals corresponding to the CH_2 protons of poly(VBT) (labeled "j") and the NCH proton of poly(NIPAM) (labeled "d") suggest that only half the amount of VBT was incorporated in the copolymer. Nevertheless, when comparing to the aromatic protons region (taking into account that the NIPAM amide signal also appears within that region), then the ratio between VBT and NIPAM in the copolymer suggests nearly complete incorporation for both monomers (1 eq. VBT and 8.25 eq. NIPAM). While the poor integration of the VBT CH_2 proton signals cannot be rationalized, further characterization by DOSY confirms the presence of the thymine moiety onto the copolymer (Figure 6.17).

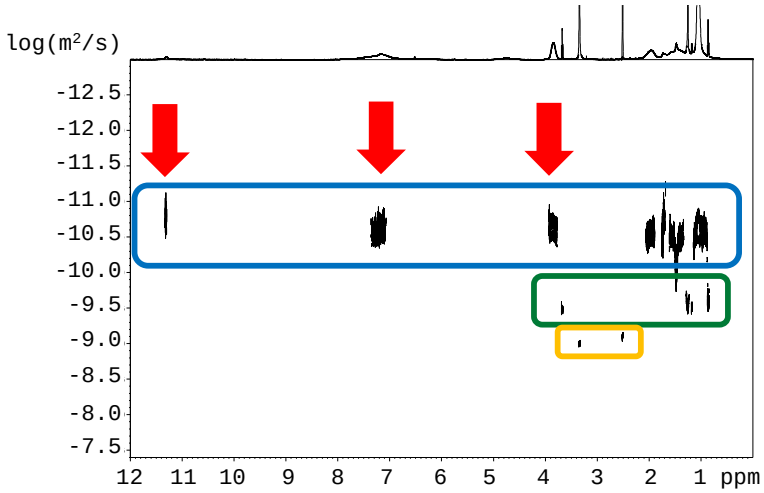

Figure 6.17. DOSY NMR spectrum of the poly(VBT)-*co*-poly(NIPAM) synthesized by emulsion polymerization (500 MHz, $(CD_3)_2SO$). The polymer (blue rectangle), the solvent (yellow rectangle), and the surfactant (green rectangle) are highlighted, as well as the signals that correspond solely to the VBT moiety (red arrows).

Signals corresponding to the VBT and the NIPAM protons were found to correspond to species with the same diffusion (2.5×10^{-11} m^2 /s) further confirming the VBT and NIPAM can be copolymerized *via* emulsion polymerization. The additional signals observed at faster diffusions correspond to the excess SDS (2.5×10^{-10} m^2/s) and the solvent (8.9×10^{-10} m^2/s). Therefore, it can be assumed that nanogels synthesized from the two co-monomers in the presence of a cross-linker will contain both species.

In a similar approach to that pursued for the hydrophobic nanogels, hydrophilic nanogels with different loadings of VBT were synthesized, with the VBT monomer feeding ratio being 2, 10, 20, and 30 wt%, while keeping the CLD constant to 0.5 wt%, thus resulting in nanogels **N6.NT2**, **N6.NT10**, **N6.NT20**, and **N6.NT30** respectively.[†] The hydrodynamic sizes of the particles were determined by DLS in water (Figure 6.18).

[†] The naming of the nanogels follows the generic format: **N6.NT**(VBT loading) whereby N denotes the copolymerization with NIPAM and T stands for thymine.

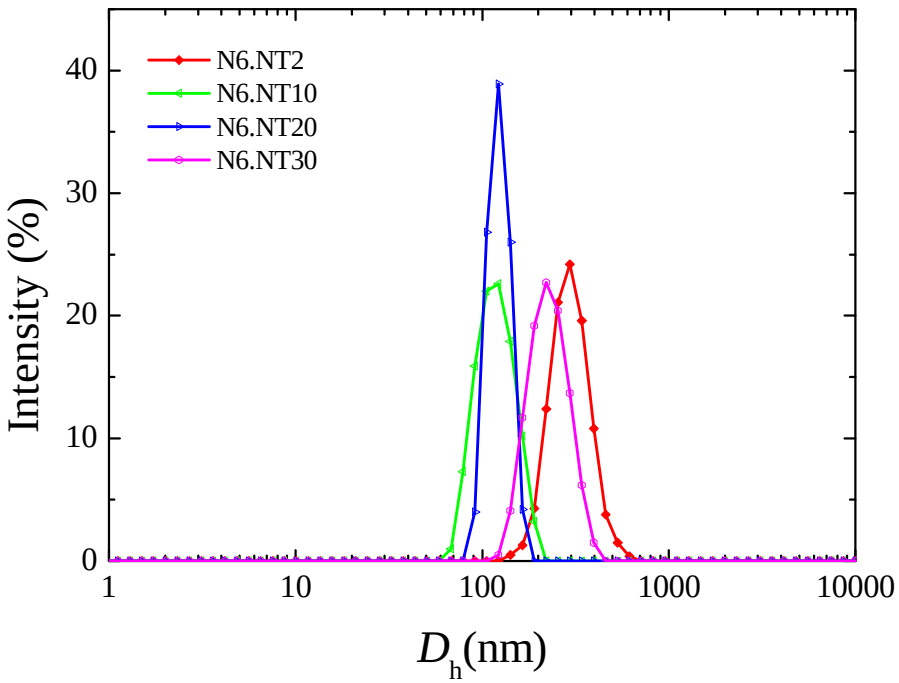

Figure 6.18. Size distributions of VBT-containing NIPAM-based nanogels, measured by DLS in water at 25 ºC.

The distributions obtained from all nanogels were found to be unimodal, suggesting uniform sized particles. However, it is apparent that the sizes of the nanogels with different VBT loadings are significantly different (Figure 6.19).

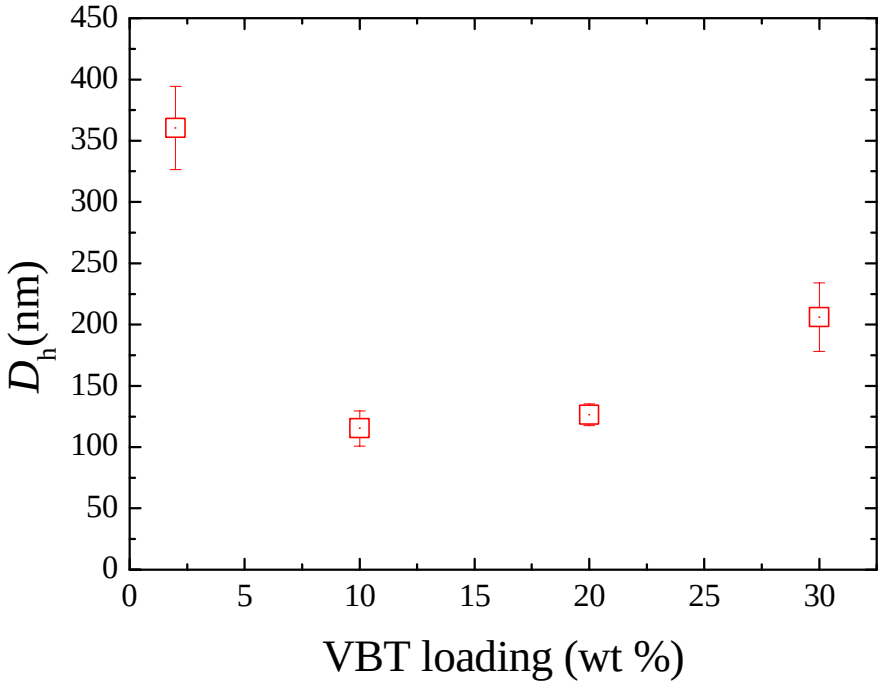

Figure 6.19. Hydrodynamic diameters of the VBT-containing NIPAM-based nanogels determined by DLS in water at 25 ºC. Error bars indicate size dispersity.

The low loading nanogels **N6.NT2** were found to have a hydrodynamic diameter of 360 nm, while at 10 wt% loading the **N6.NT10** nanogels had a hydrodynamic diameter of 115 nm. Further increase of the VBT loading results in an increase of the size of the nanogels, whereby the hydrodynamic diameter of **N6.NT20** was found to be 122 nm and that of the **N6.NT30** nanogels 209 nm. This significant distribution of sizes could be attributed to slight variations in the synthetic procedures (such as stirring rate) resulting in differences in the nucleation process during the synthesis of the nanogels. While it is apparent that optimization of the synthetic procedure in order to standardize the size of the obtained particles is necessary, for the purpose of this study, the nanogels are only compared in terms of their relative sizes. Additionally, the morphology of the **N6.NT10** and the **N6.NT30** nanogels was examined by TEM (Figure 6.20).

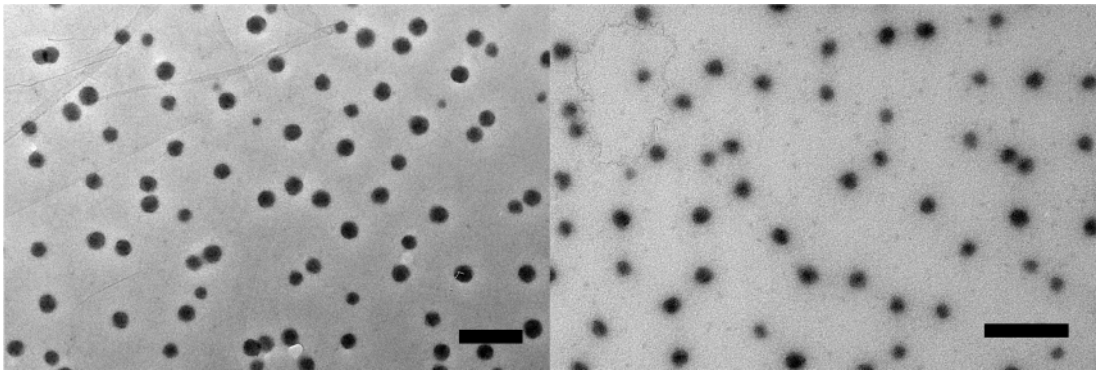

Figure 6.20. TEM images of the **N6.NT10** (left) and the **N6.NT30** (right) nanogels (Graphene oxide grid, scale bars: 200 nm)

In both cases, the particles observed are of spherical shape while the overall size distribution is narrow (Figure 6.21).

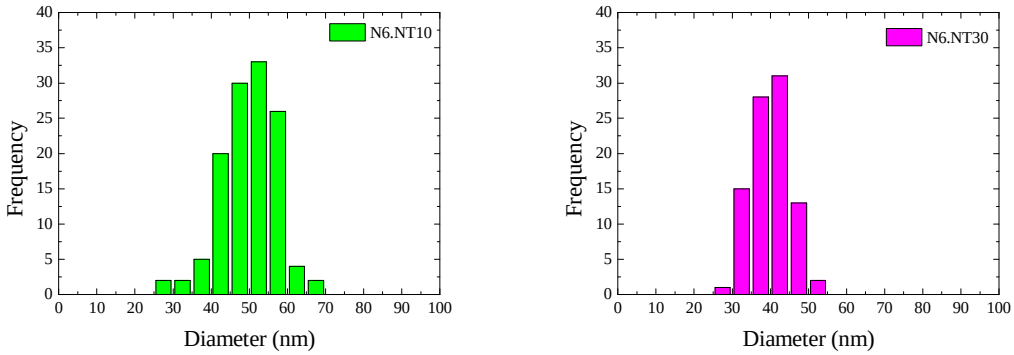

Figure 6.21. Size histograms from the **N6.NT10** and **N6.NT30** particles measured by TEM.

The TEM results further confirm the observation by DLS that the dispersity of the sizes of the particles are narrow, although it should be taken into account that with TEM the particles are in their dry collapsed state. This also explains the deviation in the measured sizes by the two techniques.

The particles were then characterized by UV-vis spectroscopy in order to observe the characteristic thymine absorbance at *ca.* 270 nm. Apart from the **N6.NT0** nanogels that

do not contain thymine, all VBT-containing nanogels were found to absorb at 270-275 nm (Figure 6.23).

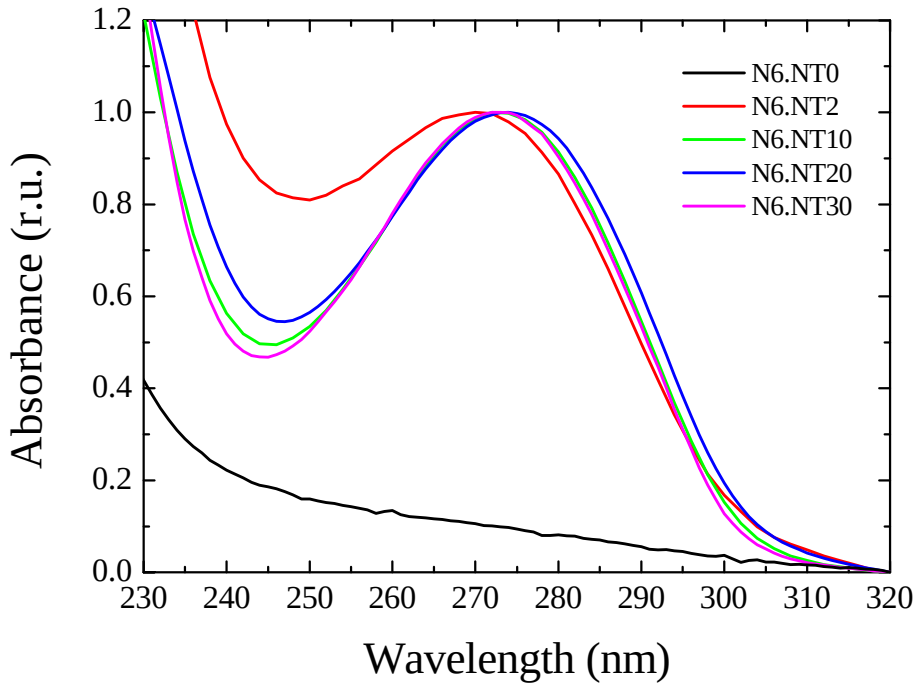

Figure 6.22. Normalized absorption spectra of **N6.NT0** poly(NIPAM)-*co*-poly(NMBA) nanogels and the VBT-containing hydrophilic nanogels **N6.NT2**, **N6.NT10**, **N6.NT20**, and **N6.NT30** in water.

The absorption of the **N6.NT0** nanogels within the studied wavelength range is weak, however it shows that there is a contribution from the nanogels themselves to the spectra obtained for the nanogels containing VBT. This contribution becomes less significant when the VBT content is high, and the absorption peaks for the **N6.NT10**, **N6.NT20**, and **N6.NT30** nanogels are similar.

The nanogels were irradiated at room temperature using the same method used for the styrene-based nanogels and the disappearance of the aforementioned characteristic thymine absorption peak was monitored by UV-vis spectroscopy (Figure 6.23). Note that each measured sample was named after its parent nanogel and the duration of the

irradiation in hours (*i.e.*, **N6.NT10-15** for the **N6.NT10** nanogels after irradiation for 15 hours).

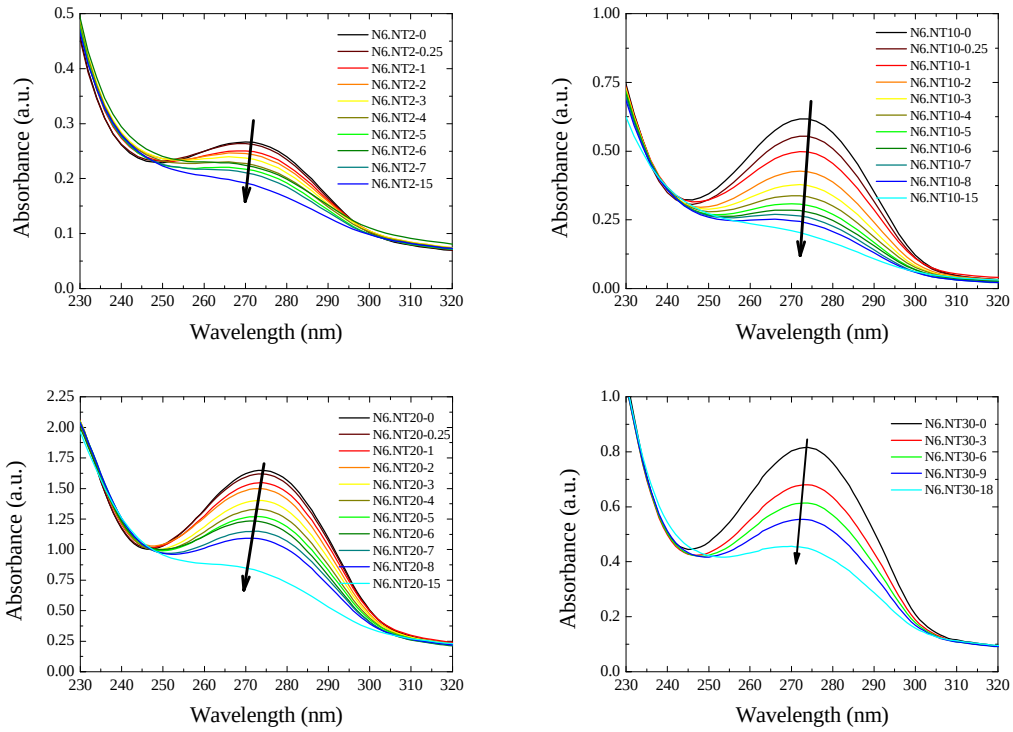

Figure 6.23. Absorption spectra for the VBT-containing hydrophilic nanogels upon irradiation.

Unlike in the case of the styrene-based nanogels, even at low thymine loadings, the **N6.NT2** nanogels show a decrease in the absorption at the 270-275 nm range, with the maxima of the absorption peaks shifting to shorter wavelengths. Similar results are observed for all irradiated samples, suggesting that the thymine moieties successfully form dimers. As previously mentioned, the increase in the cross-linking density of the hydrophilic NIPAM-based nanogels is expected to affect their size, as less water is expected to be able to swell the particles. In order to evaluate this, the size of the particles with respect to their irradiation time was determined by DLS (Figure 6.24).

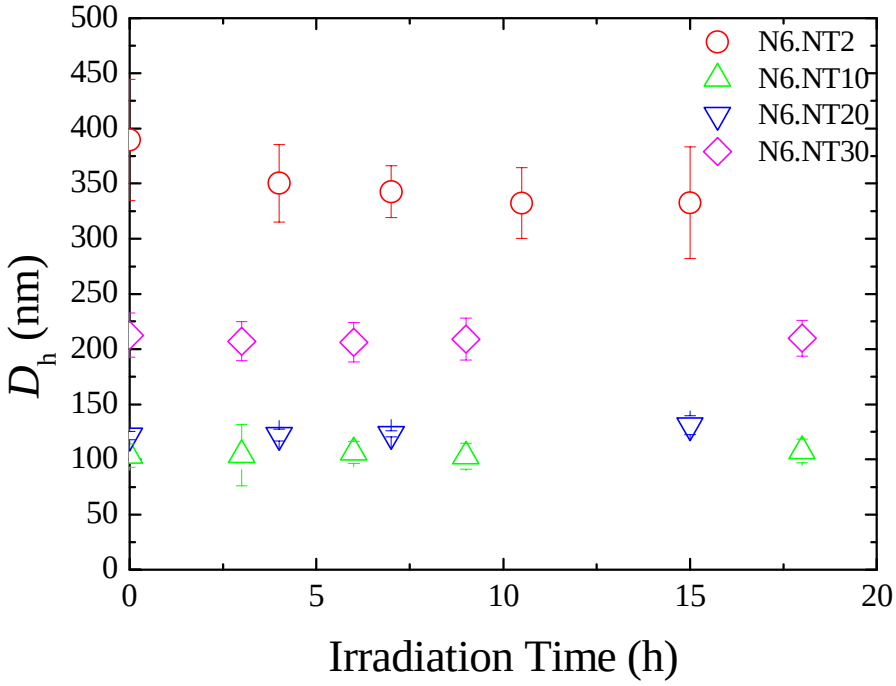

Figure 6.24. Hydrodynamic diameters of the NIPAM-based VBT-containing nanogels at different irradiation times, determined by DLS in water at 25 ºC. Lines correspond to best linear fit for each sample set of measurements. Error bars indicate size dispersity.

With the exception of **N6.NT2**, irradiation of the nanogels was not found to affect the size of the hydrophilic nanogels. While the hydrodynamic diameter of **N6.NT2** slightly decreases suggesting that irradiation, and thus increasing of the cross-linking density, results in the shrinking of the nanogels, this is not the case for **N6.NT10**, **N6.NT20**, and **N6.NT30** for which the size of the nanogels does not change with irradiation. To further investigate the effect of irradiation on the hydrophilic nanogels, the size distributions obtained by DLS were also examined, before and after irradiation (Figure 6.25).

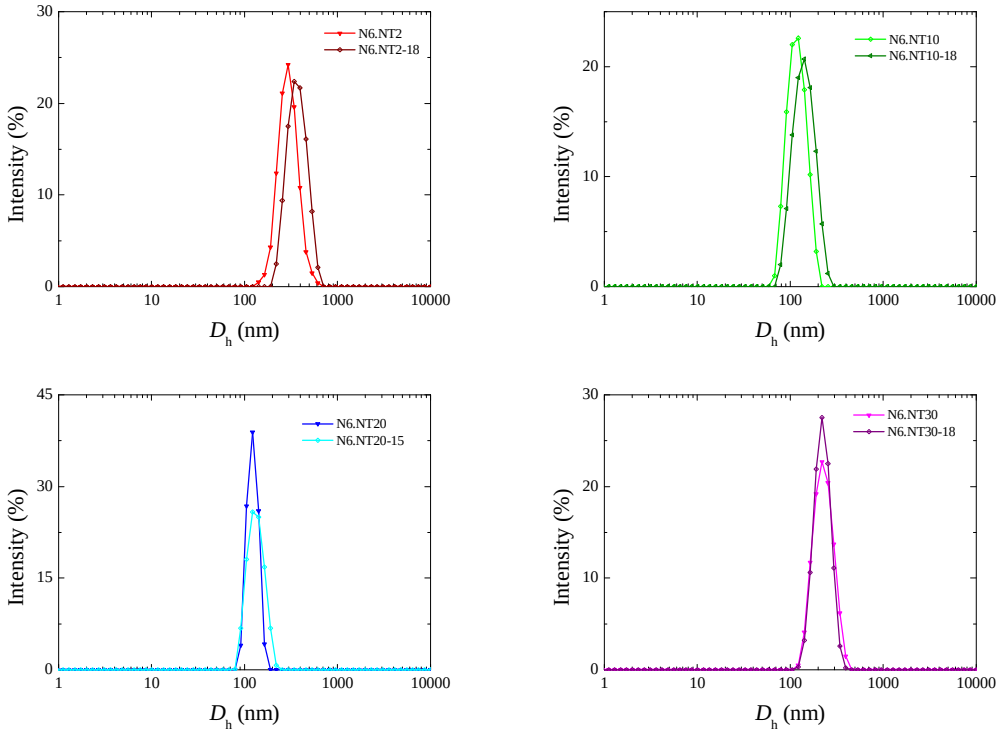

Figure 6.25. Size distributions of the hydrophilic nanogels with different VBT loadings, before and after, irradiation, determined by DLS in water at 25 ºC.

Comparison of the size distributions, in all cases, before and after irradiation shows no significant changes in the size of the particles, while no aggregation is observed. To confirm that the morphology of the particles had not been altered with irradiation, **N6.NT10-18** and **N6.NT30-18** were observed by TEM (Figure 6.26).

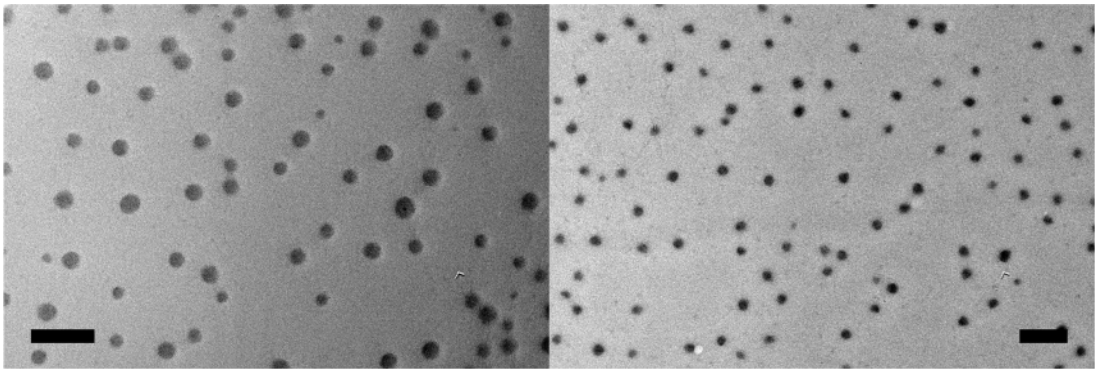

Figure 6.26. TEM images of the **N6.NT10-18** (left) and the **N6.NT30-18** (right) nanogels showing the morphology of the nanogels after irradiation. (Graphene oxide grids, scale bars: 200 nm)

The images obtained by TEM for the **N6.NT10-18** as well as the **N6.NT30-18** nanogels, both show spherical particles with relatively uniform sizes. This is consistent with the observation of the nanogels before irradiation, further suggesting that the morphology of the particles is not affected by irradiation.

Other than the decrease in the UV absorption of the nanogels, no significant change was observed from irradiation-induced dimerization of the thymine moieties. This was further confirmed by investigation of the temperature-induced size change of the nanogels by DLS measurements in water.

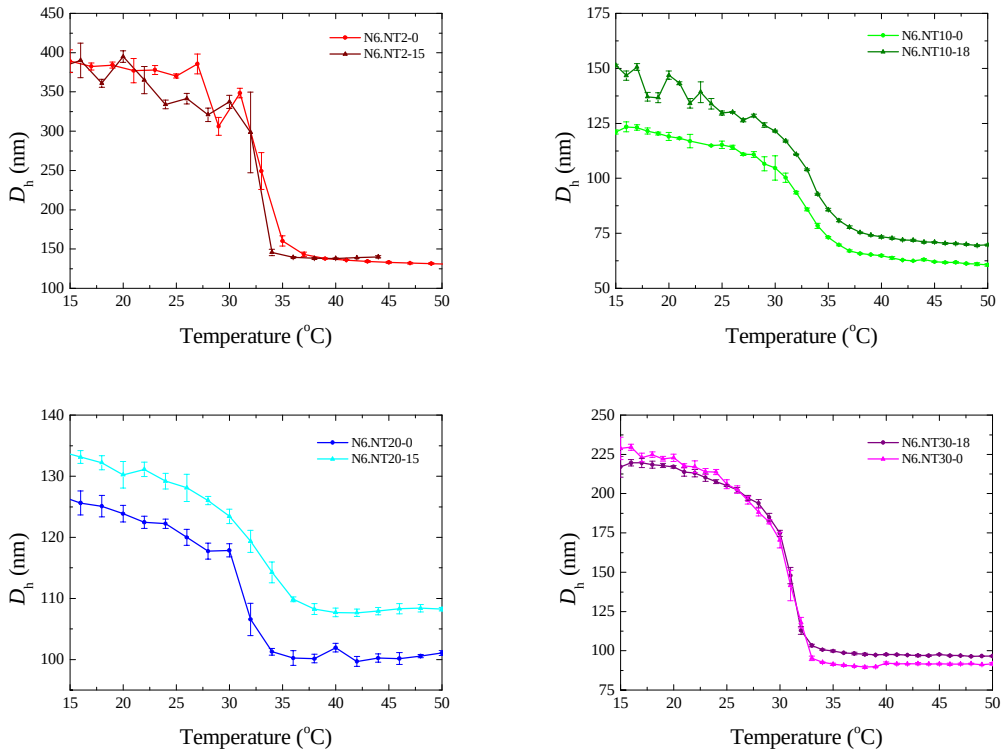

Figure 6.27. Hydrodynamic diameters of the NIPAM-based nanogels with respect to the solution temperature, measured before and after irradiation.

All nanogel dispersion were found to exhibit a transition temperature above which the particles size decreases, indicating the hydrophilic-to-hydrophobic transition of poly(NIPAM). This temperature, determined by the minima of the 1st order derivatives

of the graphs, was not found to change after irradiation of the particles and was for all samples between 31 and 33.5 ºC (Table 6.1).

Table 6.1. Transition temperatures for the NIPAM-based nanogels, before and after irradiation.

	before	after
N6.NT2	33 ºC	32.5 ºC
N6.NT10	33 ºC	33.5 ºC
N6.NT20	32 ºC	32.5 ºC
N6.NT30	31 ºC	31 ºC

Additionally, the size of the nanogels before and after irradiation was similar at elevated temperatures. These results further indicate that the properties of the nanogels are not affected by irradiation.

While in the case of the styrene-based nanogels, the successful cross-linking of the particles upon irradiation is based on the loss of the characteristic UV absorption of thymine and the gradual loss of ^{1}H NMR signals, in the case of NIPAM-based nanogels only the UV spectra provide any indication that cross-linking may have taken place. It was therefore suggested that segregation of the monomers within the particles may have resulted in thymine dimerization only taking place between close neighboring moieties (Figure 6.28-B).

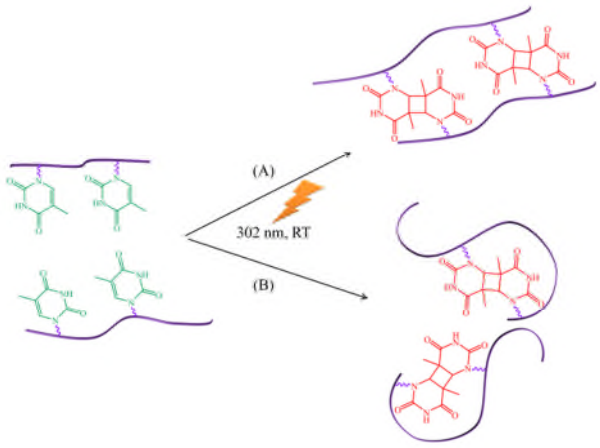

Figure 6.28. Schematic representation of the dimerization of thymine moieties present on different polymer chains within the nanogels resulting in increase of the CLD (A) and thymine moieties present on the same polymer chain not affecting the CLD (B), as a result of irradiation

This could be attributed to the high solvation of the nanogels at physiological conditions that prevents the close proximity of the thymine moieties, and therefore effectively prevents the increase of the cross-linking density of the nanogels. On the other hand, in the case of the hydrophobic styrene-based nanogels, the collapsed state of the polymer chains allows the thymine moieties to be found at close proximity, and thus dimerization to take place upon irradiation, subsequently effective cross-linking of the polymer chains.

It is proposed that cross-linking of poly(NIPAM)-*co*-poly(VBT) can take place when the polymers are in their collapsed state, such as at elevated temperatures, or in bulk. Preliminary tests to evaluate this hypothesis were conducted, whereby a linear poly(NIPAM)-*co*-poly(VBT) was synthesized *via* free radical polymerization (**G6.NT10**) and a film was formed onto a glass slide. Part of the film was masked with letters cut out from cardboard paper (Figure 6.29-A) and the slide was irradiated for 6 hours. Then, the film was rinsed with methanol to remove linear polymer chains resulting in the formation of the pattern seen in Figure 6.29-B.

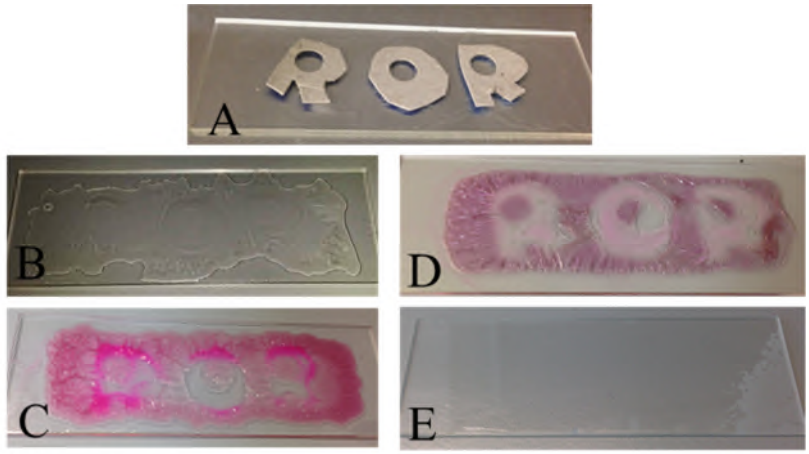

Figure 6.29. Digital photographs of the experimental setup for the patterned cross-linking of the polymer films (A), the **G6.NT10** gel after washing (B), the **G6.NT10-R** gel after washing (C), gel **G6.ST10-R** after washing (D), and **G6.NT0** after washing (E).

The obtained pattern was identical to that used to mask the polymer film, whereby the masked areas of the film were removed with rinsing, suggesting that no cross-linking had taken place, while the areas exposed to the UV light remained on the slide indicating that cross-linking had taken place, attributed to the successful dimerization of thymine. To enhance the ability to observe the resulting pattern, the experiment was repeated with the polymer being first stirred with rhodamine B before the formation of the film (**G6.NT10-R**) on the glass slide. While after rinsing with methanol to remove the residual linear polymer the same pattern is observed (Figure 6.29-C), unfortunately rhodamine B was also rinsed off, while some leaking of the dye into the voids is also observed. This preliminary result demonstrates the ability of a linear poly(NIPAM)-*co*-poly(VBT) to form macroscopic gels, as a result of irradiation successfully promoting the dimerization of the thymine moieties. As a control experiment, a linear poly(NIPAM) was synthesized using the same conditions but without adding VBT. The polymer film (**G6.NT0**) was also irradiated and upon rinsing all of the material was

removed from the surface of the glass slide, while no insoluble aggregates were visible in the solution, thus confirming that no cross-linking has taken place in the absence of VBT. Additionally, the same procedure was followed for the formation of a poly(styrene)-*co*-poly(VBT) film (also dyed with rhodamine B) (**G6.ST10**). After irradiation the linear polymer chains were removed *via* rinsing with dichloromethane, and the resulting pattern suggested that cross-linking had only taken place in the areas exposed to the UV light.

The preliminary results from the macroscopic formation of gels *via* irradiation of VBT-containing polymers support the hypothesis that the cross-linking of NIPAM-based nanogels could also take place if the polymer is less hydrated, as the polymer films were successfully cross-linked in their dry state. As a consequence, in two separate experiments the **N6.NT30** nanogels were dried and used to form a film, while in the second scenario they were heated to 30 ºC, thus reducing the amount of water in the nanogels. Both samples were subsequently irradiated without the use of a mask. For the film formed by the **N6.NT30** nanogels, when placing part of it in methanol, the immersed area was swollen, nevertheless without being removed from the slide (Figure 6.30), suggesting that inter-particle cross-linking has taken place. Similarly, despite being in an aqueous solution, **N6.NT30** nanogels at a temperature where the particles are not fully hydrated, subsequently bringing the thymine moieties to proximity, the formation of an insoluble gel was observed (Figure 6.30). This highlights that cross-linking *via* irradiation for NIPAM-based VBT-functional nanogels is possible, but optimization of the conditions, whereby the hydration of the polymer is tuned needs to be considered in order to prevent inter-particle cross-linking, such as in this demonstration.

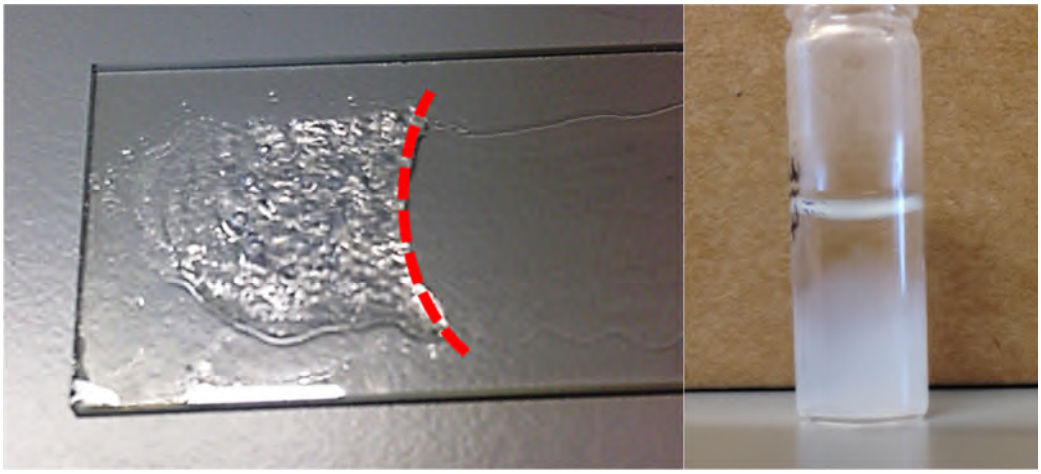

Figure 6.30. Digital photograph of the **N6.NT30** nanogel film exposed to UV irradiation (left, dotted line shows interface between dry film and swollen by immersion in methanol), and a dispersion of **N6.NT30** nanogels irradiated at elevated temperatures resulting in an insoluble gel (right).

6.4. Conclusions

In order to obtain a system where the cross-linking density can be tuned post-polymerization, in a potentially reversible manner, a thymine-containing monomer was used for the synthesis of hydrophobic nanogels. The ability of the thymine moieties to dimerize upon irradiation with UV light was shown for hydrophobic styrene-based nanogels. When the thymine-functional monomer was co-polymerized with NIPAM to form hydrophilic nanogels, irradiation with UV light did not show cross-linking of the particles, despite of the indicated dimerization of thymine. It was hypothesized that as a result of the hydration of the particles, dimerization had only taken place amongst neighboring thymine moieties, thus not altering the cross-linking density of the nanogels. To further assess the possibility to cross-link thymine-containing poly(NIPAM), a linear copolymer was synthesized and used to form a film that was exposed to UV irradiation. The subsequent cross-linking was demonstrated by the inability of the film to dissolve, unlike its non-irradiated analogues. Consequently, it is

proposed that thymine-containing monomers can be used as UV-responsive cross-linking agents in polymeric nanoparticles, while the hydration of the particles can affect the efficiency of the cross-linking.

6.5. Materials and Methods

Unless otherwise stated, all reagents were purchased from Sigma-Aldrich and used without further purification. Solvents were purchased from Fisher Scientific and used as received. Water was purified using an ion exchange cartridge (18.2 MΩ·cm). SpectraPor dialysis tubing was purchased from Spectrum Labs, with a molecular weight cut-off of 10 kDa.

Nuclear magnetic resonance (^{1}H and ^{13}C NMR) spectra were recorded in $CDCl_3$, C_3D_7NO, CD_3OD, or $(CD_3)_2SO$ solutions on a Bruker AC-250, a Bruker DPX-300, a Bruker AV-400 or a Bruker DPX- 400, a DRX-500, and a Bruker AV II-700 spectrometer. Chemical shifts are reported as δ in parts per million (ppm) and referenced to the chemical shift of the residual solvent resonances and/or internal standards (TMS ^{1}H: δ = 0.00 ppm; ^{13}C: δ = 0.00 ppm). High resolution mass spectra (HRMS) were collected using a Bruker MaXis UHR-ESI TOF. Dynamic light scattering (DLS) measurements were conducted on a Malvern Zetasizer Nano ZS instrument equipped with a 4 mW He-Ne 633 nm laser module and a detector at 173º. When required, the temperature of the solution was altered using the software built-in temperature scan mode, set to allow equilibration at each temperature interval for 60 s. All data were analyzed using Malvern DTS 6.32 software. TEM samples were prepared by drop deposition of an aqueous solution (unless otherwise stated) onto a copper/carbon grid coated with Formvar or graphene oxide sheets. The droplet was allowed to stand for one minute before excess liquid was blotted off. Images were obtained on a JEOL 2000FX

transmission electron microscope operating at 200 kV and analyzed using ImageJ software. UV-vis spectroscopy was carried out on a Perkin Elmer Lambda 35 UV/vis spectrometer using quartz cuvettes transparent above 230 nm. The spectra were corrected for background and solvent absorbance. For the UV irradiation of the samples a UPV-1000 crosslinker chamber, equipped with 5 x 8 watt UV dual bipin discharge type tubes that emit within the midrange of the UV spectrum with the maximum intensity at 302 nm was used.

6.5.1.1. Synthesis of 1-(vinylbenzyl)thymine (VBT)

A slightly modified procedure to the literature was followed for the synthesis of VBT.[9] KOH (10 g, 178 mmol, 1.12 eq.) was dissolved in H_2O (100 mL) followed by the addition of thymine (20 g, 159 mmol, 1 eq.). Upon complete dissolution of the solids, ethanol (200 mL) was added followed by a catalytic amount of *p*-methoxy phenol (0.1 g, 0.8 mmol, 0.005 eq.) and the drop-wise addition of vinyl benzyl chloride (24.3 g, 159 mmol, 1 eq.). The reaction was stirred under reflux for 15 hours before cooling. The solids were removed by filtration and the volatiles were removed under reduced pressure. The product was isolated after hot filtration with toluene and recrystallization from hexane, as a white powder (23 g, 50 % isolated yield). ^{1}H NMR ($(CD_3)_2SO$, 400 MHz) δ = 9.0 (1H, broad, NH), 7.41 (2H, d, ^3J = 8.2 Hz, Ar), 7.26 (2H, ^3J = 8.1 Hz, Ar), 6.97 (1H, app q, ^3J = 1.2 Hz, -N-CH), 6.70 (1H, ^3J = 10.9 Hz, ^3J = 17.6 Hz, vinyl), 5.57 (1H, d, ^3J = 17.6 Hz, ^2J = 0.5 Hz, vinyl), 5.27 (1H, dd, ^3J = 10.9 Hz, ^2J = 0.5 Hz, vinyl), 4.88 (2H, s, CH_2), 1.88 (3H, app d, ^3J = 1.2 Hz, CH_3); ^{13}C NMR ($(CD_3)_2SO$, 75 MHz) δ = 164.2, 151.0, 141.2, 136.3, 136.1, 127.7, 126.4, 114.5, 109.0, 49.8, 11.9; HRMS *m/z*: expected: 265.0953, found: 265.0947 $[M+Na]^+$.

6.5.1.2. Synthesis of the thymine-containing styrene-based nanogels

For a typical nanogel synthesis VBT and styrene (see Table 6.2 for quantities) were dissolved in chloroform (500 μL) and slowly added to a stirring solution of SDS (125 mg, 0.433 mmol) in water (50 mL). Then, KPS (5 mg, 0.018 mmol) was added and the reaction mixture was degassed *via* nitrogen bubbling for 5 minutes before being immersed in an oil bath at 70 ºC where the polymerization was allowed to proceed for 15 hours. The resulting nanogels were subsequently purified by dialysis against water.

Table 6.2. Reagents and quantities used for the synthesis of the styrene-based thymine containing nanogels.

	Hydrophobic monomer			VBT		DoF (wt%)
N6.ST2	styrene	487.2 mg	4.678 mmol	10 mg	0.041 mmol	2
N6.ST10	styrene	450 mg	4.321 mmol	50 mg	0.206 mmol	10
N6.ST20	styrene	400 mg	3.841 mmol	100 mg	0.413 mmol	20
N6.ST30	styrene	350 mg	3.361 mmol	150 mg	0.619 mmol	30

6.5.1.3. Synthesis of the thymine-containing NIPAM-based nanogels

For a typical nanogel synthesis VBT, NIPAM, and NMBA (see Table 6.3 for quantities) were dissolved in methanol (500 μL) and slowly added to a stirring solution of SDS (125 mg, 0.433 mmol) in water (50 mL). Then, KPS (5 mg, 0.018 mmol) was added and the reaction mixture was degassed *via* nitrogen bubbling for 5 minutes before being immersed in an oil bath at 70 ºC where the polymerization was allowed to proceed for 15 hours. The resulting nanogels were subsequently purified by dialysis against water.

Table 6.3. Reagents and quantities used for the synthesis of the NIPAM-based thymine containing nanogels.

	NIPAM	NMBA	VBT		DoF (wt%)
N6.NT2	487.5 mg 4.305 mmol	2.5 mg 0.016 mmol	10 mg	0.041 mmol	2
N6.NT10	447.5 mg 3.955 mmol	2.5 mg 0.016 mmol	50 mg	0.206 mmol	10
N6.NT20	397.5 mg 3.508 mmol	2.5 mg 0.016 mmol	100 mg	0.413 mmol	20
N6.NT30	347.5 mg 3.066 mmol	2.5 mg 0.016 mmol	150 mg	0.619 mmol	30

6.5.1.4. Dimerization of thymine *via* UV irradiation

In a typical irradiation of the nanogels, the dispersion (approximate concentration 10 $mg{\cdot}mL^{-1}$) was placed in a UV-transparent quartz cuvette and placed in the middle of the UV chamber with the transparent side facing towards the light source. For the study of the irradiation evolution, small aliquots (*ca.* 1 mL) were removed from the dispersion at different time intervals and stored for subsequent characterization without further purification.

For the irradiation of solid samples, first a solution of the sample (in CH_2Cl_2 for styrene-based materials and methanol for all other) was prepared (ca. 500 $mg{\cdot}mL^{-1}$) - when required rhodamine B (0.1 $mg{\cdot}mL^{-1}$) was also introduced in the solution - and placed on a glass slide before the solvent was removed under reduced pressure at 40 ºC. The letters "R", "O", and "R" were cut out of a 1 mm thick cardboard sheet and placed without the use of adhesive onto the formed film. The glass slide was then placed in the middle of the UV chamber with the sample side facing towards the light source. After completion of the irradiation, the slide was thoroughly rinsed with solvent (CH_2Cl_2 for styrene-based materials and methanol for all other) and allowed to dry at room temperature.

6.5.1.5. Synthesis of VBT copolymers *via* free-radical polymerization

For a typical free-radical polymerization, the monomer (450 mg of styrene or NIPAM), VBT (50 mg), and the radical initiator AIBN (5 mg) were dissolved in DMSO (5 mL) and degassed *via* nitrogen bubbling. The reaction mixture was stirred under a nitrogen blanket for 5 hours at 70 ºC and the polymer was isolated by precipitation in 10-fold excess of non-solvent (methanol for styrene-based polymers, hexane for NIPAM-based polymers) and subsequent drying under reduced pressure.

6.6. References

1. G. M. Blackburn and R. J. H. Davies, *J. Chem. Soc. C*, 1966, 2239-2244.
2. W. J. Schreier, T. E. Schrader, F. O. Koller, P. Gilch, C. E. Crespo-Hernández, V. N. Swaminathan, T. Carell, W. Zinth and B. Kohler, *Science*, 2007, **315**, 625-629.
3. B. Durbeej and L. A. Eriksson, *J. Photochem. Photobiol. A*, 2002, **152**, 95-101.
4. P. Johnston, M. T. Hearn and K. Saito, *Aust. J. Chem.*, 2010, **63**, 631-639.
5. T. Carell and R. Epple, *Eur. J. Org. Chem.*, 1998, **1998**, 1245-1258.
6. Y. Inaki, Y. Wang, M. Kubo and K. Takemoto, *J. Photopolym. Sci. Technol.*, 1991, **4**, 259-266.
7. P. Johnston, C. Braybrook and K. Saito, *Chem. Sci.*, 2012, **3**, 2301-2306.
8. Y. Dahman, J. E. Puskas, A. Margaritis, Z. Merali and M. Cunningham, *Macromolecules*, 2003, **36**, 2198-2205.
9. C. M. Cheng, M. I. Egbe, J. M. Grasshoff, D. J. Guarrera, R. P. Pai, J. C. Warner and L. D. Taylor, *J. Polym. Sci. Part A: Polym. Chem.*, 1995, **33**, 2515-2519.
10. C. Kiarie, J. Bianchini, S. Trakhtenberg and J. C. Warner, *J. Macromol. Sci., Part A: Pure Appl. Chem.*, 2005, **42**, 1489-1496.
11. S. Trakhtenberg, Y. Hangun-Balkir, J. C. Warner, F. F. Bruno, J. Kumar, R. Nagarajan and L. A. Samuelson, *J. Am. Chem. Soc.*, 2005, **127**, 9100-9104.
12. S. Trakhtenberg, J. C. Warner, R. Nagarajan, F. F. Bruno, L. A. Samuelson and J. Kumar, *Chem. Mater.*, 2006, **18**, 2873-2878.

13. J. R. Bianchini, K. Saito, T. B. Balin, V. Dua and J. C. Warner, *J. Polym. Sci. Part A: Polym. Chem.*, 2007, **45**, 1296-1303.
14. A. L. Barbarini, D. A. Estenoz and D. M. Martino, *Macromol. React. Eng.*, 2010, **4**, 453-459.
15. A. L. Barbarini, D. L. Reyna and D. M. Martino, *Green Chem. Lett. Rev.*, 2010, **3**, 231-237.
16. K. Saito, L. R. Ingalls, J. Lee and J. C. Warner, *Chem. Commun.*, 2007, 2503-2505.
17. G. Kaur, M. T. Hearn, T. D. M. Bell and K. Saito, *Aust. J. Chem.*, 2013, **66**, 952-958.
18. K. Saito and J. C. Warner, *Green Chem. Lett. Rev.*, 2009, **2**, 71-76.
19. G. Kaur, S. L. Y. Chang, T. D. M. Bell, M. T. W. Hearn and K. Saito, *J. Polym. Sci. Part A: Polym. Chem.*, 2011, **49**, 4121-4128.
20. P. Johnston, E. I. Izgorodina and K. Saito, *Photochem. Photobiol. Sci.*, 2012, **11**, 1938-1951.
21. P. Johnston, D. Wheldale, C. Braybrook and K. Saito, *Polym. Chem.*, 2014, **5**, 4375-4384.
22. G. Kaur, A. Bertrand, J. Bernard, T. D. M. Bell and K. Saito, *J. Polym. Sci. Part A: Polym. Chem.*, 2014, **52**, 2557-2561.
23. J.-F. Lutz, A. F. Thünemann and K. Rurack, *Macromolecules*, 2005, **38**, 8124-8126.
24. A. K. Whittaker, in *Annu. Rep. NMR Spectrosc.*, eds. G. A. Webb and I. Ando, Academic Press, 1997, vol. Volume 34, pp. 105-183.
25. B. R. Saunders and B. Vincent, *Adv. Colloid Interface Sci.*, 1999, **80**, 1-25.

7.1. Conclusions and future work

In this thesis three different themes towards developing new complex materials were demonstrated: sequence-controlled polymerizations, modification of the properties of a protein, and creating an enzyme mimic. All three concepts were motivated by the complex functions presented by natural enzymes that rely on their structure.

Initially, the use of norbornenes as building blocks for the synthesis of polymers with precise composition was explored. Based on the vast difference in reactivity of different norbornene isomers in ROMP, their copolymerization resulted in copolymers with a predictable location of each monomer on the polymer backbone. The rapid insertion of a functional monomer was found to show little dependence on the conversion of the slower monomer, thus allowing the synthesis of a multifunctional copolymer with a precise composition. Although the method showed moderate success when the relative concentration of the functional monomer was low, and was not efficient in the introduction of a single unit at a time, it represents a new opportunity for ROMP to be used towards the synthesis of sequence-controlled polymers. Polymers with greater precision could be obtained by combining other methods described in the literature, such as templated polymerization. It is anticipated that by designing the monomer pairs in a way that copolymerization is favored, greater precision in the monomer sequence can be obtained. Copolymers synthesized using the studied approach are currently under investigation for their use in biological applications. By incorporating a peptide-functional monomer at precise positions onto the polymer backbone, the interactions of the peptides are studied as a function of their distance. In a similar manner, hydrophilic monomers are being synthesized in an attempt to attach in precise locations saccharide groups and further investigate their binding properties onto selected proteins.

In Chapter 3, in an attempt to further examine the conditions that will allow single monomer insertion in ROMP the use of a cleavable monomer, dioxepin, was considered as it would permit locating the insertion point upon scission of the polymer backbone. However, it was found that under the examined conditions dioxepins do not readily undergo ROMP; instead they add a single monomer unit onto the polymer chain end. This insertion was not particularly efficient; nevertheless dioxepins were shown to assist with the synthesis of multiblock copolymers that could be degraded to a mixture of the individual blocks. A future consideration on this subject would be to examine different functional dioxepins and other seven-membered cyclic monomers, such as dithiepins, in order to elucidate the efficiency of their single monomer addition and optimize it.

In Chapter 4 the use of an engineered protein for the synthesis of a temperature-responsive bioconjugate was described. Different molecular weight polymers were conjugated at different positions onto the protein and the resulting temperature-related behavior was examined. Although subtly, the different conjugation positions were found to alter the coil-to-globule transition of the conjugated polymer upon increase of the temperature. At elevated temperatures the bioconjugates were not found to macroscopically precipitate, however the resulting amphiphiles were not found to form well-defined assemblies. This was ascribed to the heating rate not being optimized. While in this thesis the potential of such a system was demonstrated, it would highly benefit from the re-evaluation of the conjugation conditions. In order to increase the conjugation efficiency, the use of a more reactive alkyne in a copper-free cycloaddition is proposed in order to minimize the purification steps. Additionally, the conjugation of the introduced amino acid residues with the RAFT polymerization CTA followed by the "grafting from" polymerization of different monomers would be of interest, particularly for the double-modified protein as it would ensure minimization of steric shielding.

Furthermore, the incorporation of a RAFT polymerization CTA-functional amino acid would further minimize the steps required for the synthesis of a bioconjugate.

In Chapter 5 the simplicity of polymeric nanoreactors produced by emulsion polymerization instigated the evaluation of the synthetic parameters that determine the efficiency of such systems. By incorporating a model catalyst, L-proline, the ability of the synthesized nanogels to sequester hydrophobic reagents was examined as a function of their hydrophilicity and morphology. It was concluded that in order to enhance the efficiency of the organocatalyst, fine tuning of the hydrophobicity of the nanogel was required, which was only achieved when ethyl methacrylate was used as the co-monomer. Additionally, the recycling of the nanogels was found possible when a temperature-responsive hydrophilic cross-linked shell was added to the hydrophobic core. The efficiency of the catalytic nanogels was different at varying temperatures when the shell was homogeneously cross-linked, or a gradient. Future work on more precious catalysts should be carried out taking into account these findings, while the potential use of such particulate systems as stationary phases in flow catalyses could also be of great interest.

Taking into consideration that one of the outcomes of the Chapter 5 was that highly cross-linked particles can switch the catalysis off, the use of a reversible cross-linker based on thymine was examined in Chapter 6 as a potential “on-off” switch. The particles synthesized had successfully incorporated the cross-linker that was observed to dimerize upon irradiation. However, the properties of the hydrophilic particles were not altered, as the cross-linking occurred between proximal thymines, rather than thymines residing on different polymer segments. Future work should focus on the optimization of the photoinduced cross-linking as to effectively alter the properties of the particles. Additionally, the de-cross-linking of the particles was not found to be efficient when

employing the conditions previously reported in the literature. As such, the determination of the wavelength of the irradiation required to induce de-cross-linking of the particles should be achieved, before the use of such particles as reversible catalytic nanoreactors. Additionally, it would be of interest to investigate the potential photocycloaddition of thymine-functional particles with other moieties (such as thyamine) and their use as nanocarriers, while the enzymatic cleavage of the dimer should also be exploited.